Van reversibele additiefragmentatie-ketentransferpolymerisatie in bulk tot in (mini-)emulsie: een kinetische studie

From Reversible Addition-Fragmentation Chain Transfer Polymerization in Bulk to (Mini) Emulsion: A Kinetic Study

Dries Devlaminck

Promotoren: prof. dr. ir. D. R. D'hooge, dr. ir. P. H.M. Van Steenberge
Proefschrift ingediend tot het behalen van de graad van
Doctor in de ingenieurswetenschappen: chemische technologie

UNIVERSITEIT
GENT

Vakgroep Materialen, Textiel en Chemische Proceskunde
Voorzitter: prof. dr. P. Kiekens
Faculteit Ingenieurswetenschappen en Architectuur
Academiejaar 2018 - 2019

ISBN 978-94-6355-235-6
NUR 952
Wettelijk depot: D/2019/10.500/43

Promotoren:

prof. dr. ir. D.R. D'hooge	Universiteit Gent
dr. ir. P.H.M. Van Steenberge	Universiteit Gent

Examencommissie:

Prof. dr. Hennie De Schepper, voorzitter	Universiteit Gent
Prof. dr. ir Karen De Clerck, secretaris	Universiteit Gent
Prof. dr. Richard Hoogenboom	Universiteit Gent
Prof. dr. Anitha Ethirajan	Universiteit Hasselt
Prof. dr. Marie-Françoise Reyniers	Universiteit Gent
Prof. dr. ir. Dagmar D'hooge	Universiteit Gent
dr. ir. Paul Van Steenberge	Universiteit Gent

Universiteit Gent

Faculteit Ingenieurswetenschappen en Architectuur

Vakgroep Materialen, Textiel en Chemische Proceskunde

Laboratorium voor Chemische Techniek

Technologiepark 125

B-9052 Zwijnaarde, Gent

België

http://www.lct.ugent.be

The four years of my Phd have been an interesting journey which has brought me in contact with a lot of people, many of which I will always think back to with great joy.

Firstly, I would like to thank Prof. Marin and Prof. D'Hooge for giving me the opportunity to start a PhD at the Laboratory for Chemical Technology (LCT). Furthermore, a special thanks goes to Paul Van Steenberge, who transcended his role as copromotor and has become a dear friend. It is safe to say that the work underlying this thesis would have been much harder to achieve without your guidance and advice on the mathematics of kinetic modelling. Additionally, as a co-author of all my published work, I would like to thank Prof. Reyniers for her critical view on the performed work and raising my research to a higher level.

I have had the honor to work alongside great colleagues from the polymer part of the LCT. You never hesitated to put your own work aside when asked for help. Hence, Pieter, Gilles, Stijn, Nils, Lies and Yoshi, I will forever be grateful. Furthermore, I would like to thank all other members of the LCT for the nice lunchbreaks, especially the members of the LCT running team. Also the people from the technical team, Michaël, George, Brecht, Wim and all others, thank you for all the proper support and advice. Special thanks goes out to all the thesis students which I have guided throughout the years: Kevin, Simon and Kyann, I wish you all the best with your future career.

Moreover, thank you to my family and friends to celebrate the good times but also to provide the welcomed support during rough times. Especially my parents, who have always given me the freedom to search my own path in life. Annemie, words can't describe the love I have for you. You have always been my rock in times of trouble, in the middle of the chaos, there was you.

Finally, Arthur, you sweet and kind little man. All the sleepless nights were quickly forgotten when coming home after a hard day of work and seeing your cute smile. You have always been my deepest motivation, I am so proud to call you my son.

"Give someone a program, you frustrate them for a day; teach them how to program, you frustrate them for a lifetime." – David Leinweber

Nederlandstalige samenvatting

Gedurende de 20e eeuw heeft de industriële polymeerproductie een snelle ontwikkeling gekend, die resulteerde in één van de snelst groeiende industrieën wereldwijd. Het gevolg hiervan is dat de afwezigheid van synthetische polymeerproducten in ons dagdagelijkse leven ondenkbaar is geworden. Oorspronkelijk lag de focus vooral op de grootschalige productie van alledaagse producten omwille van de lage kost en eenvoudige productie. In de recente decennia is echter gebleken dat de veelzijdigheid van deze materialen kan aangewend worden in op maat gemaakte hoogtechnologische producten zoals biodegradeerbare bouwstenen voor weefselregeneratie of lichtgewicht vliegtuigbekleding.

Inherente limitaties en gebrek aan controle over de finale producteigenschappen in vrije radicalaire polymerisatie (Free Radical Polymerization of FRP), één van de belangrijkste polymerisatiemechanismes, kan overwonnen worden door de introductie van reversibele deactivatie radicalaire polymerisatie (reversible deactivation radical polymerization of RDRP) technieken. Door middel van RDRP wordt een groot bereik aan macromoleculaire architecturen zoals (multi-)blok copolymeren, sterpolymeren en moleculaire borstels beschikbaar.

In deze doctoraatsscriptie wordt een combinatie van kinetische modellering en experimentele technieken aangewend om een fundamenteel begrip te bekomen van het mechanisme van reversibele additie-fragmentatieketentransfer (reversible addition-fragmentation chain transfer of RAFT) polymerisatie. Dit is één van de meest veelzijdige RDRP technieken wat betreft monomeer compatibiliteit. Zowel bulk als mini-emulsie technieken worden toegepast. Enerzijds berust deze modelleringsbenadering op de essentiële bepaling van accurate RDRP gerelateerde snelheidscoëfficiënten, met inbegrip van de correcte beschrijving van diffusie limitaties en alle relevante kinetische stappen. Anderzijds is experimentele data nodig om de bekomen modelleringresultaten te valideren. Deze data berust op de doelbewuste keuze van

experimentiele condities, eventueel aangepast door preliminaire modelscreening, en karakterisatietechnieken.

Hoofdstuk 1 geeft een algemene introductie rond de chemische methodes en technieken waar de daaropvolgende hoofdstukken op verder bouwen. De concepten van FRP en RDRP technieken worden uitgelegd met als focus hoofdzakelijk RAFT polymerisatie. Aangezien in deze doctoraatsscriptie verschillende polymerisatietechnieken zoals bulk en (mini)emulsie worden toegepast, wordt ook een overzicht gegeven van de voordelen en uitdagingen rond deze technieken in combinatie met RAFT polymerisatie.

In **Hoofdstuk 2** worden moderne modelleringstechnieken besproken voor de beschrijving van de kinetiek van RAFT polymerisatie onder bulk/oplossing en emulsiecondities. Zoals vermeld hierboven kan kinetische modellering een krachtig hulpmiddel zijn om complexe chemische processen te begrijpen en optimaliseren. Voor RAFT bulk polymerisatie werden reeds meerdere inherent verschillende modelleringsmethodes ontwikkeld, die kunnen worden onderverdeeld in twee grote computationele klassen: deterministisch en stochastisch. Deterministische modellering omvat de integratie van een set van differentiaalvergelijkingen. Omdat deze vergelijkingen corresponderen met de massa-balansen voor alle species die aanwezig zijn in het reactiemengsel, kan het totale aantal vergelijkingen te hoog worden om binnen een redelijke tijdspanne op te lossen. Een elegante oplossing voor dit probleem is om de methode van momenten toe te passen waar verschillende polymeerketens niet individueel worden bekeken, maar enkel de gemiddeldes van de ketenlengtedistributie van elk type macrospecies wordt beschouwd. Als gevolg verkiest deze methode een significante reductie van de computationele tijd boven informatie over individuele ketens. Alternatief hiervoor is de kinetische Monte Carlo simulatie, de meest bekende stochastische modelleringsmethode, die elke reactie beschouwd als een willekeurig evenement waarvoor de keuze berust op de reactieprobabiliteiten en die de volledige reactiegeschiedenis bewaart. Hierdoor is het mogelijk om informatie met betrekking

tot een gedetailleerde polymeerstructuur te bekomen (comonomeer sequenties). Echter in het geval van complexe reactieschema's kan dit een hoge computationele kost eisen aangezien polymerisatieprocessen bestaan uit duizenden individuele reactiestappen, zelfs in het geval van gelimiteerde reactievolumes. Het multi-fase karakter van RAFT emulsiepolymerisatie maakt de kinetische beschrijving uitdagend en vereist een meer complexe mathematische benadering. In de meeste gevallen wordt een gelijkaardige deterministische modelleringsbenadering gebruikt zoals bij bulk polymerisatie waarbij Smith-Ewart differentiaalvergelijkingen toegevoegd worden om de evolutie van de deeltjestypedistributie te beschrijven. In dit hoofdstuk wordt een eenvoudig (intrinsiek) FRP miniemulieschema gebruikt om het gebruik van de Smith-Ewart vergelijkingen te verduidelijken. Miniemulsie polymerisatie wordt vaak verkozen boven conventionele (macro)emulsie polymerisatie zowel in experimentele als modelleringsstudies aangezien dit het deeltjesnucleatiemechanisme vereenvoudigd. Het wordt aangetoond dat accuraatheid van de modelleringsbenadering gebruikt in dit werk kan worden bevestigd door gevestigde analytische vergelijkingen voor een aantal limiterende gevallen. Verder geven de resultaten aan dat het opeenvolgende vertrek uit en de reïntroductie van radicalen in de deeltjes, mogelijk gemaakt door ketentransfer naar monomeer, de polymerisatiesnelheid verlaagt aangezien de mogelijkheid toeneemt dat twee radicalen termineren. Verder bepaalt de grootte van de (intrinsieke) terminatiesnelheidscoëfficiënt of onmiddellijke terminatie kan worden aangenomen, en dus of een maximum van één, of meerdere radicalen kan aanwezig zijn in elk deeltje.

De accuraatheid van kinetische modelleringsresultaten wordt bepaald door vele factoren. Belangrijkst is dat het direct gecorreleerd is met de volledigheid van het beschouwde reactiemechanisme, vandaar de minimalisatie van de benaderingen en vereenvoudigingen die worden gebruikt, en met de accuraatheid van de corresponderende snelheidscoëfficiënten, waaronder de juiste beschrijving van potentiele diffusielimitaties.

In **Hoofdstuk 3** worden de degeneratieve transfercoëfficiënten voor de RAFT homopolymerisatie van styrene, geïnitieerd met (O-ethyl xanthaat)-2-ethyl propionaat, een xanthaat type RAFT agens, en zijn ketenextentie met vers styreen of n-butylacrylaat bepaald door een multiresponsieve regressie-analyse toe te passen op eigen gegenereerde experimentele data. Een belangrijke eigenschap van RDRP polymeerproducten is de eindgroepfunctionaliteit, de fractie slapende macrospecies ten opzichte van de totale hoeveelheid van alle types macrospecies. Deze eigenschap is echter niet eenvoudig experimenteel te bepalen, vooral in RAFT polymerisatie die xanthaten als initiële RAFT agens gebruikt aangezien deze aanwezig blijven gedurende het volledige polymerisatieproces. In dit hoofdstuk wordt uitgelegd hoe een combinatie van dialyse, om residueel RAFT agens te verwijderen, en elementanalyse kunnen gebruikt worden om EGF data experimenteel te bekomen. De gecombineerde experimentele en modelleringsbenadering laat toe om het degeneratieve mechanisme te bevestigen. Kinetische Monte Carlo modellering werd gebruikt om het polymeer product, toegankelijk via homopolymerisatie en zijn ketenextensie, te visualiseren. Verder wordt ook uitgelicht dat het xanthaat type RAFT agens resulteert in een lage RAFT reactiviteit en beide blokken van de ketenextensie worden gevormd door middel van een enkele uitwisseling, wat een transfergedrag impliceert zoals in conventionele FRP.

Aangezien heterogene polymerisatietechnieken significante verbeteringen geven op vlak van procesveiligheid en milieuvriendelijkheid, verschuift de aandacht in **Hoofdstuk 4** naar RAFT miniemulsie polymerisatie. Een twee-dimensioneel model werd ontwikkeld dat het aantal macro- en vertrekkende groep radicalen per deeltje in aanmerking neemt. Dit model beschrijft de degeneratieve RAFT miniemulsie polymerisatie van methyl methacrylaat met cyanoprop-2-yl dithiobenzoaat als initiële RAFT agens. Bulk experimentele data uit de literatuur werd gebruikt om de micro-schaal model parameters (i.e. de snelheidscoëfficiënten en diffusielimitaties op terminatie en RAFT transfer) te bevestigen, terwijl miniemulsie literatuur

data werd gebruikt om de deactivatie en reïnitiatie coëfficiënten van het RAFT vertrekkende groep radicaal te bepalen. Het wordt aangetoond dat opeenvolgende reïntroductie/vertrek stappen met betrekking tot the RFT vertrekkende groep radicaal resulteren in een vertragingseffect gelijkaardig aan dat beschreven in Hoofdstuk 2. Echter wanneer het RAFT agens volledig geconsumeerd is wordt dit vertragend effect gestopt. In andere modellen wordt vaak een nul-één vereenvoudiging aangenomen die stelt dat enkel nul of één radicaal aanwezig kan zijn in een enkel deeltje, en dat onmiddellijke terminatie plaatsvindt wanneer twee radicalen elkaar ontmoeten. Echter, in dit hoofdstuk wordt aangetoond dat bij hoge monomeerconversies deze nul-één kinetiek niet mag aangenomen worden omwille van diffusielimitaties op terminatie. Bij een grotere gemiddelde ketenlengte wordt deze afwijking nog meer uitgesproken door diffusielimitaties op RAFT transfer.

In **Hoofdstuk 5** wordt het model uit het voorgaande hoofdstuk uitgebreid tot de 5-dimensionele Smith-Ewart vergelijkingen. Deze laten toe om ook de drie mogelijke RAFT intermediaire radicalen (R_iXR_j, R_iXR_0 and R_0XR_0) in beschouwing te nemen, en dus om de verschillen tussen het niet-degeneratieve en degeneratieve RAFT miniemulsie polymerisatiemechanisme theoretisch te verklaren. Styreen, vaak gebruikt in modelleringsstudies omwille van de beschikbaarheid van de FRP gerelateerde snelheidscoëfficiënten, werd gekozen als monomeer en een macro-RAFT agens werd beschouwd om de focus op het RAFT mechanisme te behouden, aangezien vertrek/reïntroductie van het RAFT vertrekkende groep radicaal vermeden wordt. Drie relevante RAFT kinetische parametercombinaties werden onderzocht. De eerste combinatie bootst het langzame fragmentatiemodel na, waar de RAFT vertraging wordt verklaard door een lage fragmentatie snelheidscoëfficiënt in afwezigheid van RAFT kruisterminatie. Het wordt aangetoond dat de nul-één kinetiek niet kan worden aangenomen, aangezien de R_iXR_j radicaalpopulatie zal opgebouwd worden. In navolging van het intermediaire terminatiemodel, verklaart de tweede combinatie de RAFT vertraging door een

middelmatige fragmentatiesnelheidscoëfficiënt in combinatie met een hoge kruisterminatie snelheidscoëfficiënt. Nul-één kinetiek kan worden aangenomen alhoewel alle 5 radicalen in aanmerking moeten worden genomen in het model. Tenslotte werd de derde combinatie gebruikt om een ideale RAFT agent te bestuderen, die dus niet resulteert in RAFT vertraging wat bekomen kan worden door middel van een hoge fragmentatie snelheidscoëfficiënt zonder kruisterminatie te beschouwen. Enkel in dit geval kan het degeneratieve mechanisme in alle vertrouwen worden aangenomen en een vereenvoudiging kan worden gemaakt van een beschrijving gebaseerd op een vijf dimensionele naar een twee dimensionele Smith-Ewart vergelijking. Dit resulteert in een algemeen eenvoudigere kinetische beschrijving. Belangrijk is ook dat kon worden aangetoond dat de identificatie van de aard van de RAFT vertraging bekomen kan worden door een experimentele miniemulsiestudie. Dit is omdat de trage fragmentatie en kruisterminatie hypothese resulteert in een verschillende impact van de gemiddelde deeltjesgrootte op het monomeerconversieprofiel, de dispersiteit en EGF.

Alhoewel (RAFT) miniemulsie intrinsiek de meest eenvoudige emulsiepolymerisatietechniek is wat betreft reactie- en transport mechanismes, vereist het een hoog energetisch toestel om de initiële condities te scheppen. Als gevolg is deze techniek industrieel minder relevant en wordt (RAFT) macroemulsie verkozen. Om het model uit Hoofdstuk 4 en 5 in de toekomst mogelijk uit te breiden, bespreekt **Hoofdstuk 6** een experimentele studie van RAFT macroemulsie polymerisatie van styreen met (O-ethyl xanthaat)-2-ethyl propionaat, hetzelfde controle agens die ook werd gebruikt in Hoofdstuk 2. Net zoals bij bulk polymerisatie resulteert dit xanthaat type RAFT agens niet in controle over de ketengroei, wat tot een grote dispersiteit leidt in het polymeerproduct. Desondanks kan de concentratie van dit controlerende agens gebruikt worden om de gewenste nummergemiddelde molaire massa te veranderen terwijl de polymerisatiesnelheid kan worden verhoogd door de hoeveelheid inititiator of surfactant te verhogen, of door de hoeveelheid van controlerend agens te verlagen. Verder kan de surfactant

concentratie gebruikt worden om de gemiddelde deeltjesgrootte te variëren. Het belangrijkste voordeel van het gebruik van een xanthaat type RAFT agens is gerelateerd aan zijn oppervlakteactiviteit. Het werd aangetoond dat de bekomen polystyreen latex kan worden uitgebreid door middel van een semi-batch reactie om een polystyreen-blok-poly(n-butyl acrylaat) polymeerdeeltje te creëren, die hoogstwaarschijnlijk in een kern-schil structuur zal georganiseerd zijn.

Ten slotte vat **Hoofdstuk 7** de belangrijkste conclusies van deze doctoraatsthesis samen en geeft het enkele perspectieven voor toekomstig werk.

English summary

During the 20th century, the polymer production industry has known a rapid development resulting in one of the fastest growing industries worldwide. As a result, daily life without the presence of synthetic polymer products has become unthinkable. Originally, focus was on the large scale production of everyday products due to its low cost and ease of manufacturing. However, in recent decennia, it has become apparent that its versatility can be used to design tailor-made high-tech specialty products such as biodegradable scaffolds for tissue engineering or lightweight aircraft skins.

Inherent limitations and lack of control over end product properties in free radical polymerization (FRP), one of the most important polymerization mechanisms, could be overcome by the introduction of reversible deactivation radical polymerization (RDRP) techniques. Via RDRP, a wide range of macromolecular architectures such as (multi-)block copolymers, star polymers and molecular brushes became accessible.

In this PhD thesis, a combination of kinetic modeling and experimental work is applied to gain fundamental understanding of the mechanism of reversible addition-fragmentation chain transfer (RAFT) polymerization, one of the most versatile RDRP techniques regarding monomer compatibility, applying both bulk and (mini)emulsion techniques. On the one hand, the modeling approach relies on the essential determination of accurate RAFT polymerization specific rate coefficients, including the proper description of diffusional limitations, while taking into account all relevant kinetic events, hence minimizing the integrated approximations. On the other hand, dedicated experimental data is needed to validate the obtained modeling results and relies on the purposeful choice of experimental conditions, which can be tuned by preliminary model screening, and characterization techniques.

Chapter 1 provides a general introduction to the chemical methods and techniques on which the other chapters rely on. The concepts of FRP and RDRP techniques are explained, with focus mainly on RAFT polymerization. Furthermore, as in this PhD thesis several polymerization techniques, *i.e.* bulk and (mini)emulsion, are applied, an overview of the advantages and challenges concerning these techniques in combination with RAFT polymerization are stated.

In **Chapter 2**, the state-of-the art on modeling tools for RAFT polymerization kinetics under bulk/solution and emulsion conditions is discussed. As stated above, kinetic modeling can be a powerful tool for understanding and optimizing complex chemical processes. For RAFT bulk polymerization, multiple inherently different modeling methods have already been developed which can be divided in two major computational classes: deterministic and stochastic methods. Firstly, deterministic modeling involves the integration of a set of differential equations. As these equations correspond with the mass balances for all species present in the reaction mixture, the total number of equations can become too high to solve within reasonable time. An elegant solution solving this issue is applying the method of moments approach, where different polymeric chains are not being considered individually but only the averages of the chain length distribution of each type of macrospecies are covered. Consequently, in this method, a significant reduction of the computation time is preferred over the information about individual chains. Alternatively, kinetic Monte Carlo simulations, the most notable stochastic modeling method, considers each reaction as a random event chosen based on its probability and stores the entire reaction event history, making it possible to obtain in detail the polymer structure, e.g. comonomer sequences. However, for complex reaction schemes, this can require a high computational cost as polymerization processes consist of thousands of individual reaction steps, even in limited reaction volumes. The multi-phase character of RAFT emulsion polymerization complicates the kinetic description and requires a more complex mathematical description. Mostly, a similar deterministic modeling approach as for the bulk polymerization

counterpart is used where Smith-Ewart differential equations are added to describe the evolution of the particle type distribution. In this chapter, a straightforward (intrinsic) FRP miniemulsion scheme was used to elaborate the use of the Smith-Ewart equations. Miniemulsion polymerization is often preferred over conventional (macro)emulsion polymerization in both experimental and modeling studies as this simplifies the particle nucleation mechanism. It is shown that the modeling approach used in this work can be confirmed by established analytical equations for certain limiting cases. Moreover, the results indicate that subsequent exit and reentry of radicals, made possible by chain transfer to monomer, reduces the polymerization rate as the probability for two radicals to meet and terminate increases. Additionally, the magnitude of the (intrinsic) termination rate coefficient determines if instantaneous termination can be assumed, and hence if a maximum of one or more radicals can be present in each particle.

The accuracy of kinetic modeling results is determined by many factors. Most importantly, it is directly correlated with the completeness of the considered reaction mechanism, hence the minimization of the approximations and simplifications used, and the accuracy of the corresponding rate coefficients, including the proper description of potential diffusional limitations. In **Chapter 3**, it is shown how the degenerative transfer coefficients for the RAFT homopolymerization of styrene commenced with (*O*-ethyl xanthate)-2-ethyl propionate, a xanthate type of RAFT agent, and its chain extension with fresh styrene or *n*-butylacrylate are determined by applying a multi-responsive regression analysis to in-house gathered experimental data. An important property of RDRP polymer product is the end-group functionality, which is the fraction of dormant macrospecies to the total amount of all types of macrospecies. This property however is not easily experimentally determinable, especially in RAFT polymerization employing xanthates as initial RAFT agent remains present throughout the polymerization process. In this chapter, it is explained how a combination of dialysis to

remove residual RAFT agent and elemental analysis can be used to obtain EGF experimental data. The joint experimental and modeling approach allows to confirm the degenerative mechanism and kinetic Monte Carlo modeling is used to visualize the polymer product accessible via the homopolymerization and its chain extension. Moreover, it is highlighted that the xanthate type of RAFT agent results in a low RAFT reactivity and both "blocks" of the chain extension are formed through a single exchange, which implies a transfer behavior as in conventional FRP.

As heterogeneous polymerization techniques offer significant improvements in terms of process safety and environmental friendliness, attention in **Chapter 4** is shifted towards RAFT miniemulsion polymerization. A two-dimensional model, accounting for the number of macro- and leaving group radicals per particle, is developed describing the degenerative RAFT miniemulsion polymerization of methyl methacrylate with cyanoprop-2-yl dithiobenzoate as initial RAFT agent. Bulk literature experimental data is used to confirm the micro-scale model parameters, *i.e.* rate coefficients and diffusional limitations on termination and RAFT transfer, whereas miniemulsion literature data is used to determine the exit and entry rate coefficients concerning the RAFT leaving group radical. It is shown that consecutive entry/exit events result in a retardation effect similarly as described in Chapter 2. However, when the RAFT agent is completely consumed, the retardation effect is halted in this case. In other modeling studies, a zero-one simplification is often assumed which states that only zero or one radical can be present in a single particle and that instantaneous termination occurs when two radicals meet. However, in this chapter, it is demonstrated that at high monomer conversions it is not afforded to assume zero-one kinetics, due to diffusional limitations on termination. With larger average chain lengths this deviation is more pronounced and further accelerated by diffusional limitation on RAFT transfer.

In **Chapter 5**, the model discussed in the previous chapter is extended to include 5-dimensonal Smith-Ewart equations. This allows the consideration of the three possible (R_iXR_j, R_iXR_0 and R_0XR_0) RAFT intermediate radical species and hence to theoretically understand differences between a non-degenerative and degenerative RAFT miniemulsion polymerization. Styrene, often used in modeling studies due to the availability of the FRP related rate coefficients, is chosen as monomer and a macro-RAFT agent is considered to allow the focus on the RAFT mechanism itself as exit/entry of the RAFT leaving group radical is avoided. Three relevant RAFT kinetic parameter combinations are investigated. The first combination mimics the slow fragmentation model, where RAFT retardation is explained by a low fragmentation rate coefficient in the absence of RAFT cross-termination. It is shown that zero-one kinetics cannot be assumed as the R_iXR_j radical population will build up. In order to resemble the intermediate termination model, the second combination justifies the RAFT retardation via a medium fragmentation rate coefficient in combination with a high cross-termination rate coefficient. Zero-one kinetics can be assumed although all 5 radical types need to be considered. Finally, the third combination is used to study an ideal RAFT agent, hence not resulting in RAFT retardation which is achievable via a high fragmentation rate coefficient without considering cross-termination. Only in this case, the degenerative mechanism can be safely assumed and a direct switch can be made from a five- to a two-dimensional Smith-Ewart equation based description, strongly simplifying the overall kinetic description. Importantly, it is shown that the identification of the nature of the RAFT retardation can be achieved via an experimental miniemulsion study as the slow fragmentation and cross-termination hypothesis result in a different impact of the average particle size on the monomer conversion profile, dispersity and EGF.

Although (RAFT) miniemulsion is intrinsically the most simple emulsion polymerization technique in terms of reaction and transport mechanism, it requires a high energy shear device

to establish the initial conditions. Consequently, this technique is less industrially relevant and (RAFT) macroemulsion is preferred. In order to potentially extend the model discussed in Chapter 4 and 5 in the future, **Chapter 6** discusses an experimental study of RAFT macroemulsion polymerization of styrene with (*O*-ethyl xanthate)-2-ethyl propionate, the same controlling agent as used in Chapter 2. Similar as during bulk polymerization, this xanthate type of RAFT agent does not result in control over chain growth, leading to a high dispersity polymer product. Nevertheless, the concentration of the controlling agent can be used to alter the desired number average molar mass whereas the polymerization rate can be increased by increasing the amount of initiator or surfactant or by decreasing the amount of controlling agent. Furthermore, the surfactant concentration can be used to control the average particle size as well. Importantly, the main advantage of the use of a xanthate type of RAFT agent is related to its surface activity. It is shown that the obtained polystyrene latex can be extended via semi-batch operation to create polystyrene-block-poly(n-butyl acrylate) polymer particles which will most likely be organized forming a core-shell structure.

Finally, **Chapter 7** summarizes the main conclusions of this PhD thesis and prospects for potential future work are discussed as well.

List of Symbols

Roman Symbols

$[A]$	concentration of reagent *A*	mol L^{-1}
$[A]_0$	initial concentration of reagent *A*	mol L^{-1}
C_{entry}	proportionality constant for R_0 entry into a polymer particle	-
C_{exit}	proportionality constant for R_0 exit from a polymer particle	-
C_{tr}	transfer coefficient for the exchange with the dormant macrospecies	-
$C_{tr,0}$	transfer coefficient for the exchange with the initial RAFT agent	-
$Đ$	dispersity	-
D_I	diffusion coefficient of *I* radical	m^2 s^{-1}
d_p	average particle diameter	m
D_{R0}	R_0 diffusional coefficient	m^2 s^{-1}
D_{term}	correction factor related to the rate of termination between two initiator radicals	m^2 s^{-1}
f	initiator efficiency	-
$f_n(i)$	number fraction of macroradicals with chain length *i*	-
f_{N_k}	fraction of particles with *k* (macro)radicals	-
f_{tc}	fraction of termination occurring by recombination	-
I	conventional initiator-derived radical	-
I_2	conventional radical initiator	-
i_{crit}	critical chain length for entry into a micelle/particle	-
INT_{ij}	intermediate radical with two arms of chain lenght *i* and *j*	-
i_{SL}	cross over chain length between short- and long-chain behavior	-
i_{gel}	chain length at the onset of the gel-effect	-
j_{crit}	critical chain length for precipitation	-
k_A	rate coefficient for reaction type *A*	L mol^{-1} s^{-1} or s^{-1}
$k_t^{1,1}$	(apparent) termination rate coefficient for radicals with chain length 1	L mol^{-1} s^{-1}
$<k_{tc,app}>$	average apparent termination by recombination rate coefficient	L mol^{-1} s^{-1}
M	monomer	-
m	mass	g
$M(A)$	molar mass of substance A	g mol^{-1}
M_m	mass average molar mass of polymeric species	g mol^{-1}
M_n	number average molar mass of polymeric species	g mol^{-1}
$M_{n,inst}$	instantaneous number average molar mass of polymeric species	g mol^{-1}
$n(A)$	molar amount of substance A	mol
$\bar{n}(M^\bullet)$	average number of monomeric radicals per particle	-

$\bar{n}(R_0)$	average number of leaving group radicals per particle	-
$\bar{n}(R_0XR_0)$	average number of R_0XR_0 intermediate radicals per particle	-
$\bar{n}(R_i)$	average number of macroradicals per particle	-
$\bar{n}(R_iXR_0)$	average number of R_iXR_0 intermediate radicals per particle	-
$\bar{n}(R_iXR_j)$	average number of R_iXR_j intermediate radicals per particle	-
$n_0(A)$	initial molar amount of substance A	mol
N_A	Avogadro constant	mol^{-1}
$N_{k,l,...}$	number of particles containing k radicals of type A, l radicals of type B,...	-
N_p	total number of particles	-
N_t	total number of reaction types	-
P_i	dead polymer species with chain length *i*	-
P_v^{MC}	Monte Carlo reaction probability of reaction type *v*	-
P_x	reaction probability of reaction type *x*	-
r	monomer reactivity ratio	-
R_0	RAFT leaving group	-
R_0X	initial RAFT agent	-
R_0XR_0	intermediate radical with two arms of chain length 0	-
R_0XR_i	intermediate radical of the pre-equilibrium with one arm of chain length 0 and one of chain length *i*	-
$R_{1/2/3/4}$	oligomeric radical species with chain length 1, 2, 3 or 4	-
$r_{1/2/3}$	random number used in kinetic Monte Carlo modeling	-
R_i	macroradical with chain length *i*	-
R_i'	macroradical with chain length *i* derived from a monomeric radical	-
R_iX	dormant macrospecies with chain length *i*	-
R_iXR_j	intermediate radical of the main equilibrium with two arms of chain lenght *i* and *j*	-
R_v^{MC}	the total reaction rate of reaction type *v*	s^{-1}
T	temperature	K
V	volume	L
v_p	average particle volume	L
$w(A)$	mass fraction of substance A	-
X	persistent radical	-
x_m	mass average chain length	-
X_m	monomer conversion	-
x_n	number average chain length	-
X_{R0X}	RAFT agent conversion	-
Z	stabilizing group of the RAFT chain transfer agent	-

Greek symbols

α_{gel}	exponent for termination of chains in the gel regime	-
α_L	exponent for termination of long chains in dilute solution	-
α_S	exponent for termination of short chains in dilute solution	-
δ_{ij}	Kronecker Delta function	-
λ_s	s^{th} order moment of the macroradical distribution, s = 0,1,2	mol L^{-1}
μ_s	s^{th} order moment of the distribution of dead species, s = 0,1,2	mol L^{-1}
ν	kinetic chain length	-
ν_0	kinetic chain length in the absence of chain transfer	-
ρ	(overall) radical entry (molecular) rate	s^{-1}
τ_s	s^{th} order moment of the distribution of dormant species, s = 0,1,2	mol L^{-1}
φ_0	fragmentation probability related to the RAFT preequilibrium	-
Γ	partitioning coefficient	-
$\Omega_{1/2,0/1}$	contributions related to the moments of the distribution of R_iXR_j intermediate radicals	mol L^{-1}
Ω_s^0	s^{th} order moment of the distribution of R_0XR_i intermediate radicals, s = 1,2	mol L^{-1}

Sub and Superscripts

act	activation
add	addition
app	apparent
aq/p	aqueous/particle phase
chem	intrinsic chemical contribution
deact	deactivation
diff	diffusional contribution
dis	dissociation
entry,R0	entry from aqueous phase into particle of R_0 radical
entryR2	entry of oligomeric radical with chain length 2 from aqueous phase into particle
exit,R0	exit from particle into aqueous phase of R_0 radical
exitM	exit from particle into aqueous phase of monomeric radical
frag	fragmentation
i	chain length of the involved macrospecies
nB	*n*-butyl acrylate
p	propagation
pI	chain initiation by *I*
pM	chain initiation by monomer radical
pR0	chain initiation by R_0

S	styrene
tc	termination by recombination
tc,0	termination by recombination of a macro- and leaving group radical
tc,00	termination by recombination of two leaving group radicals
tc,0I	termination by recombination of a leaving group and conventional initiator radical
tcross	cross termination
td	termination by disproportionation
tr	transfer with dormant macrospecies
tr,0	transfer with the initial RAFT agent
-tr,0	transfer between leaving group radical and dormant macrospecies
trM	chain transfer to monomer

Abbreviations

^{1}H-NMR	proton nuclear magnetic resonance
ACN	acetonitrile
AIBN	2,2'-azobis(2-methyl-propionate)
ATRP	atom transfer radical polymerization
BBO	broadband observe
BBOT	2,5-bis(5-tert-butyl-benzoxazol-2-yl) thiophene
BCPA	3-benzyltrithiocarbonyl propionic acid
BHT	butylated hydroxytoluene
CLD	chain length distribution
CMC	critical micelle concentration
CPDB	2-cyanoprop-2-yl dithiobenzoate
CRP	controlled radical polymerization
CTA	chain transfer agent
CV	coefficient of variation
DCM	dichloromethane
DLS	dynamic light scattering
DM	degenerative mechanism
EA	ethyl acrylate
EGF	end-group functionality
EP	ethyl propionate
FID	flame ionization detector
FRP	free radical polymerization
GC	gas chromatography
GPC	gel permeation chromatography
H2O	water
HPLC	high performance liquid chromatography
HQ	hydroquinone
ITM	intermediate termination model
*k*MC	kinetic Monte Carlo
KPS	potassium persulfate
LAM	less activated monomer

LCT	Laboratory for Chemical Technology
MA	methyl acrylate
MADIX	macromolecular design by interchange of xanthates
MAM	more activated monomer
MMA	methyl methacrylate
NaCl	sodium chloride
$NaHCO_3$	sodium bicarbonate
*n*BuA	*n*-butyl acrylate
NDM	non-degenerative mechanism
NMP	nitroxide mediated polymerization
OEXEP	(O-ethyl xanthate)-2-ethyl propionate
OtFOX	(O-2,2,2-trifluoro ethyl xanthate)-2-ethyl propionate
PEPDTA	1-phenylethyl phenyldithiocetate
PS	polystyrene
PS-CPDB	polystyryl-2-cryanoprop-2-yl dithiobenzoate
PSD	particle size distribution
PS-PEPDTA	polystyryl-1-phenylethylphenyl dithioacetate
PSSA	pseudo steady state approximation
PS-X	oligomeric polystyrene RAFT agent
RAFT	reversible addition-fragmentation chain transfer
RAFT-CLD-T	RAFT-chain length dependent–termination
RDRP	reversible deactivation radical polymerization
RI	refractive index
rpm	rotations per minute
SDS	sodium dodecyl sulfate
SEC	size exclusion chromatography
SFM	slow fragmentation model
Sty	styrene
TCL	targeted chain length
TEM	transmission electron microscopy
THF	tetrahydrofuran
UV-VIS	ultraviolet-visible

Chapter 1: Basic concepts of bulk and emulsion free radical and RAFT polymerization

During the 20th century, the polymer production industry has known a rapid development resulting in one of the fastest growing industries worldwide.[1] As a result, daily life without the presence of synthetic polymer products has become unthinkable. Originally, focus was on the large scale production of everyday products due to its low cost and ease of manufacturing. However, in recent decennia, it has become apparent that its versatility can be used to design tailor-made high-tech specialty products such as biodegradable scaffolds for tissue engineering or lightweight aircraft skins.[2]

Inherent limitations and lack of control over end product properties in free radical polymerization (FRP), one of the most important polymerization mechanisms, could be overcome by the introduction of reversible deactivation radical polymerization (RDRP) techniques. Via RDRP, a wide range of macromolecular architectures such as (multi-)block copolymers, star polymers and molecular brushes became accessible. This already resulted in niche applications in markets such as electronics[3–5], the coating industry[6,7] and biomedical technology.[8,9]

In this PhD thesis, a combination of experimental studies and numerical simulations is synergistically used to gain a better understanding of the kinetic aspects of reversible addition-fragmentation chain transfer (RAFT) polymerization, one of the most versatile RDRP techniques regarding monomer compatibility, in bulk, solution and dispersed media. This introductory chapter is used to elucidate the general theoretical concepts and aspects relevant for understanding the following chapters. Firstly, the principles of FRP and RDRP are explained with a strong focus on RAFT polymerization, one of the keystones of this thesis. Secondly, the differences from a kinetic point of view between carrying out a polymerization in bulk/solution

or in an emulsified system are described. Thirdly, an outline of the objectives of the remaining chapters is given.

1.1 Principle of free radical polymerization

Polymers are large molecules composed of many repeated subunits originating from small molecules, known as monomers.[10] One of the most common methods to produce synthetic polymers is FRP, of which the key reactions are shown in Figure 1.1.

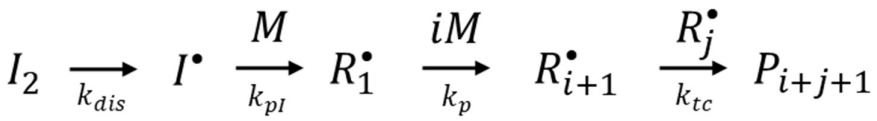

Figure 1.1*: Simplified reaction scheme showing the key elementary reactions in a free radical polymerization (FRP);* I_2*: conventional radical initiator,* I*: fragment from* I_2*,* M*: monomer,* $R_i^\bullet$*: macroradical with chain length i,* P_i*: dead polymer species with chain length I;* $k_{dis,pI,p,tc}$*: rate coefficient for dissociation, chain initiation with I, propagation and termination by recombination; not displaying for simplicity termination by disproportionation and side reactions such as transfer to monomer.*

The formation of a polymer chain commences by the decomposition of an initiator molecule (I_2) into radical fragments (I) under the influence of heat or radiation, which subsequently add to monomer molecules (M) leading to the formation of macroradicals (R_i, i: chain length). These macrospecies grow until they react with another (macro-)radical during a termination event resulting in the disappearance of the active radical center and the formation of an inactive dead polymer chain.[9,10] Additionally, (chain) transfer reactions between a macroradical and small molecules, such as monomer or solvent, or another macrospecies can occur as well, relocating the active center. The formation of branched polymer chains can even result if intramolecular chain transfer takes place. In order to limit the "uncontrolled" growing process

and to deliberately end up with low(er) molar mass polymer product, chain transfer agents such as thiols can be added to the reaction mixture as well.[11]

The popularity of FRP for the industrial production of millions of tons of synthetic polymers per year can be ascribed to its broad operating window (-80 up to 250 °C), the resistance to impurities present in the feedstock and the compatibility with a wide range of monomers and solvent including water, making it possible to perform the polymerization under both homogeneous (bulk and solution) and heterogeneous (emulsion and suspension) conditions.[12]

Nevertheless, the relatively simple and robust FRP reaction mechanism possesses some inherent disadvantages as well. The short time scale (order of magnitude of (milli)seconds) of dead polymer formation and, depending on the production conditions, the ever-changing properties of the reaction mixture throughout the polymerization process, results in the lack of control over the macromolecular structure, typically leading to broad chain length distributions (CLDs) and thus a highly inhomogeneous polymer product on a molecular level.[13,14]

1.2 Principle of reversible deactivation radical polymerization

The search for a polymerization technique capable of controlling the chain growth mechanism at the molecular level initially led to the focus on anionic and cationic polymerization. Although these so-called living polymerizations were promising techniques as termination is completely absent under ideal conditions, resulting in the "concurrent" growth of all chains and subsequently a narrow CLD, these processes require very stringent working conditions as they are very intolerant to impurities and certain functional groups. As a result, the industrial implementation never really took off and the market dominance of FRP remained.[11,15–17]

The big breakthrough in terms of control over the chain growth, end-group functionality (EGF) and macromolecular structure in a possible industrial viable setting came with the discovery of so called RDRP techniques, also known as controlled radical polymerization (CRP). Despite

not being truly living as termination still occurs, although less decisive on the final polymer product properties compared to FRP, these techniques can make use of the perks of FRP while minimizing the lack of molecular control.[3,8,11,18,19]

The general principle of RDRP techniques relies on the temporary deactivation of the active growing macroradicals into so called dormant macrospecies via the addition of a controlling/mediating agent. The fraction of dormant macrospecies to the total amount of all types of macrospecies (dormant, growing and dead) is called the end-group functionality (EGF). In case most of the chains are initiated at the same time and the activation/deactivation procedure occurs fast enough, the chains that do not terminate will grow with an equal probability leading to very narrow CLDs if a high EGF is existent. As dormant macrospecies can be made active again, it becomes possible to produce block copolymers and other macromolecular architectures inaccessible by means of FRP.[3,10,11,13,20,21]

Several RDRP techniques have been developed in the recent history which can be categorized in two groups based on the manner of forming the dormant macrospecies, namely via a reversible termination or via a reversible transfer reaction as elucidated in Figure 1.2.[3,10,13,20]

Nitroxide mediated polymerization (NMP)[22–24] and atom transfer radical polymerization (ATRP)[11,25–28] are the two most well-known examples of RDRP operating via a reversible "termination" process (Figure 1.2a). Growing macroradicals are temporarily deactivated by a persistent radical/species in the form of a nitroxide radical (NMP) or a halogen coupled with a transition metal complex (ATRP). As the persistent species are incapable of coupling with each other and termination is never truly eliminated, an excess of this deactivation agent results after an initial reaction period shifting the equilibrium towards the dormant deactivated state.[29] Moreover, the reaction temperature can be used to control the equilibrium to the favorable dormant state as well. Consequently, at any moment in time, the concentration of growing macroradicals is low and the termination reaction is suppressed.[30]

$$R_iX \underset{k_{deact}}{\overset{k_{act}}{\rightleftharpoons}} R_i^{\bullet} + X^{\bullet} \qquad \text{(a)}$$

$$R_i^{\bullet} + R_jX \overset{k_{tr}}{\rightleftharpoons} R_iX + R_j^{\bullet} \qquad \text{(b)}$$

Figure 1.2*: Key reaction mechanism for RDRP based on reversible termination (a) and reversible transfer (b);* R_iX*: dormant macrospecies with chain length i,* $R_i^{\bullet}$*: macroradical with chain length i,* $X^{\bullet}$*: persistent radical;* $k_{act,deact,tr}$*: rate coefficient for activation, deactivation and transfer with the controlling agent.*

Contrary to NMP and ATRP, reversible addition fragmentation chain transfer (RAFT) polymerization[3,8,18,20,27,31–33] utilizes as reversible transfer mechanism (Figure 1.2b) to achieve control and will be discussed thoroughly in the next subsection, as it is the technique covered in this PhD thesis.

1.3 Principle of reversible addition fragmentation chain transfer (RAFT) polymerization

The key reaction mechanism for the RAFT polymerization process is shown in Figure 1.3. Deactivation of the growing macroradical occurs initially via the addition to a chain transfer agent (CTA, R_iX with i=0) possessing a thiocarbonylthio moiety, creating a RAFT intermediate carbon centered radical ($INT_{i,j}$).[8,34,35] This intermediate radical can either fragment back to the original species or it can fragment forming a new growing macroradical and a dormant macrospecies originating from the initial growing macroradical.[36] If side reactions such as cross-termination involving the RAFT intermediate can be ignored, and RAFT fragmentation occurs sufficiently fast, a so-called degenerative mechanism as shown in Figure 1.2b is obtained.[37–39]

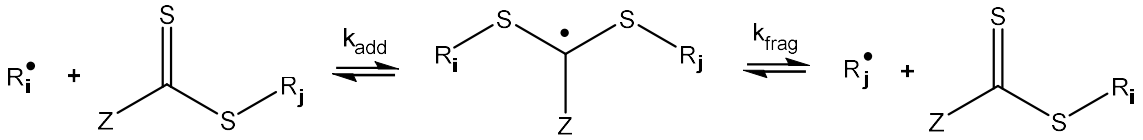

Figure 1.3: *Key reaction mechanism for the RAFT polymerization only main exchange for simplicity); $k_{add,frag}$: rate coefficient for addition of a macroradical ($R_i^{\bullet}$) to a dormant macrospecies (R_jX) forming the RAFT intermediate and fragmentation of the RAFT intermediate ($INT_{i,j}$) forming a new macroradical ($R_j^{\bullet}$) and dormant macrospecies (R_iX); i and j representations of the chain length; Z: stabilizing group of the RAFT chain transfer agent.*

The (ideal) RAFT exchange process has, in contrast to the controlling principle of NMP and ATRP, no influence on the total number of radicals present during the reaction at any moment in time. Consequently, assuming rate retardation due to cross-termination or slow fragmentation has no significant influence, the polymerization rates obtained during a RAFT polymerization are similar to comparable FRP processes.[40]

The controlling capabilities of the RAFT CTA can be accredited to the presence of a thiocarbonylthio moiety present in all RAFT mediating compounds, as shown by the general structure in Figure 1.4.[41] However, effective transfer of the active radical function between a growing macroradical and a dormant (macro)species relies on the delicate balance between stabilizing the intermediate RAFT radical in order for it to be formed but not too much as else the radical function would be trapped in this inactive state.[41,42] Consequently, the structure of the stabilizing Z group of the RAFT CTA plays a major role and the most commonly used types are shown in Figure 1.4. The tunability of this group makes it possible to achieve control over the RAFT polymerization of a wide range of monomer types. The general idea is that so-called less activated monomers (LAMs), such as ethylene and vinyl acetate, containing a saturated carbon or an oxygen/nitrogen electron pair adjacent to the vinyl group, resulting in more reactive radicals with respect to RAFT addition, rely on the use of RAFT agents reducing this

eagerness towards RAFT addition.[43] This can be achieved by the presence of a delocalizable electron pair neighboring the thiocarbonylthio group (*e.g.* xanthates and dithiocarbamates, Figure 1.4), making RAFT addition less favorable due to the resulting conjugated system in the RAFT CTA while simultaneously sufficiently destabilizing the intermediate radical in order to realize favorable RAFT fragmentation.[44] This latter is essential as more active RAFT agents (*e.g.* dithioesters and trithiocarbonates, Figure 1.4) would lead to the formation of intermediate radicals considerably more stable than the radicals formed by RAFT fragmentation, resulting in an undesired decrease of the polymerization rate.[45] In contrast, so-called more activated monomers (MAMs), such as (meth)acrylates and styrenics which possess vinyl groups conjugated by a carbonyl group or an aromatic ring, require the use of these more active RAFT agents in order to counterbalance their lower reactivity towards RAFT addition.[46–48]

Furthermore, although having limited effect on the stability of the RAFT intermediate, the appropriate choice of the RAFT leaving group (Figure 1.4) is crucial as well to achieve efficient transfer with the initial RAFT CTA as again a balance of the stability of the corresponding radical is needed.[49] On the one hand, the stability needs to be high enough to guarantee sufficient fragmentation towards this leaving group radical, otherwise the intermediate radical would fragment back to the original macroradical and RAFT CTA.[42,49,50] On the other hand, the RAFT leaving group radical also needs to be able to reinitiate the available monomer sufficiently fast to avoid retardation of the polymerization process. Leaving group structures mimicking the growing radicals or conventional initiator fragments have shown to be capable of meeting these requirements. A classic example is a cryanoisopropyl-leaving group having the same structure as the radical fragments of 2,2'-azobis(2-methyl-propionitrile) (AIBN), a common initiator in FRP.[51]

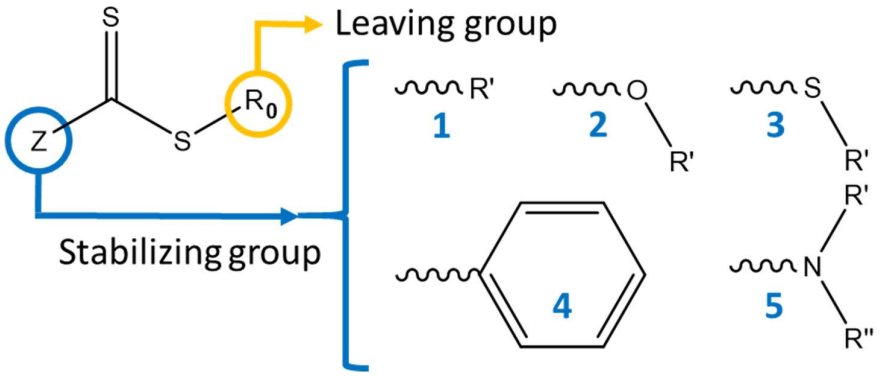

***Figure 1.4**: General structure of the thiocarbonlythio compounds used as chain transfer agent (R_0X) in RAFT polymerization. The stabilizing group (Z) can be chosen depending on the monomer type used. Typical RAFT agents are dithioesters (1), xanthates (2), trithiocarbonates (3), dithiobenzoates (4) and dithiocarbamates (5). The RAFT leaving group is chosen to achieve efficient fragmentation and reinitiation with monomer, a classic example is cyanoisopropyl.*

The reaction rates similar to conventional FRP in combination with the versatility in terms of monomer compatibility and the commercial availability in both small and larger quantities of a wide range of CTAs arguably give RAFT polymerization the highest potential of all RDRP techniques for industrial application.[8,52] Up-to-date, the new possibilities regarding well-defined narrow CLDs and polymeric architectures made achievable by the discovery of RAFT have led to the synthesis of novel materials finding use in a wide range of applications, including light-harvesting polymers[53–55], light-emitting nanoporous films,[56] optoelectronic applications,[45,57] self-assembling and stimuli responsive polymeric micelles for drug delivery applications,[58–61] and notably viscosity modifiers,[52] already commercially available present-day (Asteric™, Lubrizol).

1.4 Transition toward radical emulsion polymerization

The inherent compatibility of FRP/RAFT polymerization with a wide range of solvents allows it to be carried out operating several diverse techniques including the most commonly known and applied bulk, solution and emulsion polymerization. In its most simple configuration, the

initial reaction medium of a bulk polymerization process consists only of monomer and initiator, ultimately resulting in a highly pure polymer product. As all ingredients participate in the polymerization reactions, a high yield per reactor volume is obtained although coming at a cost of difficult temperature control due to the exothermic nature of FRP, even further intensified by the tendency toward a gel-effect and an increased viscosity even at relatively low monomer conversions (depending on monomer type and average polymer chain length). In solution polymerization, the heat transfer, and thus the process control, is greatly enhanced by introducing a solvent which dissolves the formed polymer. Careful selection of the appropriate solvent is crucial in order to avoid its participation in the reaction mechanism. Drawbacks of this technique include a lower yield per reactor volume, a reduction of the reaction rate and the difficult and costly removal of the solvents if the polymer solution is not directly usable.

Safety and environmental hazards are reduced by using a water-based process, as in conventional emulsion polymerization. This technique consists of a continuous water phase and an insoluble monomer/polymer particle phase resulting in a readily absorption and dissipation of the generated heat by the water, characterized by a high heat capacity.[62] Consequently, overheating and temperature runoff of the reactors due to the (highly) exothermic FRP process are less likely. Moreover, a similar or even higher throughput compared to bulk polymerization can be achieved as the reduction of the fraction of the reactor volume consisting of ingredients ending up in the final polymer product can be overcome by the higher rate of polymerization.[11] Furthermore, higher average molar chain lengths can be realized than with an equivalent bulk process as well, which increases the possible range of achievable chain lengths.[62] Finally, emulsion polymerizations easily reach relatively high monomer conversions, hence monomer consumption is maximized whereas problems with residual monomer are minimized. However, when the latex cannot be used as such and the polymer product needs to be separated, e.g. by coagulation and dewatering, production expenses increase, especially when the surfactant needs

be removed as well. As the removal of the latter is not only expensive but usually also very difficult, these are typically present in the final product and may be responsible for undesirable side-effects such as an unwanted color or the change of the gloss of a coating due to surfactant migration to the surface during film formation.[63] In addition, due to the heterogeneous nature, the polymerization process is extremely complex and difficult to fully understand as aspects of the mechanisms for particle formation, phase-transfer events and polymerization kinetics and their interplay need to be considered. In this PhD thesis, it is shown that the switch from FRP to RAFT polymerization further complicates the emulsion polymerization process. For completeness, it should be mentioned that emulsion polymerizations can also occur (a) with an organic continuous phase in combination with hydrophilic monomers (inverse emulsion polymerization) or (b) in the absence of surfactants (e.g. via self-assembly of amphiphilic block copolymers). However, these emulsion polymerization techniques are outside the scope of this work.

1.4.1 Principle of radical emulsion polymerization

The most commonly applied emulsion polymerization technique is so-called (radical) macroemulsion polymerization.[64,65] A macroemulsion can be formed by mixing water, (water-insoluble) monomer and surfactant above its critical micelle concentration (CMC) creating, upon stirring, an aqueous phase consisting of a small amount of monomer, large (1 - 100 μm) monomer droplets and small (5-10 nm) monomer-swollen micelles.[62] If a (water-soluble) initiator is added as well, polymerization can occur in these macroemulsions. The initiator typically decomposes in the aqueous phase forming radicals capable of reacting with the small amount of monomer units available producing oligomeric radicals. Subsequent propagation of these aqueous oligomers allows them to attain a critical chain length (i_{crit} = 2 for styrene) too hydrophobic to remain only in the aqueous phase and entry in a micelle can occur (heterogeneous nucleation) transforming it into a polymer particle.[66] Entry will predominantly

occur in micelles, despite their small size, as they are present in much larger numbers (10^{19} – 10^{21} L^{-1}) as opposed to the larger monomer droplets (10^{12} – 10^{14} L^{-1}). If heterogeneous nucleation does not occur rapidly, for example due to due to a low initial amount of micelles available, the oligomeric radicals can be allowed to grow up to a second critical chain length (j_{crit} = 5 for styrene) making the radicals insoluble in the aqueous phase[67–69] As a results, these will precipitate and attract surfactant and monomer and thereupon form particles as well (homogeneous nucleation). Nonetheless, if the surfactant concentration is well above the critical micelle concentration, mainly heterogeneous nucleation will occur (>99% for styrene).[62]

A (macro)emulsion polymerization process can typically be divided in three intervals.[70–74] During the first interval, micelles, monomer droplets and polymer particles coexist and both the number of particles and polymerization rate increases over time due to the nucleation process.[75] Once all of the micelles have disappeared (typically after 5-10% monomer conversion), either by transformation to particles or by making their surfactant molecules available for other growing particles, the total number of particles is fixed (at least in the absence of particle instabilities) and the second interval commences.[20] During this interval, monomer disappearing in the particles due to polymerization is replenished by monomer diffusing from the droplets through the aqueous phase to the particles, resulting in an approximate constant monomer concentration in the particles. As a result, neglecting chain length and viscosity effects, the polymerization rate remains constant until the monomer droplets have been completely depleted and disappeared (typically after 10-40% monomer conversion).[72] At this stage, only monomer swollen particles are present and in this third interval, the monomer concentration in the particles and hence the polymerization rate decreases (again neglecting a potential gel effect due to the increasing viscosity).[76]

In miniemulsion polymerization, the "simplified" main emulsion polymerization technique in this PhD thesis, a high shear device (*e.g.* sonicator or homogenizer) is used to form monomer droplets (100-500 nm) in the absence of micelles by employing a surfactant concentration below the critical micelle concentration, in contrast to macroemulsion polymerization as shown in Figure 1.5.[77–83] In the ideal case, each monomer droplet initially present in the mixture will be transformed into a polymer particle. Consequently, miniemulsion polymerization can avoid possible issues related to transport of hydrophobic reagents (*e.g.* RAFT agent) from monomer droplets to particles inherent to macroemulsion polymerization.[18,77,84]

Both in macro- and miniemulsion, the dispersed system is in a higher energy state compared to the related two layer organic-aqueous phase.[83,85,86] This means that in case the external force is removed, the dispersed medium could disappear in a period of seconds to days. A microemulsion however, realized by making use of a much larger amount of surfactant compared to a macroemulsion and a cosurfactant (*e.g.* pentanol), is a thermodynamically stable transparent or translucent emulsion which can form spontaneous without external shear force.[9,22,27,83,87–89] Before polymerization, a microemulsion consists of both micelles and small monomer droplets (10-100 nm) resulting in the possible nucleation of both as shown in Figure 1.5.

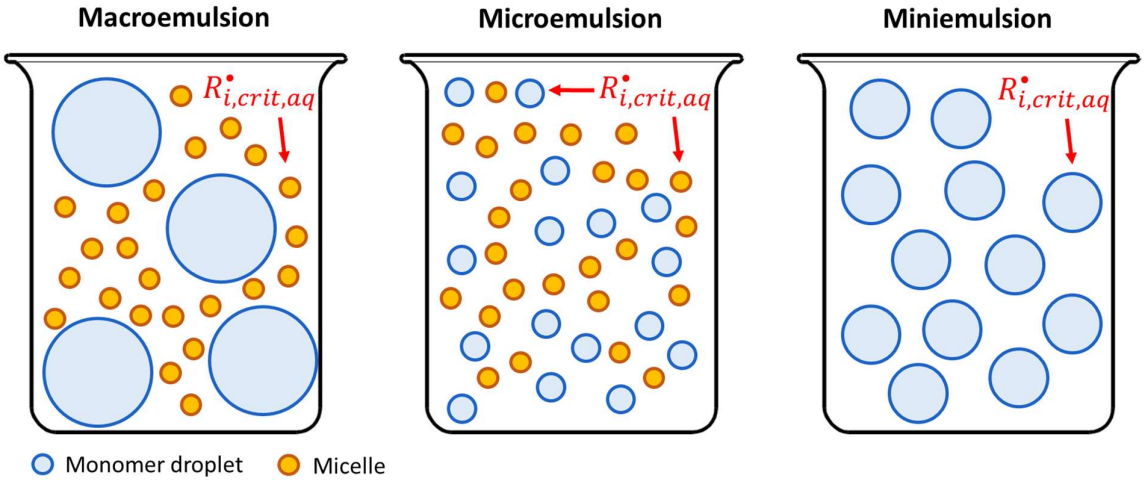

***Figure 1.5**: Representation of the initial (absence of polymer particles) dispersed medium in macro- (left; covered in Chapter 6), micro- (middle) and miniemulsion (right; mainly covered in this PhD thesis; Chapter 4 and 5) polymerization with a differentiation between monomer droplets (blue) and micelles (yellow); with $\boldsymbol{R^{\bullet}_{i,crit,aq}}$ an aqueous oligomeric radical capable of entry into a droplet (miniemulsion), micelle (macroemulsion) or both (microemulsion).*

1.4.2 Compartmentalization effects in emulsion polymerization

During bulk polymerization, all reactants are in the same space and in principle any two species can meet. For example as shown in Figure 1.6, termination can occur between any two radicals present. On the other hand, during emulsion polymerization reactants are physically confined within discrete confined spaces. This phenomenon is better known as compartmentalization and has two main consequences (Figure 1.6) providing that some fraction of particles contain a significantly low number or even none of the relevant reactants. [27,87,90–93]

Firstly, the physical confinement of reactants results in a *segregation effect* (Figure 1.6) stating that only species located in the same particle are able to react.[18,92] Consequently, even though the total number of radicals at a certain moment of time can be the same for a bulk and miniemulsion polymerization, the overall termination rate will be much lower in the latter as two radicals need to be in the same particle before termination can actually occur. This enables the increase of both the polymerization rate and the polymer average chain length by increasing the number of particles present as it becomes less likely that two radicals meet. This cannot be achieved in bulk polymerization as an increase of either the rate or the average chain length will always result in a reduction of the other property. [94,95]

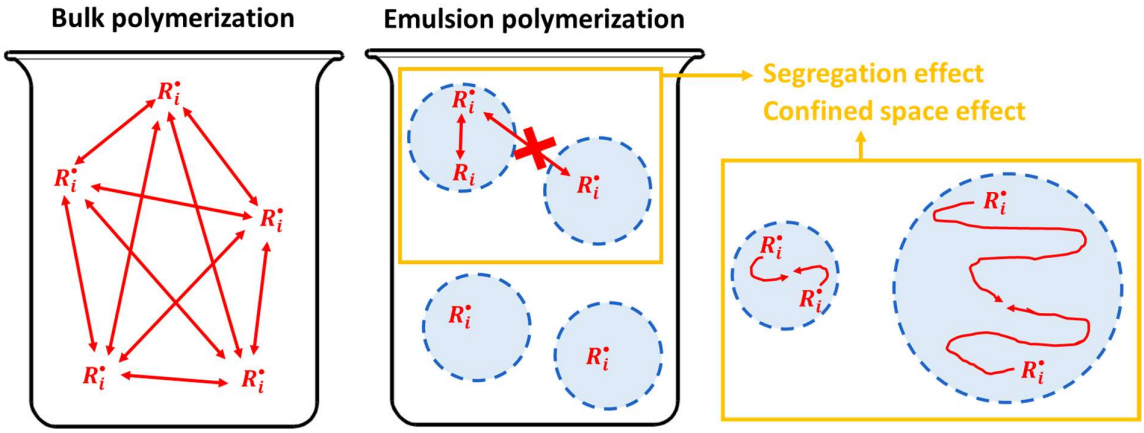

***Figure 1.6**: Schematic illustration of the difference in reaction possibilities between bulk and emulsion polymerization including a representation of the segregation and confined space effect.*

The second type of compartmentalization effect is the so-called *confined space effect* (Figure 1.6) according to which two species that are located in the same particle react at a higher rate in a small particle than in a large particle.[18,27] If the size of the particles is small enough (nanometer scale), the number of particles can exceed the number of a certain species, *e.g.* (macro)radicals, which results in a local increase of the concentration of that species in the containing particles as there exist particles that only act as monomer reservoirs.[96] Decreasing the (average) particle size will increase the number of particles at a given solid content and will result in an increase of the non-participating volume and hence of the concentration of the compartmentalized species as well.

An important prerequisite for compartmentalization to have an effect on a certain reaction is that each species involved is only present in very low amounts. If the concentration of one of the species is too high (*e.g.* monomer) the reaction (*e.g.* propagation) is almost not influenced by the segregation and confined space effect, at least to a first approximation.[27] More recent research has although shown that also the monomer concentrations can become particle size dependent.[97] This aspect is however out of the scope of the present PhD thesis.

1.5 Challenges of RAFT emulsion polymerization

Early studies focusing on the implementation of RAFT in macroemulsion polymerization did not result in the same success as observed in solution and bulk polymerization. Most experiments led to poor colloidal stability, slow polymerization rates or a loss of the control over the molar mass and dispersity.[63,98–103]

In homogeneous polymerization processes, control is typically obtained by employing high active ($C_{tr} = \frac{k_{tr}}{k_p} \gg 10$) RAFT agents.[37] Yet, during the early stages of (macro)emulsion polymerization, these RAFT agents result in the presence of particles containing large concentrations of oligomeric species.[104] The monomer in these particles have a lower chemical potential than in non-nucleated droplets resulting in a superswelling effect where monomer transfers from the droplets to the particles until an equilibrium is reached.[105] Due to this effect, particles can swell up to 100 times their unswollen volume and thereby inflict particle coagulation or even phase separation.[83,99,102,106–109] Employing low active RAFT agents, such as xanthates ($C_{tr} \ll 10$), circumvents the issues related to superswelling as polymeric instead of oligomeric species are formed from the onset of the polymerization.[110–112] However, this approach comes at the expense of the control over the chain growth, as this demands more active RAFT agents.[113] Alternatively, in an ideal miniemulsion polymerization, each droplet initially present in the reaction mixture will be transformed into a polymer particle.[77,83] Consequently, monomer transfer is not required and superswelling can be avoided by making use of a polymeric RAFT agent or by adding a sufficiently large amount of a hydrofobe (cosurfactant, *e.g.* hexadecane).[104,114,115]

Another challenge upon considering RAFT macroemulsion polymerization is the necessity of fast RAFT agent transfer from the droplets to the particles, the main locus of polymerization.[116,117] Most RAFT agents are quite water-insoluble, making the transfer process

very slow or almost nonexistent, resulting in poor molar mass control. Alternatively, water-soluble RAFT agents result in a significant amount of inhibition as it will take time for z-meric species capable of entering a particle to form. The addition of an organic solvent (*e.g.* acetone or cyclodextrins) can facilitate the transport of the RAFT agent in the aqueous phase.[118–120] Moreover, miniemulsion polymerization can once more be a suitable solution as it does not rely on transfer of the species.[121]

In free radical emulsion polymerization, exit of radicals from the particles to the aqueous phase is very limited as the entered oligomeric radicals quickly grow into macrospecies incapable of leaving. One exception is the exit of monomeric radicals if chain transfer to monomer is significant (*e.g. n*-butyl acrylate) and the water solubility of the monomer is sufficiently high.[75,122,123] In the case of RAFT emulsion polymerization, the small RAFT leaving group radical formed by the exchange reaction with the initial RAFT agent can be capable of exiting the particles.[123,124] It has been shown that this phenomenon can result in a significant polymerization rate decrease, at if the system is not operating under pseudo-bulk kinetics, as the exited radicals can terminate in the aqueous phase or after re-entry into a particle containing a growing radical.[80,99,108,125,126] Depending on the reactivity of the RAFT agent, this retardation can occur only the first few percent ($C_{tr} \ll 10$) of monomer conversion or throughout the entire polymerization process ($C_{tr} \ll 10$).[103]

Currently, xanthates are considered to be the only class of RAFT agents that can straightforwardly be employed successfully in conventional macroemulsion polymerization.[107,111,112,123,127–130] As they contain an oxygen atom in α-position to the tiocarbonlythio functional group, their RAFT transfer capability is strongly reduced resulting in the absence of superswelling issues as mentioned above.[8,103,113,131] Even though this also results in poor molar mass control, their surface activity allows the synthesis of covalently linked core-shell nanoparticles.[128] Moreover, their surface activity facilitates the transport of

the RAFT agent from droplet to particle whereas on the other hand rate retardation due to radical exit can be expected to increase as the RAFT leaving group radicals will be formed in the vicinity of the particle/aqueous phase boundary.[103] Hence, in a general RAFT emulsion polymerization research it is recommended to include also this special class of RAFT agents.

1.6 Outline of PhD thesis

The research presented in this PhD thesis focusses on the understanding and optimization of the RAFT polymerization kinetics in homogeneous and emulsion media. Modelling techniques are used to gain fundamental insights on the underlying micro- and mesoscale phenomena, with the former relating to local concentration changes and the latter to interphase mass transfer events. Whenever possible, modelled predictions are experimentally validated, either by comparison with in-house dedicated experiments or by reliable literature data. Throughout the PhD thesis, a transition from homogeneous bulk polymerization to heterogeneous emulsion polymerization techniques is targeted, as the latter possesses significant advantages in terms of environmental friendliness and process safety, as explained above.

Chapter 2 is a theoretical **introductory chapter** used to provide an overview of the possible modelling approaches for radical polymerization in general and a state-of-the art on the tools for RAFT polymerization in both bulk and emulsion polymerization. Moreover, the pioneering so-called Smith-Ewart equations are discussed for a FRP miniemulsion scheme in order to elaborate on its more general applicability in terms of complexity and completeness of modelling output compared to the simplified zero-one modelling technique which only considers zero or one radical per particle.

In Chapter 3, multi-responsive regression analysis via the extended method of moments and experimental data is used to determine the degenerative transfer coefficients of the bulk RAFT polymerization of styrene with (O-ethyl xanthate)-2-ethyl propionate, a xanthate type of

controlling agent. Moreover, kinetic Monte Carlo modelling is used to visualize the homopolymerization and chain extension with fresh styrene and *n*-butyl acrylate.

In **Chapter 4**, focus is shifted to degenerative **RAFT miniemulsion polymerization of methyl methacrylate with cyanoprop-2-yl dithiobenzoate** as initial RAFT agent. A two-dimensional Smith-Ewart model is developed accounting for the number of macro- and leaving group radicals per particle. Bulk literature data is used to determine the accuracy of micro-scale model parameters whereas available miniemulsion data is used to investigate interphase meso-scale parameters. Furthermore, the impact of diffusional limitations on the average number of (macro)radicals per particles and the (in)validity of the zero-one simplification is highlighted.

The two-dimensional Smith-Ewart model developed in Chapter 4 is expanded to a five-dimensional model, considering intermediate radical species as well, in **Chapter 5** to theoretically understand the differences between a **non-degenerative and degenerative RAFT miniemulsion polymerization of styrene**. An approach for the identification of the nature of RAFT retardation is suggested based on the influence of the average particle size on experimentally determinable polymer properties.

Chapter 6 comprises of an experimental study of **RAFT macroemulsion polymerization of styrene with (O-ethyl xanthate)-2-ethyl propionate**, the same controlling agent as used in Chapter 2. The influence of several crucial process parameters on the polymer properties is investigated. These results can be considered to be a stepping stone for future extension of the model developed and discussed in Chapter 4 and 5 in order to include macroemulsion polymerization, which is more industrially relevant compared to miniemulsion polymerization. Moreover, the use of a xanthate type of RAFT agent in combination with semi-batch RAFT copolymerization is investigated for the synthesis of more complex polymeric nanoparticle architectures, namely covalently linked core-shell nanoparticles.

Finally, **Chapter 7** summarizes the main **conclusions** of this PhD thesis and **prospects** for potential future work are discussed as well.

1.7 References:

1 G. S. Whitby, *Synthetic Rubber*, Wiley, New York, 1954.

2 A. Houben, J. Van Hoorick, J. Van Erps, H. Thienpont, S. Van Vlierberghe and P. Dubruel, *Ann. Biomed. Eng.*, 2017, **45**, 58–83.

3 M. Destarac, *Macromol. React. Eng.*, 2010, **4**, 165–179.

4 H. Wang and G. L. Rempel, *Adv. Biomed. Eng. Res.*, 2013, **1**, 62–68.

5 Z. Jun, H. Hou, J. H. Wendorff and A. Greiner, *e-polymers*, 2005, **38**, 1–7.

6 V. Mittal, Miniemulsion Polymerization Technology, Wiley, Salem, 2010.

7 S. Ren, L. Hinojosa-Castellanos, L. Zhang and M. A. Dubé, *Macromol. React. Eng.*, 2017, **11**, 1–6.

8 C. Barner-Kowollik, *Handbook of RAFT Polymerization*, Wiley-VCH, Weinheim, 2008.

9 T. P. Matyjaszewski, K.; Davies, *Handbook of Radical Polymerisation*, John Wiley & Sons, Hoboken, 2002.

10 G. Odian, *Principles of Polymerization*, John Wiley & Sons, New York, 2004.

11 J. M. Asua, *Polymer Reaction Engineering*, Blackwel Publishing Ltd, Oxford, 2007.

12 P. Nesvadba, Encyclopedia of Radicals in Chemistry, Biology and Materials, John Wiley & Sons, New York, 2012.

13 J. Qiu, B. Charleux and K. Matyjaszewski, *Prog. Polym. Sci.*, 2001, **26**, 2083–2134.

14 I. W. Hamley, *Developments in block copolymer science and technology*, John Wiley & Sons, Chichester, 2004.

15 D. J. Lunn, E. H. Discekici, J. Read de Alaniz, W. R. Gutekunst and C. J. Hawker, *J. Polym. Sci. Part A Polym. Chem.*, 2017, **55**, 2903–2914.

16 A. Kumar and R. K. Gupta, *Fundamentals of Polymer Engineering*, Marcel Dekker Inc., New York, 2003.

17 M. Hillmyer, *Curr. Opin. Solid State Mater. Sci.*, 1999, **4**, 559–564.

18 P. B. Zetterlund, S. C. Thickett, S. Perrier, E. Bourgeat-Lami and M. Lansalot, *Chem. Rev.*, 2015, **115**, 9745–9800.

19 S. K. Fierens, S. Telitel, P. H. M. Van Steenberge, M.-F. Reyniers, G. B. Marin, J.-F. Lutz and D. R. D'hooge, *Macromolecules*, 2016, **49**, 9336–9344.

20 G. Moad and D. H. Solomon, *The chemistry of radical polymerization*, Elsevier, Oxford, 2006.

21 G. T. Russell, *Aust. J. Chem.*, 2002, **55**, 399–414.

22 J. Nicolas, Y. Guillaneuf, C. Lefay, D. Bertin, D. Gigmes and B. Charleux, *Prog. Polym. Sci.*, 2013, **38**, 63–235.

23 E. Rizzardo and D. H. Solomon, *Aust. J. Chem.*, 2012, **65**, 945–969.

24 S. Fierens, D. D'hooge, P. Van Steenberge, M.-F. Reyniers and G. Marin, *Polymers (Basel).*, 2015, **7**, 655–679.

25 D. R. D'hooge, M.-F. Reyniers, F. J. Stadler, B. Dervaux, C. Bailly, F. E. Du Prez and G. B. Marin, *Macromolecules*, 2010, **43**, 8766–8781.

26 D. R. D'hooge, M.-F. Reyniers and G. B. Marin, *Macromol. React. Eng.*, 2009, **3**, 185–209.

27 P. B. Zetterlund, *Polym. Chem.*, 2011, **2**, 534–549.

28 B.-G. Li and W.-J. Wang, *Macromol. React. Eng.*, 2015, **9**, 385–395.

29 D. Greszta and K. Matyjaszewski, *Macromolecules*, 1996, **29**, 7661–7670.

30 J. W. Ma, J. A. Smith, K. B. McAuley, M. F. Cunningham, B. Keoshkerian and M. K. Georges, *Chem. Eng. Sci.*, 2003, **58**, 1163–1176.

31 J. B. McLeary and B. Klumperman, *Soft Matter*, 2006, **2**, 45–53.

32 B. Klumperman, E. T. a Van Den Dungen, J. P. a Heuts and M. J. Monteiro, *Macromol. Rapid Commun.*, 2010, **31**, 1846–1862.

33 T. Junkers, *J. Polym. Sci. Part A Polym. Chem.*, 2011, **49**, 4154–4163.

34 S. Perrier and P. Takolpuckdee, *J. Polym. Sci. Part A Polym. Chem.*, 2005, **43**, 5347–5393.

35 M. R. Hill, R. N. Carmean and B. S. Sumerlin, *Macromolecules*, 2015, **48**, 5459–5469.

36 J. Chiefari, Y. K. B. Chong, F. Ercole, J. Krstina, J. Jeffery, T. P. T. Le, R. T. A. Mayadunne, G. F. Meijs, C. L. Moad, G. Moad, E. Rizzardo, S. H. Thang and C. South, 1998, **31**, 5559–5562.

37 P. Derboven, P. H. M. Van Steenberge, M. Reyniers, C. Barner-kowollik, R. D. Dagmar, G. B. Marin, D. R. D'hooge, G. B. Marin, R. D. Dagmar and G. B. Marin, *Macromol. Theory Simulations*, 2016, **25**, 104–115.

38 G. Gody, T. Maschmeyer, P. B. Zetterlund and S. Perrier, *Macromolecules*, 2014, **47**, 639–649.

39 H. Tobita and F. Yanase, *Macromol. Theory Simulations*, 2007, **16**, 476–488.

40 A. R. Wang and S. Zhu, *Macromol. Theory Simulations*, 2003, **12**, 196–208.

41 J. Chiefari, R. T. A. Mayadunne, C. L. Moad, G. Moad, E. Rizzardo, A. Postma, M. A. Skidmore and S. H. Thang, *Macromolecules*, 2003, **36**, 2273–2283.

42 B. Y. K. Chong, J. Krstina, T. P. T. Le, G. Moad, A. Postma, E. Rizzardo and S. H. Thang, *Macromolecules*, 2003, **36**, 2256–2272.

43 M. Destarac, W. Bzducha, D. Taton, I. Gauthier-Gillaizeau and S. Z. Zard, *Macromol. Rapid Commun.*, 2002, **23**, 1049–1054.

44 D. Hua, J. Xiao, R. Bai, W. Lu and C. Pan, *Macromol. Chem. Phys.*, 2004, **205**, 1793–1799.

45 G. Moad, M. Chen, M. Häussler, A. Postma, E. Rizzardo and S. H. Thang, *Polym. Chem.*, 2011, **2**, 492–519.

46 D. J. Keddie, *Chem. Soc. Rev.*, 2014, **43**, 496–505.

47 S. Houshyar, D. J. Keddie, G. Moad, R. J. Mulder, S. Saubern and J. Tsanaktsidis, *Polym. Chem.*, 2012, **3**, 1879.

48 D. J. Keddie, G. Moad, E. Rizzardo and S. H. Thang, *Macromolecules*, 2012, **45**, 5321–5342.

49 A. Feldermann, M. H. Stenzel, T. P. Davis, P. Vana and C. Barner-Kowollik, *Macromolecules*, 2004, **37**, 2404–2410.

50 I. S. Altarawneh, V. G. Gomes and M. H. Srour, *J. Appl. Polym. Sci.*, 2009, **114**, 2356–2372.

51 L. Yang, Y. Luo, X. Liu and B. Li, *Polymer (Guildf).*, 2009, **50**, 4334–4342.

52 S. Perrier, *Macromolecules*, 2017, **50**, 7433–7447.

53 M. Chen, K. P. Ghiggino, A. Launikonis, A. W. H. Mau, E. Rizzardo, W. H. F. Sasse, S. H. Thang and G. J. Wilson, *J. Mater. Chem.*, 2003, **13**, 2696–2700.

54 W. Zhao, Z. Hou, Z. Yao, X. Zhuang, F. Zhang and X. Feng, *Polym. Chem.*, 2015, **6**, 7171–7178.

55 M. Chen, K. P. Ghiggino, A. W. H. Mau, E. Rizzardo, W. H. F. Sasse, S. H. Thang and G. J. Wilson, *Macromolecules*, 2004, **37**, 5479–5481.

56 C. Barner-Kowollik, T. P. Davis, J. P. A. Heuts, M. H. Stenzel, P. Vana and M. Whittaker, *J. Polym. Sci. Part A Polym. Chem.*, 2003, **41**, 365–375.

57 G. Moad, E. Rizzardo and S. H. Thang, *Chem. - An Asian J.*, 2013, **8**, 1634–1644.

58 A. E. Smith, X. Xu, S. E. Kirkland-York, D. A. Savin and C. L. McCormick, *Macromolecules*, 2010, **43**, 1210–1217.

59 Y. Q. Hu, M. S. Kim, B. S. Kim and D. S. Lee, *Polymer (Guildf).*, 2007, **48**, 3437–3443.

60 H. Willcock and R. K. O'Reilly, *Polym. Chem.*, 2010, **1**, 149.

61 P. Derboven, D. R. D'hooge, M.-F. Reyniers, G. B. Marin and C. Barner-Kowollik, *Macromolecules*, 2015, **48**, 492–501.

62 R. G. Gilbert, *Emulsion polymerization: a mechanistic approach*, Academic Press Inc., London, 1995.

63 M. J. Monteiro, M. Sjöberg, J. Van Der Vlist and C. M. Göttgens, *J. Polym. Sci. Part A Polym. Chem.*, 2000, **38**, 4206–4217.

64 J. M. Asua, *J. Polym. Sci. Part A Polym. Chem.*, 2004, **42**, 1025–1041.

65 M. F. Cunningham, *Prog. Polym. Sci.*, 2008, **33**, 365–398.

66 Y. Dong and D. C. Sundberg, *Macromolecules*, 2002, **35**, 8185–8190.

67 R. Rodríguez, M. J. Barandiaran and J. M. Asua, *Macromolecules*, 2007, **40**, 5735–5742.

68 B. Alhamad, J. A. Romagnoli and V. G. Gomes, *Chem. Eng. Sci.*, 2005, **60**, 2795–2813.

69 N. Sheibat-Othman, H. M. Vale, J. M. Pohn and T. F. L. McKenna, *Macromol. React. Eng.*, 2017, **11**, 201600059.

70 Y. Shang, G. Shan and P. Pan, *Macromol. Chem. Phys.*, 2015, **216**, 884–893.

71 S. Sajjadi and B. W. Brooks, *J. Appl. Polym. Sci.*, 2001, **79**, 582–597.

72 H. B. Yamak, in *Emulsion Polymerization*, Intech, 2013, pp. 35–72.

73 J. Jennings, G. He, S. M. Howdle and P. B. Zetterlund, *Chem. Soc. Rev.*, 2016, **45**, 5055–5084.

74 J. Ugelstad and F. K. Hansen, *Rubber Chem. Technol.*, 1976, 49, 536–609.

75 S. C. Thickett and R. G. Gilbert, *Polymer (Guildf).*, 2007, **48**, 6965–6991.

76 F. J. Schork and F. Lu, *Macromol. React. Eng.*, 2009, **3**, 539–542.

77 A. Butte, G. Storti and M. Morbidelli, *Macromolecules*, 2001, **34**, 5885–5896.

78 T. G. T. Jansen, P. a. Lovell, J. Meuldijk and a. M. Van Herk, *Macromol. Symp.*, 2013, **333**, 24–34.

79 F. J. Schork, G. W. Poehlein, S. Wang, J. Reimers, J. Rodrigues and C. Samer, *Colloids surfaces Physiochemical Eng. Asp.*, 1999, **153**, 39–45.

80 F. Joseph Schork and J. Guo, *Macromol. React. Eng.*, 2008, **2**, 287–303.

81 H. Tobita, *Macromol. Theory Simulations*, 2009, **18**, 108–119.

82 H. Tobita, *Macromol. Theory Simulations*, 2009, **18**, 120–126.

83 F. J. Schork, Y. Luo, W. Smulders, J. P. Russum, A. Butté and K. Fontenot, *Adv. Polym. Sci.*, 2005, **175**, 129–255.

84 G. Moad, E. Rizzardo and S. H. Thang, *Aust. J. Chem.*, 2012, **65**, 985–1076.

85 M. Oliveira, S. Lewin Behrends, I. Reis Rosa and C. Liberato Petzhold, *J. Polym. Sci. Part A Polym. Chem.*, 2017, **55**, 1–9.

86 F. Ishizuka, R. H. Utama, S. Kim, M. H. Stenzel and P. B. Zetterlund, *Eur. Polym. J.*, 2015, **73**, 324–334.

87 P. B. Zetterlund, Y. Kagawa and M. Okubo, *Chem. Rev.*, 2008, **108**, 3747–94.

88 S. Liu, K. D. Hermanson and E. W. Kaler, *Macromolecules*, 2006, **39**, 4345–4350.

89 D. J. McClements, *Soft Matter*, 2012, **8**, 1719.

90 P. B. Zetterlund and M. Okubo, *Macromolecules*, 2006, **39**, 8959–8967.

91 R. W. Simms and M. F. Cunningham, *Macromolecules*, 2008, **41**, 5148–5155.

92 P. B. Zetterlund and M. Okubo, *Macromol. Theory Simulations*, 2009, **18**, 277–286.

93 P. B. Zetterlund and M. Okubo, *Macromol. Theory Simulations*, 2007, **16**, 221–226.

94 I. González, M. Paulis, J. C. de la Cal and J. M. Asua, *Macromol. React. Eng.*, 2007, **1**, 635–642.

95 C. S. Chern, *Prog. Polym. Sci.*, 2006, **31**, 443–486.

96 Y. Kitayama, S. Tomoeda and M. Okubo, *Macromolecules*, 2012, **45**, 7884–7889.

97 Y. W. Marien, P. H. M. Van Steenberge, D. R. D'hooge and G. B. Marin, *Macromolecules*, 2019, provisionally accepted.

98 G. Moad, J. Chiefari, Y. K. Chong, J. Krstina, R. T. a Mayadunne, A. Postma, E. Rizzardo and S. H. Thang, *Polym. Int.*, 2000, **49**, 993–1001.

99 M. J. Monteiro and J. De Barbeyrac, *Macromolecules*, 2001, **34**, 4416–4423.

100 I. Uzulina, S. Kanagasabapathy and J. Claverie, *Macromol. Symp.*, 2000, **150**, 33–38.

101 D. Charmot, P. Corpart, H. Adam, S. Z. Zard, T. Biadatti and G. Bouhadir, *Macromol. Symp.*, 2000, **150**, 23–32.

102 M. J. Monteiro, M. Hodgson and H. De Brouwer, *J. Polym. Sci. Part A Polym. Chem.*, 2000, **38**, 3864–3874.

103 S. W. Prescott, University of Sydney, 2003.

104 Y. Luo, J. Tsavalas and F. J. Schork, *Macromolecules*, 2001, **34**, 5501–5507.

105 M. J. Monteiro, *Macromolecules*, 2010, **43**, 1159–1168.

106 C. N. Urbani, H. N. Nguyen and M. J. Monteiro, *Aust. J. Chem.*, 2006, **59**, 728–732.

107 M. J. Monteiro, M. M. Adamy, B. J. Leeuwen, A. M. van Herk and M. Destarac, *Polym. Prepr.*, 2005, **46**, 353–354.

108 J. G. Tsavalas, F. J. Schork, H. De Brouwer and M. J. Monteiro, *Macromolecules*, 2001, **34**, 3938–3946.

109 J. J. Vosloo, M. P. Tonge and R. D. Sanderson, *Macromolecules*, 2002, **35**, 4894–4902.

110 I. S. Altarawneh, V. G. Gomes and M. H. Srour, *Macromol. React. Eng.*, 2012, **6**, 8–16.

111 M. P. F. Pepels, C. I. Holdsworth, S. Pascual and M. J. Monteiro, *Macromolecules*, 2010, **43**, 7565–7576.

112 I. S. Altarawneh, V. G. Gomes and M. S. Srour, *Macromol. React. Eng.*, 2008, **2**, 58–79.

113 W. Smulders, R. G. Gilbert and M. J. Monteiro, *Macromolecules*, 2003, **36**, 4309–4318.

114 M. P. Tonge, J. B. Mcleary, J. J. Vosloo and R. D. Sanderson, *Macromol. Symp.*, 2003, **193**, 289–304.

115 L. Yang, Y. Luo and B. Li, *Polymer (Guildf).*, 2006, **47**, 751–762.

116 J. B. McLeary, M. P. Tonge, D. De Wet-Roos, R. D. Sanderson, B. Klumperman and D. de Wet Roos, *J. Polym. Sci. Part A Polym. Chem.*, 2004, **42**, 960–974.

117 Z. Jia and M. J. Monteiro, *ACS Symp. Ser.*, 2012, **1100**, 293–304.

118 A. Butté, A. D. Peklak, G. Storti and M. Morbidelli, *Radic. Polym. Kinet. Mech.*, 2007, **246**, 168–181.

119 B. Apostolovic, F. Quattrini, A. Butté and G. Storti, *Helv. Chim. Acta*, 2006, **89**, 1641–1659.

120 S. W. Prescott, M. J. Ballard, E. Rizzardo and R. G. Gilbert, *Macromolecules*, 2002, **35**, 5417–5425.

121 F. Zhang, P. Ni, Q. Xiong and Z. Yu, *J. Polym. Sci. Part A Polym. Chem.*, 2005, **43**, 2931–2940.

122 C. Tjiam and V. G. Gomes, *Ind. Eng. Chem. Res.*, 2014, **53**, 7526–7537.

123 S. W. Presscott, M. J. Ballard, E. Rizzardo and R. G. Gilbert, *Macromol. Theory Simulations*, 2006, **15**, 70–86.

124 M. Lansalot, T. P. Davis and J. P. A. Heuts, *Macromolecules*, 2002, **35**, 7582–7591.

125 Y. Luo, B. Liu, Z. Wang, J. Gao and B. Li, *J. Polym. Sci. Part A-Polymer Chem.*, 2007, **45**, 2304–2315.

126 J. Huang, S. Zhao, X. Gao, Y. Luo and B. Li, *Ind. Eng. Chem. Res.*, 2014, **53**, 7688–7695.

127 M. M. Adamy, A. M. van Herk, M. Destarac and M. J. Monteiro, *Macromolecules*, 2003, **36**, 2293–2301.

128 W. Smulders and M. J. Monteiro, *Macromolecules*, 2004, **37**, 4474–4483.

129 M. J. Monteiro and J. De Barbeyrac, *Macromol. Rapid Commun.*, 2002, **23**, 370–374.

130 S. Pascual, C. N. Urbani and M. J. Monteiro, *Macromol. React. Eng.*, 2010, **4**, 257–263.

131 B. Charleux, M. J. Monteiro and H. Heuts, in *Chemistry and Technology of Emulsion Polymerisation*, John Wiley & Sons, New York, 2013, pp. 105–143.

Chapter 2: The state-of-the art on modeling tools for RAFT polymerization kinetics under bulk/solution and emulsion conditions

2.1 Introduction

In recent years, modeling of polymerization kinetics using computer simulation methods is gaining prodigious interest among academic researchers and industry.[1,2] This approach has three main advantages. Firstly, simulation of the polymerization processes can be an appropriate substitute for complicated and time-consuming experiments.[3] Secondly, it can allow the gathering of process and polymer properties inaccessible via experimental methods (e.g. concentrations of short-lived radical species).[4–6] Thirdly, the vast amount of obtainable kinetic data can be used to elucidate obscurities concerning the underlying kinetic mechanism of the investigated polymerization process.[3,7,8]

There are two major computational polymerization modeling classes: deterministic and stochastic methods.[9] Deterministic modeling involves simultaneously solving the mass balances for all species present in the reaction mixture. However, considering each unique (in terms of type (*e.g.* macroradical) and chain length) macrospecies independently can result in tens of thousands of ordinary differential equations which is computationally unreasonable to integrate. Reducing the number of equations can for example be achieved by grouping chain lengths into finite intervals.[10,11]An alternative approach is the so-called method of moments, where only the averages of the chain length distribution of each type of macrospecies are covered.[1213] For example for the macroradicals, following moment equations are obtained:

$$\frac{\mathrm{d}\lambda_s}{dt} = \sum_i i^s \frac{d[R_i]}{dt} \; with\; e.g. \frac{\mathrm{d}\lambda_1}{dt} = k_p[M]\lambda_1 - k_{t,app}\lambda_1\lambda_1 + \cdots \quad (1)$$

with s=1,2,... ; i the chain length and $[R_i]$ the concentration of the macroradicals with chain length i; k_p the propagation rate coefficient; [M] the monomer concentration and $k_{t,app}$ the apparent (overall) termination rate coefficient.

Integrating these moment equations allows the calculation of the average number/mass average chain length and dispersity:

$$x_{n,R_i} = \frac{\lambda_1}{\lambda_0} \tag{2}$$

$$x_{m,R_i} = \frac{\lambda_2}{\lambda_1} \tag{3}$$

$$Đ_{R_i} = \frac{x_{m,R_i}}{x_{n,R_i}} \tag{4}$$

with $x_{n/m,R_i}$ the number/mass average chain length of the macroradicals and $Đ_{R_i}$ the dispersity of the macroradicals. Similar equations exist for all other (e.g. dead) macrospecies.

Consequently, in this method, a significant reduction of the computation time is preferred over the information about individual chains. Nonetheless, average properties of each chain population is still accessible which often suffices, especially in an industrial setting.[9]

Alternatively, stochastic approaches do not require the numerical integration of a set of coupled ordinary differential equations but each reaction is a random event that can take place with a certain probability.[14–17] Consequently, multiple possible time evolutions can exist for each time step with the probabilities of each adding up to 1. The most frequently applied stochastic method for the description of polymerization processes is the kinetic Monte Carlo (*k*MC) algorithm developed by Gillespie.[18] In the practical realization of this algorithm, for each reaction type (ν=1,...,N_t with N_t the total number of reaction types), the Monte Carlo (MC) reaction probability is defined as:

$$P_\nu^{MC} = \frac{R_\nu^{MC}}{\sum_{\nu=1}^{N_t} R_\nu^{MC}} \tag{5}$$

with R_ν^{MC} the total reaction rate of reaction type ν (in s^{-1}).

In order to determine which reaction type (μ) is to be executed, a random number (r_1), uniformly distributed between 0 and 1, is selected with the reaction type μ determined via following equation:

$$\sum_{\nu=1}^{\mu-1} \mathrm{R}_{\nu}^{MC} < r_1 < \sum_{\nu=1}^{\mu} \mathrm{R}_{\nu}^{MC} \tag{6}$$

In contrast to deterministic methods, where each time step used for integrating the differential equations is chosen by the user, the stochastic time interval between reactions (τ) is calculated based on a second random number r_2:

$$\tau = \frac{-\ln(r_2)}{\sum_{\nu=1}^{N_t} \mathrm{R}_{\nu}^{MC}} \tag{7}$$

with r_2 again uniformly distributed between 0 and 1.

Finally, a third (r_3) and when necessary fourth (r_4) random number are used when macrospecies are involved in the executed reaction in order select the chain lengths of the involved species based on their fractional occurrence.[6,16,19,20]

Consequently, the different species are tracked in a representative microscopic-scale homogeneous volume *V* (*e.g.* 10^{-17} L) and reactions are selected in a discrete manner in stochastic time steps. As a result, if the reaction event history is stored, besides the average polymer (*e.g.* $x_{n/m}$) and process properties (*e.g.* monomer conversion), a detail of the polymer structure (*e.g.* comonomer sequences) can be obtained as well.[17] However, depending on the complexity of the reaction scheme and the selected volume *V*, this can require a high computational cost. Moreover, if several particles are involved, strictly also the sampling needs to take into account this particulate nature, except in the case of a fixed particle size, as covered in this PhD thesis.

In what follows, a more detailed description and overview of modeling RAFT polymerization kinetics in bulk/solution and emulsion using either a stochastic or deterministic method will be given. This distinction is made as both polymerization types are considered in this PhD.

2.2 Kinetic modeling of RAFT bulk/solution polymerization

The kinetic modeling of RAFT polymerization systems in bulk and solution has already been extensively applied to investigate the unclear RAFT retardation mechanism[3,9,21–30], to study copolymerization processes[31–36] and to model complex polymer architectures (*e.g.* star polymers)[37–41] among other things.[42–59]

Most of the performed studies concentrate on the prediction of average properties such as $x_{n/m}$, Đ and end-group functionality (EGF) using the deterministic method of moments.[1,9,22,24,25,32,38,42–45,60–6626272829] Initial focus was on the description of linear homopolymers and more specifically on the attempt to elucidate the mechanism behind the observed rate retardation in certain RAFT polymerizations. Barner-Kowollik *et al.*[26] proposed a RAFT mechanism where a stable intermediate radical is formed resulting in a slow fragmentation rate. Alternatively, Monteiro and de Brouwer[24] suggested a RAFT cross-termination reaction between the intermediate and growing macroradicals. Clear experimental proof for a single of the proposed models is still lacking to this day. Furthermore, simulations of the average characteristics of nonlinear homopolymers have also been performed using the method of moments.[32,38] Notably, Pinto *et al.*[38] investigated the branch formation during the RAFT polymerization of vinyl acetate. Even though the presence of the RAFT agent did not affect the rate of branching, it did result in the formation of more linear polymer chains compared to a free radical polymerization (FRP) as more and shorter polymer chains are formed in general. Additionally, RAFT copolymerization processes have also been investigated employing this deterministic method.[60–66] Monteiro studied the influence of the transfer rate coefficients on the dispersity of block copolymers produced by ideal RAFT agents, hence in the absence of rate retardation, and could show that two blocks with a high dispersity can result in a lower overall dispersity due to the random coupling of the two distributions.[61] Moreover, several authors focused on the optimal operating policies aiming at obtaining specific

composition copolymers.[6063646566] For example, Sun *et al.*[65,66] employed a programmed feed rate to design copolymers of styrene and butyl acrylate with a predefined uniform and linear gradient composition distribution.

In order to gain more insight in the polymerization kinetics and polymer product properties, the prediction of the complete chain length distribution (CLD) is preferred over the calculation of the average characteristics only.[1] Nonetheless, deterministic methods capable of achieving this in a computational viable manner are limited as the number of different macrospecies can be very high, resulting in a large set of ordinary differential equations. A first method to overcome this issue is the introduction of pseudo steady state assumptions (PSSA) resulting in a set of differential-algebraic equations that is less stiff to be solved. For example, Zapata-Gonzàles *et al.*[47,48] reduced the computational load by assuming the PSSA for the calculation of the concentration of the conventional macroradical species. Additionally, if the intermediate termination model suggested by Monteiro and de Brouwer[24] was considered, the PSSA could be applied for the concentration of the RAFT intermediate species as well, reducing the computational effort even further which was confirmed by the work of De Rybel *et al.*[1] In follow-up work, these authors developed the most detailed PSSA-based model currently available for industrially relevant RAFT agents, uniquely including all chain length dependencies, *e.g.* diffusional limitations on termination.[121] Alternatively, Fortunatti *et al.*[35,44,49] have shown that the CLD can also be obtained by means of the probability generating function transform. This did not only allow the calculation of the overall CLD but also of the univariate and bivariate CLD of the conventional macroradical and intermediate macroradical species respectively. However, the most popular deterministic full CLD method is the discretized Galerkin h-*p*-method as this has been made commercially available in the PREDICI simulation software package.[21,26,31,37,40,45,68–72] This tool was for example used by Barner-Kowollik *et al.*[26] in combination with experimental data to determine the RAFT specific rate coefficients for the

polymerization of styrene mediated by cumyl dithiobenzoate. The results indicated a low fragmentation rate coefficient ($3\ 10^{-2}\ s^{-1}$) of the RAFT intermediate in agreement with the proposed slow fragmentation rate retardation mechanism. Even though Feldermann *et al.*[69] confirmed this conclusion for the same polymerization system, Pallares *et al.*[69] demonstrated that similar model profiles can be obtained with different model parameter combinations. Hence, the exact RAFT polymer mechanism is still unclear, however, for the more ideal RAFT agents, which are industrially relevant, this is much less an issue.[1] Alternatively, PREDICI has also been used to model more complex polymer architectures.[31,37,40] For example, Junkers *et al.*[37] included branch formation in their model of high temperature acrylate RAFT polymerization and suggested optimal reaction conditions. Moreover, Chaffey-Millar *et al.*[40] described the reaction kinetics and properties including the CLD of the individual arms of star polymers synthesized by means of RAFT polymerization.

Stochastic modeling of RAFT polymerization in bulk and solution has been applied less frequently than deterministic methods, even though it can also be used to obtain the CLD.[3,36,41,51,52,73–75] Notably, Tobita[51] derived analytical expressions for the overall CLD in a batch and continuous stirred tank reactor by considering the overall active and dormant periods of the macrospecies. Nonetheless, the kinetic Monte Carlo method, where the chain formation process is simulated directly by means of reaction probabilities, is mostly used.[3,36,52,73,75] Prescott[52] used this method to study termination events in more detail. It was shown that in a well-controlled RAFT system, the lifetime of the entire radical population increases at higher conversion as long chains are present. Consequently, the continually changing CLD results in the need to use apparent termination rate coefficients opposed to average values for the entire conversion profile. Furthermore, Chaffey-Millar *et al.*[41] developed a kinetic Monte Carlo code able to compete with PREDICI in terms of computation time by using a parallelized approach where the total polymerization system is divided in several smaller mini-systems, which

synchronize periodically. Gegenhuber *et al.*[76] compared experimental and bivariate kinetic Monte Carlo data to investigate the synthesis of high molar mass segmented copolymers prepared via a combination of step-growth and RAFT polymerization.

Finally, Konkolewicz et al.[67,77,78] developed hybrid models, possessing both deterministic and stochastic elements, capable of constructing the CLD and corresponding population weighted rate coefficients by integrating moment equations combined with subsequent sampling of the polymeric reaction events. The obtained model took intermediate radical termination with only oligomeric radicals into account and could accurately describe the experimental results of the RAFT polymerization of styrene mediated with cyanoisopropyl dithiobenzoate.

In this PhD, both the method of moments and the *k*MC technique is considered to describe the bulk/solution polymerization kinetics. LCT in-house codes are used for this purposes of which the details have already been covered in published work.[6,16,19,76,79–81]

2.3 Kinetic modeling of RAFT emulsion polymerization

2.3.1 Modeling techniques

Detailed kinetic modeling of RAFT emulsion polymerization has only been performed to a very limited extend as the multi-phase characteristics including possible mass transfer events make the kinetic description much more complex compared to the homogeneous processes explained in the previous section.

Not surprisingly, most of the work has focused on RAFT miniemulsion polymerization as no micelles are present and ideally each monomer droplet is transformed into a polymer particle, significantly simplifying the particle nucleation mechanism and the emulsion kinetics in general. For example, Tobita *et al.*[82–91] used *k*MC modelling to study the influence of the compartmentalized nature on the RAFT rate retardation mechanism. It was shown that the ongoing debated regarding the retardation mechanism could potentially be solved by

investigating the influence of the particle size on the polymerization rate. Retardation due to bimolecular RAFT cross-termination is expected to decrease with decreasing particle size due to segregation, whereas the slow fragmentation mechanism will not be influenced by the particle size. This approach was used by Suzuki *et al.*[88,91] to investigate the RAFT miniemulsion polymerization of styrene mediated by polystyryl dithiobenzoate. Experimental validation of *k*MC simulations indicated that the miniemulsion polymerization rate increases with decreasing particle size, hence agreeing with the RAFT cross-termination retardation model for the investigated system. The use of macro-RAFT agents neglects possible exit/entry phenomena of the small RAFT leaving group radicals, known from experimental studies[92–95] to induce additional retardation. This was confirmed by *k*MC modeling by Luo *et al.*[96] during the early stages of the RAFT miniemulsion polymerization of styrene mediated by 1-phenylethyl phenyldithioacetate (PEPDA).

Alternatively, deterministic modeling of RAFT miniemulsion copolymerization of styrene and butyl acrylate was achieved by Li et al.[97] using the pseudo-homopolymerization approach[98] consisting of conventional "bulk" method of moments equations with average pseudo-homopropagation rate coefficients combined with an equation for the average number of propagating and intermediate radicals. The ability to design (co-)monomer feeding rates corresponding with targeted copolymer composition distributions was incorporated in their model and the predefined distributions could be obtained experimentally. Optimal semi-batch operation strategies were also obtained by Jung and Gomes[99] who developed a model capable of describing the RAFT miniemulsion kinetics under pseudo-bulk conditions for the homopolymerization of styrene. A combination of population balances and approximate analytical equations was used to obtain key polymer properties including the particle size distribution and chain length distribution for the styrene polymerization mediated by O-ethyl xanthyl ethylpropionate.

However, a more fundamental and detailed deterministic modeling method for the description of the kinetics of (RAFT) emulsion polymerization is the use of (modified) Smith-Ewart differential equations.[100–102] These equations describe the time evolution of the number of particles with a given number of radicals and will be described in more detail in Section 4.[101,103,104] Luo *et al.*[105] used this method to investigate the RAFT miniemulsion of styrene by considering two radical types, *i.e.* propagating and RAFT intermediate radicals, resulting in two-dimensional Smith-Ewart equations. Experimental data was used to verify the Smith-Ewart theory and to estimate the RAFT equilibrium coefficient (k_{add}/k_{frag}) for the investigated system.

Moreover, Monteiro *et al.*[102,106] simulated the RAFT mediated microemulsion polymerization of styrene using two-dimensional Smith-Ewart equations as well. However, in contrast to Luo *et al.*[105], a differentiation between macroradicals and RAFT leaving group radicals was now made whereas RAFT intermediate radicals could be neglected by assuming the simplified degenerative RAFT mechanism. Furthermore, a constant average particle diameter (20 nm) was assumed and the nucleation process where micelles are converted into particles could be investigated by considering separate populations balances for micelles containing no or only RAFT leaving group radicals. It was shown that compartmentalization effects on termination only play a role after the complete consumption of the RAFT agent as exit and reentry of the RAFT leaving group radicals result in a retardation of the polymerization rates.

On the other hand, O'Donnel and Kaler[107] developed a simplified kinetic model for the RAFT microemulsion polymerization of butyl acrylate mediated by methyl-2-(O-ethylxanthyl)propionate. The model consisted of only four (monomer conversion, radical concentration, RAFT agent concentration and particle concentration) coupled differential equations dependent, among other things, on an analytical expression for the fraction of active radicals. The observed rate retardation was explained by slow fragmentation of the RAFT intermediate radical which reduces the concentration of active, propagating radicals.

Hermanson *et al.*[108] did not consider Smith-Ewart equations as well but developed a model based on differential equations for all possible radicals, including intermediate and RAFT leaving group radicals, while assuming negligible bimolecular termination and radical exit.[109] Nonetheless, it was assumed that the RAFT agent can diffuse from micelles to particles possibly resulting a difference in RAFT agent concentration between the two. Consequently, it was shown that the dispersity, obtained via the method om moments, will be broad with low RAFT agent concentration as uncontrolled polymerization occurred in particles nucleated at a later stage.

In silico kinetic studies of RAFT macroemulsion polymerization mostly focused on seeded systems, where a preformed latex is added to the reaction mixture before the onset of the polymerization in order to avoid the complex nucleation period[110–113] For example, Prescott *et al.* used both Monte Carlo[110] and deterministic Smith-Ewart based[111] calculations to investigate the radical loss processes in the seeded RAFT emulsion polymerization of styrene. The observed retardation was explained by a RAFT-induced exit mechanism where an entering oligomeric radical is immediately deactivated by addition to a (macro)-RAFT agent and can possibly again exit the particle after reactivation. Furthermore, exit of the RAFT leaving group radical is suggested to increase retardation at the early stages of the polymerization process. Even though these conclusions were confirmed by kinetic modeling work of Peklak and Butté[112], applying a model consisting of Smith-Ewart equations as well, Zetterlund *et al.*[114] questions the validity of the RAFT-induced exit mechanism for the observed retardation relative to a FRP process. These authors state that the probability of exit of the oligomeric species is governed by the relative rates of exit and propagation and should not be affected by prior addition to a RAFT agent. Contrarily, the use of xanthates as RAFT agents, characterized by a low transfer constant, does have an effect on the radical exit probability as discussed by Smulders *et al.*[113] Due to the surface-activity of these species, oligomeric radicals entering a

particle have a higher chance of reacting with the RAFT agent prior to propagation. Moreover, the formed RAFT leaving group radical is likely to desorb the particle, essentially resulting in a frustrated entry process as the original entry of the oligomeric radical did not result in monomer propagation inside the particle.

In this PhD, focus is on miniemulsion RAFT polymerization and the Smith-Ewart approach is considered, selecting for simplicity a fixed average particle size and an average monomer concentration. To enable a comparison with the state of the art in the next subsection the principle of this approach is highlighted, covering conventional (intrinsic) free radical polymerization.

2.3.2 Illustration of commonly used Smith-Ewart equations: free radical miniemulsion polymerization case

The kinetic description of FRP miniemulsion is inherently much more complex than the bulk/solution counterpart.[115] Not only does the two-phase system require the distinction between aqueous and organic phase species, species in the organic phase can also behave differently from an overall kinetic point of view. The physical confinement of reactants within discrete confined spaces, better known as compartmentalization, result in two fundamental effects. Firstly, the confined space effect, which states that the reaction rate of two species located in the same particle increases with decreasing particle size and secondly, the segregation effect which refers to two species located in separate particles being unable to react. Consequently, the species present in the organic phase can be divided in two groups: abundant and nonabundant species. For the abundant species (>> 10 molecules per particle), *e.g.* monomer, the concentration in the particles can be approximated by a single average concentration and the concentration time evolution can hence be described by conventional continuity equations. Moreover, the compartmentalization effects have no influence on the rates of the reactions where these species are involved. Contrarily, the nonabundant species (0-10

molecules per particle), *e.g.* macroradicals, cannot be characterized by a single average concentration as the probabilities of the reactions involving only these type of species can differ between particle types due to the compartmentalization effects. For example, termination cannot occur in particles containing no or only a single radical and hence the overall termination rate will depend on the particle type distribution. In order to account for these effects, Smith and Ewart developed a mathematical approach which describes the time evolution of the particle type distribution during FRP (mini)emulsion.[101] These Smith-Ewart equations can then be used to determine the average number of the nonabundant species in the particles which can in turn be used in the conventional continuity equations of the abundant species.

In this subsection, the Smith-Ewart equations are elaborated considering the FRP miniemulsion scheme shown in Table 1, focusing on styrene as monomer. The water soluble KPS radical initiator (I_2) decomposes in the aqueous phase forming radical anions (I) which can subsequently propagate until oligomeric species with a critical chain length of 2 are formed. Due to the hydrophobicity of these oligomeric species, only entry in the particles can occur while entry of smaller species including the radical anion are neglected. For simplicity, instantaneous monomer phase transfer to the aqueous phase is assumed resulting in a constant aqueous monomer concentration at a saturated value ($4.3\ 10^{-3}$ mol L^{-1}).[116] Based on literature data, the thermal self-initiation of styrene is neglected at the considered polymerization temperature (343K). Chain transfer to monomer in the organic phase results in the formation of small monomeric radicals capable of exiting the particles. As a first approximation, it is assumed that these monomeric radicals will always react with monomer in the aqueous phase before reentering a particle, simplifying the interphase transport scheme. Moreover, diffusional limitations on the rate coefficients of the reactions involving macrospecies are neglected as these are outside the scope of this chapter. In agreement with other modeling studies, [99,105,117]

the average particle diameter and hence the average particle volume are considered constant throughout the entire polymerization process (d_p = 200 nm).

As shown in Table 1, three (intrinsic) parameter combinations are investigated (Comb1-Comb3). Firstly, Comb1, which is characterized by a high termination and chain transfer to monomer rate coefficient. Secondly, Comb2, characterized by a high termination and a low chain transfer to monomer rate coefficient. Thirdly, Comb3 is characterized by both a relatively low termination and a low chain transfer to monomer rate coefficient.

In an ideal miniemulsion polymerization with one particle size, where the total number of particles is fixed and determined by the initial number of droplets, the number of particles with *k* macroradicals and *l* monomeric radicals are influenced by the rate coefficients of the reactions changing the number of these compartmentalized non-abundant radicals and the initial conditions (*e.g.* particle size). For the polymerization scheme discussed in Table 1, these reactions are shown in Figure 2.1 and result in a variation of the particle type distribution throughout the polymerization process.

***Table 2.1**: Overview of reactions and rate coefficients for intrinsic FRP miniemulsion of styrene at 343 K, with initiator related coefficients based on the initiator KPS and a differentiation between three parameter combinations; also included mass transfer kinetic parameters (d_p=200 nm); for simplicity only intrinsic rate coefficients are considered (typical values).*

	Reaction	Equation	k ((L mol^{-1}) s^{-1})			Ref
			Comb1	Comb2	Comb3	
Aqueous phase reactions	Dissociation of KPS[a],[b]	$I_{2,aq} \xrightarrow{f,k_{dis}} 2I_{aq}^{\bullet}$		$2.2\ 10^{-5}$		105
	Chain initiation by KPS	$I_{aq}^{\bullet} + M_{aq} \xrightarrow{k_{pI}} R_{1,aq}^{\bullet}$		$4.9\ 10^{5}$		118
	Chain initiation[c] by $M_{aq}^{\bullet}$	$M_{aq}^{\bullet} + M_{aq} \xrightarrow{k_{pM}} R_{2,aq}^{\bullet}$		$4.8\ 10^{2}$		119
	Propagation[c],[d]	$R_{1,aq}^{\bullet} + M_{aq} \xrightarrow{k_p} R_{2,aq}^{\bullet}$		$4.8\ 10^{2}$		119
Organic phase reactions	Propagation	$R_{i,p}^{\bullet} + M_p \xrightarrow{k_p} R_{i+1,p}^{\bullet}$		$4.8\ 10^{2}$		119
	Termination by recombination	$R_{i,p}^{\bullet} + R_{j,p}^{\bullet} \xrightarrow{k_{tc}} P_{i+j,p}$	$1.0\ 10^{8}$	$1.0\ 10^{8}$	$1.0\ 10^{4}$	This work,(e),(f)
	Chain transfer to monomer	$R_{i,p}^{\bullet} + M_p \xrightarrow{k_{trM}} M_p^{\bullet} + P_{i,p}$	$1.0\ 10^{1}$	$1.0\ 10^{-5}$	$1.0\ 10^{-5}$	This work,(e)
	Chain initiation[c]	$M_p^{\bullet} + M_p \xrightarrow{k_{pM}} R_{2,p}^{\bullet}$		$4.8\ 10^{2}$		119
Interphase transport	Exit[a] of $M_p^{\bullet}$	$M_p^{\bullet} \xrightarrow{k_{exitM}} M_{aq}^{\bullet}$		$1.0\ 10^{5}$		This work,(e)
	Entry[d] of $R_{2,aq}^{\bullet}$	$R_{2,aq}^{\bullet} \xrightarrow{k_{entryR_2}} R_{2,p}^{\bullet}$		$5.0\ 10^{7}$		(g)

(a) s^{-1}; (b) f= 0.2 (middle of literature[120] range of 0.1-0.3); (c) considered equal to k_p to a first approximation; (d) critical chain length for the entry of styrene is 2. Influence of initiator group is neglected to a first approximation; (e) typical values demonstrating the Smith-Ewart limiting cases as discussed in the text; (f) only termination by recombination ; (g) large values are assumed to reflect the strong entry rate of molecules possessing the critical chain length

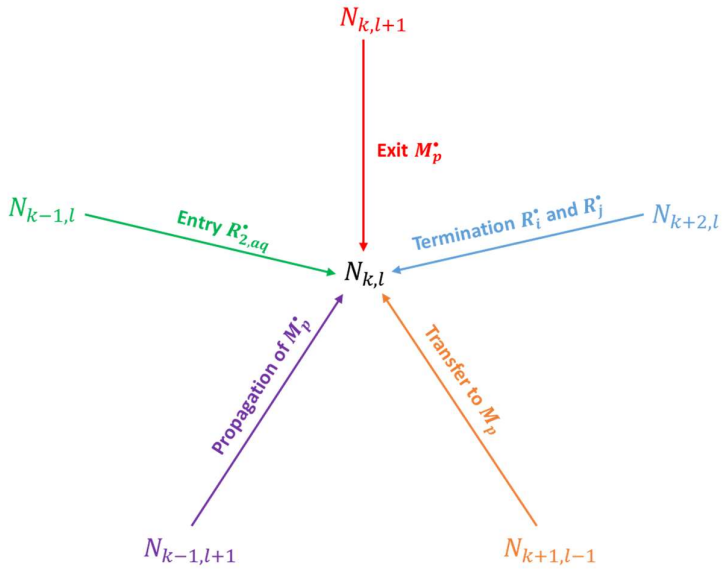

***Figure 2.1**: Schematic representation of the reactions changing the number of macroradicals and/or monomeric radicals to a particle containing k macroradicals and l monomeric radicals*

A mathematical description of the particle type distribution can be achieved by the introduction of the Smith-Ewart equations which consist of a set of population balances (Equation 8; k,l ≥ 0).

$$\begin{aligned}\frac{dN_{k,l}}{dt} = {} & \frac{k_{tc,app}}{2v_pN_A}\Big((k+2)(k+1)N_{k+2,l} - k(k-1)N_{k,l}\Big) \\ & + k_{pM}[M_p]\Big((l+1)N_{k-1,l+1} - lN_{k,l}\Big) \\ & + k_{exitM}\Big((l+1)N_{k,l+1} - lN_{k,l}\Big) \\ & + k_{ent\ \ \ _2}[R_{2,aq}](N_{k-1,l} - N_{k,l}) \\ & + k_{trM}[M_p]\Big((k+1)N_{k+1,l-1} - kN_{k,l}\Big)\end{aligned} \tag{8}$$

with $N_{k,l}$ the number of particles containing k macro- and l monomeric radicals, v_p the (average) particle volume and N_A the Avogadro constant. With the colors related to the colors in Figure 2.1.

These two-dimensional Smith-Ewart equations can only be integrated if the continuity equations of the species in the aqueous phase (Equation (9)-(14)) and the abundant species in the particles (Equation (15)-(16)) are solved as well:

$$\frac{d[I_{2,aq}]}{dt} = -fk_{dis}[I_{2,aq}] \tag{9}$$

$$\frac{d[I_{aq}]}{dt} = 2fk_{dis}[I_{2,aq}] - k_{pI}[I_{aq}][M_{aq}] \tag{10}$$

$$\frac{d[R_{1,aq}]}{dt} = k_{pI}[I_{aq}][M_{aq}] - k_p[R_{1,aq}][M_{aq}] \tag{11}$$

$$\frac{d[R_{2,aq}]}{dt} = k_p[R_{1,aq}][M_{aq}] + k_{pM}[M^{\bullet}_{aq}][M_{aq}] - k_{EntryR2}N_p\frac{[R_{2,aq}]}{N_A V_{aq}} \tag{12}$$

$$\frac{d[M_{aq}]}{dt} = -k_{pI}[I_{aq}][M_{aq}] - k_{pM}[M^{\bullet}_{aq}][M_{aq}] - k_p[R_{1,aq}][M_{aq}] \tag{13}$$

$$\frac{d[M^{\bullet}_{aq}]}{dt} = -k_{pM}[M^{\bullet}_{aq}][M_{aq}] \tag{14}$$

$$\frac{d[M_p]}{dt} = -k_p\frac{\bar{n}(R_i)}{N_a v_p}[M_p] - k_{trM}\frac{\bar{n}(R_i)}{N_a v_p}[M_p] - k_{pM}[M^{\bullet}_p][M_p] \tag{15}$$

$$\frac{d\sum_{i\geq 1}[P_{i,p}]}{dt} = \frac{k_{tc,app}}{2}\frac{\bar{n}(R_i)}{N_a v_p}\frac{\bar{n}(R_i)}{N_a v_p} + k_{trM}\frac{\bar{n}(R_i)}{N_a v_p}[M_p] \tag{16}$$

with the average number of macro – and monomeric radicals per particle defined as:

$$\bar{n}(R_i^{\bullet}) = \sum\nolimits_{k,l} k\frac{N_{k,l}}{N_p} \tag{17}$$

$$\bar{n}(M^{\bullet}) = \sum\nolimits_{k,l} l\frac{N_{k,l}}{N_p} \tag{18}$$

in which N_p is the total number of particles.

Integrating Equation (8)-(18) simultaneously allows the calculation of the concentrations of all species present throughout the polymerization process and, hence, to track the monomer conversion as well. Moreover, this set of equations can be extended to include the calculation of (average) chain length properties (number/mass average molar mass and dispersity) of the macroradicals and dead polymer chains by applying the pseudo-bulk approximation for the higher order moment equations.[121–123] However, focus of this chapter is on the concentrations of the individual species and, hence, this approach is outside the scope. Nonetheless, for more information on and examples of the calculation of the (average) chain length properties during a (mini)emulsion polymerization, the reader is referred to Chapters 4 and 5.

The resulting conversion profiles upon applying the discussed modelling approach for the parameter combinations shown in Table 1 can be found in Figure 2.2 (a-c). Comb1, characterized by a high chain transfer and termination rate coefficient, results in the slowest polymerization rate, followed by Comb2, characterized by a slow chain transfer but a high termination rate coefficient, which already leads to a significantly higher rate. However, Comb3, characterized by both a slow transfer and termination rate coefficient, clearly has the highest polymerization rate and 95% monomer conversion is achieved within the hour.

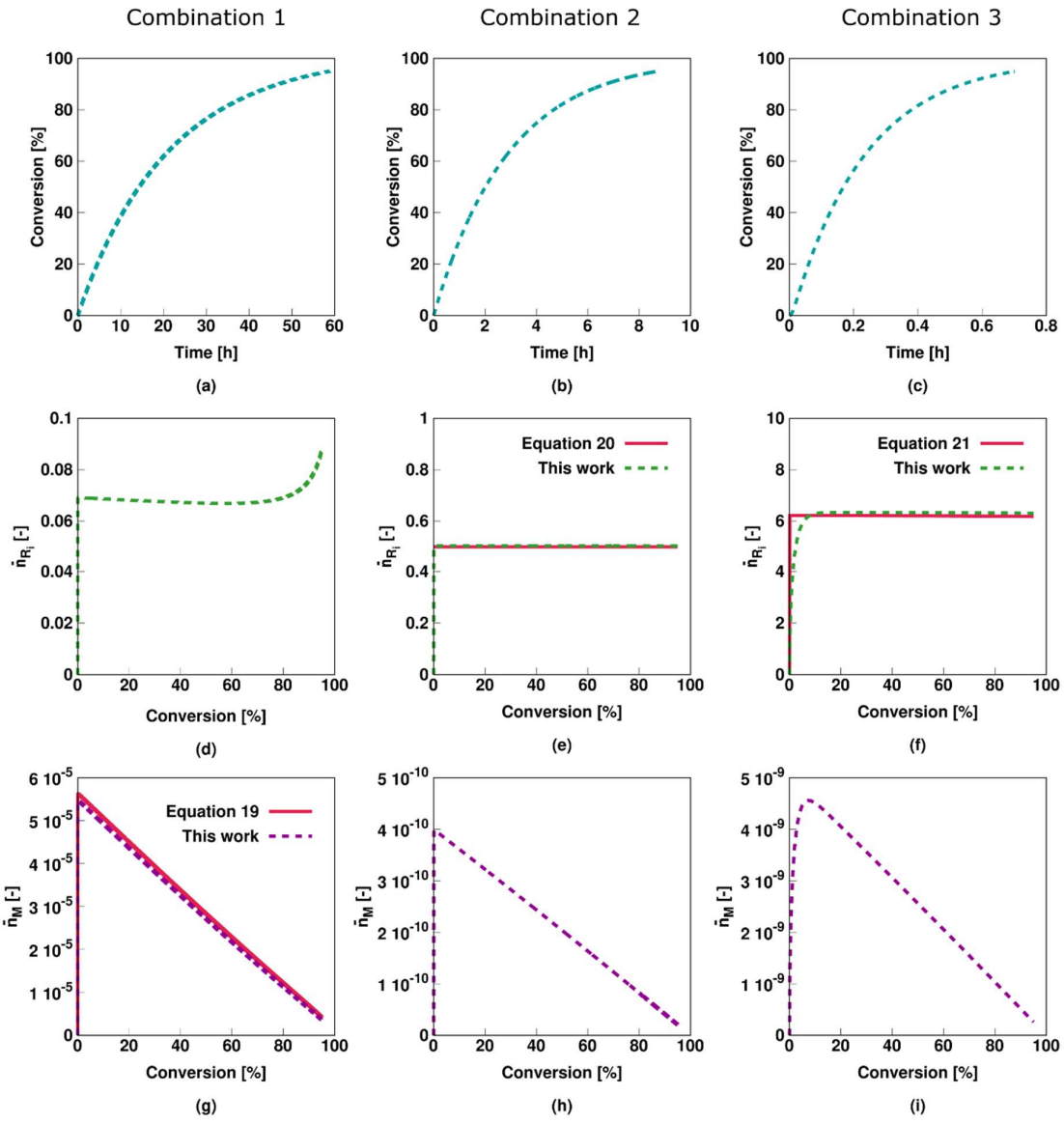

***Figure 2.2**: Overview of the monomer conversion (a-c) as a function of time and the average number of macro– (d-f) and monomeric (g-i) radicals as a function of monomer conversion for the intrinsic FRP miniemulsion of styrene at 343 K. Model parameters in Table 1. $[Sty]_0/[KPS]_0 = 1200$, $[KPS]_0 = 2\ 10^{-3}$ mol L^{-1}, $m_{sty,0} = 20$ g, $m_{H20,0} = 80$ g, and d_p=200 nm. Also shown (red lines) are the average macro/monomeric radicals as calculated via Equation 19-21 (text book examples of Smith-Ewart limits).*

Not surprisingly, this trend also manifests itself in the results for the average number of macroradicals per particle (Figure 2.2 d-f). The slow polymerization rate of Comb1 is the result of a very low (<0.1) average amount of macroradicals present in each particle throughout the

entire polymerization. Alternatively, the polymerization system corresponding with Comb2 has an average number of macroradicals per particle of 0.5, meaning that half of the particles contains only one radical whereas the other half contains none. This suggests that instantaneous termination results when a radical enters a particle already containing another (macro)radical. Finally, Comb3 results in a high yet again constant (±6) value, at least after an initial period (X_m = ± 15%), which explains the high polymerization rate. Oppositely, the average number of monomeric radicals per particle, formed after chain transfer to monomer, is the highest for Comb1 (Figure 2.2g) and decreases linearly with conversion as less monomer becomes available. Nonetheless, due to the high exit and chain initiation rate coefficients, the value is relatively low (< 10^{-5}). For Comb2 and Comb3, a much lower chain transfer rate coefficient is considered which results in a negligible value for the average number monomeric radicals per particle (Figure 2.3h/i) yet again decreasing linearly with conversion.

The three parameter combinations shown in Table 1 are similar to limiting cases originally discussed by Smith and Ewart.[101] In their pioneering work, these authors identified a first case corresponding with a system in which the radical desorption/exit rate is much faster than entry rate. As a result, the average number of radicals per particle remains very low (<<0.5). Alternatively, a second case exist where the average number of radicals per particle is equal to 0.5, corresponding to a system characterized by instantaneous termination. Finally, the third case is characterized by lower termination rates which makes it possible for particles to contain more than one radical. Importantly, as also discussed by Asua,[2] for these limiting cases, analytical solutions exists which assess the average number of radicals per particle. Adjusting these for the specific system discussed in this work, where only possible entry of R_2 radicals is considered, results in following equations:

$$Comb1: \bar{n}(M^{\bullet}) = \frac{k_{entryR2}[R_{2,aq}]}{2k_{entryR2}[R_{2,aq}] + k_{exitM}} \quad (19)$$

$$Comb2: \bar{n}(R_i^{\bullet}) = 0.5 \tag{20}$$

$$Comb3: \bar{n}(R_i^{\bullet}) = \left(\frac{k_{entryR2}[R_{2,aq}]}{\frac{k_{tc}}{v_p N_A}} \right)^{0.5} \tag{21}$$

with v_p the (average) particle volume and N_A the Avogadro constant.

As shown in Figure 2.2 (e, f and g), these equations confirm the accuracy of the modelling approach used in this work (assuming an average monomer concentration per particle at any time). The results of Figure 2.2 can be further understood by investigating Figure 2.3, showing the probabilities for the relevant reactions concerning the macro- and monomeric radicals. The higher chain transfer rate coefficient of Comb1 results in a much higher (and more significant) probability of chain transfer compared to Comb2 and Comb3. Moreover, due to the chosen high exit rate coefficient, a monomeric radical will almost exclusively exit a particle (Figure 2.3d-f). As a result, for Comb1, the generation of a significant amount of monomeric radicals followed by their (fast) exit and subsequent reentry in another particle will increase the possibility for two radicals (of which one macroradical) to be present in the same particle and, hence, to terminate. Consequently this will lead to the observed low average number of (macro)radicals per particle (Figure 2.2d). For Comb2 and Comb3, this will not occur to a significant level as the rate coefficient for chain transfer to monomer is sufficiently low. Furthermore, comparing the probability of termination for a macroradical between Comb2 and Comb3 (Figure 2.3 h and i) shows that this probability is much lower for Comb3. Therefore, in contrast to Comb2 where the average number of macroradicals is 0.5 (Figure 2.2e), instantaneous termination will not occur for Comb3 and the average number of macroradicals can be quite high (*e.g.* 6, Figure 2.2f) leading to a high polymerization rate (Figure 2.2c).

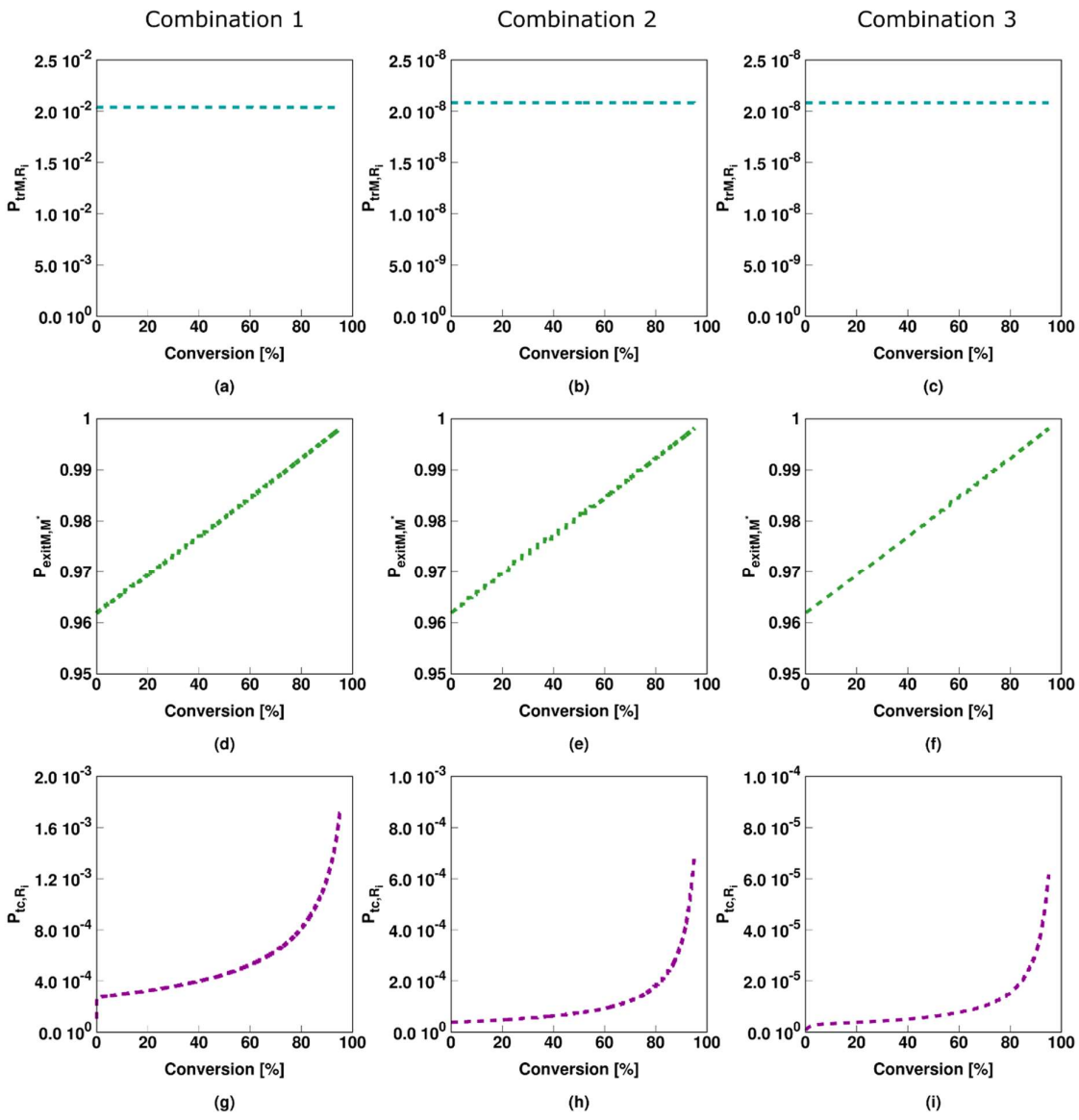

***Figure 2.3**: Probabilities of chain transfer to monomer (a-c) and termination by recombination (g-i) for the macroradicals and probability of exit for the monomeric radical, corresponding with the results shown in Figure 2.2 (calculated over all particles).*

A mathematical modelling approach based on Smith-Ewart equations also allows the description of the evolution of the radical type particle distribution as shown in Figure 2.4. For Comb1, the high probability for chain transfer and the subsequent exit, reentry and increased possibility for termination results in almost all particles containing no macro- and monomeric radicals (Figure 2.4 a/d). Alternatively, for Comb2 the absence of the relevance of chain transfer

events and the relatively high termination probability results in approximately half the particles containing no macroradicals whereas the other half contains only one (Figure 2.4b). The absence of instantaneous termination for Comb3 makes it possible for particles to contain well above one radical (Figure 2.4c). A significant amount of particles contain also a number of radicals different compared to the average of 6, highlighting that still the Smith-Ewart approach is needed. Nonetheless, as chain transfer does not significantly occur for both Comb2 and Comb3, almost all particles contain no monomeric radicals (Figure 2.4 e/f).

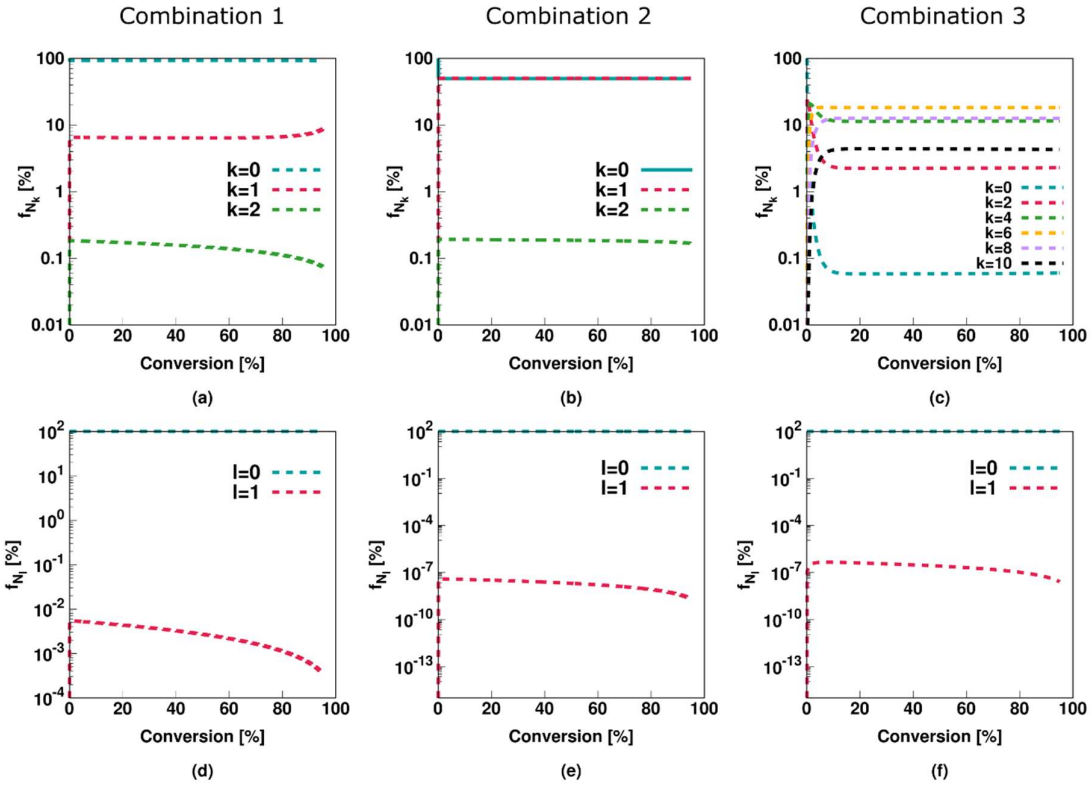

Figure 2.4*: Corresponding fraction of particles with a certain number of macro- (a-c) and monomeric (d-f) radicals as a function of conversion for Figure 2.2.*

Notably, whereas Comb1-3 represent a single limiting case as described by Equation 19-21, a more complicated polymerization system can progress from one limiting case to another throughout its process. For example, as will be explained in Chapter 4, a RAFT miniemulsion polymerization involving a leaving group radical prone to exit the particle will initially behave

similar to Comb1, with a low average number of macroradicals per particle. After complete consumption of the initial RAFT agent and at medium conversion, high termination rates will still be active and the system will behave similar to Comb2 with an average number of macroradicals per particle of 0.5. However, as the conversion increases, diffusional limitations on termination become significant and, hence, at the final stages of the polymerization process, a particle can contain more than one radical similar to Comb3. As a result, the kinetic description of these polymerization processes cannot be achieved in detail by individual analytical expressions and an elaborate computer-based modelling approach, such as developed in this work, is necessary.

In Chapter 4, the model explained in this chapter will be extended to describe the mechanism of degenerative RAFT miniemulsion polymerization including average chain length properties by means of two-dimensional Smith-Ewart equations. Subsequently, this model is extended even further in Chapter 5, where the non-degenerative RAFT miniemulsion polymerization requires five-dimensional Smith-Ewart equations.

2.4 Conclusions

Kinetic modeling has proven to be a powerful tool to investigate and design bulk and solution RAFT polymerization. The developed models can in general be divided in two groups: deterministic modeling in which a set of differential equations is integrated and stochastic modeling which considers each reaction as a random event chosen based on its probability. The multi-phase character of RAFT emulsion polymerization requires a more complex mathematical description. In most cases a deterministic modeling approach using Smith-Ewart differential equations is used to describe the evolution of the particle type distribution. Moreover, focus has mainly been on RAFT miniemulsion polymerization which simplifies the description of the particle nucleation mechanism.

A straightforward (intrinsic) FRP miniemulsion scheme was used already in this chapter to elaborate the use of the Smith-Ewart equations. It was shown that the modeling approach used in this work could be confirmed by established analytical equations for certain limiting cases. Moreover, the results show that significant chain transfer to monomer leads to a lower polymerization rate as subsequent exit and reentry increases the probability for two radicals to meet and terminate. Furthermore, absence of these chain transfer events results in an average number of macroradicals per particle of 0.5 if instantaneous termination can be assumed and of a value well above 1 if a lower termination rate coefficient is active. It should although be reminded that these averages correspond to a distribution of particle types with different radical numbers.

2.5 References

1 N. De Rybel, P. H. M. Van Steenberge, M.-F. Reyniers, C. Barner-Kowollik, D. R. D'hooge and G. B. Marin, *Macromol. Theory Simulations*, 2017, **26**, 1600048.

2 J. M. Asua, *Polymer Reaction Engineering*, Blackwel Publishing Ltd, Oxford, 2007.

3 M. Drache, G. Schmidt-Naake, M. Buback and P. Vana, *Polymer (Guildf).*, 2005, **46**, 8483–8493.

4 D. J. G. Devlaminck, P. H. M. Van Steenberge, L. De Keer, M.-F. Reyniers and D. R. D'hooge, *Polym. Chem.*, 2017, **8**, 6948–6963.

5 S. Fierens, D. D'hooge, P. Van Steenberge, M.-F. Reyniers and G. Marin, *Polymers (Basel).*, 2015, **7**, 655–679.

6 D. R. D'hooge, P. H. M. Van Steenberge, M.-F. Reyniers and G. B. Marin, *Prog. Polym. Sci.*, 2016, **58**, 59–89.

7 J. Jiang, W. J. Wang, B. G. Li and S. Zhu, *Macromol. React. Eng.*, 2017, **1700029**, 1–13.

8 I. S. Altarawneh, M. Srour and V. G. Gomes, *Polym. Plast. Technol. Eng.*, 2007, **46**, 1103–1115.

9 E. Mastan and S. Zhu, *Eur. Polym. J.*, 2015, **68**, 139–160.

10 S. Kumar and D. Ramkrishna, *Chem. Eng. Sci.*, 1996, **51**, 1311–1332.

11 S. Kumar and D. Ramkrishna, *Chem. Eng. Sci.*, 1996, **51**, 1333–1342.

12 C. H. Bamford and H. Tompa, *J. Polym. Sci.*, 1954, **50**, 1097–1115.

13 C. H. Bamford and H. Tompa, *J. Polym. Sci.*, 1953, **10**, 345–350.

14 J. Mira, C. G. Fernández and J. M. Urreaga, *J. Chem. Educ.*, 2003, **80**, 1488.

15 F. Brandl, M. Drache and S. Beuermann, *Polymers (Basel).*, 2018, **10**, 1008.

16 P. H. M. Van Steenberge, D. R. D'hooge, M.-F. Reyniers and G. B. Marin, *Chem. Eng. Sci.*, 2014, **110**, 185–199.

17 S. K. Fierens, P. H. M. Van Steenberge, M. F. Reyniers, G. B. Marin and D. R. D'hooge, *AIChE J.*, 2017, **63**, 4971–4986.

18 D. T. Gillesple, *J. Phys. Chem.*, 1977, **81**, 2340–2361.

19 P. H. M. Van Steenberge, D. R. D'hooge, Y. Wang, M. Zhong, M.-F. Reyniers, D. Konkolewicz, K. Matyjaszewski and G. B. Marin, *Macromolecules*, 2012, **45**, 8519–8531.

20 Y. W. Marien, P. H. M. Van Steenberge, C. Barner-Kowollik, M. F. Reyniers, G. B. Marin and D. R. D'Hooge, *Macromolecules*, 2017, **50**, 1371–1385.

21 P. Vana, T. P. Davis and C. Barner-Kowollik, *Macromol. Theory Simulations*, 2002, **11**, 823–835.

22 N. F. G. Wittenberg, M. Buback and R. A. Hutchinson, *Macromol. React. Eng.*, 2013, **7**, 267–276.

23 P. Drawe and M. Buback, *Macromol. Theory Simulations*, 2016, **25**, 74–84.

24 M. J. Monteiro and H. De Brouwer, *Macromolecules*, 2001, **34**, 349–352.

25 A. R. Wang and S. Zhu, *J. Polym. Sci. Part A Polym. Chem.*, 2003, **41**, 1553–1566.

26 C. Barner-Kowollik, J. F. Quinn, D. R. Morsley and T. P. Davis, *J. Polym. Sci. Part A Polym. Chem.*, 2001, **39**, 1353–1365.

27 M. Zhang and W. H. Ray, *Ind. Eng. Chem. Res.*, 2001, **40**, 4336–4352.

28 M. J. Monteiro, *J. Polym. Sci. Part A Polym. Chem.*, 2005, **43**, 3189–3204.

29 C. Li, J. He, Y. Liu, Y. Zhou and Y. Yang, *Aust. J. Chem.*, 2012, **65**, 1077–1089.

30 T. Junkers, C. Barner-Kowollik and M. L. Coote, *Macromol. Rapid Commun.*, 2011, **32**, 1891–1898.

31 P. B. Zetterlund, G. Gody and S. Perrier, *Macromol. Theory Simulations*, 2014, **23**, 331–339.

32 J. C. Hernández-Ortiz, E. Vivaldo-Lima, M. A. Dubé and A. Penlidis, *Macromol. Theory Simulations*, 2014, **23**, 147–169.

33 S. Ren, E. Vivaldo-Lima and M. Dubé, *Processes*, 2015, **4**, 1.

34 M. Ali Parsa, I. Kozhan, M. Wulkow and R. A. Hutchinson, *Macromol. Theory Simulations*, 2014, **23**, 207–217.

35 C. Fortunatti, C. Sarmoria, A. Brandolin and M. Asteasuain, *Comput. Mater. Sci.*, 2017, **136**, 280–296.

36 P. Ganjeh-Anzabi, V. Hadadi-Asl, M. Salami-Kaljahi and H. Roghani-Mamaqani, *Iran. J. Chem. Chem. Eng.*, 2012, **31**, 75–84.

37 T. Junkers and C. Barner-Kowollik, *Macromol. Theory Simulations*, 2009, **18**, 421–433.

38 M. A. Pinto, R. Li, C. D. Immanuel, P. A. Lovell and F. J. Schork, *Ind. Eng. Chem. Res.*, 2008, **47**, 509–523.

39 P. Derboven, P. H. M. Van Steenberge, J. Vandenbergh, M. F. Reyniers, T. Junkers, D. R. D'Hooge and G. B. Marin, *Macromol. Rapid Commun.*, 2015, **36**, 2149–2155.

40 H. Chaffey-Millar, M. Busch, T. P. Davis, M. H. Stenzel and C. Barner-Kowollik, *Macromol. Theory Simulations*, 2005, **14**, 143–157.

41 H. Chaffey-Millar, D. Stewart, M. M. T. Chakravarty, G. Keller and C. Barner-Kowollik, *Macromol. Theory Simulations*, 2007, **16**, 575–592.

42 A. R. Wang and S. Zhu, *Macromol. Theory Simulations*, 2003, **12**, 196–208.

43 N. V. Ulitin, A. V. Oparkin, R. Y. Deberdeev and A. A. Berlin, *Dokl. Chem.*, 2014, **456**, 107–109.

44 C. Fortunatti, C. Sarmoria, A. Brandolin and M. Asteasuain, *Macromol. React. Eng.*, 2014, **8**, 214–230.

45 Y.-N. Zhou and Z.-H. Luo, *Macromol. React. Eng.*, 2016, **10**, 516–534.

46 P. Derboven, D. R. D'hooge, M.-F. Reyniers, G. B. Marin and C. Barner-Kowollik, *Macromolecules*, 2015, **48**, 492–501.

47 I. Zapata-González, E. Saldívar-Guerra and J. Ortiz-Cisneros, *Macromol. Theory Simulations*, 2011, **20**, 370–388.

48 I. Zapata-González, E. Saldívar-Guerra, A. Flores-Tlacuahuac, E. Vivaldo-Lima and J. Ortiz-Cisneros, *Can. J. Chem. Eng.*, 2012, **90**, 804–823.

49 C. Fortunatti, C. Sarmoria, A. Brandolin and M. Asteasuain, Prediction of the full molecular weight distribution in raft polymerization using probability generating functions, Elsevier B.V., 2013, vol. 32.

50 D. S. Achilias, *Macromol. Theory Simulations*, 2007, **16**, 319–347.

51 H. Tobita, *Macromol. React. Eng.*, 2008, **2**, 371–381.

52 S. W. Prescott, *Macromolecules*, 2003, **36**, 9608–9621.

53 A. D. Peklak and A. Butté, *Macromol. Theory Simulations*, 2006, **15**, 546–562.

54 G. Johnston-Hall, M. H. Stenzel, T. P. Davis, C. Barner-Kowollik and M. J. Monteiro, *Macromolecules*, 2007, **40**, 2730–2736.

55 G. Johnston-Hall, A. Theis, M. J. Monteiro, T. P. Davis, M. H. Stenzel and C. Barner-Kowollik, *Macromol. Chem. Phys.*, 2005, **206**, 2047–2053.

56 P. Vana, T. P. Davis and C. Barner-Kowollik, *Macromol. Rapid Commun.*, 2002, **23**, 952–956.

57 T. Junkers, A. Theis, M. Buback, T. P. Davis, M. H. Stenzel, P. Vana and C. Barner-Kowollik, *Macromolecules*, 2005, **38**, 9497–9508.

58 A. Theis, T. P. Davis, M. H. Stenzel and C. Barner-Kowollik, *Macromolecules*, 2005, **38**, 10323–10327.

59 A. Theis, T. P. Davis, M. H. Stenzel and C. Barner-Kowollik, *Polymer (Guildf).*, 2006, **47**, 999–1010.

60 Y. Ye and F. J. Schork, *Ind. Eng. Chem. Res.*, 2009, **48**, 10827–10839.

61 M. J. Monteiro, *J. Polym. Sci. Part A Polym. Chem.*, 2005, **43**, 5643–5651.

62 R. Wang, Y. Luo, B. Li and S. Zhu, *Macromolecules*, 2009, 85–94.

63 A. Zargar and F. J. Schork, *Macromol. React. Eng.*, 2009, **3**, 118–130.

64 R. Wang, Y. Luo, B. Li, X. Sun and S. Zhu, *Macromol. Theory Simulations*, 2006, **15**, 356–368.

65 X. Sun, Y. Luo, R. Wang, B. G. Li, B. Liu and S. Zhu, *Macromolecules*, 2007, **40**, 849–859.

66 X. Sun, Y. Luo, R. Wang, B.-G. Li and S. Zhu, *AIChE J.*, 2008, **54**, 1073–1087.

67 D. Konkolewicz, B. S. Hawkett, A. Gray-Weale and S. Perrier, *Macromolecules*, 2008, **41**, 6400–6412.

68 M. Wulkow, *Macromol. Theory Simulations*, 1996, **5**, 393–416.

69 A. Feldermann, M. L. Coote, M. H. Stenzel, T. P. Davis and C. Barner-Kowollik, *J. Am. Chem. Soc.*, 2004, **126**, 15915–15923.

70 J. Pallares, G. Jaramillo-Soto, C. Flores-Cataño, E. Vivaldo Lima, L. M. F. Lona and A. Penlidis, A Comparison of Reaction Mechanisms for Reversible Addition-Fragmentation Chain Transfer Polymerization Using Modeling Tools, 2006, vol. 43.

71 M. Wulkow, M. Busch, T. P. Davis and C. Barner-kowollik, *J. Polym. Sci. Part A Polym. Chem.*, 2003, **42**, 1441–1448.

72 M. Wulkow, *Macromol. React. Eng.*, 2008, **2**, 461–494.

73 M. Drache and G. Drache, *Polymers (Basel).*, 2012, **4**, 1416–1442.

74 Y. Ao, J. He, X. Han, Y. Liu, X. Wang, D. Fan, J. Xu and Y. Yang, *J. Polym. Sci. Part A Polym. Chem.*, 2007, **45**, 374–387.

75 E. Pintos, C. Sarmoria, A. Brandolin and M. Asteasuain, *Ind. Eng. Chem. Res.*, 2016, **55**, 8534–8547.

76 T. Gegenhuber, L. De Keer, A. S. Goldmann, P. H. M. Van Steenberge, J. O. Mueller, M. F. Reyniers, J. P. Menzel, D. R. D'Hooge and C. Barner-Kowollik, *Macromolecules*, 2017, **50**, 6451–6467.

77 D. Konkolewicz, M. Siauw, A. Gray-Weale, B. S. Hawkett and S. Perrier, *J. Phys. Chem. B*, 2009, **113**, 7086–7094.

78 D. Konkolewicz, B. S. Hawkett, A. Gray-Weale and S. Perrier, *J. Polym. Sci. Part a-Polymer Chem.*, 2009, **47**, 3455–3466.

79 D. R. D'hooge, P. H. M. Van Steenberge, P. Derboven, M.-F. Reyniers and G. B. Marin, *Polym. Chem.*, 2015, **6**, 7081–7096.

80 D. R. D'hooge, M.-F. Reyniers and G. B. Marin, *Macromol. React. Eng.*, 2009, **3**, 185–209.

81 D. R. D'hooge, M. F. Reyniers and G. B. Marin, *Macromol. React. Eng.*, 2013, **7**, 362–379.

82 H. Tobita, *Macromol. Theory Simulations*, 2009, **18**, 108–119.

83 H. Tobita and F. Yanase, *Macromol. Theory Simulations*, 2007, **16**, 476–488.

84 H. Tobita, *Macromol. Symp.*, 2008, **261**, 36–45.

85 H. Tobita, *Macromol. Symp.*, 2010, **288**, 16–24.

86 H. Tobita, *Macromol. React. Eng.*, 2010, **4**, 643–662.

87 H. Tobita, *Polymers (Basel).*, 2011, **3**, 1944–1971.

88 H. Tobita, *Macromol. Theory Simulations*, 2011, **20**, 709–720.

89 K. Suzuki, Y. Nishimura, Y. Kanematsu, Y. Masuda, S. Satoh and H. Tobita, *Macromol. React. Eng.*, 2012, **6**, 17–23.

90 H. Tobita, *Macromol. Theory Simulations*, 2013, **22**, 399–409.

91 K. Suzuki, Y. Kanematsu, T. Miura, M. Minami, S. Satoh and H. Tobita, *Macromol. Theory Simulations*, 2014, **23**, 136–146.

92 M. Lansalot, T. P. Davis and J. P. A. Heuts, *Macromolecules*, 2002, **35**, 7582–7591.

93 Y. Luo, B. Liu, Z. Wang, J. Gao and B. Li, *J. Polym. Sci. Part A-Polymer Chem.*, 2007, **45**, 2304–2315.

94 M. J. Monteiro, M. Hodgson and H. De Brouwer, *J. Polym. Sci. Part A Polym. Chem.*, 2000, **38**, 3864–3874.

95 J. G. Tsavalas, F. J. Schork, H. De Brouwer and M. J. Monteiro, *Macromolecules*, 2001, **34**, 3938–3946.

96 Y. Luo and B. Yu, *Polym. Plast. Technol. Eng.*, 2005, **43**, 1299–1321.

97 X. Li, W. J. Wang, F. Weng, B. G. Li and S. Zhu, *Ind. Eng. Chem. Res.*, 2014, **53**, 7321–7332.

98 G. Storti, S. Carrà, M. Morbidelli and G. Vita, *J. Appl. Polym. Sci.*, 1989, **37**, 2443–2467.

99 S. M. Jung and V. G. Gomes, *Macromol. React. Eng.*, 2011, **5**, 303–315.

100 P. B. Zetterlund and M. Okubo, *Macromol. Theory Simulations*, 2009, **18**, 277–286.

101 W. V. Smith and R. H. Ewart, *J. Chem. Phys.*, 1948, **16**, 592–599.

102 Z. Jia and M. J. Monteiro, *ACS Symp. Ser.*, 2012, **1100**, 293–304.

103 M. Okubo, *Polymer Particles*, Springer, 2005.

104 S. C. Thickett and R. G. Gilbert, *Polymer (Guildf).*, 2007, **48**, 6965–6991.

105 Y. Luo, R. Wang, L. Yang, B. Yu, B. Li and S. Zhu, *Macromolecules*, 2006, **39**, 1328–1337.

106 M. P. F. Pepels, C. I. Holdsworth, S. Pascual and M. J. Monteiro, *Macromolecules*, 2010, **43**, 7565–7576.

107 G. Moad, *Macromol. Chem. Phys.*, 2014, **215**, 9–26.

108 K. D. Hermanson, S. Liu and E. W. Kaler, *J. Polym. Sci. Part A Polym. Chem.*, 2006, **44**, 6055–6070.

109 E. Mastan, X. Li and S. Zhu, *Prog. Polym. Sci.*, 2015, **45**, 71–101.

110 S. W. Prescott, M. J. Ballard, E. Rizzardo and R. G. Gilbert, *Macromolecules*, 2005, **38**, 4901–4912.

111 S. W. Prescott, M. J. Ballard, E. Rizzardo and R. G. Gilbert, *Macromol. Theory Simulations*, 2006, **15**, 70–86.

112 A. D. Peklak and A. Butte, *J. Polym. Sci. Part A Polym. Chem.*, 2006, **44**, 6114–6135.

113 W. Smulders, R. G. Gilbert and M. J. Monteiro, *Macromolecules*, 2003, **36**, 4309–4318.

114 P. B. Zetterlund, Y. Kagawa and M. Okubo, *Chem. Rev.*, 2008, **108**, 3747–94.

115 P. B. Zetterlund, *Polym. Chem.*, 2011, **2**, 534–549.

116 R. G. Gilbert, *Emulsion polymerization: a mechanistic approach*, Academic Press Inc., London, 1995.

117 P. H. M. Van Steenberge, D. D.R., M. F. Reyniers, G. B. Marin and M. F. Cunningham, *Macromolecules*, 2014, **47**, 7732–7741.

118 M. Dossi, G. Storti and D. Moscatelli, *Macromol. Theory Simulations*, 2010, **19**, 170–178.

119 M. Buback, R. G. Gilbert, R. A. Hutchinson, B. Klumberman, F.-D. Kuchta, B. G. Manders, K. F. O'Driscoll, G. T. Russell and J. Schweer, *Macromol. Chem. Phys.*, 1995, **196**, 3267–3280.

120 G. Moad and D. H. Solomon, *The chemistry of radical polymerization*, Elsevier, Oxford, 2006.

121 N. De Rybel, P. H. M. Van Steenberge, M.-F. Reyniers, D. R. D'hooge and G. B. Marin, *Chem. Eng. Sci.*, 2018, **177**, 163–179.

122 L. Bentein, D. R. D'Hooge, M. F. Reyniers and G. B. Marin, *Macromol. Theory Simulations*, 2011, **20**, 238–265.

123 D. J. G. Devlaminck, P. H. M. Van Steenberge, M.-F. Reyniers and D. R. D'hooge, *Macromolecules*, 2018, 10.1021/acs.macromol.8b02111.

Chapter 3: A detailed mechanistic study of bulk MADIX of styrene and its chain extension

3.1 Introduction

One of the major reversibsule deactivation radical polymerization (RDRP) techniques is reversible addition-fragmentation chain transfer (RAFT) polymerization.[1] Its most relevant elementary reactions are shown in Figure 3.1a, assuming for simplicity recombination as the only termination mode and ignoring RAFT cross-termination. As in traditional free radical polymerization (FRP) a conventional radical initiator (I_2) forms initiator fragments (I; blue spheres), which subsequently add to monomer (M; red spheres), leading to the formation of macroradicals (R_i; i: chain length). In contrast to FRP, these R_i species do not dominantly terminate ((5) in Figure 3.1a) to create dead polymer species P but they can also be reversibly deactivated via RAFT exchange ((2) and (4) in Figure 3.1a).

This RAFT exchange involves a (macro-)RAFT agent (R_iX; $i \geq 0$) resulting in the incorporation of end-group functionality (EGF; yellow cubes in Figure 3.1a; X), allowing further chemical modification such as the preparation of tailored block copolymers.[2–5] In the absence of RAFT degradation reactions[5,6] the amount of X moieties remains constant and under well-defined reaction conditions the number average chain length (x_n) can be tuned by varying the initial molar ratio of monomer to RAFT agent ($[M]_0/[R_0X]_0$). The latter ratio is also known as the targeted chain length (TCL), taking into account that the employed I_2 amount is typically negligible.[5]

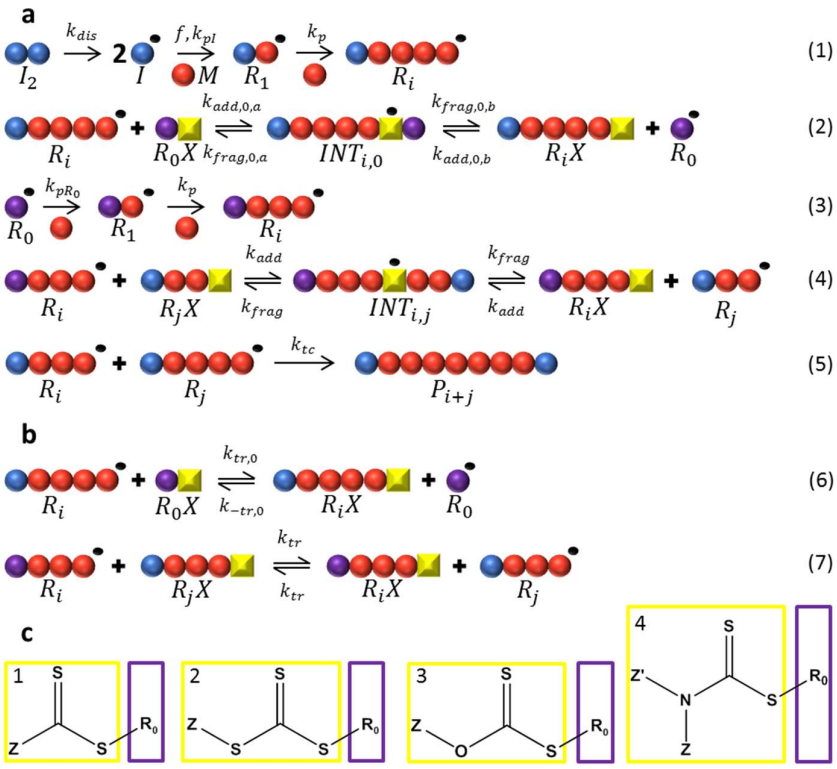

Figure 3.1*: (a) Key elementary reactions in RAFT polymerization, not displaying for simplicity termination with the RAFT intermediate and conventional termination by disproportionation; I_2: conventional radical initiator, R_0X: initial RAFT agent; I: fragment from I_2; M: monomer; R_0: RAFT leaving group; R_i: macroradical (chain length i); R_iX: dormant macrospecies; $INT_{i,j}$: intermediate RAFT radical (chain length i ("left" arm) and j ("right" arm)); P: dead polymer species; $k_{dis,pI,p,add(0,a/b),frag(0,a/b),pR0,tc}$: rate coefficient for dissociation, chain initiation with I, propagation, RAFT addition, RAFT fragmentation, chain initiation with R_0 and termination by recombination; f: conventional initiator efficiency; (b) Formal description of RAFT exchange upon validity of the degenerative RAFT mechanism (Equation (1)-(3)); (c) main classes of RAFT agents: 1: dithioesters; 2: trithiocarbonates; 3: xanthates; 4: dithiocarbamates*

For most RAFT agents, at low monomer conversions (X_m <20%), the exchange mainly occurs with the initial RAFT CTA (R_0X; (2) in Figure 3.1a), whereas at higher monomer conversions (X_m > 20%) R_0X is no longer present and only macro-RAFT species (R_iX; (4) in Figure 3.1a) are involved.[5,7,8] Mechanistically RAFT exchange is an activation/deactivation process

composed of two consecutive elementary reactions, *i.e.* (i) the addition of the (macro-)radical to the S=C group of the (macro-)RAFT agent ($k_{add(,0,a/b)}$ in Figure 3.1a) to form an intermediate RAFT radical (INT) and (ii) the fragmentation or βCS-scission ($k_{frag(,0,a/b)}$ in Figure 3.1a) of this INT species. In addition, side reactions can occur with in particular many focus on RAFT cross-termination involving INT species (reaction not shown in Figure 3.1a).[9–13]

For an efficient RAFT exchange in which these cross-termination reactions can be ignored, and chain initiation and RAFT fragmentation are sufficiently fast (no inhibition and rate retardation), a so-called degenerative mechanism is formally obtained (Figure 3.1b).[14] The introduced (RAFT) transfer "rate coefficients" $k_{tr,0}$, $k_{-tr,0}$, and k_{tr} can be calculated from the elementary RAFT addition and fragmentation rate coefficients after application of the pseudo-steady-state assumption for the calculation of the INT concentrations:[1,5,15,16]

$$k_{tr,0} = k_{add,0,a}\frac{k_{frag,0,b}}{k_{frag,0,a} + k_{frag,0,b}} = k_{add,0,a}\varphi_{0,b} \quad (1)$$

$$k_{-tr,0} = k_{add,0,b}\frac{k_{frag,0,a}}{k_{frag,0,a} + k_{frag,0,b}} = k_{add,0,b}\varphi_{0,a} \quad (2)$$

$$k_{tr} = \frac{k_{add}}{2} \quad (3)$$

in which for simplicity chain length dependencies have been neglected and $\varphi_{0,a/b}$ is the fragmentation probability. The ratios of the transfer rate coefficients to their corresponding propagation or chain initiation rate coefficients are known as degenerative RAFT transfer coefficients:[1,5,15,16]

$$C_{tr,0} = \frac{k_{tr,0}}{k_p} \quad (4)$$

$$C_{-tr,0} = \frac{k_{-tr,0}}{k_{pR_0}} \quad (5)$$

$$C_{tr} = \frac{k_{tr}}{k_p} \quad (6)$$

with typical values ranging between 10^{-2} and 10^{4}.[17–19] As a rule of thumb, $C_{tr(,0)}$ values larger than 10 are necessary to achieve excellent microstructural control (*e.g.* dispersity ($Đ$) <1.5).[20]

These transfer coefficients are strongly dependent on the chemical structure surrounding the reactive thiocarbonylthio moiety.[15] An overview of the main classes of RAFT agents is provided in Figure 3.1c, with the purple/yellow colour boxes for a direct link to Figure 3.1a/b. Specifically for xanthates (RAFT agent 3 in Figure 3.1c), which contain an oxygen atom in α-position to the thiocarbonylthio functional group, the RAFT transfer capability is strongly reduced. The presence of a delocalizable oxygen electron pair decreases the S=C double-bond character and, consequently, RAFT addition becomes less favourable.[21] The corresponding RAFT polymerization is often referred to as macromolecular design by interchange of xanthates (MADIX), due to historical reasons of its discovery.[22,23]

As a result of the low S=C double-bond character with xanthates, microstructural control ($Đ$<1.5) can typically only be achieved employing so-called less activated monomers (LAMs) such as ethylene and vinyl acetate. These monomers typically contain a saturated carbon or an oxygen/nitrogen electron pair adjacent to the vinyl group resulting in more reactive radicals with respect to RAFT addition ($C_{tr(,0)}$ >10).[17,19,21,24–28] [29] Other more active RAFT agents such as dithioesters and trithiocarbonates (Figure 3.1c) lead to the formation of INT radicals considerably more stable than the radicals formed by RAFT fragmentation, resulting in an undesired lowering of the polymerization rate. With xanthates, the increased stability of R_0X, due to the delocalizable lone electron pairs, and the sufficient destabilization of the radical centre of the corresponding INT species allow to simultaneously lower the RAFT addition reactivity and to realize a more favourable RAFT fragmentation as compared to other types of RAFT agents.

On the other hand, bulk or solution MADIX of so-called more activated monomers (MAMs), such as (meth)acrylates and styrenics which possess vinyl groups conjugated by a carbonyl

group or an aromatic ring, can typically not be easily conducted with a good control over chain length. Research in this area is thus still challenging as the radicals are less reactive for RAFT addition and the less active xanthate may not actively participate during polymerization ($C_{tr(,0)}$ <<10). Rate retardation and inhibition are also typically absent so that a degenerative RAFT mechanism (Figure 3.1b) can be often assumed, strongly simplifying the overall kinetic description.[5,7,30–34]

A crucial design parameter, as for every RAFT polymerization,[15,16,35] is thus the selection of the appropriate MADIX agent substituents as this determines $C_{tr(,0)}$. For MADIX of MAMs, several kinetic studies have been performed with styrene as monomer.[7,17,19,25,32,34,36,37] For example, Adamy *et al.*[7] investigated the influence of the chemical structure of the initial RAFT agent for MADIX of styrene in toluene and reported that with (O-ethyl xanthate)-2-ethyl propionate (OEXEP) as initial RAFT agent a $Đ$ close to 2 (X_m = 20%) can merely be obtained. In contrast, by increasing the electron-withdrawing capacity of the Z group by incorporation of fluorinated groups in β-position to the oxygen atom, as for instance in (O-2,2,2-trifluoro ethyl xanthate)-2- ethyl propionate (OtFOX), a lower but still high $Đ$ of 1.6 can be achieved (X_m > 20%), in agreement with an earlier experimental study of Destarac *et al.*[36] The latter observation was attributed to an increased reactivity of the S=C bond due to the decreased availability of the oxygen lone pair to conjugate with the thiocarbonyl group. This also followed from a comparison of the $C_{tr,0}$ (Equation (4)) values.[7 37]

It should be stressed that solely focusing on $C_{tr,0}$ is very likely insufficient to unequivocally predict the success of a MADIX process. For example, for O-ethyl-S-[(2-phenyl)prop-2-yl] dithiocarbonate, Destarac *et al.*[37] determined a rather high $C_{tr,0}$ of 3.8 at 110 °C for styrene, which has been related to the higher stability of the leaving tertiary benzylic radical as compared to the styryl radical. Despite this promising $C_{tr,0}$ value, only polystyrene with a high $Đ$ (≈2) could be obtained (X_m > 80%), which has been attributed to a lower C_{tr} (Equation (6)) value

close to 1, as assessed using Müller's equation.[38] In several studies[7,32,34] C_{tr} has although been taken equal to $C_{tr,0}$, which can thus be expected to be an oversimplification of the description of the RAFT/MADIX polymerization kinetics.

For MADIX, main focus has been on the determination of $C_{tr,0}$. In general, the applicability of the methods used to determine $C_{tr,0}$ strongly depends on the validity of their model assumptions.[20] Under the common assumption of a degenerative RAFT mechanism (sufficiently fast RAFT fragmentation), the Mayo[39] and CLD method[40] have been mostly applied.[20] Alternatively, Moad and coworkers[15,16,35] demonstrated that $C_{tr,0}$ can be evaluated from the slope of a plot of $\ln[R_0X]$ *vs.* $\ln[M]$, at least in case the RAFT exchange with R_0 radicals ($k_{-tr,0}$; Figure 3.1b) can be assumed to be negligible.

Unfortunately for C_{tr}, as recently highlighted by Derboven *et al.*,[20] no reliable (analytic) method exists which can be safely used for a broad range of conditions and RAFT reactivities, in particular in case $C_{tr,0}$ strongly differs from C_{tr}. Only very recently, a novel method based on measured dispersities has been proposed to jointly determine $C_{tr,0}$ and C_{tr} in a single experimental run.[8] This method requires a rather controlled degenerative RAFT polymerization with sufficiently low dispersities (<1.3), which are typically not encountered in MADIX. Currently, for MADIX, C_{tr} could only be assessed using size exclusion chromatography (SEC) data. In particular, Smulders *et al.*[30] applied the method of Goto[41–43] to assess C_{tr} during chain extension of dormant polystyrene in toluene with *n*-butyl acrylate and OEXEP as RAFT agent. A C_{tr} value of 1.04 (60 °C) resulted, which is rather approximate, taking into account the overlap between the SEC traces for the dormant polystyrene and the obtained block copolymer at the low molar mass region of the SEC trace.

Despite the somewhat restricted mediating capacities of xanthates under bulk and solution conditions and the difficulty to map the impact of the chemical structure on the RAFT transfer reactivities, MADIX remains of particular interest for all monomer types. This becomes clearer

by highlighting that MADIX can be successfully conducted in water-based media (*e.g.* (mini)emulsion), without issues related to colloidal instability.[5,7,44–47] A key feature is the xanthate surface activity, which allows the synthesis of covalently linked core-shell nanoparticles with typically styrene as core.[30,33,48] Be that as it may, exit/entry and even re-entry phenomena can disturb the desired growth so that the identification of the most suited conditions is non-trivial.[49–52]

To facilitate the identification of the suited MADIX/RDRP bulk, solution and emulsion conditions, model-based design has shown to be a powerful and indispensable tool, as it minimizes the need of long trial and error based experimental approaches with a full mapping of the relation of process parameters and RDRP characteristics.[11,53–60] A prerequisite for model-based design are accurate intrinsic rate coefficients. As explained above, for MADIX, only a limited number of exchange kinetic parameters are available.[7,15,16,20,36,61] Hence, further research on the determination of MADIX-specific kinetic parameters is still needed to fully exploit its potential, in particular in view of emulsion applications.

In the present work, a detailed combined experimental and simulation study is presented of bulk MADIX of styrene at 70°C with OEXEP as initial RAFT agent and AIBN as conventional radical initiator. Average characteristics are simulated deterministically and detailed microstructural properties are obtained through parallel stochastic kinetic Monte Carlo (*k*MC) simulations. Dedicated regression analysis is applied to determine both $C_{tr,0}$ and C_{tr}, considering an extensive set of experimental data, including data on RAFT agent conversion, $Đ$, and EGF. The EGF data are reliably measured by consecutively performing dialysis to remove residual OEXEP and elemental analysis to determine the sulphur and nitrogen content for the polymer samples. It should be noted that in general EGF determination is challenging,[62] especially for high molar mass polymers for which the accuracy of techniques such as proton nuclear magnetic resonance (^{1}H-NMR),[63–68] ultraviolet (UV) spectroscopy,[69,70] matrix-assisted laser

desorption/ionization time-of-flight,[61,62] and even elemental analysis[73] is limited. The modelling tools are used to better understand the MADIX mechanism and to visualize - for the first time - the monomer sequences along the individual chains during chain extension with (i) styrene or (ii) n-butyl acrylate (*n*BuA).

3.2 Experimental

3.2.1 Materials

Styrene (Sty, monomer (*M*), ≥99%, Sigma-Aldrich) was passed through a column filled with basic aluminium oxide (Sigma-Aldrich) to remove the stabilizer (4-tert-butylcatechol). 2,2-Azobis(2-methyl-propionitrile) (AIBN, conventional radical initiator (I_2), ≥98.0%, Sigma-Aldrich) was purified twice by recrystallization from methanol (≥99.6%, Sigma-Aldrich) and stored afterwards at -18°C. *n*-decane (≥99%; internal standard), tetrahydrofuran (THF, ≥99%), dichloromethane (DCM, ≥99%), ethanol, diethyl ether (≥98%), pentane (98%), ethyl 2-bromopropionate (99%), and potassium O-ethyl dithiocarbonate (96%) were purchased from Sigma-Aldrich and used as received. Ethanol (>99.8%) was purchased from Chem-Lab and used as received as well. Distilled water was further purified through a Millipore Milli-Q Plus system. Cellulose ester dialysis membranes with a molar mass cut-off between 5 x 10^2 and 10^3 g mol^{-1} were obtained from Spectrum Labs and soaked in deionized water and subsequently rinsed thoroughly prior to usage in order to remove the sodium azide preservative agent.

3.2.2 MADIX synthesis procedures

A typical isothermal MADIX homopolymerization was performed as follows (entry 7 in Table A1 in Appendix A which presents an overview of all the initial homopolymerization conditions). A mixture of styrene (35 mL), OEXEP (0.697 g; synthesis procedure in Section A2 of Appendix A), AIBN (0.050 g), and *n*-decane (2 mL) was added to a 100-mL two-neck glass flask, containing a magnetic stirrer bar. A stopcock was attached to one neck and a rubber

septum to the other. The solution was degassed by three freeze-pump-thaw cycles after which an argon environment was established. The flask was immersed in a preheated oil bath at the desired polymerization temperature (70°C) and constantly stirred at 300 rpm. This temperature has been selected in view of a future extension to MADIX emulsion polymerization.[33,74,75] Moreover, the self-initiation of styrene is suppressed, simplifying the overall kinetic description.[76] Temperature control was possible through *in situ* measurements via a thermocouple inserted in the rubber septum. Samples (1.5 mL) were withdrawn from the reaction flask at distinct, predefined reaction times, using 2 mL degassed syringes with stainless-steel needles, and immediately quenched in liquid nitrogen.

For the MADIX chain extensions (Table A2 in Appendix A for an overview of all conditions), an analogous synthesis procedure was used as for the homopolymerizations. The necessary polystyrene reactant (*RX*) was first synthesized by performing a homopolymerization experiment on a larger scale (100 mL styrene; entry 3 in Table A1 in Appendix A). Importantly, the polystyrene as obtained during this first synthesis step was purified by means of dialysis in order to remove unreacted OEXEP (R_0X). The samples were loaded into the dialysis tubing and placed in toluene (volume ≈ 50 times the sample volume). The dialysis was run for 96h at room temperature while renewing the toluene dialysate five times at approximately 8, 24, 48, 56, and 72h. Afterwards, the samples were extracted from the membrane and toluene was removed by means of rotary evaporation (80°C; 250 mbar; 2h) and freeze-drying (~10^{-2} mbar; 1h). As explained in Section A5 of Appendix A, the molar amount of *RX* in the purified samples (n_{RX}) was determined using:

$$n_{RX} = \frac{m_{PS}}{M_n} EGF \tag{7}$$

in which m_{PS} is the polystyrene mass and M_n the number average molar mass.

Both the homopolymerization and chain extension experiments were performed in duplicate and the reproducibility was always identified as very high.

The elemental analysis samples for the EGF measurements of the homopolymerizations were obtained by a similar dialysis procedure (toluene volume ≈ 200 times the sample volume; dialysis time 48h; renewing of dialysate at approximately 3, 18, 22, 27, 38, and 41h). The successful removal of R_0X could be confirmed by ^{1}H NMR and size exclusion chromatography (SEC) analysis (see Results and Discussion).

3.2.3 Analytic techniques

Monomer and RAFT agent conversion (X_m and X_{R0X}) were determined by gas chromatography (GC). GC analysis was carried out using a trace-GC ultra-Gas Chromatograph equipped with an AS3000 auto sampler, a flame ionization detector (FID), and a CP WAX 52 CB 30 m capillary column. Helium (flow rate: 1.5 mL min^{-1}) was used as carrier gas and the following stepwise temperature program was applied: (i) 50°C during 4 min; (ii) heating ramp of 20°C min^{-1} until 300 °C was reached; (iii) 300°C for 5 min. DCM was used as solvent to prepare the samples and *n*-decane was present in the reaction mixture as internal standard. Data acquisition and processing were performed using Chrom-Card Trace-Focus GC software. The GC results were successfully confirmed by ^{1}H NMR (Figure A2 in Appendix A). The spectra were recorded at 400 MHz and ambient temperature with $CDCl_3$ as solvent, using a Bruker Avance II spectrometer equipped with a Broadband Observe (BBO) probe. GC analysis and ^{1}H NMR were also applied to investigate the efficiency of the OEXEP synthesis (molar purity: 97±1%; Figure A1 in Appendix A). Only a significant amount of ethyl 2-bromopropionate remained (±3%) but no other impurities or side products could be detected. Number/mass average molar mass ($M_{n/m}$) and dispersity ($Đ$) were measured via SEC, injecting polymer samples diluted with THF. A PL-GPC50 plus instrument equipped with a PL-AS RT auto sampler and a refractive index (RI) detector, one Resipore 50 x 7.5 mm guard column and two Resipore 300 X 7.5 mm

columns in series were used. The flow rate was 1 mL min^{-1} and the analysis temperature was 30 °C. Calibration for homopolymerization and chain extension of styrene was performed with narrow polystyrene standards (Medium EasiVials kit, Agilent Technologies), ranging from 1.62 x 10^2 to 4.83 x 10^5 g mol^{-1}. Data acquisition and processing were performed using the PL Cirrus GPC/SEC software. EGF values of polymer samples after dialysis, hence, after removal of R_0X, were determined by means of elemental analysis, using a Flash 2000 Organic Elemental Analyser (Thermo Scientific) equipped with a thermal conductivity detector (TCD). Calibration was performed with a 2,5-bis(5-tert-butyl-benzoxazol-2-yl) thiophene (BBOT) standard.

The EGF value, which reflects the amount of *X* end-groups for the total number of chains, follows from:

$$EGF = \frac{n(X)}{0.5[n(I) + n(R_0) + n(X)]} \quad (8)$$

in which *n(A)* (*A*=R_0, *X*, and *I*) is the molar amount of *A* groups in the polystyrene sample (calculation see Section A7 of Appendix A), neglecting end-groups originating from chain transfer of macroradicals to monomer as verified in Section A9 of Appendix A. The factor 0.5 reflects that all chains possess two chain ends of one of the three considered end-group types in the denominator of Equation (8) (see also Figure 3.3; top right).

3.3 Kinetic modelling and regression analysis

MADIX of styrene and its chain extension are modelled both with a fast deterministic and a detailed stochastic method, assuming a degenerative RAFT exchange mechanism (Figure 3.1b). This mechanism can be assumed taking into account that the RAFT fragmentation can expected to be fast and the RAFT addition slow. [7,19,21,32,77] As shown by De Rybel *et al.*,[11] for low RAFT addition rate coefficients (<$10^{2.5}$ L mol^{-1} s^{-1}) with styrene, even an extremely low RAFT fragmentation rate coefficient of 10^{-2} s^{-1} still results in no observable rate retardation or RAFT-cross-termination, further supporting the use of a degenerative mechanism.

For the deterministic modelling, the so-called extended method of moments[78–82] is used, allowing the simulation of the evolution of the monomer and R_0X conversion and average polymer characteristics such as the number and mass average chain length ($x_{n/m}$), $Đ$, and EGF. Since this method is very fast it facilitates the estimation of the RAFT exchange parameters (*cf.* Equation (1)-(3)). Moreover, population weighted or thus averaged apparent termination rate coefficients are considered. For the calculation of these averages, the macroradical CLD can be approximated by the Flory-Schulz distribution (see further). For the stochastic modelling, the kinetic Monte Carlo technique (*k*MC) is employed, following the basic algorithm of Gillespie[83] extended as previously described to map the polymer microstructure with a high level of detail.[57,84,85] More details on this approach are provided in Section A10 of Appendix A. Importantly, it has been verified that the simulated average characteristics of both computational methods converge (see Figure A6 in Appendix A).

The transfer rate coefficients $k_{tr,0}$ and k_{tr}, allowing the calculation of the corresponding degenerative RAFT coefficients $C_{tr,0}$ and C_{tr} (Equation (4)-(6)), have been estimated based on an extensive set of polymerization data, using the deterministic kinetic model and the Levenberg-Marquardt algorithm (ODRPACK v2.01).[86] For a detailed description on the regression analysis procedure, the reader is referred to earlier work.[87,88] The transfer coefficient $k_{-tr,0}$ could be neglected based on preliminary simulations (see Section A12 of Appendix A) indicating that reaction of R_0 radicals with monomer is strongly preferred over reaction with R_oX. Similarly, exchange between conventional initiator radicals (I) and R_0X is kinetically insignificant as the addition of monomer to I is sufficiently fast (see Section A13 of Appendix A).

An overview of the reactions considered in the degenerative RAFT kinetic model and their associated kinetic parameters is provided in Table A3 (styrene) and Table A6 (*n*BuA) in Appendix A. For the chain extension with *n*BuA, for simplicity and taking into account the

expected limited impact, a possible penultimate monomer unit effect is ignored. Specifically for termination, apparent rate coefficients are considered to account for diffusional limitations, according to the well-established RAFT-chain length dependent–termination (RAFT-CLD-T) technique. These coefficients are chain length and X_m dependent and their model parameters are listed in Section A15 of Appendix A. For the "block copolymer radicals", an averaging according to the overall copolymer composition is performed, as explained in Section A14 of Appendix A and in agreement with a previous kinetic modelling study.[89–99] Diffusional limitations on the other reaction steps are neglected, based on literature data,[80,92,100,101] taking into account that the maximal X_m is limited and the RAFT addition rate coefficients are relatively low.

3.4 Results and discussion

In this section, attention is first paid to the EGF determination by combining dialysis and elemental analysis, with AIBN/OEXEP as MADIX initiation system and styrene as monomer. Next focus is on the validity of the kinetic model assumptions to ensure a reliable *in silico* interpretation of the MADIX characteristics and mechanism. Finally, a detailed kinetic analysis of both the MADIX homopolymerization and the chain extension with fresh styrene or *n*BuA, starting from isolated (dormant) polystyrene is performed. The monomer sequences and end-groups of each chain of a representative (co)polymer sample are visualized, considering the $C_{tr(,0)}$ values as determined based on tuning to experimental data.

3.4.1 Validation of EGF determination

As indicated above, it is not straightforward to retrieve reliable EGF data for RDRP processes. An additional complication in the present work is the rather slow OEXEP (R_0X) consumption, resulting in a significant amount of unreacted OEXEP during the homopolymerization with styrene making elemental analysis without prior purification challenging. Moreover, to

facilitate chain extension and to accurately estimate k_{tr} (or C_{tr}), reactions with R_0X need to become kinetically insignificant and, hence, unreacted OEXEP needs to be removed.

For R_0X removal, as shown in Section A16 of Appendix A, conventional precipitation is not recommended as SEC analysis shows that a significant amount of oligomeric species is also removed along with R_0X. On the other hand, in case dialysis is performed a successful R_0X removal is realized as shown in Figure 3.2. For a typical homopolymerization (entry 1 in Table A1 in Appendix A; X_m=33%), dialysis ensures a complete removal of the initial RAFT agent (Figure 3.2; top ^{1}H-NMR data) without altering the polymer part of the SEC trace (Figure 3.2; bottom).

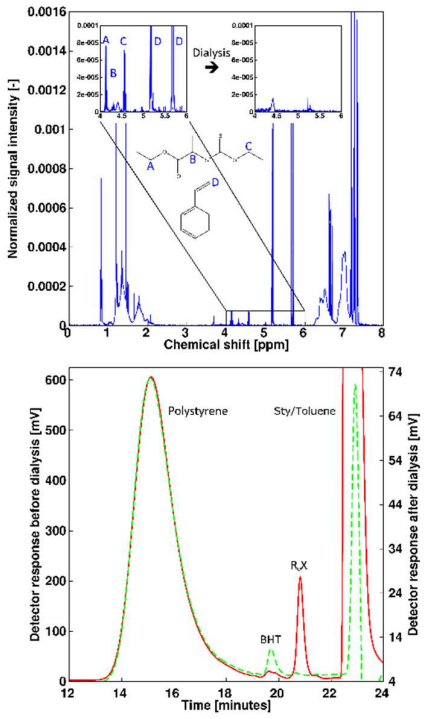

Figure 3.2*: Verification of reliability of dialysis to remove the initial RAFT agent (OEXEP); top: 1H-NMR spectrum before (main spectrum and detail top left) and after (only in detail top right) dialysis with assignment of relevant peaks for OEXEP and styrene; bottom: SEC trace before (solid red line) and after (dashed green line) dialysis; BHT: butylated hydroxytoluene (THF (SEC eluent) stabilizer); M_n (before)=6.1 x 10^3 g mol^{-1}, M_m (before)=12.2 x 10^3 g mol^{-1}, and Đ (before)=2.0; M_n (after)= 5.9 x 10^3 g mol-1, M_m (after)= 12.2 x 10^3, and Đ (after)=2.1; entry 1 in Table A1 in Appendix A, X_m=33%.*

After dialysis, elemental analysis of the purified polystyrene samples is performed to determine the mass fractions of carbon, hydrogen, nitrogen, and sulphur. The associated chromatogram for the purified product in Figure 3.2 is depicted in Figure 3.3. As the polymer is linear and consists of styrene units, carbon and hydrogen generate the largest peaks. In contrast, nitrogen and sulphur are only present in the end-groups (Figure 3.3; top right) and, hence, result only in minor peaks. This implies that the most reliable EGF data are only obtainable at lower TCLs at which the relative importance of the end-groups is higher.

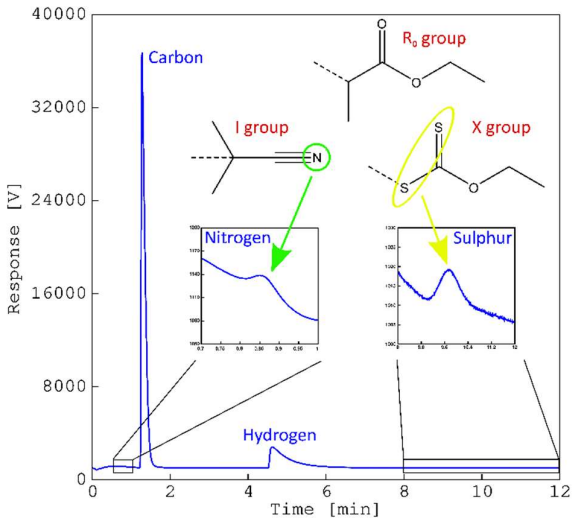

Figure 3.3*: Typical elemental analysis chromatogram for MADIX homopolymerization of styrene (entry 1 in Table A1 in Appendix A; X_m=33%; related purified SEC trace in Figure 3.2), allowing EGF measurement according to Equation (8)-(11). Reliable assumption of linear chains with as end-groups either R_0 and X; I and X; I and I; R_0 and R_0; and R_0 and I; negligible contribution of chain transfer to monomer (see Section A9 of Appendix A) and R_0R_0 formation (see Section A8 of Appendix A).*

3.4.2 Validation of kinetic modelling assumptions

For a fast simulation of the MADIX process, as explained above, the deterministic extended method of moments is applied. This method only aims at the description of the temporal evolution of X_m and the average CLD characteristics but takes into account (apparent) chain length dependencies. This is done by the calculation of averaged apparent termination rate

coefficients while assessing the macroradical concentrations using a predetermined distribution. For example, the zeroth order averaged apparent termination (by recombination) rate coefficient (<$k_{tc,app}$>), as needed to integrate the moment equations, is defined by:

$$\langle k_{tc,app} \rangle = \frac{\sum_{i=1}^{\infty}\sum_{j=1}^{\infty} k_{tc,app}^{i,j}(1+\delta_{ij})[R_i][R_j]}{\left(\sum_{i=1}^{\infty}[R_i]\right)^2} \quad (12)$$

in which $k_{tc,app}^{i,j}$ is the apparent termination (by recombination) rate coefficient between macroradicals with a chain length *i* and *j* (values: Section A14 of Appendix A), δ_{ij} the Kronecker Delta function, and $[R_i]$ and $[R_j]$ are the corresponding concentrations. In the present work, these individual concentrations are assumed to follow a Flory-Schulz distribution:

$$f_n(i) = \frac{[R_i]}{\sum_{i=1}^{\infty}[R_i]} = \frac{1}{x_{n,r}} \exp\left(-\frac{i}{x_{n,r}}\right) \quad (13)$$

with $f_n(i)$ the number fraction of macroradicals with a chain length *i* and $x_{n,r}$ the associated number average chain length.

For homopolymerization the use of the Flory-Schulz distribution is valid, as shown in Figure 3.4 (entry 3 in Table A2 in Appendix A) focusing on the simulation of X_m (0-8h; top left) and in Figure A6 of Appendix A focusing on the simulation of the average CLD characteristics. A perfect match is obtained between the results for the (approximate) deterministic simulations (green full lines) and the *k*MC simulations (red dotted lines) which fully take into account chain length dependencies. The validity of Equation (13) is also reflected in the simulated number macroradical CLDs (*e.g.* Figure 3.4 bottom left; X_m= 10%), which also match leading to similar variations for <$k_{tc,app}$> (Figure 3.4 top right; Equation (12)). This result cannot be generalized to a typical RAFT polymerization[102] but is specific for the selected MADIX process in which a Flory-Schulz character is obtained for the control over chain length.

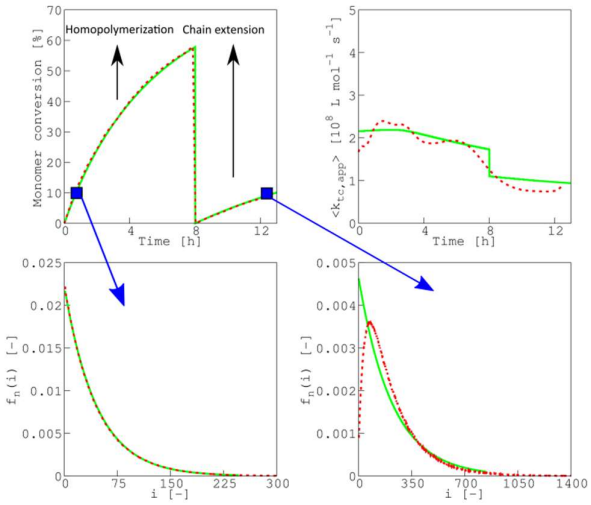

***Figure 3.4**: Comparison of main simulation results for MADIX homopolymerization and chain extension with fresh styrene obtained with the deterministic extended method of moments, assuming a Flory-Schulz macroradical CLD (Equation (13)) (full green lines) and with a kMC model explicitly accounting for all chain length dependencies (dotted red lines). Monomer conversion (top left) and zeroth order average apparent rate coefficient (Equation (12); top right); conditions homopolymerization: 0-8h: entry 3 Table A1 in Appendix A) and chain extension 8-13h: entry 3 Table A2 in Appendix A); Bottom left: macroradical CLD at X_m=10% for MADIX homopolymerization and bottom right for chain extension at the same conversion; dotted line in top right for a single kMC run.*

Also for the chain extensions the deterministic method can be used for the reliable calculation of the average MADIX characteristics. Despite a mismatch at the low chain lengths for the macroradical CLDs (*e.g.* bottom right in Figure 3.4; X_m=10%; entry 3 in Table A2 in Appendix A), the monomer conversions and average CLD characteristics are still identical for the deterministic and *k*MC simulations, as shown in Figure 3.4 (top left; X_m evolution for 8-13 h) and as shown in Figure A6 in Appendix A (average CLD characteristics). Note that the chain extended macroradicals are not Schulz-Flory distributed. To obtain Flory-Schulz behavior both segments should be of a similar length, *e.g.* short original segments should be extended again

with short ones which is statically unlikely. Instead of a Flory-Schulz distribution a Gamma like distribution results (Figure 3.4 bottom right).

3.4.3 Microstructural control for MADIX styrene homopolymerization

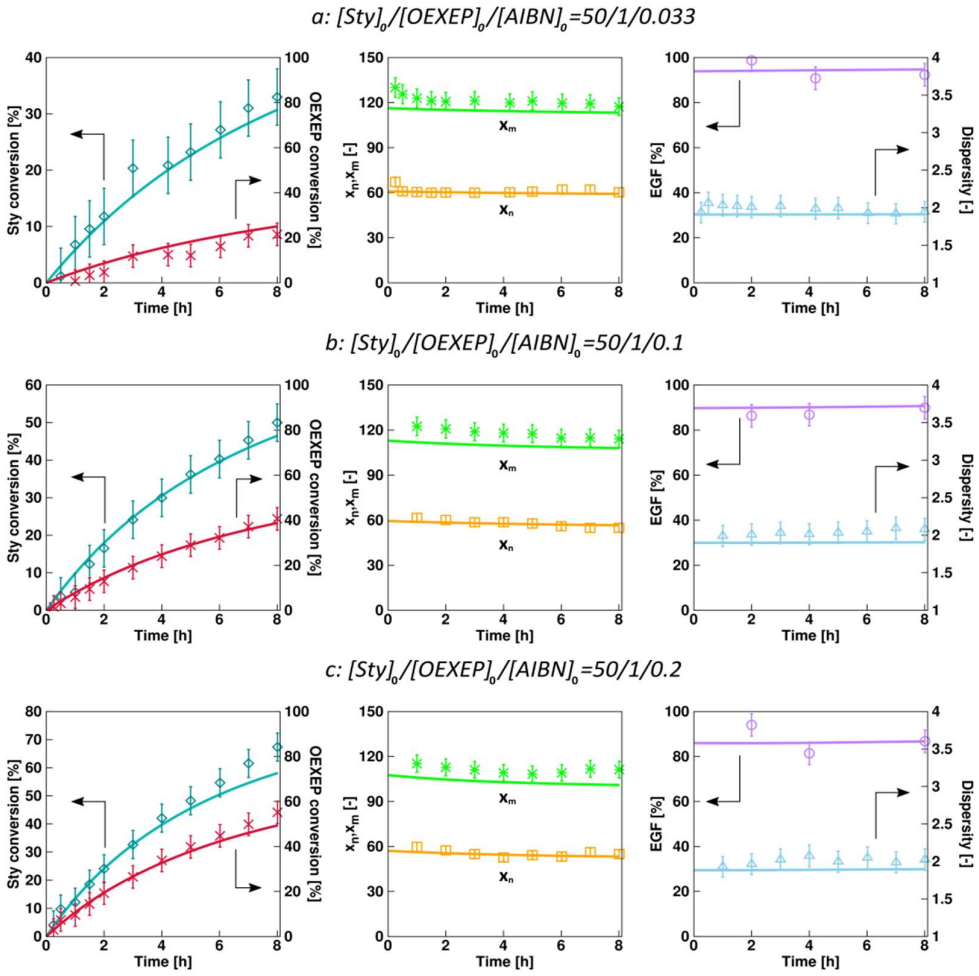

***Figure 3.5**: Comparison between simulation and experimental data for a variation of* $[OEXEP]_0/[AIBN]_0$ *for MADIX homopolymerization of styrene at 70°C with AIBN and OEXEP; Monomer conversion (X_m, dark blue), R_0X conversion (X_{R0X}, red), number-average chain length (x_n, orange), mass-average chain length (x_m, green), dispersity (Đ, purple), and end-group functionality (EGF, light blue) as a function of time; Lines correspond to calculated values with rate coefficients given in Table A3 in Appendix A and accounting for diffusional limitations (parameters in Table A4); entry 1-3 in Table A1 in Appendix A; simulated output with deterministic method.*

To obtain a better understanding of the homopolymerization kinetics, a systematic experimental study has been conducted under isothermal conditions (70°C), including a variation of all initial batch concentrations. In Figure 3.5 and 3.6, the experimental data on X_m, R_0X conversion (X_{R0X}), number and mass average chain length (x_n and x_m), EGF, and $Đ$ are provided under several initial conditions (entry 1-6 in Table A1 in Appendix A) along with the corresponding simulation results (parameters Table A3 in Appendix A).

For all data, an excellent agreement between the experimental and simulated data is obtained. Similarly, for the additional data in Figure A10 in Appendix A (entry 7 in Table A1), the experimental data are well-described. Investigation of Figure 3.5 allows to conclude that an increase of the initial I_2 concentration (lower $[R_0X]_0/[I_2]_0$) leads to an increase of both X_m and X_{R0X} (Figure 3.5; left) while having limited effect on the average chain length characteristics x_n, x_m, and $Đ$ (Figure 3.5; middle and right). At all times high x_n values, roughly 10% higher than the TCL, are obtained with constant $Đ$ values close to 2. The EGF data (Figure 3.5; right) indicate a relatively high livingness (>80%), which is also time independent. Greater EGF values are obtained for decreasing I_2 amounts, further highlighting the relevance of the optimization of $[R_0X]_0/[I_2]_0$. On the other hand, as can be derived from Figure 3.6, an increase of TCL ($[M]_0/[R_0X]_0$) at a given $[I_2]_0$ (4 x 10^{-3} mol L^{-1}) has no notable influence on X_m and X_{R0X} (Figure 3.6; left) while it results in a reduction of x_n and x_m (Figure 3.6; middle). The chain length characteristics again remain constant throughout the MADIX. A lower livingness is obtained at higher TCLs (Figure 3.6; right) whereas $Đ$ remains again constant around a value of 2. Hence, on an overall basis the effect of TCL is relatively restricted aside from its natural influence on the average chain lengths.

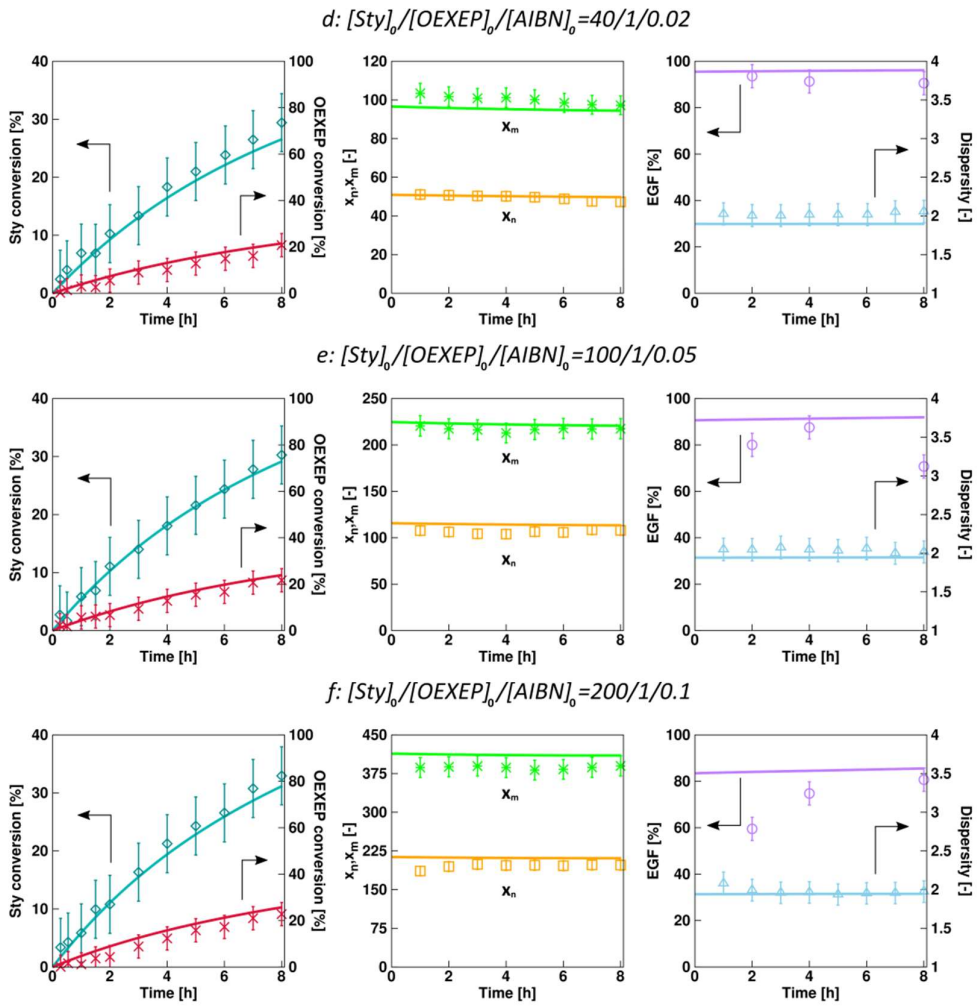

***Figure 3.6**: Comparison between simulated and experimental data for a variation of TCL ($[M]_0/[OEXEP]_0$)) at a given $[I_2]0$ (4 x 10^{-3} mol L^{-1}) for MADIX homopolymerization of styrene at 70°C with AIBN and OEXEP; Monomer conversion (X_m, dark blue), R_0X conversion (X_{R0X}, red), number-average chain length (x_n, orange), mass-average chain length (x_m, green), dispersity (Đ, purple), and end-group functionality (EGF, light blue) as a function of time; Lines correspond to calculated values with rate coefficients given in Table A3 in Appendix A and accounting for diffusional limitations (parameters in Table A4); entry 4-6 in Table A1 in the Appendix A; simulated output with deterministic method.*

Further model analysis shows that for the studied MADIX homopolymerization RAFT exchange involving macropecies (k_{tr}) is negligible. As illustrated in Section A18 in Appendix

A, identical simulations results are obtained for a k_{tr} (Equation (6)) value equal to 0 L mol^{-1} s^{-1} and if k_{tr} is taken equal to ten times $k_{tr,0}$. From this it can be concluded that the rate of exchange between macrospecies is too low to significantly affect the concentration of macroradicals. The latter are only involved in propagation, termination or in RAFT exchange with R_0X. Since, the rate of re-initiation is in addition significantly higher than the rate of exchange of R_0 radicals and dormant macrospecies, the latter exchange, characterized by $k_{-tr,0}$, is also kinetically insignificant as shown in Section A12 of Appendix A. The homopolymerization data in Figure 3.5, 3.6, and A10 in Appendix A are therefore only affected by a single RAFT transfer parameter, *i.e.* $C_{tr,0}$ (Equation (4)). Hence, for the current MADIX system, several of the reactions/exchanges of Figure 3.1 are kinetically insignificant and the reaction scheme can be represented by the one in Figure 3.7. It is clear from the reduced scheme that the formation of the dormant species can be formally compared to chain transfer with a conventional chain transfer agent such as 1-butanethiol, although with a single transfer of X instead of H.[104] Note that in this context transfer is thus defined as a consecutive addition and fragmentation to the "right".

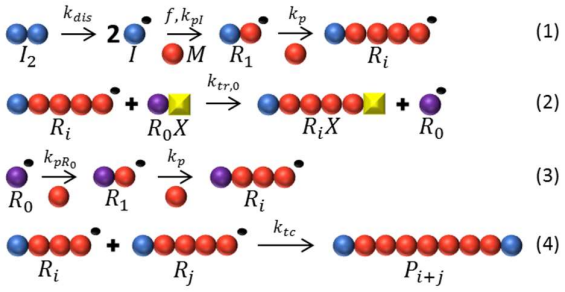

Figure 3.7*: Simplified reaction scheme for MADIX homopolymerization of styrene with OEXEP as initial RAFT agent, starting from the general RAFT polymerization reaction scheme (Figure 3.1). Other steps of Figure 3.1 are kinetically insignificant.*

The $C_{tr,0}$ value obtained through multi-response regression analysis (0.80 ± 0.02) is larger than the value obtained following the previously developed methods of Mayo (0.71 ± 0.02; Section A19 of Appendix A) and Moad (0.69 ± 0.04; Section A19 of Appendix A), [7,15,16,20,35] which focus only on x_n and $X_{M/R0X}$ data, respectively. As demonstrated in Figure 3.8 (entry 4 in Table A1 in Appendix A), the increased $C_{tr,0}$ value results in a good prediction of all average MADIX characteristics, whereas the use of the lower values obtained from the literature methods lack the capability of accurately predicting experimental x_n and x_m data. With the two literature methods, too high average chain lengths are simulated at all times. For the Mayo method, this inaccurate reflection of the x_n data seems at first sight surprising as the $C_{tr,0}$ is determined based on this response only. As explained in Section A20 in Appendix A, the Mayo method is only fully accurate if the theoretical kinetic chain length can be represented by the experimentally accessible x_n, which is only true in the absence of dead chains formed by termination by recombination. This highlights the relevance of multi-response regression analysis using the detailed modelling strategy in the present work.

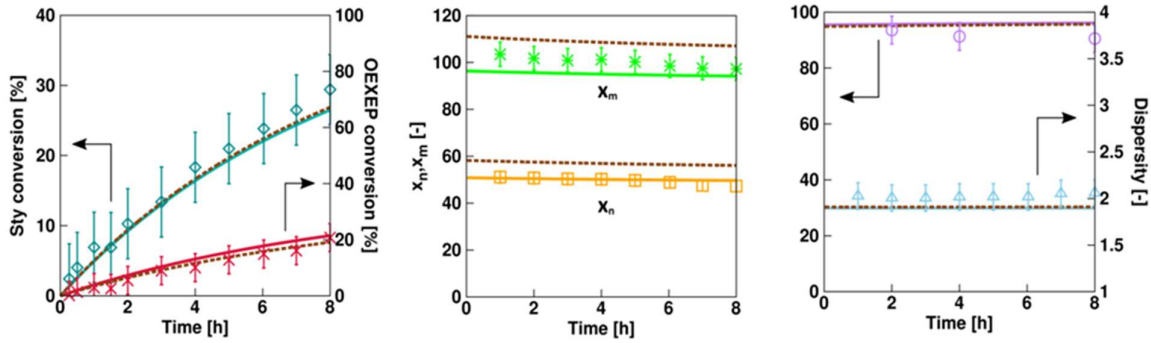

***Figure 3.8**: Relevance of applying multi-response regression analysis to all average MADIX characteristics to estimate $C_{tr,0}$ compared to previously developed methods by Mayo[39] and Moad[15,16,35] which focus only on respectively x_n and $X_{M/R0X}$ data; entry 4 in Table A1 of Appendix A with full lines corresponding to the results with the multi-response regression analysis ($C_{tr,0}$= 0.80; this work) and the brown dashed lines ($C_{tr,0}$= 0.69) after application of the literature methods (Section A19 of Appendix A).*

Another advantage of the modelling strategy is the possibility to map the MADIX characteristics over a broad operating window, as shown in Figure 3.9 focusing on the simultaneous prediction of the reaction time, x_n, EGF, and $Đ$ at a fixed X_m of 20%, with $[M]_0/[\mathrm{R_0X}]_0$ and $[\mathrm{R_0X}]_0/[I_2]_0$ values ranging respectively from 10 to 500 and from 1 to 50. As shown in Figure A14 in Appendix A for every condition in Figure 3.9 the R_0X conversion (X_{R0X}) is equal to *ca.* 16%, again highlighting the low reactivity of xanthates towards styryl macroradicals and that the exchange with the initial RAFT agent is dominant in the selected MADIX homopolymerization.

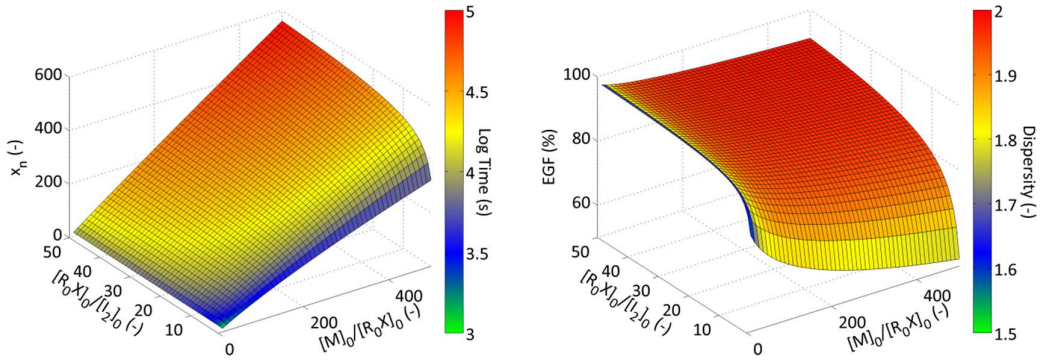

Figure 3.9*: Number-average chain length (x_n, left) and end-group functionality (EGF, right) as a function of $[R_0X]_0/[I_2]_0$ (ranging from 1 to 50) and $[M]_0/[R_0X]_0$ (ranging from 10 to 500) and the corresponding polymerization time (left; color) and dispersity (right; colour); simulated data have been achieved by means of the parameters given in Table A3 with R_0X equal to (O-ethyl xanthate)-2-ethyl propionate, M=Sty, and I_2=AIBN; 70°C; X_m=20%*

Since R_0X acts as a conventional CTA, as indicated above, it follows from Figure 3.9 (left) that x_n can be controlled by varying its initial concentration. In agreement with the results in Figure 3.5, an increase of $[\mathrm{R_0X}]_0/[I_2]_0$ leads to higher EGF values (Figure 3.9; right) but also to higher reaction times (Figure 3.9; left). Additionally, high $Đ$ (close to 2; Figure 3.9 right) values are obtained under all conditions, except at very low $[M]_0/[\mathrm{R_0X}]_0$ for which $Đ$ is reduced to a value close to 1.5. As shown in Table 3.1, the coefficients of variation of both the dormant and

dead polymer CLD ($CV(RX)$ and $CV(P)$), which are defined as the ratio of the standard deviations (that are related to the dispersities) to the number average chain lengths, are lower for a decreasing $[M]_0/[\mathrm{R_0X}]_0$ explaining the aforementioned trend for the (overall) *Đ*. Note that the dormant population is the key contributor to *Đ*, as high EGF values always result. As explained above (Figure 3.7), the latter population is formed by a single RAFT exchange. Hence, by adding more R_0X for a given initial M amount a more rapid chain transfer takes place. This leads to a lowering of *Đ*, eventually to a value of 1.5.

***Table 3.1**: Đ, EGF, and x_n for two different $[M]_0/[R_0X]_0$ in Figure 3.9 (X_m=20%) with the coefficient of variation CV (ratio of CLD standard deviation to mean value ($\underline{x_n}$)), differentiating between dormant (RX) and dead (P) polymer*

$[M]_0/[R_0X]_0/[I_2]_0$	*Đ*	*EGF*	x_n	CV_{tot}	$CV(RX)$	$CV(P)$
10/1/0.2	1.66	0.91	14.18	0.81	0.95	0.68
50/1/0.2	1.88	0.86	55.78	0.94	0.99	0.71

In addition, the detailed *k*MC simulations allow to explicitly visualize the microstructure of individual chains, including a differentiation according to the end-groups as defined in Figure 3.3 (top right). For instance for entry 3 in Table A1 in Appendix A, Figure 3.10 (top) shows the lengths and end-groups of *ca.* 1500 randomly selected chains out of a *k*MC simulation system consisting of *ca.* 10^8 chains, at t=8h (X_m=60%). Below the white dashed line the dormant chains are depicted and above this line the dead chains. In agreement with the previous results and discussions, it follows that most chains are dormant as the majority of chains are below the white dashed line. A more detailed analysis shows that a significant part of the dormant and dead chains have the undesired *I* end-group, confirming the difficult R_0X consumption. Clearly, a high scatter in chain lengths is obtained with in particular a strong deviation in the contribution

of the dormant and dead macrospecies which are respectively shorter and longer than the mean value (x_n=51).

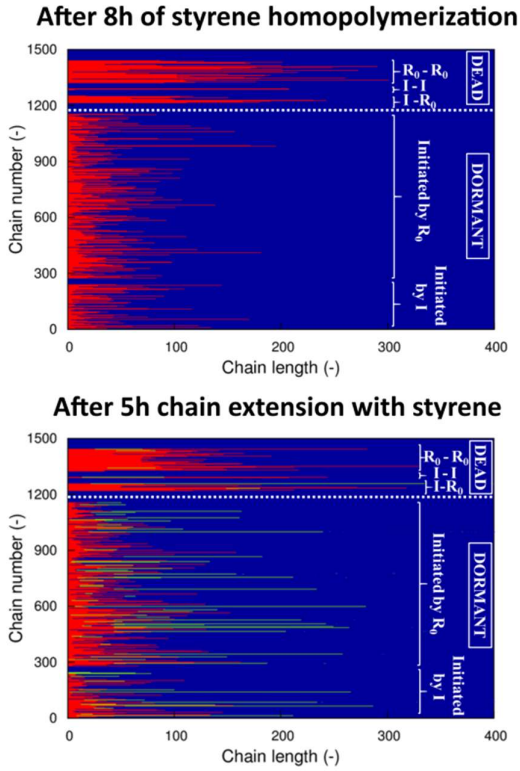

***Figure 3.10**: Visualization of the detailed microstructure of ca. 1500 individual chains for homopolymerization of styrene (top, after 8h, red, x_n=51) and its subsequent chain extension with fresh styrene (bottom, after 5h; green, x_n=60); simulated with kMC with ca. 10^8 chains. Conditions: top: entry 3 in Table A1; bottom: entry 3 in Table A2; model parameters: Table A3.*

3.4.4 Microstructural control upon chain extension with styrene

As explained above, an efficient R_0X removal is obtained without altering the original SEC trace upon dialysis of the homopolymer. Consequently, by addition of fresh styrene and AIBN to the purified polymer, potential chain extension can be investigated. Importantly k_{tr} is then the only relevant transfer rate coefficient as exclusively styrene macrospecies are present. Hence, by regression analysis based on X_m, x_n, x_m, and $Đ$ data from chain extension experiments (points in Figure 3.11; 70 °C) this RAFT exchange parameter can be estimated.

As shown in Figure A15 of Appendix A, the most valuable data for this parameter tuning are the x_m and $Đ$ data, resulting in $k_{tr} = (2.1 \pm 0.4)$ x 10^2 L mol^{-1} s^{-1}. The corresponding C_{tr} reaches a value of 0.44 ± 0.07. Narrow confidence intervals are thus obtained for the macro-RAFT exchange kinetic parameters which is reflected in the good agreement between the experimental and deterministic simulation results in Figure 3.11. Notably, the obtained k_{tr} (Equation (3)) value is 45% lower than the estimated $k_{tr,0}$ (Equation (1)) value of (3.8 ± 0.1) x 10^2 L mol^{-1} s^{-1}. This lowering is kinetically significant as demonstrated in Figure A15 in Appendix A in which different simulation results of several polymer characteristics are obtained in case k_{tr} is assumed equal to $k_{tr,0}$.

Based on Equation (3) it further follows that $k_{add} = 2k_{tr} = 4.2$ x 10^2 L mol^{-1} s^{-1} (70°C). Reminding that $k_{tr,0}$ is on a fundamental level related to the addition and fragmentation reactions in Figure 3.12 also here further mechanistic insights can be obtained *a posteriori*, based on Equation (1). If it is assumed that $k_{add,0,a}$ (RAFT addition of R_i to R_0X) is equal to k_{add}, consistent with the common claim that the RAFT addition rate coefficient is mainly influenced by the nature of the Z group, it follows from Equation (1) that the fragmentation probability $\varphi_{0,b}$ for the intermediate R_0XR_1 toward R_0 is equal to 0.9 (see also Table A3 in Appendix A). The latter is unexpected as this would imply a much higher stability for R_0 (bond dissociation energy[105] of R_0-H = 394 kJ mol^{-1}) compared to the secondary benzylic R_i radical (bond dissociation energy[106] of R_i-H = 354-378 kJ mol^{-1}). More plausible is thus to assume $\varphi_{0,b}$ lower than 0.9 resulting in a $k_{add,0,a}$ higher than k_{add}. Hence, both the Z and R group are important in determining the RAFT addition reactivity and by extension the overall transfer coefficient. Nonetheless, the Z group remains paramount as it determines the order of magnitude of $k_{tr(,0)}$ as for instance demonstrated by the difference for xanthates and trithiocarbonates in combination with LAMs/MAMs.

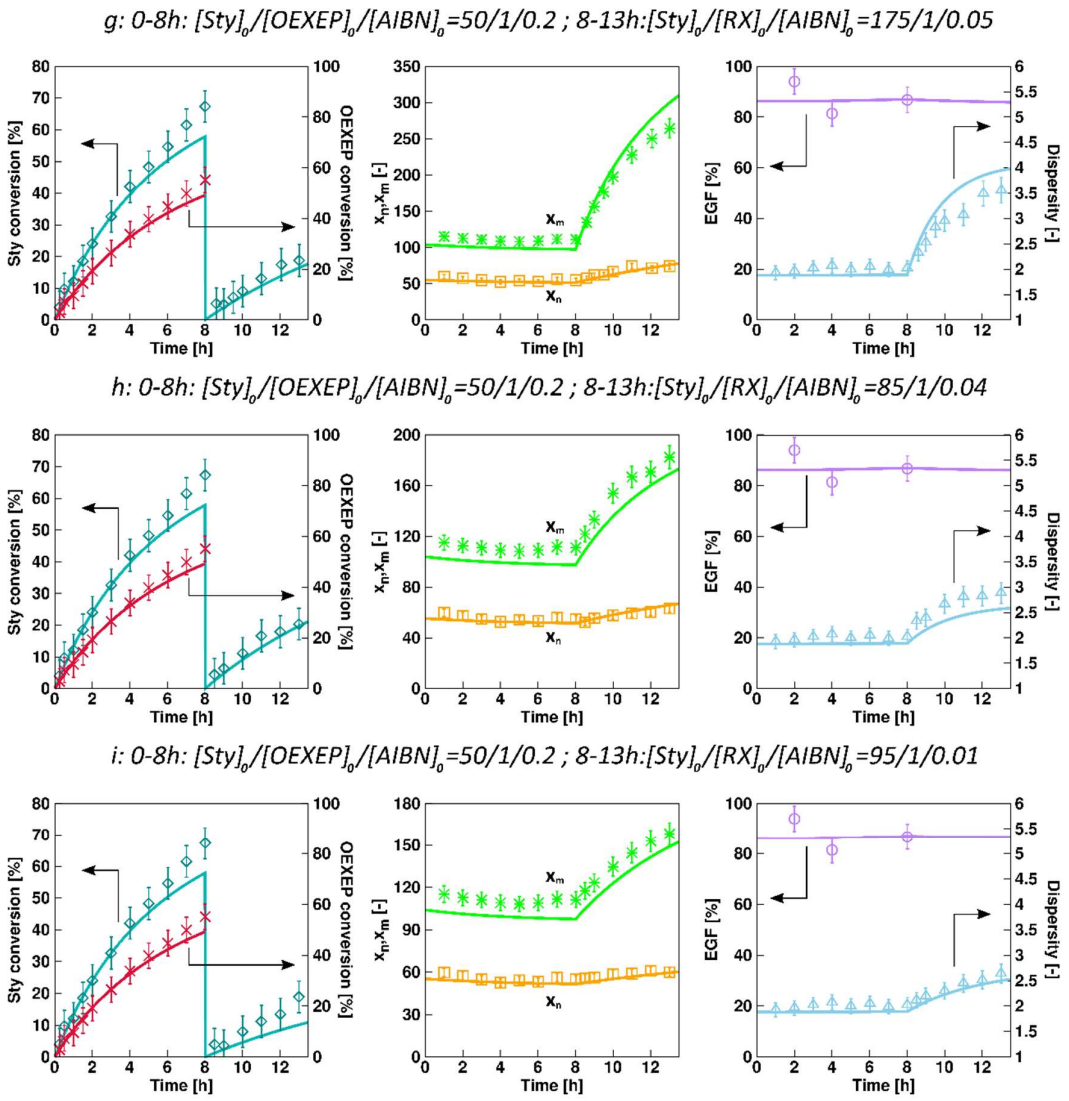

***Figure 3.11**: Comparison between simulated and experimental data for MADIX homopolymerization of styrene (0-8h; entry 3 in Table A1 in Appendix A) and subsequent chain extension of (dormant) polystyrene (after purification via dialysis) with fresh styrene (8-13h; entry 1-3 in Table A2 in Appendix A); 70°C; Monomer conversion (X_m, dark blue), R_0X conversion (X_{R0X}, red), number-average chain length (x_n, orange), mass-average chain length (x_m, green), dispersity (Đ, purple), and end-group functionality (EGF, light blue) as a function of time; Lines correspond to calculated values with rate coefficients given in Table A3 in Appendix A and accounting for diffusional limitations (parameters in Table A4); simulated output with deterministic method.*

Further inspection of Figure 3.11 shows that the chain extension with fresh styrene results in an increase of x_n, x_m and $Đ$ while having a negligible effect on EGF. This weak dependence for EGF is due to the relatively low amount of newly formed dead chains. The latter can be most easily derived from Figure 3.10 (bottom) which shows the explicit growth of the chains as accessible via the *k*MC simulations (conditions: entry 3 in Table A2 in Appendix A) with the freshly incorporated styrene units in green colour and again making a distinction between the different end-groups. As can be seen, the fresh styrene is mainly incorporated in the macroradicals formed by the activation of the dormant species originating from the first synthesis step and much more "block"-copolymer chains are present than "green" homopolymer chains. Again a single (net) transfer, as countable via the *k*MC simulations,[107] takes place similar to the reaction scheme shown in Figure 3.7 with R_0X replaced by the dormant macrospecies (*RX*), taking into account that the additional styrene conversion remains sufficiently low (Figure 3.11).

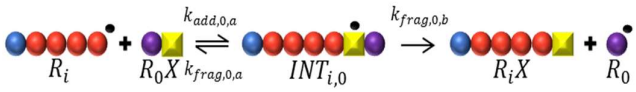

***Figure 3.12**: Exchange (2) in Figure 3.7 on the elementary level. Interpretation of Equation (1) starting from the estimated value for $k_{tr,0}$ with the kinetic model.*

The accuracy of the determination of $k_{tr,0}$ and k_{tr} is further confirmed in the SEC traces in Figure 3.13 which show good agreement between the experimental and simulated mass CLD after 8h of homopolymerization (green; X_m=65%; entry 3 in Appendix A Table A1) and subsequent 5h of chain extension with fresh styrene (blue; X_m=20%; entry 1 in Appendix A Table A2). A high molar mass shoulder is present after the chain extension, consistent with the simulations results in Figure 3.10 (middle). Consequently, although no typical RDRP control over the chain growth is possible, reactivation of the dormant species can still be achieved under the right circumstances, *i.e.* upon R_0X removal.

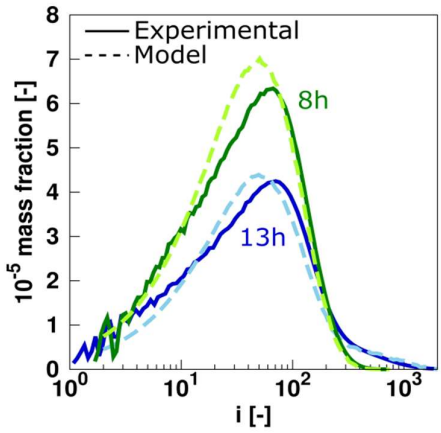

***Figure 3.13**: Comparison between the experimental (full lines) and simulated (dashed lines) mass CLD after 8h of homopolymerization (green; X_m=65%; entry 3 in Appendix A Table A1) and subsequent 5h of chain extension with fresh styrene (blue; X_m=20%; entry 1 Table A2 in Appendix A).*

3.4.5 Microstructural control upon chain extension with nBuA

To further illustrate the potential of the visualization tool, focus is on a second monomer in view of the synthesis of actual block copolymer chains. Not any monomer can be selected as the intermediate formed by exchange between the dormant species consisting of the first monomer (here styrene) and the macroradicals consisting of the second monomer must effectively fragment toward macroradicals of the first monomer type. An efficient reinitiation involving these radicals with the second monomer is needed as well to allow for chain extension and, hence, block copolymer formation.[108]

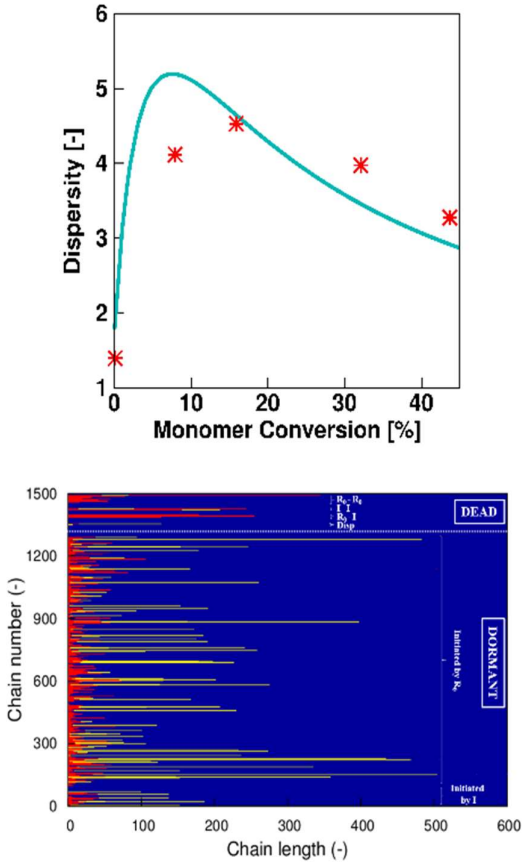

***Figure 3.14**: Top: Comparison between simulated (blue) and experimental (red) dispersity data[30] for MADIX chain extension of dormant polystyrene with n-butyl acrylate; reaction conditions: [Toluene]$_0$= 6 mol L^{-1}, [n-BuA]$_0$=2.0 mol L^{-1}, [n-BuA]$_0$/[$R_{i,sty}$X]$_0$/[AIBN]$_0$=198/1/1; T=60°C ;Bottom: Visualization of monomer sequences using kinetic Monte Carlo modelling after 20% monomer conversion of chain extension: red: styrene unit; yellow: n-butyl acrylate; parameters: Table A6 of Appendix A*

Based on the experimental work of Smulders et al.[30] *n*BuA is an interesting monomer. For example, Figure 3.14 (top) shows the model description of the experimental dispersity data[30] for the chain extension in toluene of dormant polystyrene synthesized with OEXEP. The corresponding simulated monomer sequences are provided in Figure 3.14 (bottom). Based on literature data and for simplicity backbiting and thus short chain branching is neglected.[109]

For the simulations in Figure 3.14, at first sight, four macro-RAFT exchange reactions are needed due to the possible presence of two macroradical and dormant species types, with either a styrene or *n*BuA terminal unit. Mathematically this implies an extension of Equation (3)

through the introduction of $k_{tr,XY}$ with X referring to the radical terminal unit and Y to the dormant terminal unit ($k_{tr,nB,nB}$; $k_{tr,nB,S}$; $k_{tr,S,S}$; $k_{tr,S,nB}$; S: styrene; nB: *n*BuA). However, as shown in Figure A16 in Appendix A and as explained in detail in Section A23 of Appendix A, for the low *n*BuA conversions as covered in the present work (≤ 45%), only the transfer coefficient for a macroradical with a *n*BuA terminal unit and a dormant species with a styrene terminal unit ($k_{tr,nBS}$) can be seen as kinetically significant. Styryl macroradicals which have been formed by activation of the original dormant polystyrene chains have already reacted with *n*BuA before RAFT exchange can occur, due to the typical low k_{tr} values for xanthates in combination with MAMs. Hence, only *n*BuA terminal radicals are present which reduces the number of exchange reactions already safely from 4 to 2 (remaining rate coefficients: $k_{tr,nBS}$ and $k_{tr,nBnB}$). Furthermore, due to the low concentration of dormant poly(styrene-block-*n*BuA) compared to the initial dormant polystyrene at low *n*BuA conversions, transfer of *n*BuA macroradicals with the dormant block copolymer species ($k_{tr,nBnB}$) is less relevant and can be neglected (Figure A17 in Appendix A). Supportive for this claim is also the expectation that $k_{tr,nB,nB}$ is lower than $k_{tr,nB,S}$, taking into account that the bond dissociation energy[110] of the benzylic C-H bond of ethyl benzene (354-378 kJ mol^{-1}) is lower than the one of the C-H bond in the alpha position of ethyl propionate (400 kJ mol^{-1}).[110] This implies that $k_{tr,nB,S}$ can be seen as the only kinetically relevant RAFT transfer coefficient, at least to a first approximation. The resulting simplified reaction scheme is shown in Figure 3.15, considering all kinetically relevant MADIX reactions for the chain extension of dormant polystyrene with *n*BuA up to intermediate conversion.

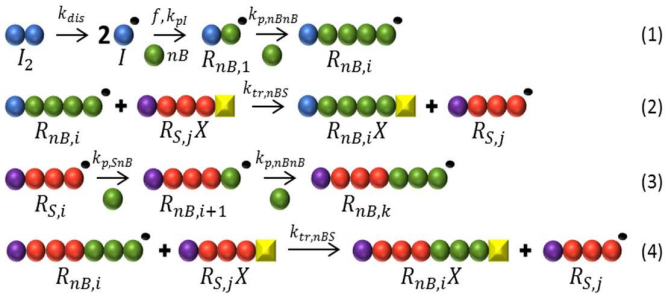

Figure 3.15*: Kinetically relevant MADIX reactions (termination by recombination/disproportionation not shown for simplicity) for the chain extension of dormant polystyrene (after dialysis to remove OEXEP) with nBuA up to intermediate conversions;* $R_{nB/S}$*: macroradical with n-butyl acrylate (nB; green spheres) or styrene (S; red spheres) as terminal unit. Similar notation for dormant species; styrene: red; nBuA: green as in Figure 3.10.*

Based on the data in Figure 3.14 (top), a preliminary value of 4.6 x 10^4 L mol^{-1} s^{-1} results for $k_{tr,nBS}$ which corresponds to a $C_{tr,nB,S}$ equal to 1.35 in agreement with the kinetic study of Smulders et al.[30] Such C_{tr} value can still be seen as relatively low but suffices to enable a successful MADIX chain extension, as confirmed by the *k*MC simulation results in Figure 3.14 (bottom).

3.5 Conclusions

A detailed understanding of MADIX under bulk/solution conditions is obtained by successfully combining experimental and modelling analysis tools, focusing both on conversion, chain length and EGF data. The latter data can be obtained by a combination of dialysis and elemental analysis, an insight relevant for all RAFT polymerizations and, hence, not restricted to exchange processes based on xanthates.

To accurately estimate $C_{tr,0}$ for the OEXEP/styrene MADIX system, multi-response regression analysis to homopolymerization data is recommended. On the other hand, C_{tr} can be reliably estimated to specifically x_m data upon polymer isolation, using dialysis and applying chain extension. For OEXEP and styrene, a $C_{tr,0}$ and C_{tr} of respectively 0.80±0.02 and 0.44±0.07

result, highlighting the influence of both the R and Z group of the agent on the RAFT addition and fragmentation coefficients. For chain extension with *n*BuA, a C_{tr} of 1.35 is put forward in the present work, reflecting the reactivity for RAFT exchange of macroradicals with a *n*BuA terminal unit and dormant macrospecies with a styrene terminal unit.

The use of advanced kinetic Monte Carlo simulations enables visualization of the chain growth and end-groups of individual macrospecies, both during homopolymerization and chain extension. For the selected MAM systems and monomer conversions, the dormant macrospecies are always formed via a single exchange, which implies a transfer behaviour as in a conventional free radical polymerization, although with a slight delay due to the reversible nature of the first addition/fragmentation step. Hence, bulk MADIX with MAMs behaves mechanistically different than classical bulk RAFT polymerizations with consecutive well-defined activation-growth-deactivation cycles.

3.6 References

1 J. Chiefari, Y. K. B. Chong, F. Ercole, J. Krstina, J. Jeffery, T. P. T. Le, R. T. A. Mayadunne, G. F. Meijs, C. L. Moad, G. Moad, E. Rizzardo, S. H. Thang and C. South, *Macromolecules*, 1998, **31**, 5559–5562.

2 G. Gody, T. Maschmeyer, P. B. Zetterlund and S. Perrier, *Macromolecules*, 2014, **47**, 3451–3460.

3 G. Gody, T. Maschmeyer, P. B. Zetterlund and S. Perrier, *Macromolecules*, 2014, **47**, 639–649.

4 X. Zhang, S. Boissé, W. Zhang, P. Beaunier, F. D'Agosto, J. Rieger and B. Charleux, *Macromolecules*, 2011, **44**, 4149–4158.

5 C. Barner-kowollik, *Handbook of RAFT Polymerization*, Wiley-VCH, Weinheim, 2008.

6 P. Lebreton, B. Ameduri, B. Boutevin and J. M. Corpart, *Macromol. Chem. Phys.*, 2002, **203**, 522–537.

7 M. M. Adamy, A. M. van Herk, M. Destarac and M. J. Monteiro, *Macromolecules*, 2003, **36**, 2293–2301.

8 P. Derboven, P. Van Steenberge, M.-F. Reyniers, C. Barner-Kowollik, D. R. D'hooge and G. B. Marin, *Polym. Chem.*, 2016, **7**.

9 Y. Kwak, A. Goto, Y. Tsujii, Y. Murata, K. Komatsu and T. Fukuda, *Macromolecules*, 2002, **35**, 3026–3029.

10 Y. Kwak, A. Goto and T. Fukuda, *Macromolecules*, 2004, **37**, 1219–1225.

11 N. De Rybel, P. H. M. Van Steenberge, M.-F. Reyniers, C. Barner-Kowollik, D. R. D'hooge and G. B. Marin, *Macromol. Theory Simulations*, 2017, **26**, 1600048.

12 D. Konkolewicz, B. S. Hawkett, A. Gray-Weale and S. Perrier, *Macromolecules*, 2008, **41**, 6400–6412.

13 C. Barner-Kowollik and S. Perrier, *J. Polym. Sci. Part A Polym. Chem.*, 2008, **46**, 5715–5723.

14 C. Barner-Kowollik, J. F. Quinn, D. R. Morsley and T. P. Davis, *J. Polym. Sci. Part A Polym. Chem.*, 2001, **39**, 1353–1365.

15 J. Chiefari, R. T. A. Mayadunne, C. L. Moad, G. Moad, E. Rizzardo, A. Postma, M. A. Skidmore and S. H. Thang, *Macromolecules*, 2003, **36**, 2273–2283.

16 B. Y. K. Chong, J. Krstina, T. P. T. Le, G. Moad, A. Postma, E. Rizzardo and S. H. Thang, *Macromolecules*, 2003, **36**, 2256–2272.

17 M. Destarac, *Polym. Rev.*, 2011, **51**, 163–187.

18 G. Moad, C. M. Flagship and B. Ave, 2015.

19 G. Moad, E. Rizzardo and S. H. Thang, *Aust. J. Chem.*, 2012, **65**, 985–1076.

20 P. Derboven, P. H. M. Van Steenberge, M. Reyniers, C. Barner-kowollik, D. R. D'hooge and G. B. Marin, *Macromol. Theory Simulations*, 2016, **25**, 104–115.

21 M. R. Hill, R. N. Carmean and B. S. Sumerlin, *Macromolecules*, 2015, **48**, 5459–5469.

22 S. Perrier and P. Takolpuckdee, *J. Polym. Sci. Part A Polym. Chem.*, 2005, **43**, 5347–5393.

23 L. Seiler, J. Loiseau, F. Leising, P. Boustingorry, S. Harrisson and M. Destarac, *Polym. Chem.*, 2017, Accepted.

24 E. Rizzardo and D. H. Solomon, *Aust. J. Chem.*, 2012, **65**, 945–969.

25 A. Ilchev, R. Pfukwa, L. Hlalele, M. Smit and B. Klumperman, *Polym. Chem.*, 2015, **6**, 7945–7948.

26 G. Pound, J. B. McLeary, J. M. McKenzie, R. F. M. Lange and B. Klumperman, *Macromolecules*, 2006, **39**, 7796–7797.

27 G. Pound, F. Aguesse, J. B. McLeary, R. F. M. Lange and B. Klumperman, *Macromolecules*, 2007, **40**, 8861–8871.

28 I. Van Nieuwenhove, S. Maji, M. Dash, S. Van Vlierberghe, R. Hoogenboom and P. Dubruel, *Polym. Chem.*, 2017, **8**, 2433–2437.

29 M. H. Stenzel, L. Cummins, G. E. Roberts, T. P. Davis, P. Vana and C. Barner-Kowollik, *Macromol. Chem. Phys.*, 2003, **204**, 1160–1168.

30 W. Smulders and M. J. Monteiro, *Macromolecules*, 2004, **37**, 4474–4483.

31 WO 1998058974, 1998.

32 W. Smulders, R. G. Gilbert and M. J. Monteiro, *Macromolecules*, 2003, **36**, 4309–4318.

33 M. J. Monteiro and J. De Barbeyrac, *Macromolecules*, 2001, **34**, 4416–4423.

34 M. P. F. Pepels, C. I. Holdsworth, S. Pascual and M. J. Monteiro, *Macromolecules*, 2010, **43**, 7565–7576.

35 G. Moad, J. Chiefari, Y. K. Chong, J. Krstina, R. T. A. Mayadunne, A. Postma, E. Rizzardo and S. H. Thang, *Polym. Int.*, 2000, **49**, 993–1001.

36 M. Destarac, W. Bzducha, D. Taton, I. Gauthier-Gillaizeau and S. Z. Zard, *Macromol. Rapid Commun.*, 2002, **23**, 1049–1054.

37 M. Destarac, C. Brochon, J. M. Catala, A. Wilczewska and S. Z. Zard, *Macromol. Chem. Phys.*, 2002, **203**, 2281–2289.

38 A. H. E. Muller, R. G. Zhuang, D. Y. Yan and G. Litvinenko, *Macromolecules*, 1995, **28**, 4326–4333.

39 F. R. Mayo, *J. Am. Chem. Soc.*, 1943, **65**, 2324–2329.

40 P. A. Clay and R. G. Gilbert, *Macromolecules*, 1995, **28**, 552–569.

41 A. Goto, T. Terauchi, T. Fukuda and T. Miyamoto, *Macromol. Rapid Commun.*, 1997, **18**, 673–681.

42 T. Fukuda and A. Goto, *Macromol Rapid Commun*, 1997, **18**, 683–688.

43 A. Goto, K. Sato, Y. Tsujii, T. Fukuda, G. Moad, E. Rizzardo and S. H. Thang, *Macromolecules*, 2001, **34**, 402–408.

44 S. W. Prescott, M. J. Ballard, E. Rizzardo and R. G. Gilbert, *Aust. J. Chem.*, 2002, **55**, 415.

45 M. F. Cunningham, *Prog. Polym. Sci.*, 2008, **33**, 365–398.

46 P. B. Zetterlund, *Polym. Chem.*, 2011, **2**, 534–549.

47 P. B. Zetterlund, S. C. Thickett, S. Perrier, E. Bourgeat-Lami and M. Lansalot, *Chem. Rev.*, 2015, **115**, 9745–9800.

48 P. B. Zetterlund, Y. Kagawa and M. Okubo, *Chem. Rev.*, 2008, **108**, 3747–94.

49 J. M. Asua, *Prog. Polym. Sci.*, 2014, **39**, 1797–1826.

50 E. Mastan, X. Li and S. Zhu, *Prog. Polym. Sci.*, 2015, **45**, 71–101.

51 D. R. D'hooge, P. H. M. Van Steenberge, M.-F. Reyniers and G. B. Marin, *Prog. Polym. Sci.*, 2016, **58**, 59–89.

52 M. J. Monteiro and M. F. Cunningham, *Macromolecules*, 2012, **45**, 4939–4957.

53 M. J. Monteiro, *J. Polym. Sci. Part A Polym. Chem.*, 2005, **43**, 5643–5651.

54 Y. Luo, R. Wang, L. Yang, B. Yu, B. Li and S. Zhu, *Macromolecules*, 2006, **39**, 1328–1337.

55 I. S. Altarawneh, V. G. Gomes and M. S. Srour, *Macromol. React. Eng.*, 2008, **2**, 58–79.

56 S. M. Jung and V. G. Gomes, *Macromol. React. Eng.*, 2011, **5**, 303–315.

57 D. R. D'hooge, P. H. M. Van Steenberge, P. Derboven, M.-F. Reyniers and G. B. Marin, *Polym. Chem.*, 2015, **6**, 7081–7096.

58 P. H. M. Van Steenberge, D. R. D'hooge, M. F. Reyniers, G. B. Marin and M. F. Cunningham, *Macromolecules*, 2014, **47**, 7732–7741.

59 Y. N. Zhou, C. M. Guan and Z.-H. Luo, *Eur. Polym. J.*, 2010, **46**, 2164–2173.

60 Z.-H. Luo, X.-L. Zhan and Y.-R. Yang, *J. Shanghai Univ.*, 2006, **10**, 274–276.

61 W. W. Smulders, Technische Universiteit Eindhoven, 2002.

62 J. Vandenbergh and T. Junkers, *Macromolecules*, 2014, **47**, 5051–5059.

63 J. C. Bevington, J. R. Ebdon and T. N. Huckerby, *Eur. Polym. J.*, 1985, **21**, 685–694.

64 C. Lefay, J. Belleney, B. Charleux, O. Guerret and S. Magnet, *Macromol. Rapid Commun.*, 2004, **25**, 1215–1220.

65 J. C. Bevington and T. N. Huckerby, *Eur. Polym. J.*, 2006, **42**, 1433–1436.

66 A. Postma, T. P. Davis, a. R. Donovan, G. Li, G. Moad, R. Mulder and M. S. O'Shea, *Polymer (Guildf).*, 2006, **47**, 1899–1911.

67 J.-F. Lutz and K. Matyjaszewski, *J. Polym. Sci. Part A Polym. Chem.*, 2005, **43**, 897–910.

68 K. Matyjaszewski, S. M. Jo, H. Paik and D. a Shipp, *Macromolecules*, 1999, **32**, 6431–6438.

69 H. Willcock and R. K. O'Reilly, *Polym. Chem.*, 2010, **1**, 149.

70 M. Rodlert, E. V. A. Harth, I. A. N. Rees and C. J. Hawker, *J. Polym. Sci. Part A Polym. Chem.*, 2000, **38**, 4749–4763.

71 M. Dourges, B. Charleux, J. Vairon and J. Tabet, *Macromolecules*, 1999, **32**, 2495–2502.

72 M. Bednarek, T. Biedron and P. Kubisa, *Macromol. Chem. Phys.*, 2000, **201**, 58–66.

73 S. O. Hammouch and J. Catala, *Macromol. Rapid Commun.*, 1996, **17**, 149–154.

74 M. J. Monteiro, M. M. Adamy, B. J. Leeuwen and A. M, *Society*, 2005, **46**, 4–5.

75 M. J. Monteiro, M. Sjöberg, J. Van Der Vlist and C. M. Göttgens, *J. Polym. Sci. Part A Polym. Chem.*, 2000, **38**, 4206–4217.

76 J. D. Woloszyn and K. B. Mcauley, *Macromol. React. Eng.*, 2011, **5**, 453–466.

77 P. Derboven, P. H. M. Van Steenberge, M. Reyniers, C. Barner-kowollik, R. D. Dagmar and G. B. Marin, *Macromol. Theory Simulations*, 2016, **25**, 104–115.

78 E. Mastan and S. Zhu, *Eur. Polym. J.*, 2015, **68**, 139–160.

79 D. R. D'hooge, M.-F. Reyniers and G. B. Marin, *Macromol. React. Eng.*, 2009, **3**, 185–209.

80 D. R. D'hooge, M. F. Reyniers and G. B. Marin, *Macromol. React. Eng.*, 2013, **7**, 362–379.

81 W. Wang, Y. Zhou, L. Shi and Z.-H. Luo, *Ind. Eng. Chem. Res.*, 2014, **53**, 11873–11883.

82 Y.-N. Zhou and Z.-H. Luo, *Macromol. React. Eng.*, 2016, **10**, 516–534.

83 D. T. Gillesple, *J. Phys. Chem.*, 1977, **81**, 2340–2361.

84 P. H. M. Van Steenberge, D. R. D'hooge, M.-F. Reyniers and G. B. Marin, *Chem. Eng. Sci.*, 2014, **110**, 185–199.

85 P. H. M. Van Steenberge, D. R. D'hooge, Y. Wang, M. Zhong, M.-F. Reyniers, D. Konkolewicz, K. Matyjaszewski and G. B. Marin, *Macromolecules*, 2012, **45**, 8519–8531.

86 R. H. Byrd, P. T. Boggs, J. E. Rogers and R. B. Schnabel, *ODRPACK Software for Orthogonal Distance Regression*, 1992.

87 I. Chavez-Sumarriva, P. H. M. Van Steenberge and D. R. D'hooge, *Ind. Eng. Chem. Res.*, 2016, **55**, 9387–9396.

88 C. Toloza Porras, D. R. D'hooge, P. H. M. Van Steenberge, M. F. Reyniers and G. B. Marin, *Ind. Eng. Chem. Res.*, 2014, **53**, 9674–9685.

89 A. Theis, T. P. Davis, M. H. Stenzel and C. Barner-Kowollik, *Polymer (Guildf).*, 2006, **47**, 999–1010.

90 P. Vana, T. P. Davis and C. Barner-Kowollik, *Macromol. Rapid Commun.*, 2002, **23**, 952–956.

91 G. Johnston-Hall, M. H. Stenzel, T. P. Davis, C. Barner-Kowollik and M. J. Monteiro, *Macromolecules*, 2007, **40**, 2730–2736.

92 P. Derboven, D. R. D'hooge, M.-F. Reyniers, G. B. Marin and C. Barner-Kowollik, *Macromolecules*, 2015, **48**, 492–501.

93 T. Junkers, A. Theis, M. Buback, T. P. Davis, M. H. Stenzel, P. Vana and C. Barner-Kowollik, *Macromolecules*, 2005, **38**, 9497–9508.

94 G. Johnston-Hall, A. Theis, M. J. Monteiro, T. P. Davis, M. H. Stenzel and C. Barner-Kowollik, *Macromol. Chem. Phys.*, 2005, **206**, 2047–2053.

95 A. Theis, T. P. Davis, M. H. Stenzel and C. Barner-Kowollik, *Macromolecules*, 2005, **38**, 10323–10327.

96 A. Theis, A. Feldermann, N. Charton, T. P. Davis, M. H. Stenzel and C. Barner-Kowollik, *Polymer (Guildf).*, 2005, **46**, 6797–6809.

97 A. Theis, A. Feldermann, N. Charton, M. H. Stenzel, T. P. Davis and C. Barner-kowollik, *Macromolecules*, 2005, **38**, 2595–2605.

98 A. Feldermann, M. H. Stenzel, T. P. Davis, P. Vana and C. Barner-Kowollik, *Macromolecules*, 2004, **37**, 2404–2410.

99 S. K. Fierens, P. H. M. Van Steenberge, M.-F. Reyniers, D. R. D'hooge and G. B. Marin, *AIChE J.*, 2017, Provisionally accepted.

100 A. M. Rabea and S. Zhu, *Polymers (Basel).*, 2015, **7**, 819–835.

101 G. Johnston-Hall and M. J. Monteiro, *J. Polym. Sci. Part a-Polymer Chem.*, 2008, **46**, 3155–3176.

102 N. De Rybel, P. H. M. Van Steenberge, M.-F. Reyniers, D. R. D'hooge and G. B. Marin, *Chem. Eng. Sci.*, 2017, **177**, 163-179

103 R. V. Hogg, A. Craig and J. W. McKean, *Introduction to Mathematical Statistics*, 6th edn., 2005.

104 G. Odian, *Principles of Polymerization*, John Wiley & Sons, New Jersey, 2004.

105 A. M. El-Nahas, M. V. Navarro, J. M. Simmie, J. W. Bozzelli, H. J. Curran, S. Dooley and W. Metcalfe, *J. Phys. Chem. A*, 2007, **111**, 3727–3739.

106 A. O'Mally and B. K. Hodnett, *Stud. Surf. Sci. Catal.*, 1997, **110**, 1137–1144.

107 S. K. Fierens, S. Telitel, P. H. M. Van Steenberge, M.-F. Reyniers, G. B. Marin, J.-F. Lutz and D. R. D'hooge, *Macromolecules*, 2016, **49**, 9336–9344.

108 D. J. Keddie, *Chem. Soc. Rev.*, 2014, **43**, 496–505.

109 D. Konkolewicz, S. Sosnowski, R. D. Dagmar, R. Szymanski, G. B. Marin and K. Matyjaszewski, *Macromolecules*, 2011, **44**, 8361–8373.

110 Y.-R. Luo, *Handbook of Bond Dissociation Energies in Organic Compounds*, CRC Press, 2003.

Chapter 4: Deterministic modeling of degenerative RAFT miniemulsion polymerization rate and average polymer characteristics: invalidity of zero-one nature at higher monomer conversions

4.1 Introduction

The exploitation of reversible deactivation radical polymerization (RDRP) has allowed the synthesis of narrow molar mass distributed polymers possessing well-defined end-group functionalities, enabling the design of tailor-made molecular architectures such as block, star, comb-like, and dendritic (co)polymers.[1–5] Although several types of RDRP have been developed over the last decennia, reversible addition-fragmentation chain transfer (RAFT) polymerization has demonstrated to be one of the most valuable ones, due to its applicability over a wide monomer range (*e.g.* styrene, methyl methacrylate (MMA), vinyl acetate, *etc.*) and working temperatures (258 to 453 K) while being compatible with a variety of solvents.[1,6–8]

$$I_2 \xrightarrow{k_{dis}} 2I^{\bullet} \xrightarrow[M]{f,k_{pI}} R_1^{\bullet} \xrightarrow[M]{k_p} R_i^{\bullet} \quad (1)$$

$$R_i^{\bullet} + R_0X \underset{k_{-tr,0}}{\overset{k_{tr,0}}{\rightleftharpoons}} R_iX + R_0^{\bullet} \quad (2)$$

$$R_0^{\bullet} \xrightarrow[M]{k_{pR_0}} R_1^{\bullet} \xrightarrow[M]{k_p} R_i^{\bullet} \quad (3)$$

$$R_i^{\bullet} + R_jX \underset{k_{tr}}{\overset{k_{tr}}{\rightleftharpoons}} R_iX + R_j^{\bullet} \quad (4)$$

$$R_i^{\bullet} + R_j^{\bullet} \xrightarrow{k_{tc}} P_{i+j} \quad (5)$$

$$R_i^{\bullet} + R_j^{\bullet} \xrightarrow{k_{td}} P_i + P_j \quad (6)$$

Figure 4.1*: Representation of the simplified degenerative RAFT mechanism; I_2: conventional radical initiator, $I^{\bullet}$: fragment originating from I_2, M: monomer, $R_i^{\bullet}$: macroradical with chain length i (≥1), R_0X: initial (small) RAFT agent, $R_0^{\bullet}$: RAFT leaving group radical, R_iX: dormant macrospecies (i≥1), P_i: dead polymer species; $k_{dis,pI,p,tr0,-tr0,pR0,tr,tc,td}$: rate coefficient for dissociation, chain initiation with $I^{\bullet}$, propagation, transfer (or exchange) with initial RAFT agent (R_0X) and macroradical, transfer between RAFT leaving group ($R_0^{\bullet}$) and dormant macrospecies (RX), chain initiation with $R_0^{\bullet}$, transfer between macroradicals ($R^{\bullet}$) and dormant macrospecies (RX), termination by recombination, and termination by disproportionation; f: conventional initiator efficiency.*

In RAFT polymerization, control over chain growth is obtained by the introduction of a small initial agent R_0X to otherwise a conventional free radical polymerization (FRP) process. The essential reactions are shown in Figure 4.1, assuming for simplicity a so-called degenerative mechanism for the RAFT exchange. A fast exchange/transfer between a macroradical ($R_i^\bullet$; i= chain length) and a dormant (macro-)species ($R_iX, i \geq 0$) ensures a concurrent growth of all the dormant macrospecies. If the amount of dead polymer chains formed due to inevitable termination is low compared to the total amount of polymer chains and the R_0X consumption is fast, a low-dispersity "living" polymer is obtained.

The RAFT transfers shown in Figure 4.1 ("reaction" 2 and 4) in principle consist of two elementary steps, namely a radical addition to C=S followed by a fragmentation or β-scission. However, if the fragmentation rate coefficients are sufficiently high and side reactions involving the formed intermediate radicals (*e.g.* RAFT cross-termination leading to star formation) can be neglected, the mechanism can be simplified to a degenerative one characterized by formal transfer "rate coefficients" ($k_{(-),tr,(0)}$).[9–14] Previous research[15–21] suggests that this is the case for the RAFT agent/monomer combination considered in the present work, *i.e.* 2-cyanoprop-2-yl dithiobenzoate (CPDB)/MMA. In particular, Buback *et al.*[15] highlighted that the decrease of the bulk polymerization rate of MMA with increasing initial CPDB concentration can be adequately explained by the chain-length dependency of the (average) apparent termination rate coefficient and no slow fragmentation or RAFT cross-termination is needed to explain the kinetic data.

From an industrial point of view, the application of RAFT polymerization in dispersed media is favored due to the absence of organic volatile solvents, easily manageable control of the generated reaction heat, process flexibility including semi-batch addition of reagents, high yield, and straightforwardly isolatable product.[22–28] Specifically RAFT polymerization in "compartmentalized nanoreactors" as encountered under emulsion polymerization conditions

is promising. Emulsion polymerization allows to lower the number of radicals per particle and therefore to increase the rate and livingness of the RAFT polymerization.[1,29–31] In the limit one radical per active particle can be achieved, which is impossible under bulk conditions in which radicals can easily find each other in one "big particle" with thus no segregation as shown in Figure 4.2 for two nanoparticles (black box; middle). The most commonly applied emulsion technique is macro-emulsion polymerization,[22,23] in which large monomer droplets are present along with aqueous phase initiator and monomer swollen micelles, the latter being converted into polymer particles because of radical entry (heterogeneous nucleation), chain initiation/propagation, and supply of monomer from the droplets (monomer transport). At one point these large droplets disappear and the polymerization largely takes place in the polymer particles, for which the reaction probabilities depend on the particle size, *e.g.* two radicals in a smaller particle terminate more likely (confined space effect in Figure 4.2; black box: middle). In contrast to bulk polymerization not only chemistry and micro-scale diffusional limitations therefore matter but also meso-scale mass transfer phenomena, with notably (re-)entry and exit events (Figure 4.2; grey box; bottom) resulting in particle type dynamics.[14,32–40]

To somewhat simplify the emulsion kinetics focus has been on miniemulsion RAFT polymerization with an oil-soluble RAFT in which the polymer formation takes place in nanoscale monomer droplets so that the particle nucleation mechanism is less an issue (Figure 4.2; blue box).[22,23,41,42] RAFT miniemulsion polymerization can be achieved by applying high shear homogenization or ultrasonication to a mixture of monomer, water, initiator, RAFT agent, surfactant, and long-chain costabilizer which results in kinetically stable droplets with a diameter in the range of 50-500 nm.[7,8,37,43–45] Consequently, before the onset of the polymerization, the (oil soluble) RAFT agent is already evenly distributed over the droplets which obviates the necessity of aqueous phase transport of these hydrophobic molecules.[46] Under well-defined conditions the droplets/particles are stabilized to such degree that they do

not coalesce or aggregate during polymerization and, hence, the final latex particle size distribution is very similar to the initial monomer droplet size distribution.

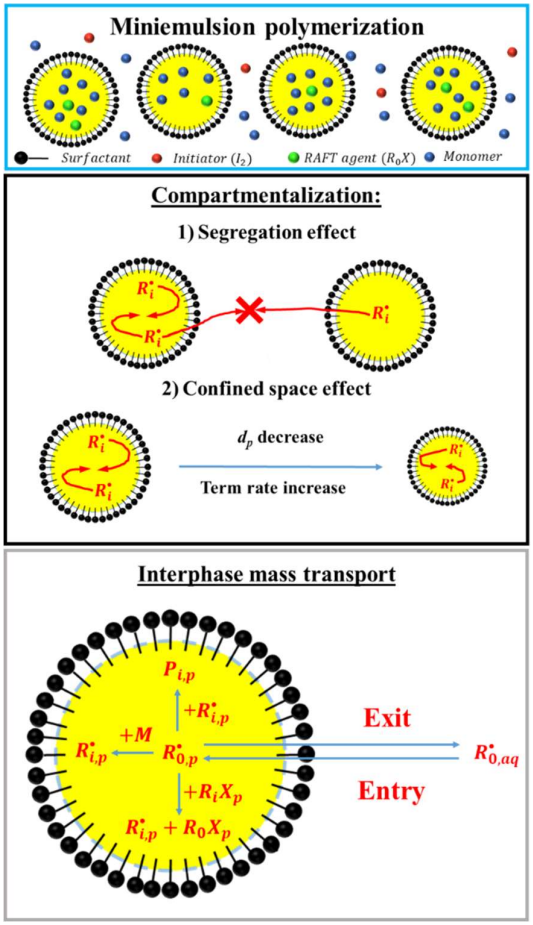

Figure 4.2*: top: representation of RAFT miniemulsion with a water-based initiator; middle: compartmentalization for miniemulsion polymerization kinetics; bottom: meso-scale interphase mass transport phenomena involving R_0 radicals.*

Several research groups[4,5,25,43,45–56] have focused on the experimental understanding of RAFT miniemulsion polymerization. Initial issues regarding colloidal instability as for example reported by Tsavalas *et al.*[48] during RAFT miniemulsion of styrene with 2-phenylprop-2-yl dithiobenzoate and later ascribed by Luo *et.al.*[54,57] to superswelling have been resolved. This superswelling is caused by the large number of oligomers formed at the beginning of the polymerization and could be overcome by either replacement of the common small RAFT agent

by a RAFT-end-capped oligomer or by using high levels of surfactant and cosurfactant (*e.g.* hexadecane), as described by Tonge *et.al.*[49] Attention has also been paid to the role of interphase mass transfer phenomena.[25,48,52,58] Despite that no retardation of the RAFT bulk polymerization of styrene with 1-phenylethyl phenyldithioacetate (PEPDTA) could be observed, the polymerization rate significantly reduced under miniemulsion conditions. This was explained by the exit of the RAFT leaving group radical and subsequent termination in the aqueous phase or after re-entry into a particle containing a growing radical, during the early stages of the polymerization. These hypotheses were supported by the absence of this rate decrease if an oligomerized PEPDTA based agent was used.

Several kinetic models have been also developed to better grasp RAFT miniemulsion polymerization.[2,3,24,41,59–66] Focus has been on both stochastic and deterministic methods, typically neglecting diffusional limitations at the micro-scale, considering an average particle size, and simulating only the polymerization rate and thus the monomer conversion profile. By means of intrinsic kinetic Monte Carlo (*k*MC) modeling the influence of the RAFT agent during the early stages of the miniemulsion RAFT polymerization (< 25% monomer conversion) on the monomer conversion and the relevance of exit/entry has been for instance investigated by Luo *et al.*,[64] with styrene and 1-phenylethyl phenyldithioacetate (PEPDTA). It was assumed that a zero-one system exists, *i.e.* a particle contains either no radicals or one radical, implying instantaneous termination if a radical enters a particle already containing one radical. It was shown that for an average particle diameter of 100 nm exit of the RAFT leaving group (R_0) radical cannot be neglected. *k*MC modelling was also used by Tobita to describe the conversion profile for intrinsic "ideal" miniemulsion polymerization of styrene, hence, in the absence of exit/entry phenomena. To mimic these conditions polystyryl dithiobenzoate was taken as macro-RAFT agent.[47,67] The observed rate retardation, as expected with this type of RAFT agent based on bulk data,[47,68] could be explained by termination of the intermediate RAFT

radicals.[47,67] Deterministic modeling of the miniemulsion RAFT polymerization rate is commonly achieved by the introduction of Smith-Ewart (differential) equations that describe the time evolution of the number of particles with a given number of radicals.[69–71] Luo *et al.* considered two radical types, *i.e.* propagating radicals and RAFT intermediate radicals leading to two-dimensional Smith-Ewart equations, to investigate RAFT miniemulsion polymerization of styrene with polystyryl-2-cryanoprop-2-yl dithiobenzoate (PS-CPDB) and polystyryl-1-phenylethylphenyl dithioacetate (PS-PEPDTA) up to intermediate monomer conversions (60%).[24] As macro-RAFT agents were considered exit and entry events were ignored and with the intrinsic kinetic model the observed rate retardation was attributed to the establishment of a zero-one system in which intermediate radicals inside particles do not propagate. Also pseudo-bulk minimemulsion kinetics have been modeled, for instance with O-ethylxanthyl ethyl propionate as RAFT agent and styrene as a monomer (semi-batch operation mode) by a combination of population balances and approximate analytical equations.[41] Focus was on high monomer conversions (*e.g.* 95%) while accounting for diffusional limitations on termination, although neglecting entry and exit phenomena originating from the initial RAFT agent.

Limited focus has been on the simulation of the miniemulsion RAFT polymerization (average) chain length characteristics and if they are considered strong simplifications are often made.[2,41,59,62,65,66] For example, Li *et al.*[66] simulated the number average chain length and dispersity for the RAFT miniemulsion copolymerization of styrene and *n*-butyl acrylate with 3-benzyltrithiocarbonyl propionic acid (BCPA) using for simplicity the conventional "bulk" method of moments equations and pseudo-homopropagation rate coefficients with no Smith-Ewart equations accounted for. Model development while accounting for such equations is recommended, as demonstrated for nitroxide miniemulsion polymerization (NMP) miniemulsion, with NMP another important RDRP technique.[72–75] Furthermore, to best of the authors knowledge, no modeling studies on miniemulsion RAFT polymerization calculate the

end-group functionality (EGF; fraction of dormant polymer chains) despite that this property is essential in view of further polymer modifications.

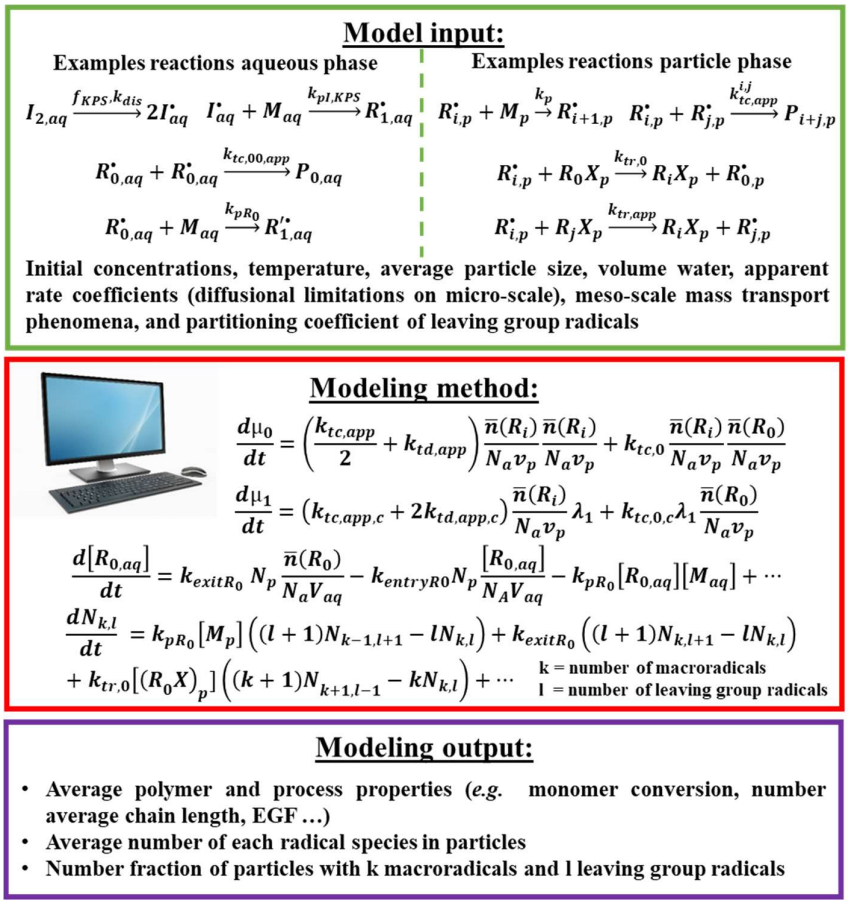

***Figure 4.3**: Output (bottom, purple box) as accessible with the developed model (basics in middle red box) , along with the necessary input parameters (top, green box).*

In this work, a deterministic model framework (Figure 4.3) – based on two-dimensional Smith-Ewart equations (middle part: red box) - is therefore developed for miniemulsion RAFT polymerization up to very high monomer conversion. The framework accounts for meso-scale exit and entry phenomena for small radicals and micro-scale diffusional limitations on both termination and RAFT exchange, the former often ignored, as explained above, and the latter always neglected up to now. As shown in Figure 4.3, the model allows to simulate the monomer conversion, EGF, number average chain length, and dispersity as a function of time while

considering the kinetic disturbance because of compartmentalization (Figure 4.2; black box). The model is also capable of providing the number fractions of particles with a given number of macroradicals (k) and R_0 radicals (l) to properly evaluate the validity of zero-one kinetics. Focus is also on different average particle sizes, in view of the particle size dependence of the reaction and mass transfer probabilities (*cf.* Figure 4.2; black and grey box).[30,31,34,72]

The model is applied to degenerative isothermal RAFT miniemulsion polymerization of MMA with CPDB (R_0X), with model validation based on literature data on radical polymerization in general and bulk and miniemulsion experimental data from Yang *et al.*[5] in particular. Importantly, the miniemulsion RAFT polymerization data are only used to tune entry/exit, hence, meso-scale and miniemulsion specific parameters. It is shown that only at the lower monomer conversions and for the lower average particle sizes a zero-one system can be established. At higher monomer conversions and particle sizes diffusional limitations on termination are shown to be too strong to avoid the formation of particles with more than one radical. This effect is further enhanced for high chain lengths where additionally diffusional limitations on RAFT transfer are active. In any case, the miniemulsion polymerization rate is faster than the bulk counterpart despite a retardation at low monomer conversions due to consecutive exit/entry of R_0 radicals.

4.2 Modeling methodology

To describe the miniemulsion RAFT polymerization of MMA with CPDB as agent and potassium persulfate (KPS) as radical initiator at 333 K a multi-scale modeling strategy is needed. In the present work, a deterministic multi-scale model development is performed with the particle level described by Smith-Ewart equations accounting for meso-scale interphase mass transport, *i.e.* exit/entry phenomena, as evaluated at the average particle size.[34,72–74] At the micro-scale, corrections are made for diffusional limitations by apparent rate coefficients, in agreement with bulk kinetic studies.[9,32,76–82]

In what follows an overview is first given of the reactions and interphase mass transfers considered. Next focus is on the Smith-Ewart equations, which are constructed considering these reactions and transfers, and the determination of the model parameters is highlighted, separating micro- from meso-scale parameters by explaining how model validation is performed to consecutively bulk and miniemulsion RAFT polymerization data.

4.2.1 Reactions and interphase mass transport

To describe the miniemulsion RAFT polymerization of MMA with CPDB as agent and potassium persulfate (KPS) as radical initiator at 333 K a degenerative mechanism (Figure 4.1) can be assumed, as explained above.[15–21] In the present work, in agreement with other modeling studies,[24,41,72] the particle size distribution is represented for simplicity by an average particle diameter d_p and, hence, the average particle volume v_p is considered constant throughout the entire polymerization process, as also density difference are ignored for simplicity.

An overview of the reactions and interphase mass transport phenomena is given in Table 4.1. It follows that initiator decomposition occurs only in the aqueous phase of the miniemulsion. The conventional radical anion initiator fragment formed out of KPS (I) is allowed to propagate until an oligomeric species is formed with a critical chain length of 4 ($R_{4,aq}$), upon which entry in the particles is assumed.[83] Entry of smaller radicals initiated by an I fragment is thus neglected. The RAFT leaving group capped oligomeric radicals in the aqueous phase, originating from exit of the R_0 radical from a particle, can already enter a new particle if a critical chain length of 2 is obtained in the aqueous phase ($R'_{2,aq}$). This lower critical value is justified by the lower water solubility of the R_0 radical compared to the water solubility of the sulfate radical anion fragment originating from KPS.[84]

***Table 4.1**: Overview of reactions and rate coefficients for RAFT miniemulsion polymerization of MMA with CPDB and potassium persulfate (KPS) at 333 K. Also provided are the exit/entry parameters that describe interphase transport, and the reactions/parameters if a bulk polymerization is performed (switch of conventional radical initiator to AIBN).*

	Reaction	Bulk	Mini-emulsion	Equation	k ((L mol^{-1}) s^{-1})	Ref
Aqueous phase reactions	Dissociation of KPS[(a),(b)]		X	$I_{2,aq} \xrightarrow{f_{KPS},k_{dis,KPS}} 2I^{\bullet}_{aq}$	$5.3\ 10^{-6}$	24
	Chain initiation by KPS		X	$I^{\bullet}_{aq} + M_{aq} \xrightarrow{k_{pI,KPS}} R^{\bullet}_{1,aq}$	$3.4\ 10^{6}$	85
	Chain initiation by $R^{\bullet}_0$		X	$R^{\bullet}_{0,aq} + M_{aq} \xrightarrow{k_{pR_0}} R'^{\bullet}_{1,aq}$	$9.5\ 10^{3}$	(d),(g)
	Propagation		X	$R^{\bullet}_{1\le i\le 3,aq} + M_{aq} \xrightarrow{k_p} R^{\bullet}_{i+1,aq}$	$8.2\ 10^{2}$	(e),(f)
			X	$R'^{\bullet}_{1,aq} + M_{aq} \xrightarrow{k_p} R'^{\bullet}_{2,aq}$	$8.2\ 10^{2}$	(e),(g)
	Termination by recombination		X	$R^{\bullet}_{0,aq} + R^{\bullet}_{0,aq} \xrightarrow{k_{tc,00,app}} P_{0,aq}$	$1.3\ 10^{9}$	(h)
			X	$R^{\bullet}_{0,aq\prime} + R^{\bullet}_{1\le i\le 3,aq} \xrightarrow{k_{tc,0(1\le i\le 3),app}} P_{1\le i\le 3,aq}$	$1.3\ 10^{9}$	(h)
			X	$R^{\bullet}_{0,aq} + R'^{\bullet}_{1,aq} \xrightarrow{k_{tc,01',app}} P_{1,aq}$	$1.3\ 10^{9}$	(g),(h)
Organic phase reactions	Dissociation of AIBN[(a),(c)]	X		$I_{2,b} \xrightarrow{f_{AIBN,app},k_{dis,AIBN}} 2I^{\bullet}_{b}$	$1.1\ 10^{-5}$	86
	Chain initiation by AIBN	X		$I^{\bullet}_{b} + M_b \xrightarrow{k_{pI,AIBN}} R^{\bullet}_{1,b}$	$9.5\ 10^{3}$	(d)
	Chain initiation by $R^{\bullet}_0$	X	X	$R^{\bullet}_{0,p} + M_p \xrightarrow{k_{pR_0}} R^{\bullet}_{1,p}$	$9.5\ 10^{3}$	(d)
	Propagation	X	X	$R^{\bullet}_{i,p} + M_p \xrightarrow{k_p} R^{\bullet}_{i+1,p}$	$8.2\ 10^{2}$	87
	Termination by recombination	X	X	$R^{\bullet}_{0,p} + R^{\bullet}_{0,p} \xrightarrow{k_{tc,00,app}} P_{0,p}$	$1.3\ 10^{9}$	(h)
		X	X	$R^{\bullet}_{0,p} + R^{\bullet}_{i,p} \xrightarrow{k_{tc,0,app}} P_{i,p}$	$1.3\ 10^{9}$	(h)
		X	X	$R^{\bullet}_{i,p} + R^{\bullet}_{j,p} \xrightarrow{k^{i,j}_{tc,app}} P_{i+j,p}$	$1.3\ 10^{9}$	88,(h)
	Termination by disproportionation	X	X	$R^{\bullet}_{i,p} + R^{\bullet}_{j,p} \xrightarrow{k^{i,j}_{td,app}} P_{i,p} + P_{j,p}$	$1.3\ 10^{9}$	88,(h)
	RAFT exchange	X	X	$R^{\bullet}_{i,p} + R_0X_p \xrightarrow{k_{tr,0}} R_iX_p + R^{\bullet}_{0,p}$	$1.6\ 10^{4}$	20,(i)
		X	X	$R^{\bullet}_{i,p} + R_jX_p \xrightarrow{k_{tr,app}} R_iX_p + R^{\bullet}_{j,p}$	$6.2\ 10^{4}$	20,(i),(l)
Interphase transport	Entry of $R^{\bullet}_{4,aq}$		X	$R^{\bullet}_{4,aq} \xrightarrow{k_{entryR_4}} R^{\bullet}_{4,p}$	$5.0\ 10^{7}$	(f),(j)
	Entry of $R'^{\bullet}_{2,aq}$		X	$R'^{\bullet}_{2,aq} \xrightarrow{k_{entryR'_2}} R'^{\bullet}_{2,p}$	$5.0\ 10^{7}$	(g),(j)
	Exit[(a)] of $R^{\bullet}_{0,p}$		X	$R^{\bullet}_{0,p} \xrightarrow{k_{exitR_0}} R^{\bullet}_{0,aq}$	$1.5\ 10^{5}$	(k)
	Entry of $R^{\bullet}_{0,aq}$		X	$R^{\bullet}_{0,aq} \xrightarrow{k_{entryR_0}} R^{\bullet}_{0,p}$	$4.8\ 10^{11}$	(k)

(a) s^{-1}; (b) f_{KPS} = 0.2 (middle of literature[89] range of 0.1-0.3); (c) $f_{AIBN,app}$ as explained in Section B1 of Appendix B (d) Section B2 in Appendix B; (e) considered equal to k_p to a first approximation; (f) critical chain length for the entry of MMA is 4 [83]; (g) oligomeric radicals with an R_0 end-group in the aqueous phase are accounted for separately with a critical chain length of 2 as lower water solubility of the R_0 compared to the I fragment; (h) given value of $k^{1,1}_{t,app}$, see Section B3 in Appendix B for other chain lengths and as a function of monomer conversion. Fraction of term. of two macroradicals by recombination[90–92] : 0.32; (i) calculated assuming $C_{tr,0} = \frac{k_{tr,0}}{k_p} = 20$ and $C_{tr} = \frac{k_{tr}}{k_p} = 76$, both values determined at 353K [20] (j) large values are assumed to reflect the strong entry rate of molecules possessing the critical chain length and values given for d_p=1.0 10² nm; (k) Values (this work) given for d_p=1.0 10² nm, see Figure 4.4 for general formulas as a function of d_p; (l) apparent rate coefficients based on Equation (B12) (Appendix B4).

No R_0X species are considered to be present in the aqueous phase. Furthermore, chain transfer to monomer can be neglected, as explained in Section B5 in Appendix B. The RAFT exchange of R_0 radicals with R_0X in the particles is much less important than chain initiation, resulting in a kinetically insignificant transfer coefficient $k_{-tr,0}$, as shown in Section B5 in Appendix B, further supporting the assumption of a degenerative mechanism. At lower monomer conversion, the aqueous monomer concentration is considered at its saturated value ($5.6\ 10^{-1}$ mol L^{-1}),[93] implying instantaneous monomer phase transfer. As the polymerization proceeds, a point is reached at which the monomer concentration in both phases is equal (monomer conversion ca. 90%), after which it is assumed for simplicity that both concentrations remain equal and decrease together.

For comparison, in Table 4.1, also bulk RAFT reactions are provided. All reactions are the same than for the miniemulsion case, except those related to the conventional radical initiator, which is now AIBN. The latter switch is due the water solubility of KPS. Furthermore, bulk polymerization does not feature interphase mass transport.

4.2.2 Smith-Ewart and moment equations

The species present in the organic phase can be divided in two groups. The first group consists of the abundant species (>> 10 molecules per particle), *e.g.* monomer and R_0X, whose concentrations in the particles are approximated by a single average concentration over all particles at any time and their concentration time evolution is accounted for by means of conventional continuity equations. The second group consists of nonabundant species, here macroradicals and RAFT initiator radicals, with typically only 0 to 10 molecules per particle so that the reaction kinetics do not follow pseudo-bulk kinetics and, hence, a single average concentration as for the abundant species cannot be considered. Due to the low number of radicals per particle the kinetics can be influenced by compartmentalization (Figure 4.2; black box)[94,95] so that the reaction probabilities in one particle can be completely different than those

in another particle, with the possibility that many particles undergo no changes at a given integration time step as they contain no radicals.

In order to account for compartmentalization effects for the miniemulsion kinetics so-called 2-dimensional Smith-Ewart equations (Equation (1)) have been implemented to characterize the time evolution of the radical numbers in the polymer particles, in agreement with previous modeling work on nitroxide mediated polymerization (NMP).[69,72,96] These population balances describe the temporal evolution of polymer particles having k macroradicals and l R_0 radicals ($N_{k,l}$,; $k,l \geq 0$):

$$\begin{aligned}\frac{dN_{k,l}}{dt} = {} & \frac{k_{tc,app} + k_{td,app}}{2v_p N_A}\Big((k+2)(k+1)N_{k+2,l} - k(k-1)N_{k,l}\Big) \\ & + k_{entryR_4}[R_{4,aq}](N_{k-1,l} - N_{k,l}) + k_{entry\ 2'}[R'_{2,aq}](N_{k-1,l} - N_{k,l}) \\ & + k_{pR_0}[M_p]\Big((l+1)N_{k-1,l+1} - lN_{k,l}\Big) \\ & + \frac{k_{tc,00}}{2v_p N_A}\Big((l+2)(l+1)N_{k,l+2} - l(l-1)N_{k,l}\Big) \\ & + \frac{k_{tc,0}}{v_p N_A}\Big((k+1)(l+1)N_{k+1,l+1} - klN_{k,l}\Big) \\ & + k_{entryR_0}[R_{0,aq}]\big(N_{k,l-1} - N_{k,l}\big) + k_{exitR_0}\Big((l+1)N_{k,l+1} - lN_{k,l}\Big) \\ & + k_{tr,0}[(R_0X)_p]((k+1)N_{k+1,l-1} - kN_{k,l})\end{aligned} \tag{1}$$

These Smith-Ewart equations need to be integrated along the continuity equations of species in the aqueous phase (Equation ((2)-(14)) and of the abundant species in the particles (Equation (15)-(19)):

$$\frac{d[I_{2,aq}]}{dt} = -fk_{dis}[I_{2,aq}] \tag{2}$$

$$\frac{d[I_{aq}]}{dt} = 2fk_{dis}[I_{2,aq}] - k_{pI}[I_{aq}][M_{aq}] - k_{tc,0I}[I_{aq}][R_{0,aq}] \tag{3}$$

$$\frac{d[R_{0,aq}]}{dt} = k_{exitR_0} N_p \frac{\bar{n}(R_0)}{N_a V_{aq}} - k_{entryR0} N_p \frac{[R_{0,aq}]}{N_A V_{aq}} - k_{tc,0I}[I_{aq}][R_{0,aq}] - k_{tc,0(1\le i\le 3)}[R_{1\le i\le 3,aq}][R_{0,aq}] - k_{tc,00}[R_{0,aq}][R_{0,aq}] - k_{tc,01'}[R_{0,aq}][R'_{1,aq}] - k_{pR_0}[R_{0,aq}][M_{aq}] \quad (4)$$

$$\frac{d[R_{1,aq}]}{dt} = k_{pI}[I_{aq}][M_{aq}] - k_p[R_{1,aq}][M_{aq}] - k_{tc,01}[R_{1,aq}][R_{0,aq}] \quad (5)$$

$$\frac{d[R_{2,aq}]}{dt} = k_p[R_{1,aq}][M_{aq}] - k_p[R_{2,aq}][M_{aq}] - k_{tc,02}[R_{2,aq}][R_{0,aq}] \quad (6)$$

$$\frac{d[R_{3,aq}]}{dt} = k_p[R_{2,aq}][M_{aq}] - k_p[R_{3,aq}][M_{aq}] - k_{tc,03}[R_{3,aq}][R_{0,aq}] \quad (7)$$

$$\frac{d[R_{4,aq}]}{dt} = k_p[R_{3,aq}][M_{aq}] - k_{entryR_4} N_p \frac{[R_{4,aq}]}{N_A V_{aq}} \quad (8)$$

$$\frac{d[M_{aq}]}{dt} = -k_{pI}[I_{aq}][M_{aq}] - k_p[R_{1,aq}][M_{aq}] - k_p[R_{2,aq}][M_{aq}] - k_p[R_{3,aq}][M_{aq}] - k_{pR_0}[R_{0,aq}][M_{aq}] - k_p[R'_{1,aq}][M_{aq}] \quad (9)$$

$$\frac{d[P_{0,aq}]}{dt} = k_{tc,0I}[I_{aq}][R_{0,aq}] + \frac{k_{tc,00}}{2}[R_{0,aq}][R_{0,aq}] \quad (10)$$

$$\frac{d[P_{1\le i\le 3,aq}]}{dt} = k_{tc,0(1\le i\le 3)}[R_{0,aq}][R_{1\le i\le 3,aq}] \quad (11)$$

$$\frac{d[P_{1,aq}]}{dt} = k_{tc,01'}[R_{0,aq}][R'_{1,aq}] \quad (12)$$

$$\frac{d[R'_{1,aq}]}{dt} = k_{pR_0}[R_{0,aq}][M_{aq}] - k_p[R'_{1,aq}][M_{aq}] - k_{tc,01'}[R_{0,aq}][R'_{1,aq}] \quad (13)$$

$$\frac{d[R'_{2,aq}]}{dt} = k_p[R'_{1,aq}][M_{aq}] - k_{entryR'_2} N_p \frac{[R'_{2,aq}]}{N_A V_{aq}} \quad (14)$$

$$\frac{d[M_p]}{dt} = -k_p \frac{\bar{n}(R_i)}{N_a v_p}[M_p] - k_{pR_0} \frac{\bar{n}(R_0)}{N_a v_p}[M_p] \tag{15}$$

$$\frac{d\tau_0}{dt} = \frac{d\sum_{i>0}[R_i X_p]}{dt} = k_{tr,0} \frac{\bar{n}(R_i)}{N_a v_p}[R_0 X_p] \tag{16}$$

$$\frac{d\mu_0}{dt} = \frac{d\sum_{i\geq 1}[P_{i,p}]}{dt} = \left(\frac{k_{tc,app}}{2} + k_{td,app}\right) \frac{\bar{n}(R_i)}{N_a v_p} \frac{\bar{n}(R_i)}{N_a v_p} + k_{tc,0} \frac{\bar{n}(R_i)}{N_a v_p} \frac{\bar{n}(R_0)}{N_a v_p} \tag{17}$$

$$\frac{d[P_{0,p}]}{dt} = \frac{k_{tc,00}}{2} \frac{\bar{n}(R_0)}{N_a v_p} \frac{\bar{n}(R_0)}{N_a v_p} \tag{18}$$

$$\frac{d[R_0 X_p]}{dt} = -k_{tr,0} \frac{\bar{n}(R_i)}{N_a v_p}[R_0 X_p] \tag{19}$$

with the average number of macroradicals and R_0 radicals defined as:

$$\bar{n}(R) = \sum_{k,l} k \frac{N_{k,l}}{N_p} \tag{20}$$

$$\bar{n}(R_0) = \sum_{k,l} l \frac{N_{k,l}}{N_p} \tag{21}$$

in which N_p is the total number of particles.

Based on Equation (2)-(19) the monomer conversion and EGF evolution can be directly calculated. For the calculation of the number-average chain length (x_n) and the dispersity as a function of time, the pseudo-bulk approximation for the higher order moment equations is applied, following again previous work on NMP miniemulsion.[72,96] An overview of all higher order moment equations is given Section B6 in Appendix B. To account for issues related to size exclusion chromatography calibrations the experimental data for x_n were corrected with a constant factor of 0.8. A constant factor could be used for all experimental data, highlighting its relevance and leading to the expected relation under well-defined RDRP conditions.

The bulk counter case is modeled as described in previous work,[9,78,97–100] considering the extended method of moments, allowing the simulation of the evolution of the monomer and R_0X conversion, the EGF change, and the variation of x_n and the dispersity as a function of monomer conversion. As explained below all model parameters are taken here from literature.

4.2.3 Model parameters

The parameter tuning for the modeling of the RAFT miniemulsion polymerization was conducted with the aim of ensuring maximum reliability of all model parameters. Hence, to separate bulk-specific from emulsion-specific phenomena, a distinction is made between tuning model parameters based on dedicated bulk reaction conditions (first step) and emulsion conditions (second step). Benchmarking against experimental data under bulk conditions (entry B1 in Table 4.2) allows fine-tuning the miniemulsion model toward the prediction of the RAFT polymerization kinetics. This tuning is therefore free of any interference caused by compartmentalization and phase-transfer meso-scale phenomena such as exit/entry model parameters. As explained below, this two-phase parameter tuning strategy results in a set of model parameters which can be largely taken directly from bulk literature kinetic studies (see Table 4.1 and see further Figure 4.5), except for the exit/entry parameters which needed to be tuned based on miniemulsion experimental data (entry ME1-ME3 in Table 4.2; see further Figure 4.6).

***Table 4.2**: Overview of the initial conditions used in the isothermal experimental study of bulk (exp 1) and miniemulsion (exp 2-4) RAFT polymerization of MMA performed by Yang et al.[5a]*

Entry	$[MMA]_0/[CPDB]_0$	$[CPDB]_0/[I_2]_0$	d_p (nm)[b]
B1	192	4.88	-
ME1	192	4.68	2.0 10^2
ME2	192	4.68	1.4 10^2
ME3	590	1.53	1.0 10^2

[a]T=333 K; AIBN as conventional initiator (I_2) for the bulk experiment and KPS for the miniemulsion experiments; $m_{MMA,0}$ = 20 g; m_{H2O} = 80g; [b]average particle diameter

Micro-scale diffusional limitations

To account for diffusional limitations on termination, the composite k_t model,[88] also known as the RAFT-chain length dependent-termination (RAFT-CLD-T) model,[101] is used. For simplicity, average apparent termination rate coefficients are evaluated at the number average radical chain length $x_{n,r}$. The RAFT-CLD-T literature parameters, as determined in bulk, are given in Section B3 of Appendix B.

Based on the recent overview of De Rybel *et al.*[77] it is clear that also the RAFT exchange can become diffusion controlled already at intermediate monomer conversions, as typical RAFT-specific intrinsic reactivities are higher than conventional propagation reactivities and the RAFT exchange involves two macrospecies as in termination. In the present work, apparent RAFT exchange rate coefficients are therefore used. These have been obtained by relying on the coupled parallel encounter pair model approach as introduced by D'hooge *et al.*[78]:

$$k_{tr,app} = \left(\frac{1}{k_{tr,chem}} + \frac{2}{k_{tr,diff}}\right)^{-1} \quad (22)$$

with $k_{tr,app}$ the apparent RAFT transfer rate coefficient, $k_{tr,chem}$ the intrinsic RAFT transfer rate coefficient (see Table 4.1), and $k_{tr,diff}$ the diffusional contribution for RAFT transfer as

calculated in Section B4 in Appendix B based on bulk data. As the initial RAFT agent is completely consumed at relatively low monomer conversions, diffusional limitations on $k_{tr,0}$ can be neglected. Similarly the exit rate coefficient for R_0 can be assumed as intrinsic.

To account for the increasing viscosity during the bulk polymerization simulations,[77] an apparent conventional initiator efficiency f_{app} has been calculated based on the free volume theory as described by Buback *et al.*[102] and as explained in more detail in Section B1 in Appendix B, in line with the work of De Rybel *et al.*[77] In contrast, in the miniemulsion polymerization, an intrinsic initiator efficiency is used, as this relates to an initiator decomposition in a low viscous aqueous environment. For the same reason, intrinsic entry coefficients can be considered. To minimize the effect of diffusional limitations on propagation, which are ignored in the present work, only experimental data until a monomer conversion of 95% are considered.[103–105]

Meso-scale exit and entry coefficients

In agreement with previous work,[72,73,75] an inverse quadratic and linear relationship with respect to d_p is regarded for the exit and entry rate coefficients of the R_0 species respectively, as shown in Figure 4.4. The ease of performing a meso-scale mass transfer with a given concentration gradient is reflected in $C_{exit/entry}$. The entry and exit rate coefficients are interrelated by the partitioning coefficient Γ which is a thermodynamic quantity for a solute in a two-phase system and, in case of an organic-aqueous phase system, is defined as the ratio of the equilibrium concentration of the compound in the organic phase to its equilibrium concentration in the aqueous phase (Figure 4.4).[37,106] Γ is dimensionless and independent of the particle diameter.

In this work, a Γ value of 10 was assumed which is a typical value for an AIBN radical fragment (resembling R_0 as CPDB is the initial RAFT agent) in a monomer/aqueous system.[107,108] Hence, focus is on tuning of either the exit or the entry rate coefficient and not both as they need to follow the partitioning coefficient. The exit rate coefficient was tuned in the present work by

varying $C_{exit}D_{R_0,org}$ and comparing with the available experimental data at different d_p values (see further; Figure 4.6). The diffusion coefficient in the organic phase and thus $C_{exit}D_{R_0,org}$ can be considered constant to a first approximation as R_0X is completely consumed at relatively low monomer conversion (<40%, see further: Figure 4.6). The tuning of k_{exit,R_0} and the calculation of k_{entry,R_0} is justified by the observation that the simulated output is more sensitive to individually adjusting k_{exit,R_0} at fixed Γ as opposed to adjusting only k_{entry,R_0} as explained in Section B7 in Appendix B. It can thus be concluded that only one parameter needed to be tuned for the minemulsion data description and all other parameters are thus literature based.

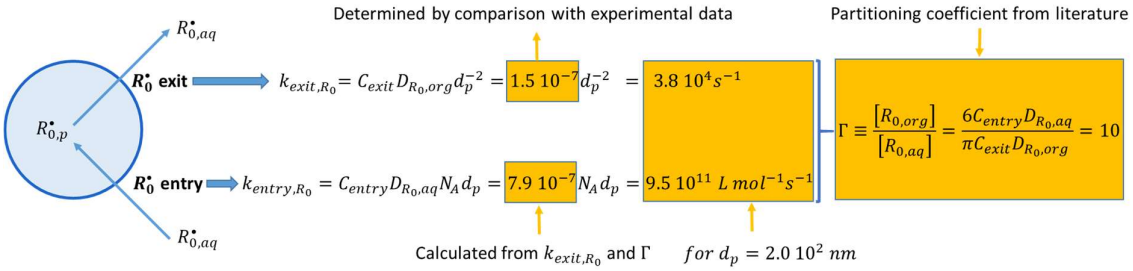

Figure 4.4*: Schematic representation of the calculation of the exit and entry rate coefficient for the RAFT leaving group radical ($R^{\bullet}_0$) from/into a polymer particle with average diameter d_p in the RAFT miniemulsion polymerization of MMA at 333K with CPDB as RAFT agent and KPS as conventional radical initiator. These are the only parameters tuned based on miniemulsion RAFT polymerization data;* Γ *= partitioning coefficient;* $C_{exit}D_{R_0,org}$ *has been determined by comparison with experimental miniemulsion data[5] (entry ME1-3 in Table 4.2) with all other model parameters obtained based on bulk literature data and assuming a literature[107,108] based* Γ *of 10;* $C_{exit/entry}$ *= proportionality constant for* R_0 *exit/entry from/into a polymer particle (-),* $D_{R_0,org/aq}$ *=* R_0 *diffusional coefficient in the organic/aqueous phase (dm² s⁻¹),* N_a *= Avogadro constant (mol⁻¹);* $D_{R_0,org/aq}$ *can be assumed constant as the RAFT agent is completely consumed at low monomer conversion (see Results and Discussion); values for* $k_{exit,R0}$ *and* $k_{entry,R0}$ *are given for* $d_p = 2.0\ 10^2\ nm$ *(entry ME1 in Table 4.2) as an example.*

4.3 Results and discussion

4.3.1 Bulk RAFT polymerization: model validation of micro-scale model parameters

For bulk RAFT polymerization of MMA mediated by CPDB (Entry B1 in Table 4.2), the comparison between the simulation results obtained with the parameters in Table 4.1 and the experimental data acquired by Yang *et al.*[5] is shown in Figure 4.5. A good agreement for both the monomer conversion profile (Figure 4.5a) and the change of the average polymer properties with increasing monomer conversion (Figure 4.5b-c) is obtained, highlight the significance of the micro-scale parameters in Table 4.1 and the accurate description of the apparent kinetics. The conversion profile has a typical S shape, confirming the similarity between RAFT polymerization and FRP. The linear growth of the number average chain length (x_n, Figure 4.5b) with monomer conversion, the high EGF (>90%, Figure 4.5c) and the low dispersity (Đ < 1.5, Figure 4.5c), at least up to a monomer conversion of 80%, confirm the excellent microstructural control. Consistent with this statement is the fast simulated disappearance of the initial RAFT agent, as shown in Figure 4.5a.

Figure 4.5d illustrates that diffusional limitations play an important role in the bulk case. Not only diffusional limitations on the average termination rate coefficient ($\langle k_{t,app} \rangle$, dashed line) matter but also those on the average RAFT transfer rate coefficient ($\langle k_{tr,app} \rangle$, dotted line). Diffusional limitations on termination result in an auto-acceleration, better known as the gel-effect,[109] with a dominance at intermediate monomer conversions (±50%) and also confirmed by the reduction of the slope of the EGF profile (Figure 4.5d). Note that the $\langle k_{t,app} \rangle$ line is characterized by a sudden downward step at intermediate monomer conversion, which is due to the variation of a change in diffusion regime as predicted by the literature based RAFT-CLD-T parameters.

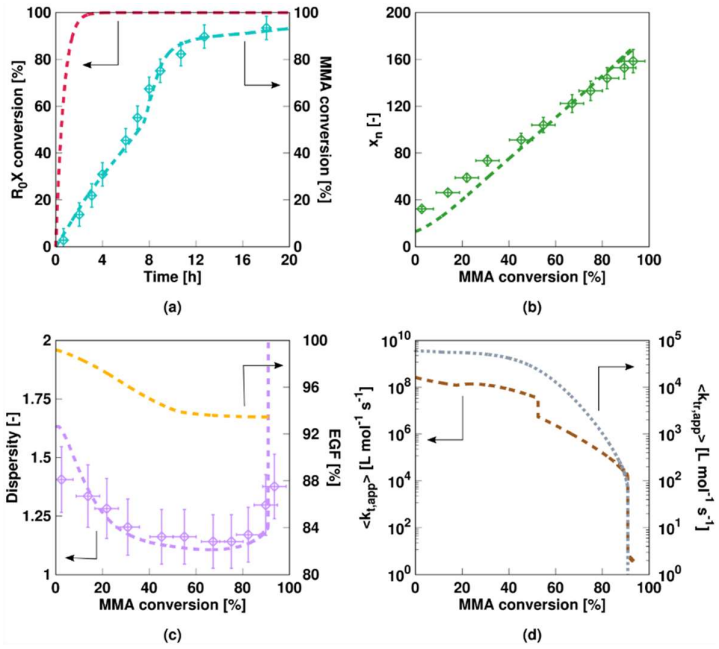

***Figure 4.5**: Comparison of simulation and experimental data (entry B1 in Table 4.2)[5] for bulk RAFT polymerization of MMA at 333 K with AIBN and CPDB. Monomer conversion (a) as a function of time, number average chain length x_n (b), and dispersity (c) as a function of monomer conversion. In (a) also the simulated initial RAFT agent (R_0X) conversion. In (c) also the simulated end-group functionality (EGF); (d) shows the variation of the overall average (zeroth order) apparent termination rate coefficient (brown, $\langle k_{t,app} \rangle = \langle k_{tc,app} \rangle + \langle k_{td,app} \rangle$) and average RAFT transfer coefficient (grey) as a function of MMA conversion; variation of the apparent initiator efficiency in Figure B1 of Appendix B; lines correspond to calculated values with the model parameters given in Table 4.1; typical average error bars.*

The importance of diffusional limitations on RAFT transfer is visible in the sharp increase of the dispersity at higher monomer conversions (> 80%). RAFT exchange, as termination, involves two macrospecies and therefore diffusional limitations are relevant. As RAFT exchange is intrinsically slower than termination (Table 4.1), the RAFT exchange kinetics become only diffusion-limited at much more viscous environments and thus higher monomer conversion and x_n values. Note that the steepness of the increase in dispersity is directly correlated with the steepness of the drop of $\langle k_{tr,app} \rangle$. A better microstructural control is

therefore very likely in case this viscosity dependency of the RAFT exchange can be controlled, keeping in mind that diffusional limitation on propagation can be ignored at such monomer conversions. Furthermore, the apparent initiator efficiency decreases due to diffusional limitations (Figure B1 of Appendix B), leading at very high monomer conversions to a cessation of the polymerization.

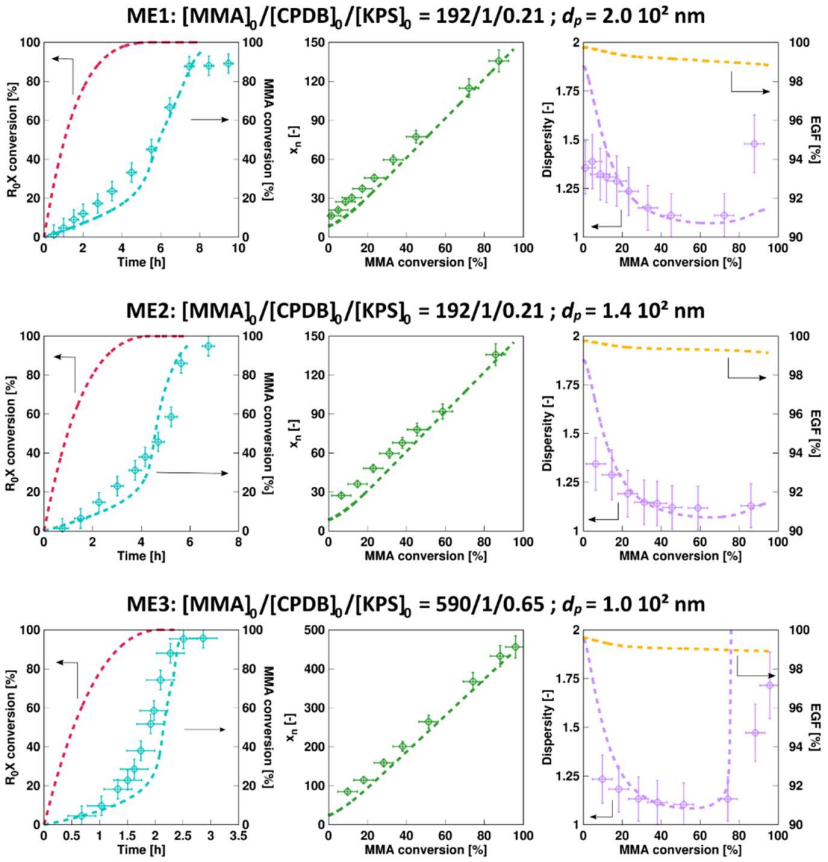

Figure 4.6*: Comparison of simulated and experimental data (entry ME1-ME3 in Table 4.2)[5] for miniemulsion of MMA at 333 K with KPS and CPDB. Left column: monomer conversion (X_m, blue) as a function of time; middle column: number-average chain length (x_n, green) as a function of monomer conversion; Right column: dispersity (Đ, purple) as a function of monomer conversion. In left column also the simulated initial RAFT agent (R_0X) conversion (red line). In the right column also the simulated end-group functionality (EGF; orange line) as a function of monomer conversion; lines correspond to calculate values with model parameters given in Table 4.1; typical average error bars.*

4.3.2 Miniemulsion RAFT polymerization: model validation of meso-scale model parameters

A good agreement between the simulated and the experimental miniemulsion RAFT polymerization data of Yang *et al.*[5] is shown in Figure 4.6 (conditions: Table 4.2; same initial RAFT agent as bulk case but KPS as initiator; *cf.* Table 4.1). The observed linear growth of x_n (green, middle column), the high EGF (orange, right column) and the low dispersity (<1.5; right column) at low and intermediate monomer conversions indicate that a well-controlled RAFT polymerization is taking place. It should be reminded that all reaction rate coefficients are fixed in the simulations and only tuning is done for the R_0 exit rate coefficient (*cf.* Figure 4.4).

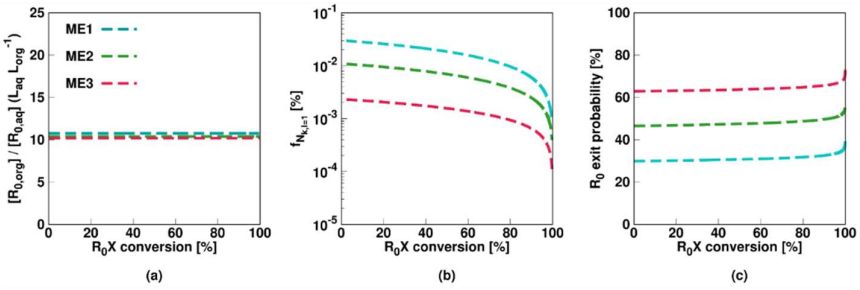

Figure 4.7*: (a) Ratio of the average concentration of the leaving group radical (R_0) in the organic phase (all particles) to the concentration in the aqueous phase, (b) the fraction of particles with 1 R_0 (middle) and (c) the exit probability, i.e. the ratio of the rate of the exit of the leaving group to the sum of the exit rate and R_0 total consumption rate, in all the particles as a function of the initial RAFT agent (R_0X) conversion for Experiment ME1 (blue), Experiment ME2 (green), and Experiment ME3 (red). Conditions as mentioned in Table 4.2. Simulated values calculated with model parameters in Table 4.1; from ME1 to ME3: higher relevance of exit of R_0 as decreasing average particle size; X_{R0X} = 100% at X_m = 40 % for all experiments; average particle size for ME1-3: 2 10^2, 1.4 10^2 and 1.0 10^2 nm.*

Figure 4.7 shows for experiment ME1, ME2, and ME3 (decreasing (average) particle size) the ratio of the average concentration of the leaving group radical in the organic phase to the concentration of that radical in the aqueous phase (subplot a), the fraction of particles with one R_0 radical (subplot b), and the leaving group exit probability considering all possible reaction and mass transfer events (subplot c) as a function of the R_0X conversion. It can be seen in Figure

4.7a that on an overall basis equilibrium of R_0 between the two phases is quickly achieved, consistent with the literature based value of 10 for the partitioning coefficient.[107,108] Moreover, most of the particles do not possess a R_0 radical (Figure 4.7b), indicating a fast consumption by termination or propagation, or a fast exit. As shown in Figure 4.7 (c), the ratio of the exit rate to the overall consumption/disappearance rate increases with decreasing particle size due to the inverse quadratic relation between the average particle size and the exit rate coefficient. Hence, the simulation and experimental results for ME3 (lowest average particle size) in Figure 4.6 are most affected by exit of R_0.

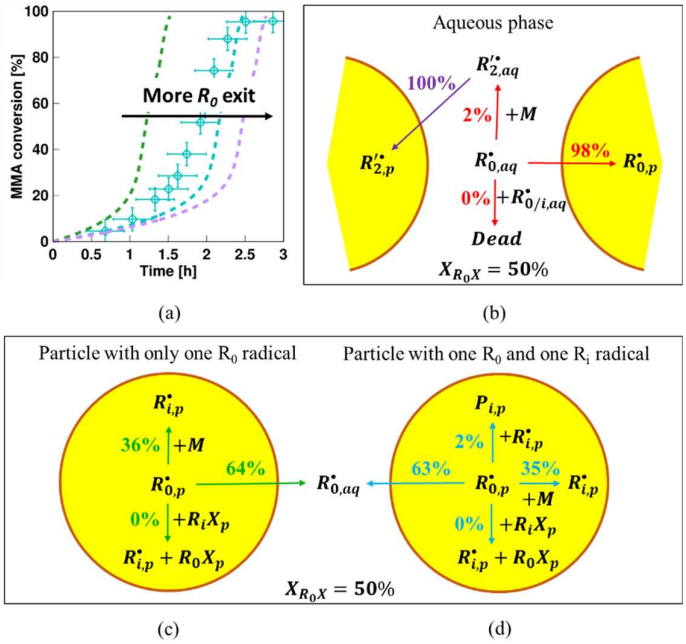

***Figure 4.8**: (a): the theoretical influence of the exit rate coefficient on the conversion plot of Experiment ME3 in Table 4.2;* $C_{exit}D_{R_0,or} = 1.5\ 10^{-8} dm^2 s^{-1}$ *(green)* $C_{exit}D_{R_0,or} = 1{,}5\ 10^{-7} dm^2 s^{-1}$ *(blue; line as in Figure 4.5 bottom; left + experimental data)* $C_{exit}D_{R_0,or} = 1{,}5\ 10^{-6} dm^2 s^{-1}$ *(purple line); other parameters as in Table 4.1; more exit leading to more delay at low monomer conversions. b-d: Reaction probabilities involving the leaving group R_0 radicals in aqueous phase (b) and particles with zero and one macroradical (c and d); situation at 50% conversion of initial RAFT agent (X_m = 3.5%); these results highlight that delay is due to a dominant occurrence of re-entry/exit of R_0; other model parameters in Table 4.1.*

The latter is also theoretically illustrated in Figure 4.8a by comparing the tuned conversion profile in Figure 4.6 (same blue line) with the profiles for which the exit rate coefficient is lowered and increased with a factor 10 (green and purple line). As long as initial RAFT agent is present (monomer conversions below 20%; *cf.* left column Figure 4.6), the lines strongly differ with an increased exit rate coefficient retarding the polymerization. At higher monomer conversions (>20%), at which the initial RAFT agent is depleted, the exit rate coefficient does not influence the polymerization rate so that all monomer conversion temporal changes become parallel. To further investigate the origin of the retardation at the lower monomer conversions, Figure 4.8b-d show the reaction probabilities at 50% initial RAFT agent conversion for the R_0 radical in the aqueous phase (subplot b), in a particle containing only a R_0 radical (subplot c), and in a particle containing both a R_0 and a macroradical (subplot d). As shown in Figure 4.8b, termination involving the aqueous R_0 radical is negligible and almost all these radicals will entry a particle before they can react with monomer. The small amount of R_0 radicals that are able to take up monomer will enter a particle as well once the critical length of 2 is obtained, similar as macroradicals of chain length 4 as formed from KPS dissociation and consecutive aqueous chain initiation and propagation (Table 4.1). As shown in Figure 4.8c, in particles, exit of R_0 radicals to the aqueous phase is dominant and, hence, these will undergo re-entry (to another particle). R_0 radicals which do not exit a particle will mainly react with monomer resulting in the formation of macroradicals that cannot exit. However, if a radical is already present or formed by (re-)entry, at one point termination can occur as in a conventional FRP process as RAFT exchange is not infinitely fast as shown in Section B10 in Appendix B. It can thus be concluded that the observed retardation effect at lower monomer conversions is mainly caused by alternating R_0 exit and (re-)entry, resulting in a negligible monomer consumption.

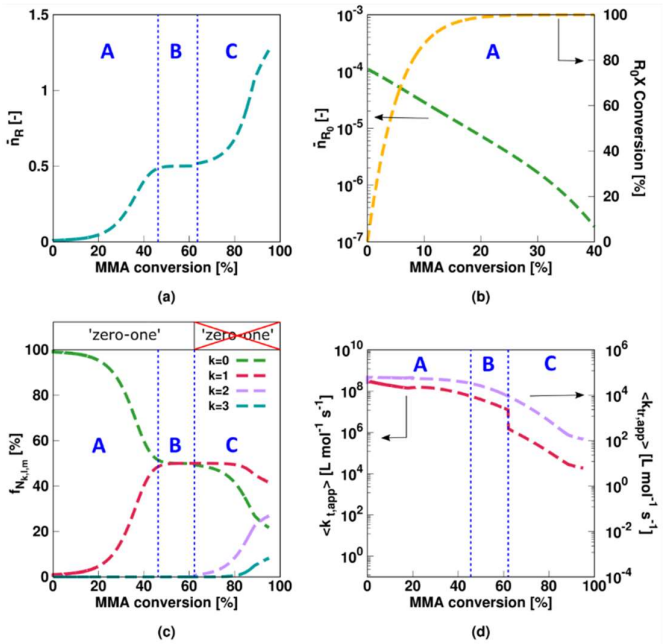

Figure 4.9*: Results with complete model (diffusional limitations on termination and RAFT transfer; used for Figure 4.6) for the average number of macroradicals per particle ($\bar{n}_R$, (a), blue), average number of leaving group radicals per particle ($\bar{n}_{R_0}$, (b), green), R_0X conversion ((b), orange), fraction of particles with 0 up to 3 macroradicals (c), average apparent overall termination rate coefficient ($\langle k_{t,app} \rangle = \langle k_{tc,app} \rangle + \langle k_{td,app} \rangle$, (d), red, for calculation see Section B3 in Appendix B) and the average apparent transfer rate coefficient ($\langle k_{tr,app} \rangle$, (d), purple, for calculation see Section B4 in Appendix B) as a function of MMA conversion for Experiment ME2; conditions as mentioned in Table 4.2 and calculated with model parameters given in Table 4.1. Similar results for ME1 in Table 4.1 (see Section B8 in Appendix B); A-C regimes related to dominance of entry/exit; termination; diffusional limitations on termination (see in detail in Figure 4.10).*

Despite this retardation - on an overall basis - the miniemulsion polymerizations are much faster than the bulk polymerization case, as can be derived from comparing Figure 4.5 (a) vs. Figure 4.6 (first column), ignoring for simplicity differences in initiator loading and initiator mechanism (aqueous *vs.* organic). In any case, the kinetics are influenced by segregation (Figure B11 in Appendix B; dominance of active particles with one radical), with very low average radical amounts as *e.g.* shown in Figure 6.9(a) for ME2 in Table 4.2 (average amount

below 1.5 and mostly well below 1) consistent with the higher EGF values in Figure 4.6 (right column).

4.3.3 Miniemulsion RAFT polymerization: invalidity of zero-one kinetics

As shown in Figure 4.9a, the average number of macroradicals per particle ($\bar{n}_R$) as a function of MMA conversion for experiment ME2 is characterized by three regimes. At low monomer conversions (< ±45%, regime A), $\bar{n}_R$ is very low (close to 0) and thus zero-one kinetics result. This can be explained by the dominance of R_0 exit and (re-)entry at low monomer conversion, as explained above. As long as R_0X is present $\bar{n}_R$ remains low (values of *ca.* 10^{-2}) and the average number of R_0 radicals per particle ($\bar{n}_{R0}$; Figure 4.9b green) decreases. The latter average is always very low ($<10^{-4}$) as R_0 species are rapidly involved in propagation and exit. The relevance of R_0 exit and re-entry based retardation is also highlighted in Figure 4.9c as the fraction of particles containing no radical (green dashed line) is always dominant. At intermediate monomer conversion (±45% - ±60%, regime B in Figure 4.9), half the particles contain no macroradicals and half of them possess just one so that the benchmark $\bar{n}_R$ value of 0.5 related to (quasi)-instantaneous termination is obtained. Note that the fraction of particles containing two radicals is *e.g.* 3 10^{-2} % at 50 % monomer conversion (cf. Figure B11 in Appendix B) further confirming this statement. The B regime is characterized by the absence of exit of radicals (X_{R0X}=100%) and a sufficiently high average apparent termination rate coefficient (red, Figure 4.9d) results in a negligible amount of short-lived particle types containing two radicals.

The situation is different at higher monomer conversions (> ±60%; regime C). The high number average chain length (Figure 4.6: middle column) and thus high particle viscosity result in a significant decrease of the apparent termination coefficient, as shown in Figure 4.9(d). As a result, termination events do not necessarily occur sufficiently fast and it becomes possible for particle to possess more than one radical (Figure 9c). Consequently, $\bar{n}_R$ can increase above 0.5,

as shown in Figure 4.9a. In other words, the zero-one kinetics approximation is no longer valid, which is an important insight overlooked in previous studies which typically either focus on lower monomer conversion or intrinsic kinetics.

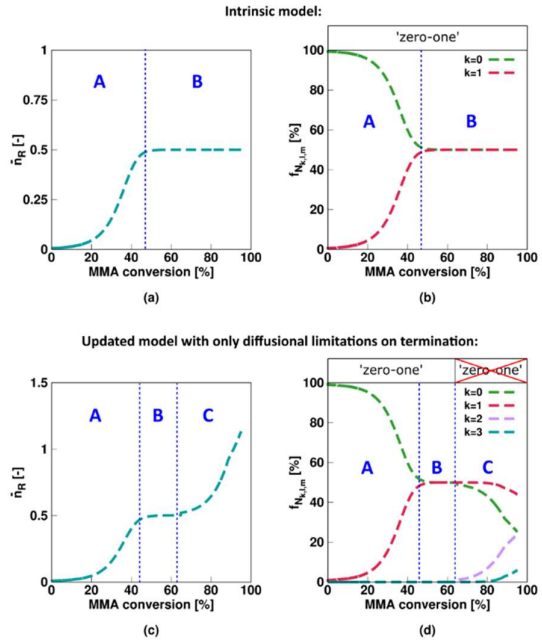

Figure 4.10*:(a)-(b): the average number of macroradicals per particle ($\bar{n}_{R_i}$blue) and the average number of leaving group radicals per particle ($\bar{n}_{R_0}$) in case intrinsic kinetics are assumed for ME2 in Table 4.2 (no diffusional limitations on termination and RAFT transfer); (c)-(d): updates in case diffusional limitations on termination are accounted for. Identical results as in Figure 4.9 implying that the invalidity of zero-one kinetics is due to diffusional limitations on termination only ; same conclusion for ME1 in Table 4.1 (see Section B8 in Appendix B).*

Figure 4.10 further demonstrates the importance of diffusional limitations and thus apparent kinetics. For intrinsic miniemulsion kinetics only two regions can be distinguished in the $\bar{n}_R$ plot and particles possessing more than one radical are almost unachievable. Note that only diffusional limitations on termination are relevant as Figure 4.9 (a) and (c) match with Figure 4.10 (a) and (c), in which intrinsic RAFT transfer rate coefficients are used. In contrast to the bulk case (Figure 4.5) diffusional limitations on RAFT transfer (Figure 4.9(d)) are thus

kinetically less relevant and a better microstructural control results. The same is true for ME1 in Table 4.2, as explained in Appendix B.

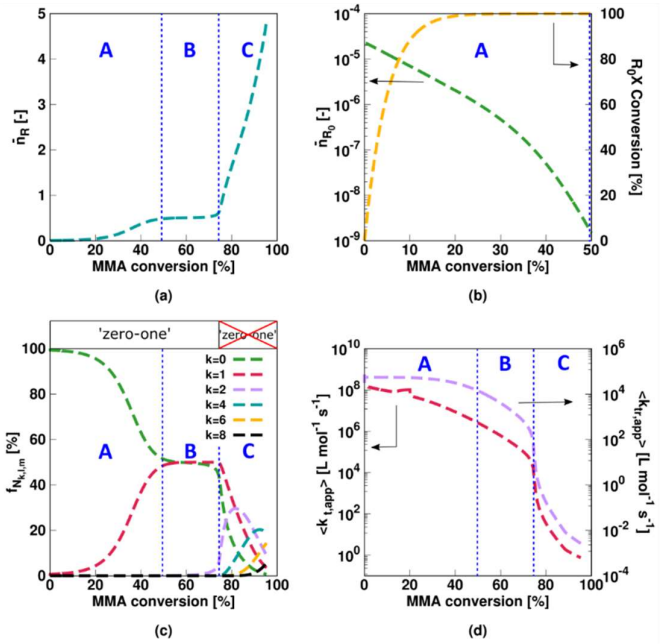

***Figure 4.11**: Results with complete model (diffusional limitations on termination and RAFT transfer; used for Figure 4.6) for the average number of macroradicals per particle ($\bar{n}_R$; (a); blue), average number of leaving group radicals per particle ($\bar{n}_{R_0}$; (b); green), R_0X conversion ((b); orange), fraction of particles with 0 up to 8 macroradicals (c), average apparent overall termination rate coefficient ($\langle k_{t,app} \rangle = \langle k_{tc,app} \rangle + \langle k_{td,app} \rangle$; (d); red ; for calculation see Section B3 in Appendix B) and the average apparent transfer rate coefficient ($\langle k_{tr,app} \rangle$; (d); purple ; for calculation see Section B4 in Appendix B) as a function of MMA conversion for Experiment ME3; conditions as mentioned in Table 4.2) and calculated with model parameters in Table 4.1.*

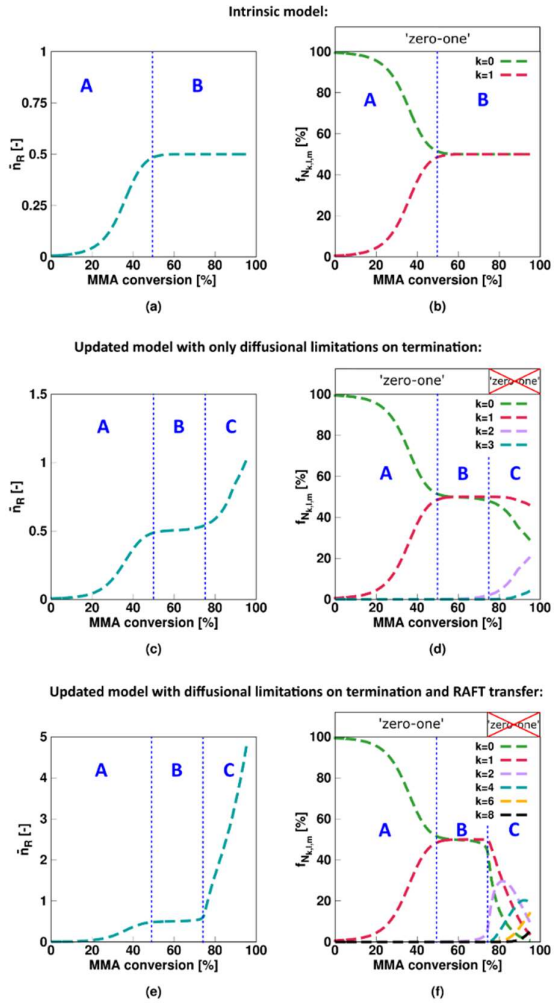

Figure 4.12*: (a-b): the average number of macroradicals per particle ($\bar{n}_R$ blue) and the average number of leaving group radicals per particle ($\bar{n}_{R_0}$) in case intrinsic kinetics are assumed for ME3 in Table 4.2 (no diffusional limitations on termination and RAFT transfer); (c)-(d): updates in case diffusional limitations on termination are accounted for; (e)-(f): updates in case diffusional limitations on termination and RAFT exchange are accounted for. Identical results as in Figure 4.11 only for the bottom row implying that the invalidity of zero-one kinetics is due to diffusional limitation on termination and RAFT transfer.*

Care should be taken for the generalization of this finding. Higher chain length polymer is for instance obtained for ME3 compared to ME1/2 (Figure 4.6; middle column) due to the lower amount of initial R_0X used (Table 4.2). As a result, diffusional limitations on termination and

RAFT transfer result in a more profound decrease of the apparent termination and transfer rate coefficient in regime C, as shown in Figure 4.11(d). Despite that regime A and B in Figure 4.11 are very similar to the corresponding regimes of experiment ME2 in Figure 4.9, with an initial $\bar{n}_R$ well below 0.5 due to exit and re-entry events of R_0 and an $\bar{n}_R$ very close to 0.5 after complete consumption of the initial R_0X (Figure 4.11(b)), the invalidity of the zero-one kinetics in regime C is much more far-reaching. At monomer conversions greater than 80%, the majority of particles even contain more than one radical (Figure 4.11(c)).

For ME3, chain length dependencies are therefore more crucial and diffusional limitations on both termination and RAFT transfer need to be considered, as gradually shown in Figure 4.12. Diffusional limitations on termination already result in the establishment of the three regimes (Figure 4.12 (c)-(d)) but diffusional limitation on RAFT transfer are needed to describe the complete build-up of radicals in regime C up to the higher monomer conversion (Figure 4.12 (e)-(f)). This extra increase of the number of radicals due to apparent RAFT exchange kinetics results in a dispersity increase as in the bulk case albeit at a lower chain length (Figure 4.5). Overall it follows from Figure 4.12(f) that still a significant amount of particles contain less than two radicals, making segregation as characteristic for miniemulsion still relevant.

4.3.4 Miniemulsion RAFT polymerization: relevance of process conditions

Applying a modeling strategy in order to fully understand the kinetics of RAFT miniemulsion polymerization allows the possibility to investigate the process and polymer characteristics over a broad operating window. A first example is shown in Figure 4.13 in which the influence of the targeted chain-length (TCL, $[MMA]_0/[CPDB]_0$) on the time to reach a certain monomer conversion, and the number average chain length, the dispersity, the EGF, and the average number of radical per particle for those monomer conversions are depicted. The other initial amounts are taken as in ME1 in Table 4.1. Focus is on a monomer conversion of 50 (dashed lined) and 80% (full lines).

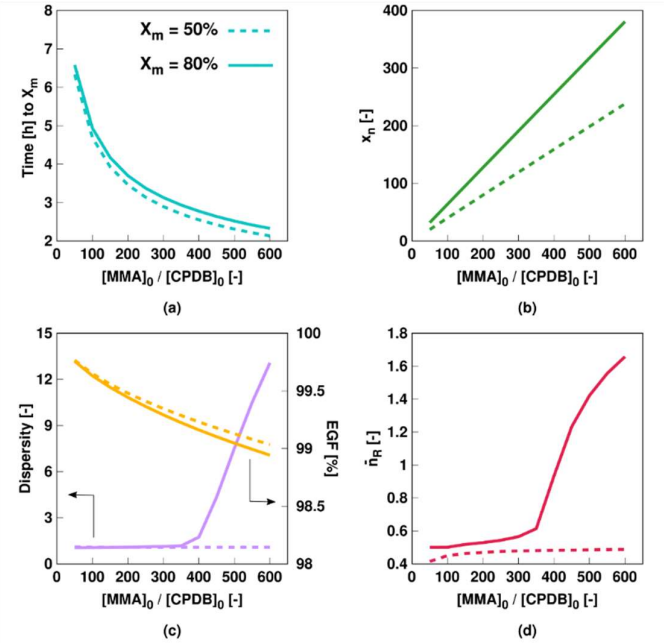

***Figure 4.13**: Influence of the targeted chain length (TCL; $[MMA]_0/[CPDB]_0$) on the time to reach 50% (dashed line) and 80% (full line) monomer conversion (blue, (a)), the number average chain length (x_n, green, (b)), the dispersity (purple, (c)), the end group functionality (orange, (c)), and the average number of macroradicals per particle ($\bar{n}_R$, red, (d)) at those monomer conversions; d_p = 100 nm, all other initial amounts as in experiment ME1 in Table 4.2 except for $m_0(R_0X)$; model parameters as given in Table 4.1.*

Figure 4.13 (a) indicates that a higher TCL leads to shorter polymerization times (see also Section B12 in Appendix B). This is the result of several factors. First of all a smaller initial amount of R_0X results in a less pronounced retardation caused by the leaving group radical R_0 (Figure B12 in Appendix B). While the probability of exit is unaffected by the TCL (Figure B9 in Appendix B) less R_0 radicals are generated. Furthermore, the gel-effect is stronger if higher chain lengths are involved and relatively more conventional radical initiator is present. The latter gives the process a higher FRP character and also explains the lower EGF values (Figure 4.13 (c)).[110] Detailed model inspection also reveals that at medium monomer conversions (50%), the RAFT transfer is not yet influenced by diffusional limitations (similar to Figure 4.9d and Figure 4.11d), even at the highest TCL. The excellent control over the chain growth is at

those monomer conversions thus not influenced by the TCL as shown in Figure 4.13 (c) with a constant dispersity of approximately 1.1 obtained for all TCLs (dashed line). In contrast, at high monomer conversion (*ca.* 80%), diffusional limitations on the RAFT transfer (and termination) result in a sharp increase of the dispersity at higher TCL (full line), consistent with the discussion of Figure 4.12. Consistently at medium monomer conversion (50%; dashed line), the slight reduction of the apparent termination rate coefficient results in only in a negligible increase of $\bar{n}_R$ (Figure 4.13(d); full line), whereas at high monomer conversion (80%) diffusional limitations on both termination and transfer lead to a significant increase of $\bar{n}_R$ with increasing TCL.

As a second example, the influence of the average particle size (d_p) is shown in Figure 4.14. The other process conditions are taken as for ME1 in Table 4.1 (TCL= 192). Focus is on a monomer conversion of 10, 50 and 95% (dotted/dashed/full lines). It follows from Figure 4.14 (a) that a decrease of d_p results in a shorter time to reach a certain monomer conversion, as the total number of radicals present in all particles increases (Figure 4.14 (f)) due to a higher importance of the segregation effect capable of compensating for a more pronounced initial delay due to R_0 exit/entry (*cf.* Figure 4.7-8). The (degenerative) RAFT transfer reactions are however not influenced by this segregation effect as the both the initial RAFT agent and the dormant macrospecies are not kinetically compartmentalized. As a result, both the number average chain length (Figure 4.14(b)) and the dispersity (Figure 4.14 (c)) are not influenced by d_p. Similar to the results shown in Figure 4.6, the dispersity first decreases between 10 and 50% monomer conversion after which it again increases due to diffusional limitations. As the initial molar ratio of R_0X to conventional radical initiator is maintained, too much I_2 derived chains are relatively formed at higher d_p and, hence, more termination events occur resulting in a decrease of the EGF with increasing d_p (Figure 4.14 (d)).

Figure 4.14(e) (vertical dotted blue line) shows that at d_p = 120 nm for $\bar{n}_R$ the three regimes as introduced in Figure 4.10 can be detected: Regime A: very low $\bar{n}_R$ values (close to 0); Regime B: plateau values for $\bar{n}_R$ at 0.5; and Regime C: $\bar{n}_R$ values higher than 1. More in detail, for the very low monomer conversions, Regime A is always active. For example, $\bar{n}_R$ increases steadily with d_p for a monomer conversion of 10% (dotted red line in Figure 4.14(e)) but never a value as high as 0.5 is reached. At such low monomer conversion R_0X is still present and thus the polymerization rate is lowered by exit/entry of R_0 but this effect is less relevant for an increasing average particle size (*cf.* Figure 4.4), explaining the increase of $\bar{n}_R$ along the whole d_p range.

For a monomer conversion at which R_0X is absent the particle size dependence for $\bar{n}_R$ is more complex and also the other two regimes (B and C) can be established. For example, at 50% monomer conversion (dashed line in Figure 4.14(e)) a zero-one system with $\bar{n}_R$ equal to 0.5 results for d_p between ±90 and 120 nm. In this regime, any variation in exit/entry rates (due to a change in particle size) is effectively counteracted by instantaneous termination, keeping $\bar{n}_R$ equal to 0.5. Below 90 nm, however, the delay caused by R_0 exit at low monomer conversion (<40%) is not yet compensated due to the larger amount of particles present (Figure B14 in Appendix B) and thus regime A remains. For d_p larger than 120 nm, the pseudo-bulk kinetic regime C is observed, as $\bar{n}_R$ varies with d_p^3 consistent with the work of Zetterlund and Okubo on NMP.[95] In this regime, $\bar{n}_R$ steadily increases with d_p as termination does not occur fast enough anymore (weaker confined space effect) making it possible for a particle to contain more than one radical.

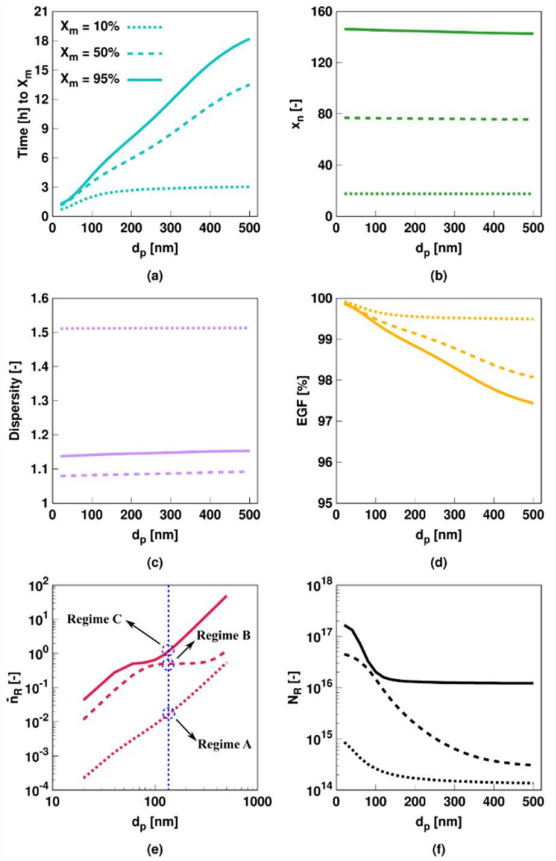

***Figure 4.14**: Influence of the (average) particle size (d_p) on the time to reach 10% (dotted line), 50% (dashed line) and 95% (full line) monomer conversion (blue, (a)), and the number average chain length (x_n, green, (b)), the dispersity (purple, (c)), the end-group functionality (orange, (d)), the average number of radicals per particle ($\bar{n}_R$, red, (e)) and the total number of radicals in the organic phase (all particles, black, (f)) at those monomer conversions; Blue line in e for comparison with Figure 4.9a; experimental conditions as in experiment ME1 in Table 4.2 (targeted chain length of 192); model parameters as given in Table 4.1.*

Finally, for a monomer conversion of 95% (full line in Figure 4.14(e)), similar to the results at 50% monomer conversion, at very low average particle sizes an $\bar{n}_R$ of 0.5 is still not achieved as no full compensation for the delay by R_0 exit is still not obtained. As diffusional limitations on termination are now stronger it is also less likely that one radical can be maintained per particle at already lower particle sizes. Only the particles with an intermediate size (but lower than the suited sizes at 50% monomer conversion) can still ensure fast termination, enabling a

zero-one system with $\bar{n}_R$ equal to 0.5. In other words, Regime C is more easily encountered at the expense of Regime B. Hence, the view that zero-one kinetics are simply established in RAFT polymerization, should be revisited in a more nuanced way, especially upon fully appreciating diffusional limitations at higher monomer conversions. In general, a RAFT polymerization conducted in miniemulsion can display three kinetic regimes: (i) a zero-one system with rate control by R_0 exit, (ii) a zero-one system featuring instantaneous termination, and (iii) a pseudo-bulk regime, with the possibility of more than one radical per particle.

4.4 Conclusions

For degenerative miniemulsion RAFT polymerization with a small RAFT agent R_0X at the start it is demonstrated with a two-dimensional Smith-Ewart based model coupled with moment equations under the pseudo-bulk approximation that it is not afforded to assume zero-one kinetics, as often done in previous studies. At one point in the polymerization, the reaction mixture becomes too viscous and the apparent termination reactivity cannot be high enough to minimize the contribution of nanoparticles with more than 1 (macro)radical. In other words, "instantaneous" termination cannot be established. Moreover, if the average chain length can become sufficiently high also diffusional limitation on RAFT transfer become relevant and a significant fraction of the nanoparticles contains several (macro)radicals.

For higher average particle sizes, this invalidity of the zero-one kinetics is already visible at lower monomer conversions due a lesser importance of the confined space effect. Furthermore, at the lower average particle sizes exit of R_0 at the lower monomer conversions is more relevant and the polymerization slows more down. However, as soon as R_0X is completely consumed, the segregation effect is dominant and higher polymerization rates are obtained as for the bulk counterpart, at least if the monomer conversion is allowed to become sufficiently high.

Under the range of conditions studied the end-group functionality is always high but too high monomer conversions should be avoided to allow for the synthesis of low dispersity polymers.

The developed model thus allows to identify the optimal average particle size in view of design of the polymerization rate and control over the average polymer properties.

4.5 References

1 Barner-Kowollik, C. *Handbook of RAFT Polymerization*; Wiley-VCH: Weinheim, 2008.

2 Tobita, H. Modeling Controlled/Living Radical Polymerization Kinetics: Bulk and Miniemulsion. *Macromol. React. Eng.* **2010**, *4* (11–12), 643–662.

3 Tobita, H. Threshold Particle Diameters in Miniemulsion Reversible-Deactivation Radical Polymerization. *Polymers (Basel).* **2011**, *3* (4), 1944–1971.

4 Luo, Y.; Liu, X. Reversible Addition-Fragmentation Transfer (RAFT) Copolymerization of Methyl Methacrylate and Styrene in Miniemulsion. *J. Polym. Sci. Part A Polym. Chem.* **2004**, *42* (24), 6248–6258.

5 Yang, L.; Luo, Y.; Liu, X.; Li, B. RAFT Miniemulsion Polymerization of Methyl Methacrylate. *Polymer (Guildf).* **2009**, *50* (18), 4334–4342.

6 Hill, M. R.; Carmean, R. N.; Sumerlin, B. S. Expanding the Scope of RAFT Polymerization: Recent Advances and New Horizons. *Macromolecules* **2015**, *48*, 5459–5469.

7 Prescott, S. W.; Ballard, M. J.; Rizzardo, E.; Gilbert, R. G. RAFT in Emulsion Polymerization: What Makes It Different? *Aust. J. Chem.* **2002**, *55*, 415.

8 Matahwa, H.; Mcleary, J. B.; Sanderson, R. D. Comparative Study of Classical Surfactants and Polymerizable Surfactants (Surfmers) in the Reversible Addition-Fragmentation Chain Transfer Mediated Miniemulsion Polymerization of Styrene and Methyl Methacrylate. *J. Polym. Sci. Part A Polym. Chem.* **2006**, *44* (1), 427–442.

9 Devlaminck, D. J. G.; Van Steenberge, P. H. M.; De Keer, L.; Reyniers, M.-F.; D'hooge,

D. R. A Detailed Mechanistic Study of Bulk MADIX of Styrene and Its Chain Extension. *Polym. Chem.* **2017**, *8* (45), 6948–6963.

10 Derboven, P.; Steenberge, P. H. M. Van; Reyniers, M.; Barner-kowollik, C.; Dagmar, R. D.; Marin, G. B.; D'hooge, D. R.; Marin, G. B.; Dagmar, R. D.; Marin, G. B. Chain Transfer in Degenerative RAFT Polymerization Revisited : A Comparative Study. *Macromol. Theory Simulations* **2016**, *25* (1), 104–115.

11 Gody, G.; Maschmeyer, T.; Zetterlund, P. B.; Perrier, S. Exploitation of the Degenerative Transfer Mechanism in RAFT Polymerization for Synthesis of Polymer of High Livingness at Full Monomer Conversion. *Macromolecules* **2014**, *47*, 639–649.

12 Kubo, K.; Goto, A.; Sato, K.; Kwak, Y.; Fukuda, T. Kinetic Study on Reversible Addition-Fragmentation Chain Transfer (RAFT) Process for Block and Random Copolymerizations of Styrene and Methyl Methacrylate. *Polymer (Guildf).* **2005**, *46* (23), 9762–9768.

13 Zetterlund, P. B.; Gody, G.; Perrier, S. Sequence-Controlled Multiblock Copolymers via RAFT Polymerization: Modeling and Simulations. *Macromol. Theory Simulations* **2014**, *23*, 331–339.

14 Pepels, M. P. F.; Holdsworth, C. I.; Pascual, S.; Monteiro, M. J. RAFT-Mediated Emulsion Polymerization of Styrene with Low Reactive Xanthate Agents: Microemulsion-like Behavior. *Macromolecules* **2010**, *43*, 7565–7576.

15 Buback, M.; Meiser, W.; Vana, P. Mechanism of CPDB-Mediated RAFT Polymerization of Methyl Methacrylate: Influence of Pressure and RAFT Agent Concentration. *Aust. J. Chem.* **2009**, *62* (11), 1484–1487.

16 Gao, J.; Luo, Y.; Wang, R.; Bogeng, L.; Zhu, S. Kinetics of Methyl Methacrylate and N-Butyl Acrylate Copolymerization Mediated by 2-Cyanoprop-2-Yl Dithiobenzoate as a RAFT

Agent. *J. Polym. Sci. Part A Polym. Chem.* **2007**, *45*, 3098–3111.

17 Chong, B. Y. K.; Krstina, J.; Le, T. P. T.; Moad, G.; Postma, A.; Rizzardo, E.; Thang, S. H. Thiocarbonylthio Compounds [S=C(Ph)S-R) in Free Radical Polymerization with Reversible Addition-Fragmentation Chain Transfer (RAFT Polymerization). Role of the Free-Radical Leaving Group (R). *Macromolecules* **2003**, *36*, 2256–2272.

18 Benaglia, M.; Rizzardo, E.; Alberti, A.; Guerra, M. Searching for More Effective Agents and Conditions for the RAFT Polymerization of MMA: Influence of Dithioester Substituents, Solvent, and Temperature. *Macromolecules* **2005**, *38* (8), 3129–3140.

19 Matyjaszewski, K.; Spanswick, J. Controlled / Living Radical Polymerization. *Materialstoday* **2005**, *8*, 26–33.

20 Derboven, P.; Van Steenberge, P.; Reyniers, M.-F.; Barner-Kowollik, C.; D'hooge, D. R.; Marin, G. B. A Novel Method for the Measurement of Degenerative Chain Transfer Coefficients: Proof of Concept and Experimental Validation. *Polym. Chem.* **2016**, *7*, 3334–3349.

21 Moad, G. Mechanism and Kinetics of Dithiobenzoate-Mediated RAFT Polymerization: Status of Dilemma. *Macromol. Chem. Phys.* **2014**, *215*, 9–26.

22 Cunningham, M. F. Controlled/living Radical Polymerization in Aqueous Dispersed Systems. *Prog. Polym. Sci.* **2008**, *33* (4), 365–398.

23 Save, M.; Guillaneuf, Y.; Gilbert, R. G. Controlled Radical Polymerization in Aqueous Dispersed Media. *Aust. J. Chem.* **2006**, *59* (10), 693–711.

24 Luo, Y.; Wang, R.; Yang, L.; Yu, B.; Li, B.; Zhu, S. Effect of Reversible Addition-Fragmentation Transfer (RAFT) Reactions on (Mini)emulsion Polymerization Kinetics and Estimate of RAFT Equilibrium Constant. *Macromolecules* **2006**, *39*, 1328–1337.

25 Lansalot, M.; Davis, T. P.; Heuts, J. P. A. RAFT Miniemulsion Polymerization:

Influence of the Structure of the RAFT Agent. *Macromolecules* **2002**, *35* (20), 7582–7591.

26 Smulders, W.; Gilbert, R. G.; Monteiro, M. J. A Kinetic Investigation of Seeded Emulsion Polymerization of Styrene Using Reversible Addition-Fragmentation Chain Transfer (RAFT) Agents with a Low Transfer Constant. *Macromolecules* **2003**, *36* (12), 4309–4318.

27 Guo, Y.; Tysoe, M. E.; Zetterlund, P. B. Rate Enhanced Nitroxide-Mediated Miniemulsion Polymerization: Effect of Nitroxide Water Solubility. *Polym. Chem.* **2013**, *4* (11), 3256–3264.

28 Drache, M.; Brandl, K.; Reinhardt, R.; Beuermann, S. Ab Initio Kinetic Monte Carlo Simulation of Seeded Emulsion Polymerizations of Styrene. *Phys. Chem. Chem. Phys.* **2018**, *20* (16), 10796–10805.

29 Russum, J. P.; Barbre, N. D.; Jones, C. W.; Schork, F. J. Miniemulsion Reversible Addition Fragmentation Chain Transfer Polymerization of Vinyl Acetate. *J. Polym. Sci. Part A Polym. Chem.* **2005**, *43* (10), 2188–2193.

30 Altarawneh, I. S.; Gomes, V. G.; Srour, M. H. Polymer Chain Extension in Semibatch Emulsion Polymerization with RAFT-Based Transfer Agent: The Influence of Reaction Conditions on Polymerization Rate and Product Properties. *J. Appl. Polym. Sci.* **2009**, *114*, 2356–2372.

31 Monteiro, M. J.; De Barbeyrac, J. Free-Radical Polymerization of Styrene in Emulsion Using a Reversible Addition - Fragmentation Chain Transfer Agent with a Low Transfer Constant: Effect on Rate, Particle Size, and Molecular Weight. *Macromolecules* **2001**, *34*, 4416–4423.

32 D'hooge, D. R.; Van Steenberge, P. H. M.; Reyniers, M.-F.; Marin, G. B. The Strength of Multi-Scale Modeling to Unveil the Complexity of Radical Polymerization. *Prog. Polym. Sci.* **2016**, *58*, 59–89.

33 Prescott, S. W.; Ballard, M. J.; Rizzardo, E.; Gilbert, R. G. Radical Loss in RAFT-Mediated Emulsion Polymerizations. *Macromolecules* **2005**, *38* (11), 4901–4912.

34 Prescott, S. W.; Ballard, M. J.; Rizzardo, E.; Gilbert, R. G. Rate Optimization in Controlled Radical Emulsion Polymerization Using RAFT. *Macromol. Theory Simulations* **2006**, *15* (1), 70–86.

35 Sen, M. Y.; Puskas, J. E. Green Polymer Chemistry: Telechelic Poly(ethylene Glycol)s via Enzymatic Catalysis. *Am. Chem. Soc. Polym. Prepr. Div. Polym. Chem.* **2008**, *49* (1), 487–488.

36 Zetterlund, P. B.; Kagawa, Y.; Okubo, M. Controlled/living Radical Polymerization in Dispersed Systems. *Chem. Rev.* **2008**, *108* (9), 3747–3794.

37 Zetterlund, P. B.; Thickett, S. C.; Perrier, S.; Bourgeat-Lami, E.; Lansalot, M. Controlled/Living Radical Polymerization in Dispersed Systems: An Update. *Chem. Rev.* **2015**, *115*, 9745–9800.

38 Prescott, S. W.; Ballard, M. J.; Rizzardo, E.; Gilbert, R. G. Successful Use of RAFT Techniques in Seeded Emulsion Polymerization of Styrene: Living Character, RAFT Agent Transport, and Rate of Polymerization. *Macromolecules* **2002**, *35* (14), 5417–5425.

39 McLeary, J. B.; Klumperman, B. RAFT Mediated Polymerisation in Heterogeneous Media. *Soft Matter* **2006**, *2*, 45–53.

40 Stoffelbach, F.; Tibiletti, L.; Rieger, J.; Charleux, B. Surfactant-Free, Controlled/living Radical Emulsion Polymerization in Batch Conditions Using a Low Molar Mass, Surface-Active Reversible Addition-Fragmentation Chain-Transfer (RAFT) Agent. *Macromolecules* **2008**, *41*, 7850–7856.

41 Jung, S. M.; Gomes, V. G. Miniemulsion Polymerisation via Reversible Addition Fragmentation Chain Transfer in Pseudo-Bulk Regime. *Macromol. React. Eng.* **2011**, *5*, 303–

315.

42 Asua, J. M. Challenges for Industrialization of Miniemulsion Polymerization. *Prog. Polym. Sci.* **2014**, *39* (10), 1797–1826.

43 Brouwer, H. De; Tsavalas, J. G.; Schork, F. J.; Michael, J. Living Radical Polymerization in Miniemulsion Using Reversible Addition - Fragmentation Chain Transfer. *Macromolecules* **2000**, *33*, 9239–9246.

44 Qi, G.; Schork, F. J. On the Stability of Miniemulsions in the Presence of RAFT Agents. *Langmuir* **2006**, *22* (22), 9075–9078.

45 Schork, F. J.; Luo, Y.; Smulders, W.; Russum, J. P.; Butté, A.; Fontenot, K. Miniemulsion Polymerization. *Adv. Polym. Sci.* **2005**, *175*, 129–255.

46 Zhou, X.; Ni, P.; Yu, Z. Comparison of RAFT Polymerization of Methyl Methacrylate in Conventional Emulsion and Miniemulsion Systems. *Polymer (Guildf).* **2007**, *48* (21), 6262–6271.

47 Suzuki, K.; Nishimura, Y.; Kanematsu, Y.; Masuda, Y.; Satoh, S.; Tobita, H. Experimental Validation of Intermediate Termination in RAFT Polymerization with Dithiobenzoate via Comparison of Miniemulsion and Bulk Polymerization Rates. *Macromol. React. Eng.* **2012**, *6* (1), 17–23.

48 Tsavalas, J. G.; Schork, F. J.; De Brouwer, H.; Monteiro, M. J. Living Radical Polymerization by Reversible Addition-Fragmentation Chain Transfer in Ionically Stabilized Miniemulsions. *Macromolecules* **2001**, *34*, 3938–3946.

49 Tonge, M. P.; Mcleary, J. B.; Vosloo, J. J.; Sanderson, R. D. RAFT Polymerisation in Water-Borne Organic Dispersions. *Macromol. Symp.* **2003**, *193*, 289–304.

50 Butte, A.; Storti, G.; Morbidelli, M. Miniemulsion Living Free Radical Polymerization by RAFT. *Macromolecules* **2001**, *34*, 5885–5896.

51 Yang, L.; Luo, Y.; Bogeng, L. I. RAFT Miniemulsion Polymerization Targeting to Polymer of Higher Molecular Weight. *J. Polym. Sci. Part A Polym. Chem.* **2005**, *43* (20), 4972–4979.

52 Luo, Y.; Liu, B.; Wang, Z.; Gao, J.; Li, B. Butyl Acrylate RAFT Polymerization in Miniemulsion. *J. Polym. Sci. Part A-Polymer Chem.* **2007**, *45*, 2304–2315.

53 Uzulina, I.; Gaillard, N.; Guyot, A.; Claverie, J. Controlled Radical Polymerization of Styrene in Miniemulsion Polymerization Using Reversible Addition Fragmentation Chain Transfer. *Comptes Rendus Chim.* **2003**, *6* (11–12), 1375–1384.

54 Yang, L.; Luo, Y.; Li, B. Reversible Addition Fragmentation Transfer (RAFT) Polymerization of Styrene in a Miniemulsion: A Mechanistic Investigation. *Polymer (Guildf).* **2006**, *47* (2), 751–762.

55 Bowes, A.; Mcleary, J. B.; Sanderson, R. D. AB and ABA Type Butyl Acrylate and Styrene Block Copolymers via RAFT-Mediated Miniemulsion Polymerization. *J. Polym. Sci. Part A Polym. Chem.* **2007**, *45*, 588–604.

56 Zayas, H. a.; Truong, N. P.; Valade, D.; Jia, Z.; Monteiro, M. J. Narrow Molecular Weight and Particle Size Distributions of Polystyrene 4-Arm Stars Synthesized by RAFT-Mediated Miniemulsions. *Polym. Chem.* **2013**, *4*, 592–599.

57 Luo, Y.; Tsavalas, J.; Schork, F. J. Theoretical Aspects of Particle Swelling in Living Free Radical Miniemulsion Polymerization. *Macromolecules* **2001**, *34* (16), 5501–5507.

58 Monteiro, M. J.; Hodgson, M.; De Brouwer, H. Influence of RAFT on the Rates and Molecular Weight Distributions of Styrene in Seeded Emulsion Polymerizations. *J. Polym. Sci. Part A Polym. Chem.* **2000**, *38*, 3864–3874.

59 Tobita, H. RAFT Miniemulsion Polymerization Kinetics, 2 - Molecular Weight Distribution. *Macromol. Theory Simulations* **2009**, *18* (2), 120–126.

60 Tobita, H.; Yanase, F. Monte Carlo Simulation of Controlled/living Radical Polymerization in Emulsified Systems. *Macromol. Theory Simulations* **2007**, *16* (4), 476–488.

61 Tobita, H. Kinetics of Controlled/living Radical Polymerization in Emulsified Systems. *Macromol. Symp.* **2008**, *261* (1), 36–45.

62 Tobita, H. Fundamentals of RAFT Miniemulsion Polymerization Kinetics. *Macromol. Symp.* **2010**, *288* (1), 16–24.

63 Tobita, H. On the Discrimination of RAFT Models Using Miniemulsion Polymerization. *Macromol. Theory Simulations* **2013**, *22* (8), 399–409.

64 Luo, Y.; Yu, B. Monte Carlo Simulation of Droplet Nucleation in RAFT Free Radical Miniemulsion Polymerization. *Polym. Plast. Technol. Eng.* **2005**, *43* (5), 1299–1321.

65 Wang, Z.; Zhang, Q.; Zhan, X.; Chen, F.; Rao, G.; Xiong, J. Preparation, Kinetics and Microstructures of Well-Defined PS-B-PS/Bd Diblock Copolymers via RAFT Miniemulsion Polymerization. *J. Polym. Res.* **2013**, *20* (11), 288–301.

66 Li, X.; Wang, W. J.; Weng, F.; Li, B. G.; Zhu, S. Targeting Copolymer Composition Distribution via Model-Based Monomer Feeding Policy in Semibatch RAFT Mini-Emulsion Copolymerization of Styrene and Butyl Acrylate. *Ind. Eng. Chem. Res.* **2014**, *53*, 7321–7332.

67 Suzuki, K.; Kanematsu, Y.; Miura, T.; Minami, M.; Satoh, S.; Tobita, H. Experimental Method to Discriminate RAFT Models between Intermediate Termination and Slow Fragmentation via Comparison of Rates of Miniemulsion and Bulk Polymerization. *Macromol. Theory Simulations* **2014**, *23* (3), 136–146.

68 Kwak, Y.; Goto, A.; Tsujii, Y.; Murata, Y.; Komatsu, K.; Fukuda, T. A Kinetic Study on the Rate Retardation in Radical Polymerization of Styrene with Addition−Fragmentation Chain Transfer. *Macromolecules* **2002**, *35* (8), 3026–3029.

69 Smith, W. V.; Ewart, R. H. Kinetics of Emulsion Polymerization. *J. Chem. Phys.* **1948**,

16, 592–599.

70 Okubo, M. *Polymer Particles*; Springer, 2005.

71 Thickett, S. C.; Gilbert, R. G. Emulsion Polymerization: State of the Art in Kinetics and Mechanisms. *Polymer (Guildf).* **2007**, *48* (24), 6965–6991.

72 Van Steenberge, P. H. M.; D.R., D.; Reyniers, M. F.; Marin, G. B.; Cunningham, M. F. 4-Dimensional Modeling Strategy for an Improved Understanding of Miniemulsion NMP of Acrylates Initiated by SG1-Macroinitiator. *Macromolecules* **2014**, *47*, 7732–7741.

73 Bentein, L.; D'hooge, D. R.; Reyniers, M.-F.; Marin, G. B. Kinetic Modeling of Miniemulsion Nitroxide Mediated Polymerization of Styrene: Effect of Particle Diameter and Nitroxide Partitioning up to High Conversion. *Polymer (Guildf).* **2012**, *53* (3), 681–693.

74 Cano-Valdez, A.; Saldívar-Guerra, E.; González-Blanco, R.; Cunningham, M. F.; Herrera-Ordóñez, J. Nitroxide Mediated Radical Emulsion Polymerization: Mathematical Modeling. *Macromol. Symp.* **2017**, *374* (1), 1–11.

75 Sugihara, Y.; Zetterlund, P. B. Synergistic Effects of Compartmentalization and Nitroxide Exit/Entry in Nitroxide-Mediated Radical Polymerization in Dispersed Systems. *Macroletters* **2012**, *696* (1), 12–16.

76 De Rybel, N.; Van Steenberge, P. H. M.; Reyniers, M.-F.; D'hooge, D. R.; Marin, G. B. How Chain Length Dependencies Interfere with the Bulk RAFT Polymerization Rate and Microstructural Control. *Chem. Eng. Sci.* **2018**, *177*, 163–179.

77 De Rybel, N.; Van Steenberge, P. H. M.; Reyniers, M.-F.; Barner-Kowollik, C.; D'hooge, D. R.; Marin, G. B. An Update on the Pivotal Role of Kinetic Modeling for the Mechanistic Understanding and Design of Bulk and Solution RAFT Polymerization. *Macromol. Theory Simulations* **2017**, *26*, 1600048.

78 D'hooge, D. R.; Reyniers, M. F.; Marin, G. B. The Crucial Role of Diffusional

Limitations in Controlled Radical Polymerization. *Macromol. React. Eng.* **2013**, *7*, 362–379.

79 Johnston-Hall, G.; Theis, A.; Monteiro, M. J.; Davis, T. P.; Stenzel, M. H.; Barner-Kowollik, C. Accessing Chain Length Dependent Termination Rate Coefficients of Methyl Methacrylate (MMA) via the Reversible Addition Fragmentation Chain Transfer (RAFT) Process. *Macromol. Chem. Phys.* **2005**, *206* (20), 2047–2053.

80 Van Steenberge, P. H. M.; D'hooge, D. R.; Reyniers, M.-F.; Marin, G. B. Improved Kinetic Monte Carlo Simulation of Chemical Composition-Chain Length Distributions in Polymerization Processes. *Chem. Eng. Sci.* **2014**, *110*, 185–199.

81 Rabea, A. M.; Zhu, S. Modeling the Influence of Diffusion-Controlled Reactions and Residual Termination and Deactivation on the Rate and Control of Bulk ATRP at High Conversions. *Polymers (Basel).* **2015**, *7* (5), 819–835.

82 Wang, A. R.; Zhu, S. Effects of Diffusion-Controlled Radical Reactions on RAFT Polymerization. *Macromol. Theory Simulations* **2003**, *12* (23), 196–208.

83 Dong, Y.; Sundberg, D. C. Radical Entry in Emulsion Polymerization: Estimation of the Critical Length of Entry Radicals via a Simple Lattice Model. *Macromolecules* **2002**, *35* (21), 8185–8190.

84 Perry, R. H.; Green, D. W. *Perry's Chemical Engineers' Hand-Book*; McGraw-Hill: New York, 1998.

85 Dossi, M.; Storti, G.; Moscatelli, D. Initiation Kinetics in Free-Radical Polymerization: Prediction of Thermodynamic and Kinetic Parameters Based on Ab Initio Calculations. *Macromol. Theory Simulations* **2010**, *19* (4), 170–178.

86 Erben, M. T.; Bywater, S. The Thermal Decomposition of 2,2'-Azo-Bis-Isobutyronitrile. Part I. Products of the Reaction. *J. Am. Chem. Soc.* **1955**, *77* (14), 3712–3714.

87 Beuermann, S.; Buback, M. Rate Coefficients of Free-Radical Polymerization Deduced

from Pulsed Laser Experiments. *Prog. Polym. Sci.* **2002**, *27* (2), 191–254.

88 Johnston-Hall, G.; Monteiro, M. J. Bimolecular Radical Termination: New Perspectives and Insights. *J. Polym. Sci. Part a-Polymer Chem.* **2008**, *46* (10), 3155–3176.

89 Moad, G.; Solomon, D. H. *The Chemistry of Radical Polymerization*; Elsevier, 2006.

90 Fierens, S. K.; Van Steenberge, P. H. M.; Reyniers, M. F.; Marin, G. B.; D'hooge, D. R. How Penultimate Monomer Unit Effects and Initiator Influence ICAR ATRP of N-Butyl Acrylate and Methyl Methacrylate. *AIChE J.* **2017**, *63* (11), 4971–4986.

91 Nakamura, Y.; Yamago, S. Termination Mechanism in the Radical Polymerization of Methyl Methacrylate and Styrene Determined by the Reaction of Structurally Well-Defined Polymer End Radicals. *Macromolecules* **2015**, *48* (18), 6450–6456.

92 Buback, M.; Günzler, F.; Russell, G. T.; Vana, P. Determination of the Mode of Termination in Radical Polymerization via Mass Spectrometry. *Macromolecules* **2009**, *42* (3), 652–662.

93 Gilbert, R. G. *Emulsion Polymerization: A Mechanistic Approach*; Academic Press Inc., 1995.

94 Zetterlund, P. B. Controlled/living Radical Polymerization in Nanoreactors: Compartmentalization Effects. *Polym. Chem.* **2011**, *2* (3), 534–549.

95 Zetterlund, P. B.; Okubo, M. Compartmentalization in Nitroxide-Mediated Radical Polymerization in Dispersed Systems. *Macromolecules* **2006**, *39* (26), 8959–8967.

96 Bentein, L.; D'Hooge, D. R.; Reyniers, M. F.; Marin, G. B. Kinetic Modeling as a Tool to Understand and Improve the Nitroxide Mediated Polymerization of Styrene. *Macromol. Theory Simulations* **2011**, *20*, 238–265.

97 Mastan, E.; Zhu, S. Method of Moments: A Versatile Tool for Deterministic Modeling of Polymerization Kinetics. *Eur. Polym. J.* **2015**, *68*, 139–160.

98 D'hooge, D. R.; Reyniers, M.-F.; Marin, G. B. Methodology for Kinetic Modeling of Atom Transfer Radical Polymerization. *Macromol. React. Eng.* **2009**, *3*, 185–209.

99 Wang, W.; Zhou, Y.; Shi, L.; Luo, Z.-H. Modeling of the Atom Transfer Radical Copolymerization Processes of Methyl Methacrylate and 2-(Trimethylsilyl) Ethyl Methacrylate under Batch, Semibatch, and Continuous Feeding: A Chemical Reactor Engineering Viewpoint. *Ind. Eng. Chem. Res.* **2014**, *53*, 11873–11883.

100 Zhou, Y.-N.; Luo, Z.-H. State-of-the-Art and Progress in Method of Moments for the Model-Based Reversible-Deactivation Radical Polymerization. *Macromol. React. Eng.* **2016**, *10* (6), 516–534.

101 Derboven, P.; D'hooge, D. R.; Reyniers, M.-F.; Marin, G. B.; Barner-Kowollik, C. The Long and the Short of Radical Polymerization. *Macromolecules* **2015**, *48*, 492–501.

102 Buback, M.; Huckestein, B.; Kuchta, F.; Russell, G. T. Initiator Efficiencies in 2,2'-Azoisobutyronitrile-Initiated Free Radical Polymerizations of Styrene. *Macromol. Chem. Phys.* **1994**, *195*, 2117–2140.

103 Garg, D. K.; Serra, C. A.; Hoarau, Y.; Parida, D.; Bouquey, M.; Muller, R. Analytical Solution of Free Radical Polymerization: Applications- Implementing Gel Effect Using AK Model. *Macromolecules* **2014**, *47* (21), 7370–7377.

104 Tefera, N.; Weickert, G.; Westerterp, K. R. Modeling of Free Radical Polymerization up to High Conversion . I . A Method for the Selection of Models by Simultaneous Parameter Estimation. *J. Appl. Polym. Sci.* **1996**, *63*, 1649–1661.

105 Carswell, T. G.; Hill, D. J. T.; Londero, D. I.; O'Donnell, J. H.; Pomery, P. J.; Winzor, C. L. Kinetic Parameters for Polymerization of Methyl Methacrylate at 60°C. *Polymer (Guildf).* **1992**, *33* (1), 137–140.

106 Zetterlund, P. B.; Okubo, M. Nitroxide-Mediated Radical Polymerization in

Miniemulsion at Stationary State: Rationale for Independence of Polymerization Rate on Nitroxide Partitioning Using Oil-Phase Initiation. *Macromol. Theory Simulations* **2005**, *14* (7), 415–420.

107 Shang, Y.; Shan, G.-R. IBN Partition between St Monomer/Polymer and Water and Its Application in Miniemulsion Polymerization Initiated by AIBN. *AIChE J.* **2012**, *58* (10), 3135–3143.

108 Shang, Y.; Shan, G.; Pan, P. Kinetic and Molecular Weight Modeling of Miniemulsion Polymerization Initiated by Oil-Soluble Initiators. *Macromol. Chem. Phys.* **2015**, *216*, 884–893.

109 O'Driscoll, K. F. *Comprehensive Polymer Science*; Pergamon Press London, 1989.

110 D'Hooge, D. R.; Konkolewicz, D.; Reyniers, M. F.; Marin, G. B.; Matyjaszewski, K. Kinetic Modeling of ICAR ATRP. *Macromol. Theory Simulations* **2012**, *21* (1), 52–69.

Chapter 5: A theoretical comparison of non-degenerative and degenerative RAFT polymerization of Styrene under miniemulsion conditions with macro-RAFT agent and water soluble initiator

5.1 Introduction

Free radical polymerization (FRP) is currently one of the most commonly applied industrial polymerization techniques, due to its relative insensitivity to impurities, compatibility with a wide range of monomers, and the possibility to use multiple reaction media including bulk, solution, suspension and emulsion.[1–10] A drawback is the limited structural control at the molecular level, with a high dispersity (>1.5) and a restricted functionality degree in view of the synthesis of complex well-defined macromolecular architectures. To overcome this drawback, reversible deactivation radical polymerization (RDRP) or controlled radical polymerization (CRP) techniques have been developed, allowing to regulate the molecular structure of individual polymer chains and design novel molecular architectures such as block, star, comb-like, and dendritic (co)polymers inaccessible by FRP.[2,4,5,7,11–16]

Despite that several RDRP techniques have been proposed over the last decennia, reversible addition-fragmentation chain transfer (RAFT) polymerization is one of the most promising ones due to its direct resemblance to FRP regarding the order of magnitude of the polymerization rate.[17–19] In view of prospective industrial operation, RAFT polymerization in a dispersed medium with water as the continuous phase is preferred, as it reduces the risks of overheating and runaway as a result of the highly exothermic nature of radical polymerization.[2,20–25] High monomer conversions can also be targeted without the increasing viscosity becoming a very critical issue as in bulk polymerization, which minimizes potential problems with residual monomer removal.[26,27] Moreover, for well-chosen (average) particle sizes the kinetics are influenced by compartmentalization as reactants are physically confined within discrete

confined spaces with active particles even possessing only one radical so that the livingness of the RAFT polymerization can be increased compared to the bulk RAFT process.[28–36]

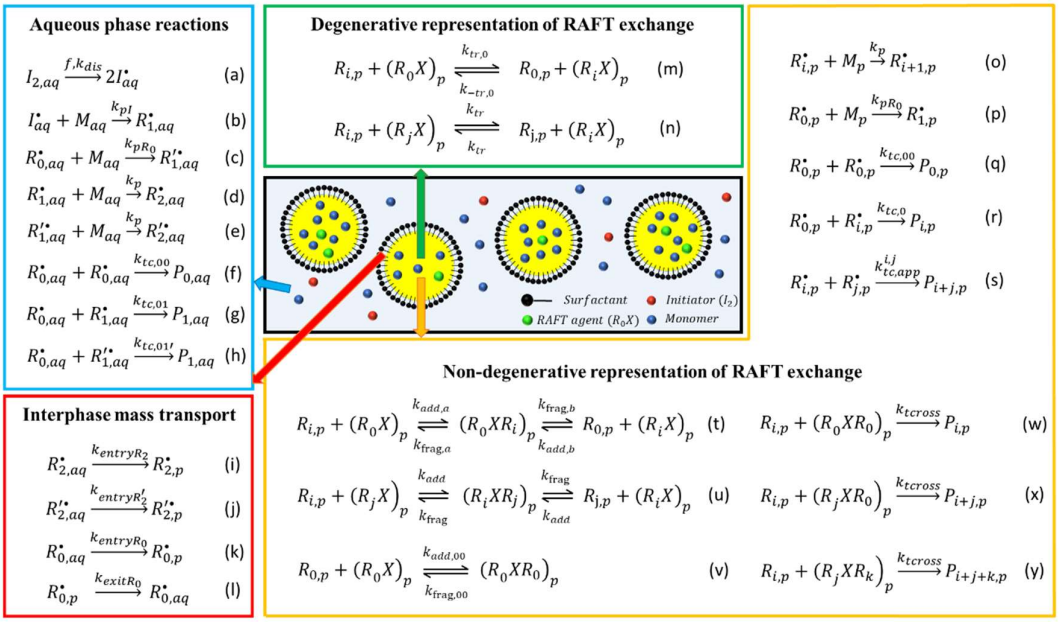

Figure 5.1: *Representation of the RAFT miniemulsion process (black box: initialization with water soluble initiator and oil soluble initial RAFT agent) and an overview of the main reactions and interphase mass transfers. A subdivision is made between the reactions occurring in the aqueous phase (blue box, reaction (a)-(h)), in the organic phase (orange box, reaction (o)-(y)), and interphase mass transport phenomena (red box, (i)-(l); selected number of phenomena). In case a degenerative RAFT mechanism can be assumed, the reaction sequences (t)-(v) in the orange box can be simplified to the exchange events (m) and (n) (green box; also no RAFT-cross termination; reaction (w)-(y)). Conventional termination only shown for the recombination mode (w) as this is dominant for styrene, the monomer investigated in this work; no mass transfer for RAFT intermediate radicals, as they are likely too hydrophobic due to their size.*

A special class of RAFT emulsion polymerization is RAFT miniemulsion polymerization (Figure 5.1; black box; water soluble initiator and oil soluble initial RAFT agent) in which the polymerization occurs in kinetically stable monomer droplets (50-500 nm) realized by high shear homogenization or ultrasonification, making aqueous phase transport of hydrophobic

RAFT agent, as in conventional (macro)emulsion, not an issue. [4,21,34,37–40] Under well-defined conditions, droplet coalescence or aggregation, and monomer diffusion can be restricted and, hence, the initial monomer droplet size distribution is more or less the particle size distribution.[41] A challenge remains to control the reaction rates, taking into account that radicals (besides monomer) can undergo mass transfer due to the heterogeneous nature of the process, as displayed in Figure 5.1 with reactions in the aqueous phase in a blue box, reactions in the organic phase in an orange box, and phase-transfer events in a red box.

As shown Figure 5.1, the water soluble initiator ($I_{2,aq}$) forms initiator fragments (I_{aq}) which subsequently add to monomer (M) until oligomeric species are formed that are too hydrophobic (e.g. critical chain length for styrene, monomer in the present work: 2) to remain in the aqueous phase so that entry (interphase mass tranport (i) in Figure 5.1) into a droplet/particle occurs. There the oligomers can grow to 'true' macroradicals (R_i; i: chain length), which in contrast to FRP do not dominantly terminate to create dead polymer species (P) but can also add to the initial RAFT chain transfer agent (CTA, R_0X), forming a *first* RAFT intermediate radical type (R_iXR_0, , reaction (t) in Figure 5.1). Due to the instability of this adduct-radical, fragmentation occurs resulting in either the starting compounds ($k_{frag,a}$) or a dormant macrospecies (R_iX) and a RAFT CTA derived leaving group radical (R_0) ($k_{frag,b}$). The latter radical is capable of re-initiating the polymerization ($k_{p,R0}$, reaction (s) in Figure 5.1) but can also undergo mass transfer to the aqueous phase (event (l) in Figure 5.1). Furthermore, addition of a macroradical to a dormant macrospecies leads to the formation of a *second* type of RAFT intermediate radical characterized by two arms of in general two different lengths (R_iXR_j, reaction (u) in Figure 5.1). Its fragmentation (k_{frag}) can result in the reactivation of the dormant macrospecies while temporary deactivating the original growing macroradical. If the resulting exchange/transfer of the radical function between growing and dormant macrospecies occurs fast enough, concurrent growth of all the dormant chains can be achieved. Note that a *third* type of RAFT intermediate

radical (R_0XR_0) can be present in the particles, formed by the addition of the leaving group radical R_0 to the initial RAFT CTA R_0X (reaction (v) in Figure 5.1). Hence, 5 types of radicals ($R_0XR_{0,p}$, $R_iXR_{0,p}$, $R_iXR_{j,p}$, $R_{0,p}$ and $R_{i,p}$) can exist in the particles. Considering also the aqueous phase (and the maximal chain lengths) 6 more radicals (I_{aq}, $R(')_{1,aq}$, $R(')_{2,aq}$, and $R_{0,aq}$) exist, ignoring the exit/entry of RAFT intermediate radicals as they are in most cases too hydrophobic.

Under ideal RAFT conditions, implying no-RAFT cross-termination (reaction (w)-(y) in Figure 5.1) and no slow RAFT fragmentation, the consecutive/competitive RAFT additions/fragmentations (reactions (t)-(v) in orange box of Figure 5.1) can be simplified to the so-called degenerative transfer mechanism ("reactions/exchanges" (m) and (n) in the green box in Figure 5.1) in which the intermediate radical species ($R_0XR_{0,p}$, $R_0XR_{i,p}$ and $R_iXR_{j,p}$) are not explicitly mentioned as the pseudo steady-state approximation (PSSA) can be applied to calculate their concentrations.[19,42–45] The corresponding transfer "rate coefficients" ($k_{tr,0}$, $k_{-tr,0}$ and k_{tr}), as defined based on the (conventional) radical and dormant species concentrations, are a function of the elementary RAFT addition and fragmentation parameters:

$$k_{tr,0} = k_{add,0,a}\frac{k_{frag,0,b}}{k_{frag,0,a} + k_{frag,0,b}} \quad (1)$$

$$k_{-tr,0} = k_{add,0,b}\frac{k_{frag,0,a}}{k_{frag,0,a} + k_{frag,0,b}} \quad (2)$$

$$k_{tr} = \frac{k_{add}}{2} \quad (3)$$

with in the last equation, for simplicity, chain length dependencies neglected. Intrinsically this assumption can be realistic[46] but at higher monomer conversion the RAFT exchanges can be influenced by diffusional limitations.[19,47–53] Hence, apparent exchange kinetics can be operative similar to diffusional limitation on termination inducing the well-known gel-effect.[1,34,54–56]

A research question that arises is which experimental and/or modeling tools are most suited to test if a simplified degenerative RAFT mechanism can be applied or if the detailed non-degenerative one needs to be considered. Most focus has been on the bulk monomer conversion profile in which the RAFT polymerization case is compared with the corresponding FRP case (same initial conditions except no initial RAFT agent), with a (strong) rate retardation associated with the need of a non-degenerative mechanism. Barner-Kowollik *et al.*[57] hypothesized that the rate retardation could be explained by a low RAFT fragmentation rate resulting in an accumulation of non-propagating RAFT intermediate species. In contrast, Monteiro *et al.*[58] attributed the retardation to RAFT cross-termination reactions involving conventional and intermediate radicals, resulting - even with high fragmentation rates – in the formation of three and four armed dead species. Which of both explanations is most plausible is although still under debate,[45,59–63] even after a large number of both experimental[57–59,64–76] and theoretical studies.[47,63,77–87] Interestingly, recent research has indicated that bulk RAFT rate retardation can even occur under the validity of the degenerative mechanism.[47,88,89] As lower chain length polymer chains are always formed in a well-defined homogeneous RAFT polymerization compared to the corresponding FRP process the gel-effect is less established in the former so that the conversion profile is less steep.

Tobita *et al.*[90–92] suggested that miniemulsion RAFT polymerization with macro-RAFT agents is interesting to study the nature of rate retardation leading to a non-degenerative RAFT mechanism. The use of macro-RAFT agents allows to neglect to a first approximation the exit/entry phenomena of R_0 (mass transfer events (k) and (l) in the red box in Figure 5.1), which is known to induce additional retardation.[36,93–96] Still the kinetics are influenced by compartmentalization with the bimolecular RAFT cross-termination rate expected to decrease with decreasing (average) particle size, whereas the particle size should not have an influence on the RAFT fragmentation rate, at least for a given RAFT intermediate concentration. For

RAFT miniemulsion polymerization of styrene mediated by polystyryl dithiobenzoate, this aspect was exploited by Suzuki *et al.*[91,97] who showed with intrinsic kinetic Monte Carlo simulations that the miniemulsion polymerization rate and thus monomer conversion increases with decreasing droplet size, agreeing with the theoretical bulk predictions of the RAFT cross-termination model for the investigated system.

Despite that the investigation of RAFT in (mini)emulsion polymerization can be advantageous to investigate the plausibility of the chosen retardation model, a detailed kinetic study over a wide range of theoretically relevant RAFT addition, fragmentation and cross-termination rate coefficients as a function of the average particle size is still lacking. Most kinetic modeling studies on RAFT (mini)emulsion polymerization are simplified[23,32,98–110] with the common assumption[23,101,102,108,110] of a zero-one system, hence, either droplets/particles contain one or no radical at all. For example, Altarawneh *et al.*[101,102] used a zero-one model to describe the RAFT emulsion polymerization of styrene mediated by *O*-ethylxanthyl ethyl propionate. The zero-one model implied that instantaneous termination occurs if a radical enters a particle containing a conventional or intermediate radical. Similarly, Luo *et al.*[103] showed that for the miniemulsion polymerization of styrene with styrene oligomers of 1-phenylethylphenyl dithioacetate (PS-PEPDTA) and 2-cyranoprop-2-yl dithiobenzoate (PS-CPDB) as RAFT agents, a zero-one model assuming cross-termination can be used to describe the experimental data. Li *et al.*[104] investigated the copolymerization of styrene and butyl acrylate in miniemulsion using 3-benzyltrithiocarbonyl propionic acid (BCPA) as initial RAFT agent taking into account RAFT cross-termination but no insights on the conflicting rate retardation models were given. Assuming a priori the validity of a zero-one system is although not recommended. In the recent work of Devlaminck *et al.*[96] it was shown that for a degenerative RAFT system (polymerization of methyl methacrylate (MMA) with cyanoprop-2-yl dithiobenzoate (CPDB, R_0X) and potassium persulfate (KPS, I_2);

$[MMA]_0/[CPDB]_0/[KPS]_0$ = 590/1/0.65; d_p=100nm) at higher monomer conversions particles with several radicals can exist due to diffusional limitation on termination and additionally RAFT exchange in case the (average) chain length is sufficiently high.

In this work, non-degenerative and degenerative RAFT miniemulsion polymerization are theoretically compared for a wide range of RAFT exchange kinetic parameters, focusing both on the monomer/initial RAFT agent conversion profile and the average polymer properties, which is rarely done. This comparison is made by means of a 5-dimensional Smith-Ewart based model, allowing the mapping of all radical types and numbers per particle, starting from the code developments in previous work on degenerative RAFT polymerization.[96] It is shown that the nature of the RAFT exchange process affects the limits for the maximal radical type numbers and is dependent on the (average) particle size, with the most detailed differentiation possible upon the joint consideration of the trends for the polymerization rate and the control over average polymer properties.

5.2 Modeling methodology

In this work, a multi-scale Smith-Ewart based modeling methodology, as recently introduced for degenerative RAFT polymerization,[96] is extended to describe degenerative and non-degenerative RAFT miniemulsion polymerization of styrene (Figure 5.1) at 343 K.

***Table 5.1**: Overview of reactions and intrinsic rate coefficients for RAFT miniemulsion polymerization of styrene at 343 K, with initiator related coefficients based on KPS and a differentiation between RAFT exchange parameters: Combination 1-3 (slow RAFT fragmentation/high RAFT cross-termination/ideal RAFT agent). Further differentiation between reactions for a simplified degenerative model (DM) and non-degenerative model (NDM); an oligomeric styrene RAFT agent is assumed; all rate coefficients in L mol^{-1} s^{-1} except k_{dis} and $k_{frag,R0/I,R0/IX}$; also included interphase mass transfer parameters; for termination and RAFT exchange apparent rate coefficients are used (Section C1 and C2 of Appendix C).*

Reaction	DM	NDM	Equation	*Comb1*	*Comb2*	*Comb3*	*ref*
			Aqueous phase reactions				
Diss.[a],[b] of I_2	x	x	$I_{2,aq} \xrightarrow{f,k_{dis}} 2I^{\bullet}_{aq}$		$2.2\ 10^{-5}$		[103]
Chain ini *I*	x	x	$I^{\bullet}_{aq} + M_{aq} \xrightarrow{k_{pI}} R^{\bullet}_{1,aq}$		$4.9\ 10^{5}$		[113]
Propagation [c],[d]	x	x	$R^{\bullet}_{1,aq} + M_{aq} \xrightarrow{k_p} R^{\bullet}_{2,aq}$		$4.8\ 10^{2}$		[114]
			Organic phase reactions				
Chain ini $R^{\bullet}_0$[e]	x	x	$R^{\bullet}_{0,p} + M_p \xrightarrow{k_{pR_0}} R^{\bullet}_{1,p}$		$4.8\ 10^{2}$		[114]
Propagation	x	x	$R^{\bullet}_{i,p} + M_p \xrightarrow{k_p} R^{\bullet}_{i+1,p}$		$4.8\ 10^{2}$		[114]
Termination [f]	x	x	$R^{\bullet}_{0,p} + R^{\bullet}_{0,p} \xrightarrow{k_{tc,00}} P_{0,p}$		$1.0\ 10^{9}$		[115,116]
[f]	x	x	$R^{\bullet}_{0,p} + R^{\bullet}_{i,p} \xrightarrow{k_{tc,0}} P_{i,p}$		$1.0\ 10^{9}$		[115,116]
[f]	x	x	$R^{\bullet}_{i,p} + R^{\bullet}_{j,p} \xrightarrow{k_{tc}^{i,j}} P_{i+j,p}$		$1.0\ 10^{9}$		[115,116]
RAFT add/frag [i]		x	$R_{0,p} + (R_iX)_p \xrightarrow{k_{add,R_0,R_iX}} (R_0XR_i)_p$	$1.0\ 10^{5}$	$1.0\ 10^{6}$	$1.0\ 10^{7}$	[j]
[i]		x	$R_{i,p} + (R_jX)_p \xrightarrow{k_{add,R_iR_jX}} (R_iXR_j)_p$	$1.0\ 10^{5}$	$1.0\ 10^{6}$	$1.0\ 10^{7}$	[j]
[i]		x	$R_{0,p} + (R_0X)_p \xrightarrow{k_{add,R_0,R_0X}} (R_0XR_0)_p$	$1.0\ 10^{5}$	$1.0\ 10^{6}$	$1.0\ 10^{7}$	[j]
[i]		x	$R_{i,p} + (R_0X)_p \xrightarrow{k_{add,R_iR_0X}} (R_iXR_0)_p$	$1.0\ 10^{5}$	$1.0\ 10^{6}$	$1.0\ 10^{7}$	[j]
[a],[i]		x	$(R_0XR_i)_p \xrightarrow{k_{frag,R_0,R_iX}} R_{0,p} + (R_iX)_p$	$1.0\ 10^{1}$	$1.0\ 10^{3}$	$1.0\ 10^{8}$	[j]
[a],[i]		x	$(R_0XR_i)_p \xrightarrow{k_{frag,R_i,R_0X}} R_{i,p} + (R_0X)_p$	$1.0\ 10^{1}$	$1.0\ 10^{3}$	$1.0\ 10^{8}$	[j]
[a],[i]		x	$(R_iXR_j)_p \xrightarrow{k_{frag,R_iR_jX}} R_{i,p} + (R_jX)_p$	$1.0\ 10^{1}$	$1.0\ 10^{3}$	$1.0\ 10^{8}$	[j]
[a],[i]		x	$(R_0XR_0)_p \xrightarrow{k_{frag,R_0,R_0X}} R_{0,p} + (R_0X)_p$	$1.0\ 10^{1}$	$1.0\ 10^{3}$	$1.0\ 10^{8}$	[j]
RAFT cross-t[i]		x	$R_{i,p} + (R_jXR_0)_p \xrightarrow{k_{tcross}} P_{i+j,p}$	0	$1.0\ 10^{8}$	0[k]	[j]
[i]		x	$R_{i,p} + (R_jXR_k)_p \xrightarrow{k_{tcross}} P_{i+j+k,p}$	0	$1.0\ 10^{8}$	0	[j]
[i]		x	$R_{i,p} + (R_0XR_0)_p \xrightarrow{k_{tcross}} P_{i,p}$	0	$1.0\ 10^{8}$	0	[j]
[i]		x	$R_{0,p} + (R_iXR_0)_p \xrightarrow{k_{tcross}} P_{i,p}$	0	$1.0\ 10^{8}$	0	[j]
[i]		x	$R_{0,p} + (R_iXR_j)_p \xrightarrow{k_{tcross}} P_{i+j,p}$	0	$1.0\ 10^{8}$	0	[j]
[i]		x	$R_{0,p} + (R_0XR_0)_p \xrightarrow{k_{tcross}} P_{0,p}$	0	$1.0\ 10^{8}$	0	[j]
RAFT exchange	x		$R^{\bullet}_{i,p} + R_0X_p \xrightarrow{k_{tr,0}} R_iX_p + R^{\bullet}_{0,p}$	$5.0\ 10^{4}$	$5.0\ 10^{5}$	$5.0\ 10^{6}$	[g]
	x		$R^{\bullet}_{0,p} + R_iX_p \xrightarrow{k_{-tr,0}} R_0X_p + R^{\bullet}_{i,p}$	$5.0\ 10^{4}$	$5.0\ 10^{5}$	$5.0\ 10^{6}$	[g]
	x		$R^{\bullet}_{i,p} + R_jX_p \xrightarrow{k_{tr}} R_iX_p + R^{\bullet}_{j,p}$	$5.0\ 10^{4}$	$5.0\ 10^{5}$	$5.0\ 10^{6}$	[g]
			interphase mass transport				
Entry of $R^{\bullet}_{2,aq}$	x	x	$R^{\bullet}_{2,aq} \xrightarrow{k_{entryR_2}} R^{\bullet}_{2,p}$		$5.0\ 10^{7}$		[d],[h]

(a) s^{-1}; (b) f=0.2 (middle of literature[117] range of 0.1-0.3); (c) considered equal to k_p to a first approximation; (d) critical chain length for the entry of styrene is 2; (e) equal to k_p due to oligomeric RAFT agent; (f) given value is that of $k_{t,app}^{1,1}$, see Section C1 in Appendix C; only termination by recombination; (g) calculated from corresponding addition and fragmentation rate coefficients (Equation (6)-(8); (h) large values are assumed to reflect the strong entry rate of molecules possessing the critical chain length and values given for d_p=1.0 10² nm; (i) given value is the intrinsic rate coefficient, for calculation of the apparent rate coefficients see Section C2 in Appendix C; (j) this work; (k) can be taken as 0 as kinetically insignificant (Figure C1 of Appendix C).

5.2.1 Reactions, rate coefficients and mass transfer parameters

The RAFT miniemulsion of styrene mediated by an oligomeric polystyrene-RAFT agent (PS-X) and initiated by potassium persulfate (KPS) as radical initiator at 343 K is theoretically investigated for several RAFT kinetic parameter combinations. Each combination is investigated considering both the simplified degenerative (DM) and the detailed non-degenerative (NDM) RAFT polymerization mechanism. Three types of RAFT parameter combinations are investigated (Comb1-Comb3). Firstly, Comb1, similar to the slow fragmentation model (SFM),[57,63,97] is characterized by a high RAFT addition and a low fragmentation rate coefficient in the absence of RAFT cross-termination. Secondly, Comb2, similar to the intermediate termination model (ITM) described in literature,[58,78,97,111,112] is characterized by a high RAFT addition and cross-termination rate coefficient and a medium RAFT fragmentation rate coefficient. Thirdly, Comb3 is characterized by a high RAFT addition and fragmentation rate coefficient with a kinetically insignificant RAFT cross termination so that the rate coefficient can be given a value of 0 mol L^{-1} s^{-1}. This parameter combination mimics an ideal RAFT agent, as confirmed in Appendix C (Section C4).

The use of an oligomeric RAFT agent allows neglecting interphase mass transport (entry/exit) of the RAFT leaving group (R_0) which is known to have a significant impact on the polymerization kinetics at low monomer conversion.[96] Nevertheless, a differentiation is made between the initial oligomeric RAFT agent and the polymeric dormant species in order to isolate the RAFT initiation stage from the overall kinetics. For simplicity, the average particle diameter d_p and the average particle volume v_p are considered constant throughout the entire polymerization process, in agreement with other modeling studies.[103,105,118]

Table 5.1 gives an overview of the reactions considered, with the reactions necessary to investigate the simplified degenerative and the detailed non-degenerative RAFT model also mentioned. The water soluble KPS radical initiator (I_2) decomposes only in the aqueous phase.

The formed radical anion (*I*) propagates until an oligomeric species with a critical chain length of 2 is formed after which only entry in the particles can occur (mass transfer event in Table 5.1). Entry of smaller oligomeric species and the radical anion is neglected as well as chain transfer to monomer.[43,119–121] All initial oligomeric PS-X is considered to be present in the particles and no exit can occur. For simplicity monomer transport is ignored. Considering the limited maximum conversion investigated (<95%), the aqueous monomer concentration can be considered constant at its saturated value ($4.3\ 10^{-3}$ mol L^{-1})[20] and, hence, instantaneous monomer phase transfer to the aqueous phase is assumed. Thermal self-initiation is neglected at the polymerization temperature considered, based on literature data.[119,122–124]

Diffusional limitations on termination are taken into account through apparent rate coefficients (subscript "app") that are calculated by means of the composite k_t model,[115] also sometimes referred to as the RAFT-chain length dependent-termination (RAFT-CLD-T) model.[116] More information regarding this model and the necessary parameters are given in Section C1 of Appendix C. The average apparent termination rate coefficient is evaluated using the number radical average radical chain length $x_{n,r}$.

As previously indicated already at intermediate monomer conversions RAFT specific reactions, i.e. RAFT addition, fragmentation, cross termination and transfer (when assuming the degenerative mechanism), can become diffusion controlled, as only macrospecies are involved similar to conventional termination.[47–49,51,53,125,126] Consequently, apparent rate coefficients need to be considered for these RAFT specific reactions as well. A fundamental approach is the coupled parallel encounter pair model, as introduced by D'hooge *et al.* [49] In such model for instance the apparent macro-RAFT addition and fragmentation rate coefficient follow from:

$$k_{add,app} = \left(\frac{1}{k_{add,chem}} + \frac{1}{k_{add,diff}}\right)^{-1} \quad (4)$$

$$k_{frag,app} = \left(\frac{1}{k_{frag,chem}} + \frac{K_{eq,1}}{k_{frag,diff}}\right)^{-1} \quad (5)$$

with $k_{add/frag,chem}$ the intrinsic RAFT macro-addition/fragmentation rate coefficient (see Table 5.1), $k_{add/frag,diff}$ the diffusional contribution for RAFT macro-addition/fragmentation (which can be approximated by the termination diffusional contribution), and $K_{eq,1}$ the ratio between the intrinsic macro-RAFT addition and fragmentation rate coefficient, highlighting the coupled nature of these reactions. For a degenerative model the following equations formally result:

$$k_{tr,0,app} = \left(\frac{1}{k_{tr,0,chem}} + \frac{1}{k_{tr,0,diff}} + \frac{1}{K_{eq,2}k_{-tr,0,diff}}\right)^{-1} \quad (6)$$

$$k_{-tr,0,app} = \left(\frac{1}{k_{-tr,0,chem}} + \frac{1}{k_{-tr,0,diff}} + \frac{K_{eq,2}}{k_{tr,0,diff}}\right)^{-1} \quad (7)$$

$$k_{tr,app} = \left(\frac{1}{k_{tr,chem}} + \frac{2}{k_{tr,diff}}\right)^{-1} \quad (8)$$

with $k_{(-)tr(,0),app}$ the apparent RAFT transfer rate coefficients, $k_{(-)tr(,0),chem}$ the intrinsic RAFT transfer rate coefficient (see Table 5.1), $k_{(-)tr(,0),diff}$ the diffusional contribution for RAFT transfer and $K_{eq,2}$ equal to:

$$K_{eq,2} = \frac{k_{tr,0,chem}}{k_{-tr,0,chem}} \quad (9)$$

For more information regarding these RAFT apparent rate coefficients, the reader is referred to Section C2 of Appendix C. Diffusional limitations on propagation, typically observed at very high monomer conversions (≥95%)[127–129] are ignored in the present work, which is justified reminding the limited maximal monomer conversion investigated.

5.2.2 Compartmentalization model: Smith-Ewart and moment equations

In RAFT miniemulsion polymerization, some species will be present in each particle in large amounts (a number per particle much higher than 10 for *e.g.* monomer and R_0X) whereas only 0 up to *e.g.* 10 species of a certain radical type are present in each particle. The concentration of the abundant species can - for simplicity - be approximated by a single average concentration over all particles at any time and if a deterministic solution strategy is followed their concentration vs time evolution is accounted for by means of continuity equations or mass balances.[43,49,130–133] For the non-abundant species, pseudo-bulk kinetics are very likely not obtained. Here, no averaging is allowed and thus the kinetics can be significantly affected by compartmentalization. This implies that the number of particles with each possible set of given number of radical types needs to be followed alongside the aforementioned differential equations. So-called multi-dimensional Smith-Ewart equations are therefore needed, with the number of radical types determining the degree of dimensionality.[134–138]

In our previous work[96] on degenerative RAFT polymerization a two-dimensional Smith-Ewart modeling methodology with the calculation of the number of R_0 and macroradicals per particle has been put forward, accounting for interphase mass transfer and diffusional limitations up to high monomer conversions. Both the calculation of the polymerization rate and average polymer characteristics as a function of time is covered, with the average chain length characteristics following from an extended method of moments. Based on Figure 5.1 - with a non-degenerative model- a five-dimensional Smith-Ewart model is now required. The population balances in this model describe the temporal evolution of polymer particles having k macroradicals, l R_0 radicals, m R_iXR_0 radicals, n R_iXR_j radicals and o R_0XR_0 radicals ($N_{k,l,m,n,o}$; $k,l,m,n,o \geq 0$) (Appendix C: Section C8). The continuity equations of the species in the aqueous phase, the abundant species in the particles and the associated equations for the average chain

length characteristics are provided in Appendix C (Section C9). In these equations, the average numbers of each radical type are defined as:

$$\bar{n}(R) = \sum_{k,l,m,n,o} k \frac{N_{k,l,m,n,o}}{N_p} \tag{10}$$

$$\bar{n}(R_0) = \sum_{k,l,m,n,o} l \frac{N_{k,l,m,n,o}}{N_p} \tag{11}$$

$$\bar{n}(R_i X R_0) = \sum_{k,l,m,n,o} m \frac{N_{k,l,m,n,o}}{N_p} \tag{12}$$

$$\bar{n}(R_i X R_j) = \sum_{k,l,m,n,o} n \frac{N_{k,l,m,n,o}}{N_p} \tag{13}$$

$$\bar{n}(R_0 X R_0) = \sum_{k,l,m,n,o} o \frac{N_{k,l,m,n,o}}{N_p} \tag{14}$$

in which N_p is the total number of particles.

5.3 Results and discussion

In this section, attention is first focused on the impact of the RAFT exchange parameters on the main miniemulsion polymerization characteristics, assuming the detailed non-degenerative mechanism. Here an average particle size of 100 nm and a targeted chain length (TCL) of 200 ($[R_0X]_0/[KPS]_0 = 3$, $[KPS]_0 = 4\ 10^{-3}$ mol L^{-1}, $m_{MMA,0} = 20$ g, $m_{H2O,0} = 80$ g) are considered for the parameter variations Comb1-Comb3 in Table 5.1. Next a comparison is made with the descriptions following the simplified degenerative mechanism. Finally, it is investigated whether a variation of the average particle size enables to differentiate between the nature of the RAFT mechanism making a distinction between slow RAFT fragmentation and pronounced RAFT cross-termination. Focus is here on both the changes of the monomer conversion and polymer properties.

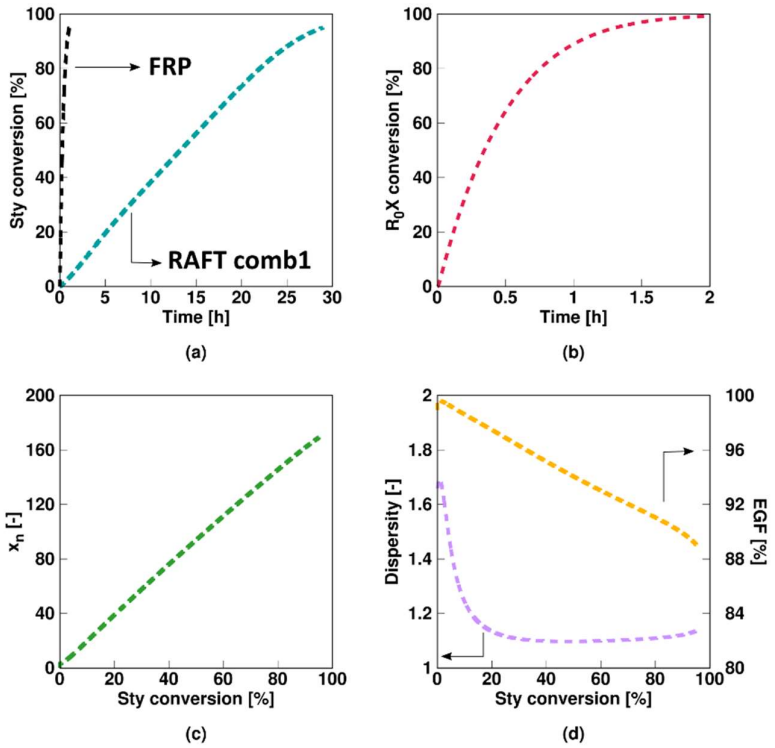

***Figure 5.2**: Overview of average characteristics for non-degenerative miniemulsion RAFT polymerization of styrene at 343 K with KPS and an oligomeric RAFT agent. Monomer conversion (a) and initial RAFT agent (R_0X) conversion (b) as a function of time and number average chain length x_n (c), dispersity (d) and end-group functionality (EGF) (d) as a function of styrene conversion. Model parameters for Comb1 (slow fragmentation case) in Table 5.1. $[Sty]_0/[R_0X]_0 = 200$, $[R_0X]_0/[KPS]_0 = 3$, $[KPS]_0 = 4\ 10^{-3}$ mol L^{-1}, $m_{MMA,0} = 20$ g, $m_{H2O,0} = 80$ g; $d_p = 100$ nm; this slow fragmentation case leads specifically to a much slower polymerization compared to the FRP case (black line in (a)).*

5.3.1 Results considering a non-degenerative mechanism at an average particle size of 100 nm

As shown in Figure 5.2a, a slow fragmentation model (**Comb 1** in Table 5.1; non-degenerative parameters) results in a much lower polymerization rate compared to the corresponding FRP. As RAFT intermediate radicals cannot propagate, the low fragmentation rate coefficients involving these species result in a decrease of the macroradical (R_i) amount available for propagation. The low fragmentation rate coefficient of the RAFT intermediate species R_0XR_0

and R_iXR_0 results in a prolonged presence of the initial RAFT agent, as shown in Figure 5.2b. Nevertheless, a linear growth for the number average chain length (x_n; Figure 5.2c) with monomer conversion and a low dispersity (<1.5, Figure 5.2d) are obtained. Unavoidable termination events result in a steady decrease of the EGF, although the latter remains high (>88%) as shown in Figure 5.2d. Overall a reasonable chain growth control is achieved.

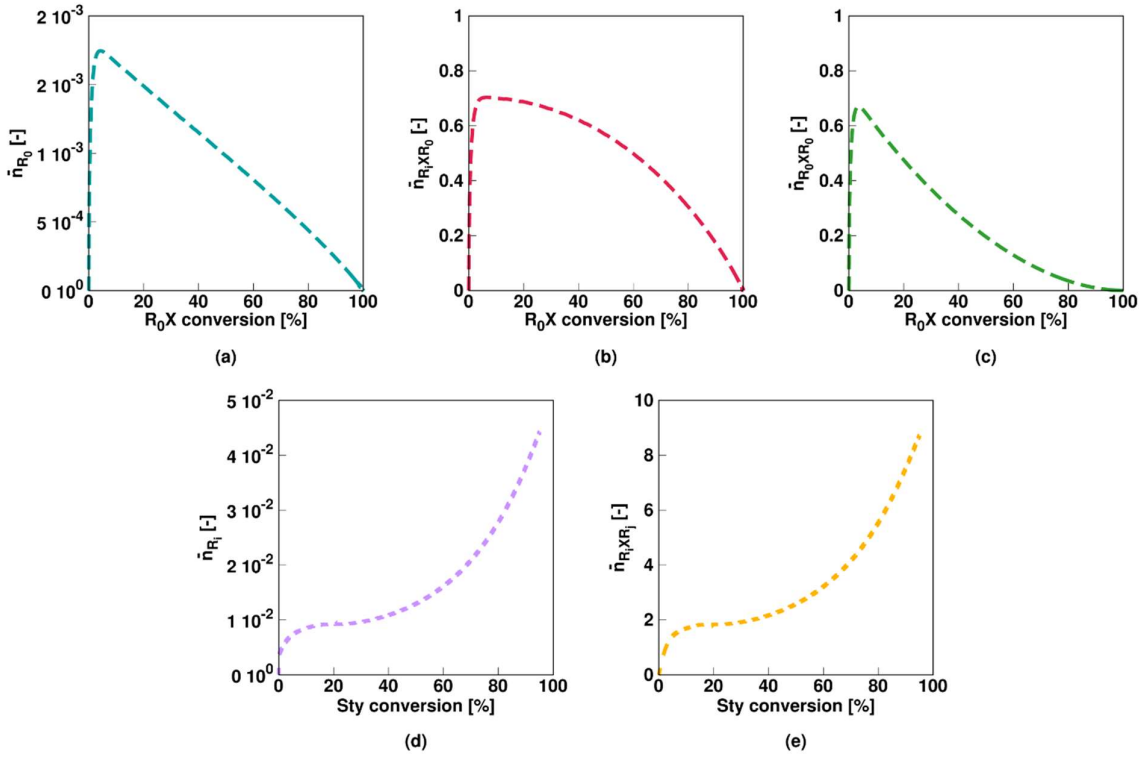

Figure 5.3*: Corresponding evolution of the average number of radicals of a given type (Equation (10)-(14)) as a function of initial RAFT agent (R_0X) agent or styrene conversion for Figure 5.2; the slow fragmentation case leads to a strong build-up of the intermediate RAFT radical (see (e)) resulting in much higher values then 0.5, the value characteristic value for 0-1 kinetics, from intermediate styrene conversions onwards.*

For the slow fragmentation model, the average number of R_0, R_iXR_0, and R_0XR_0 radicals all steadily decrease as a function of the RAFT agent conversion as shown in Figure 5.3a, 5.3b and 5.3c, due to the formation of macroradicals R_i after addition of monomer to R_0. However, the slow fragmentation results in an initially large (>0.5) average number of R_iXR_0 and R_0XR_0

radicals per particle. The average number of R_i radicals is low throughout the entire polymerization (< 5 10^{-2}, Figure 5.3d) as the radical function is mainly stored in the intermediate R_iXR_j form (Figure 5.3e). Above 50% monomer conversion, diffusional limitations on termination (Figure C3 of Appendix C) even result in a steep increase of the average number of these radicals (>>2). It can thus be concluded that a multi-dimensional Smith-Ewart description is needed, with a considered maximal radicals per particle beyond a value of 1. In other words, for a slow RAFT fragmentation model zero-one kinetics are not obtained.

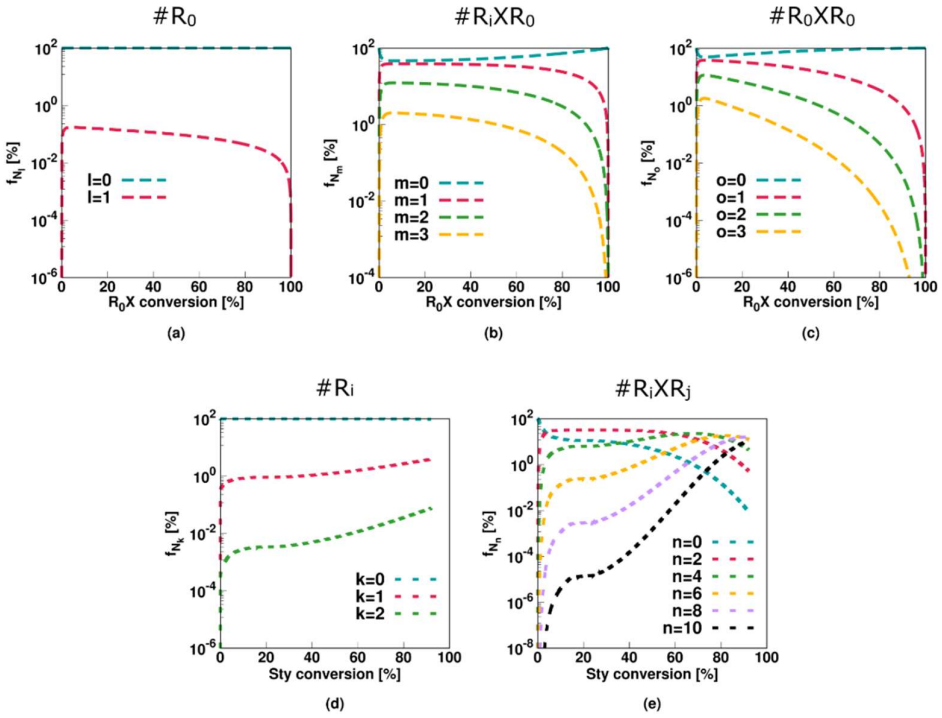

***Figure 5.4**: Corresponding fraction of particles with a given number of radicals as a function of initial RAFT agent (R_0X) agent or styrene conversion for Figure 5.2. Averages are depicted in Figure 5.3.*

This is also confirmed in Figure 5.4 (Comb 1) displaying the particle distributions. For R_0 and R_i (Figure 5.4a and 5.4d), the high termination, propagation and addition rate coefficients result in almost all particles containing none of these radicals, consistent with the very low average numbers in Figure 5.3a and 5.3d. For R_iXR_0 and R_0XR_0 radicals (Figure 5.4a and 5.4b), on the other hand, 'empty' particles are less present and even at the initial stage of the polymerization

process, a 0-1 description is inappropriate. This is even more pronounced for R_iXR_j radicals as shown in Figure 5.4e as most particles contain at least one of these radicals already after a few percentages of monomer conversion. At the final stages of the polymerization, a significant amount of particles even contain up to 10 radicals, again highlighting the importance of the use of the multidimensional Smith-Ewart equations.

Figure 5.5 shows the evolution of the main miniemulsion average characteristics, considering **Comb2** non-degenerative model parameters of Table 5.1. Here, in contrast to Comb1, the intermediate radicals can terminate significantly by reaction with both leaving group and macroradicals again resulting in a significant rate reduction compared to the FRP countercase (Figure 5.5a). The initial RAFT agent is now consumed much faster as shown in Figure 5.5b. A linear growth of x_n and a low dispersity (Figure 5.5c and 5.5d), except at very high (>85%) monomer conversion again indicate an acceptable controlled character of the polymerization further exemplified by a relatively high EGF (Figure 5.5d).

The average number of R_0 radicals per particle for Comb2 is again very low, as shown in Figure 5.6a. The average number of R_iXR_0 and R_0XR_0 radicals (Figure 5.6b and 5.6c) is slightly lower for Comb2 as a larger fragmentation rate coefficient is considered and cross-termination is plausible as well. The average number of macroradicals remains low (Figure 5.6d) and more or less constant, indicating that diffusional limitations do not have a significant effect. Notably the average number of R_iXR_j radicals (Figure 5.6e) is constant as well but with a value of roughly 0.5, as cross-termination withholds the build-up of these radical species. As shown in Figure 5.6f, the concentration of RAFT star cross product steadily increases with increasing monomer conversion and the majority of the dead polymer species is this star product. Hence, for Comb 2, the dominant role of RAFT-cross termination is clear in the radical and dead polymer spectrum.

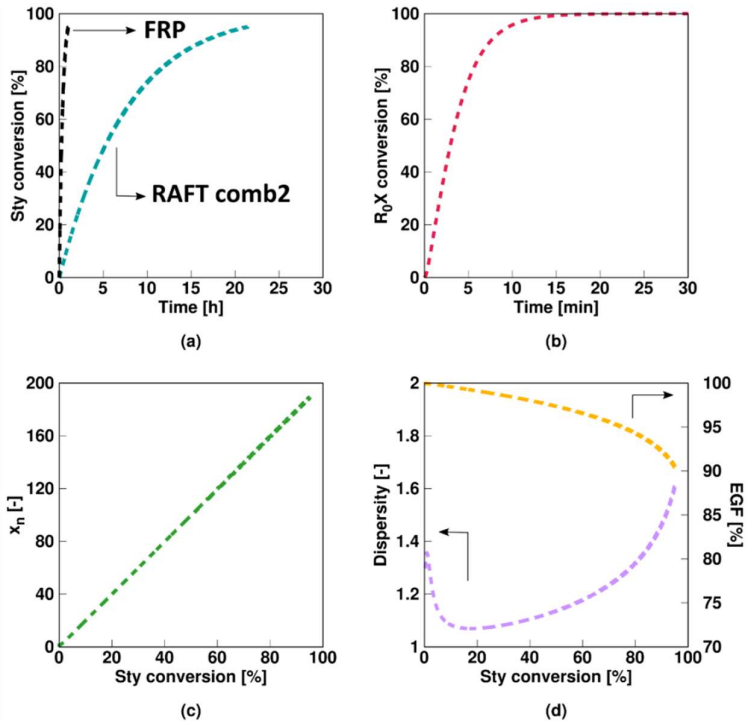

Figure 5.5: *Changes for Figure 5.2 in case Comb2 model parameters from Table 5.1 instead of Comb 1 model parameters (RAFT cross termination case); a less controlled RAFT polymerization is observed, with again a strongly lower polymerization rate as in the corresponding FRP case.*

This conclusion also follows from the radical distributions in Figure 5.7 with most particles containing no or only a single radical of each radical type. Moreover, for R_iXR_j *radicals (Figure 5.7e), roughly half the particles contain none of these species whereas the other half contains one, resulting in an average value of approximately 0.5 (Figure 5.6e). Only at the higher monomer conversions 1% of the particles contain 2* R_iXR_j *radicals, again highlighting the limited impact of diffusional limitations and thus the acceptable approximation of zero-one kinetics, albeit with multiple radical types.*

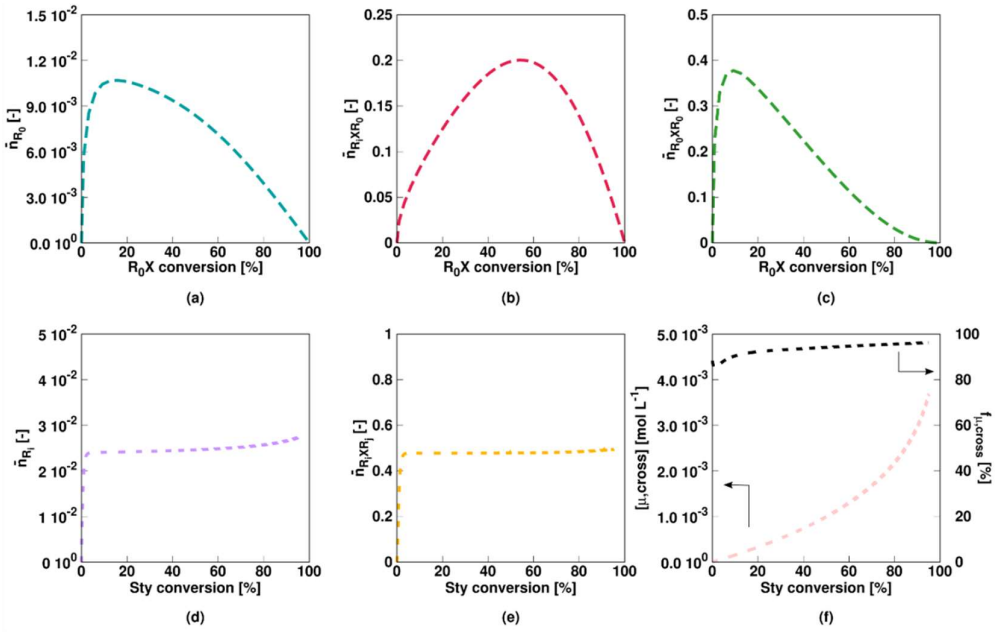

***Figure 5.6**: Corresponding evolution of the average number of radicals of a given type as a function of initial RAFT agent (R_0X) agent or styrene conversion for Figure 5.5 (Comb 2), with a value of 0.5 in (e). Also subfigure (f) with the evolution of the concentration of RAFT-cross termination product (left) and the fraction for this polymer in the overall dead polymer amount (right). Most of the dead polymer is thus star polymer product.*

Figure 5.8 shows the results for **Comb3**, mimicking an ideal RAFT agent as a high RAFT addition and fragmentation rate coefficient are considered. No rate retardation compared to the FRP case is observed indicating that the fraction of radicals in the inactive intermediate form is negligible at any time and that the gel-effect impact as for the bulk case is much less an issue, also bearing in mind that the monomer is styrene which is less prone to rate acceleration as e.g. methyl methacrylate polymerization.[47] Moreover, the RAFT agent is almost instantaneously consumed completely, as shown in Figure 5.8b. It can be confirmed that a RAFT agent characterized by parameter set Comb3 behaves as ideal RAFT agent as x_n increases linearly with monomer conversion, the dispersity is very close to the theoretical lower limit of 1, and the EGF is >99% (Figure 5.8b-d).

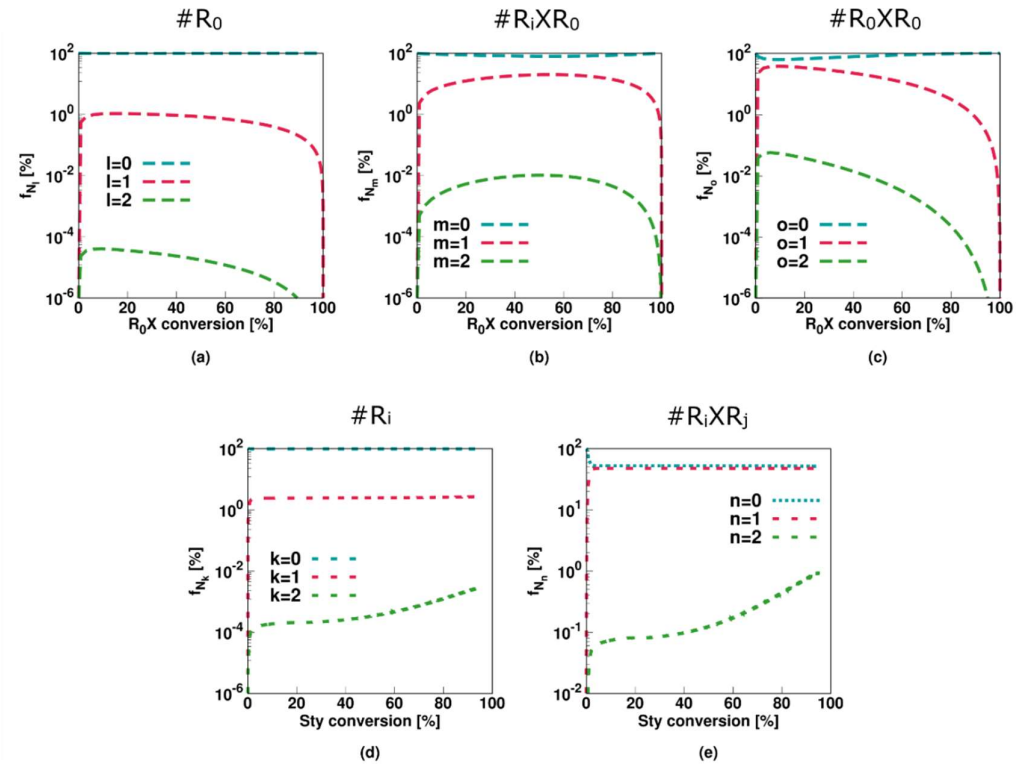

Figure 5.7*: Corresponding fraction of particles with a given number of radicals as a function of initial RAFT agent (R_0X) agent or styrene conversion for Figure 5.5; averages in Figure 5.6; zero-one kinetics are now established but several radical types are needed.*

As mentioned previously, a RAFT polymerization and corresponding FRP conversion profile can only coincide if the RAFT intermediate radicals are formed rapidly and extremely short-lived, which is confirmed by the average radical values for Comb 3 shown in Figure 5.9. A constant value of 0.5 is obtained for the average number of macroradicals (Figure 5.9d), indicating instantaneous termination if two macroradicals are present in a particle. Under the Comb3 miniemulsion conditions the assumption of zero-one kinetics is thus again acceptable.

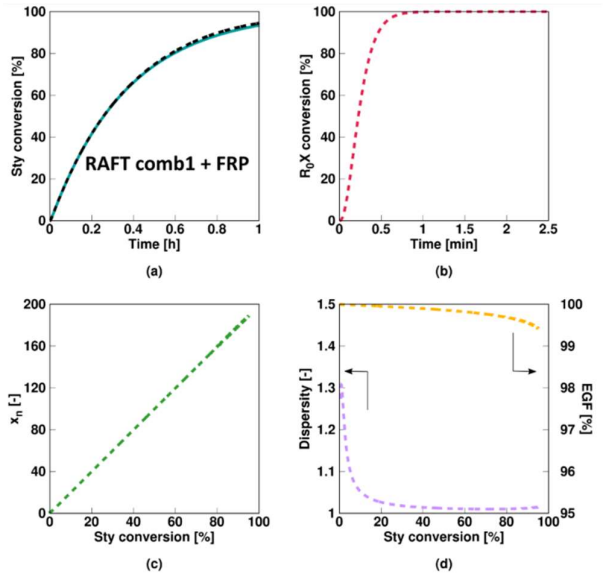

Figure 5.8*: Change of Figure 5.2 in case Comb3 model parameters (ideal RAFT agent case) from Table 5.1 instead of Comb 1 model parameters; identical results are obtained in case a degenerative model is used (see Section C4 in Appendix C). This is also consistent with the identical line under the corresponding FRP conditions.*

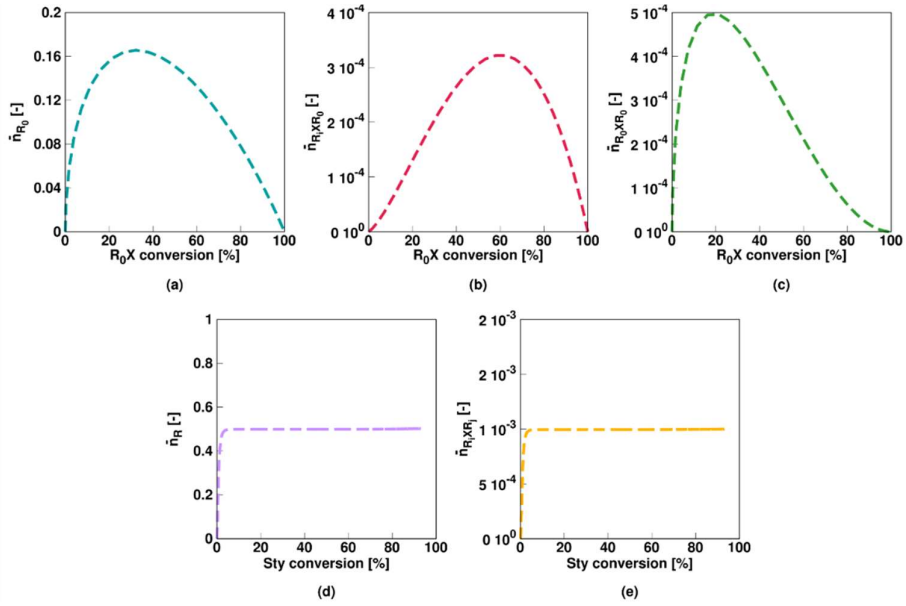

Figure 5.9*: Corresponding evolution of the average number of radicals of a given type as a function of initial RAFT agent (R_0X) agent or styrene conversion for Figure 5.9; for (d) an average value of 0.5, highlighting the targeted instantaneous termination with conventional macroradicals and the validity of zero-one kinetics.*

The average values of Figure 5.9 (Comb 3) can be further understood by considering the particle type distributions of Figure 5.10. The only radical type which can be significantly present in a particle is a macroradical. More specifically, half of the particles contain zero macroradicals whereas the other half contains only one macroradical. As opposed to Comb 2 the key 0.5 value is thus now established with the population of macroradicals.

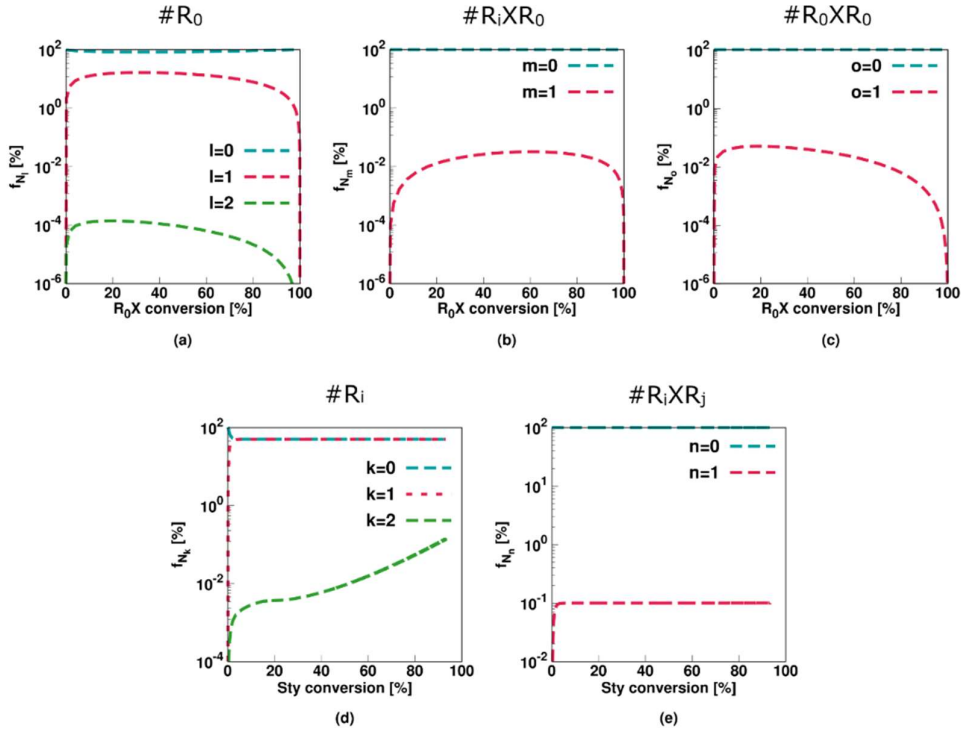

Figure 5.10: *Corresponding fraction of particles with a given number of radicals as a function of initial RAFT agent (R_0X) agent or styrene conversion for Figure 5.9; averages in Figure 5.10.*

5.3.2 Relevance of non-degenerative description

The next logical step is to explicitly validate whether a simplified degenerative mechanism enables to obtain the detailed kinetic descriptions as produced with the non-degenerative mechanism. Only for Comb3 (ideal RAFT agent) this is case (Figure C2 in Appendix C). For the other two combinations this is not the case as shown in Figure 5.11 (dashed lines: non-degenerative description from before; full lines: degenerative approximation; Comb 1: red; Comb 2: green). It follows that for Comb1 (red lines) both the styrene (Figure 5.11a) and RAFT

agent consumption rate (Figure 5.11b) are significantly reduced when the intermediate radicals are considered compared to the simplified degenerative approximation. This is not surprising as the slow fragmentation results in the formation of radicals incapable of propagating whereas in the degenerative approach the RAFT mechanism is described by a direct exchange which does formally not include the formation of these intermediate species. The x_n (Figure 5.11c) and dispersity (Figure 5.11d) are only minorly affected by switching from the non-degenerative to the degenerative approach. The EGF is however significantly lower for the non-degenerative description but this is related to the longer polymerization time needed to reach the final conversion.

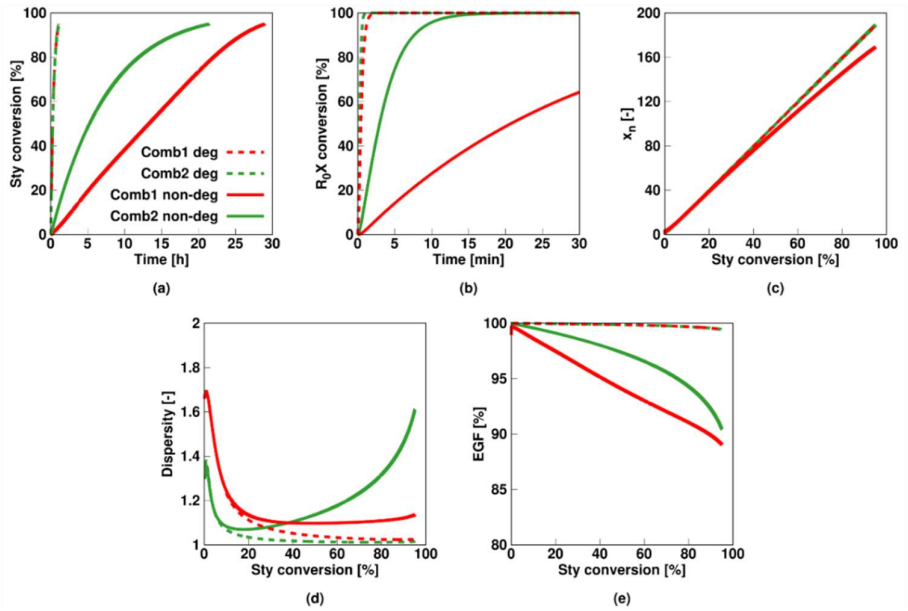

***Figure 5.11**: Comparison of non-degenerative results (full lines) of Figure 5.2 / 5 with the simplified degenerative model results (dashed lines) for Comb1 (red) / Comb2 (green) model parameters in Table 5.1. The non-degenerative models are needed for these combinations. For Comb3, the degenerative description is allowed (see Appendix C).*

Similarly, for Comb2 (green lines), the monomer and initial RAFT agent conversion are again much slower for the non-degenerative description as not only the non-propagating intermediate species are explicitly taken into account but these can also terminate with macroradicals.

Nonetheless, the x_n is unaffected as both models are coincident. However, in the non-degenerative approach, the domination event is RAFT cross-termination, resulting in star product whereas in the degenerative approach only conventional termination can occur resulting in linear dead species. As star product will inherently be larger than linear dead product, the overall dispersity for the non-degenerative description will be larger as well which can be seen in Figure 5.11d. Finally, the EGF for the non-degenerative description is again much lower due to the prolonged reaction time. Hence, only for very well-defined RAFT systems the degenerative assumption is afforded.

5.3.3 Relevance of the (average) particle size

Figure 5.12 shows the influence of d_p on the reaction time to reach a monomer conversion (X_M) of 30% and the main average polymer properties at this X_M for the three model parameter combinations in Table 5.1, with Column *i* relating to Comb *i* and d_p varying between 50 and 150 nm. This low monomer conversion is selected for illustration purposes and to avoid too long simulation times. It is clear that for all three models the time to reach a X_M of 30% increases with increasing d_p (Figure 5.12 (a)-(c)). Nevertheless, for Comb1 (Figure 5.12a) the increase slows down with increasing d_p whereas for Comb2 (Figure 5.12b) and Comb3 (Figure 5.12c) the increases become more pronounced. The EGF decreases (Figure 5.12 (j)-(l)) are related to the monomer conversion changes, with higher losses implying more conventional radical initiator consumption before the targeted monomer conversion is reached. This again illustrates the link between the reaction time and the loss of the RAFT polymerization livingness and further highlights the relevance of EGF measurements.

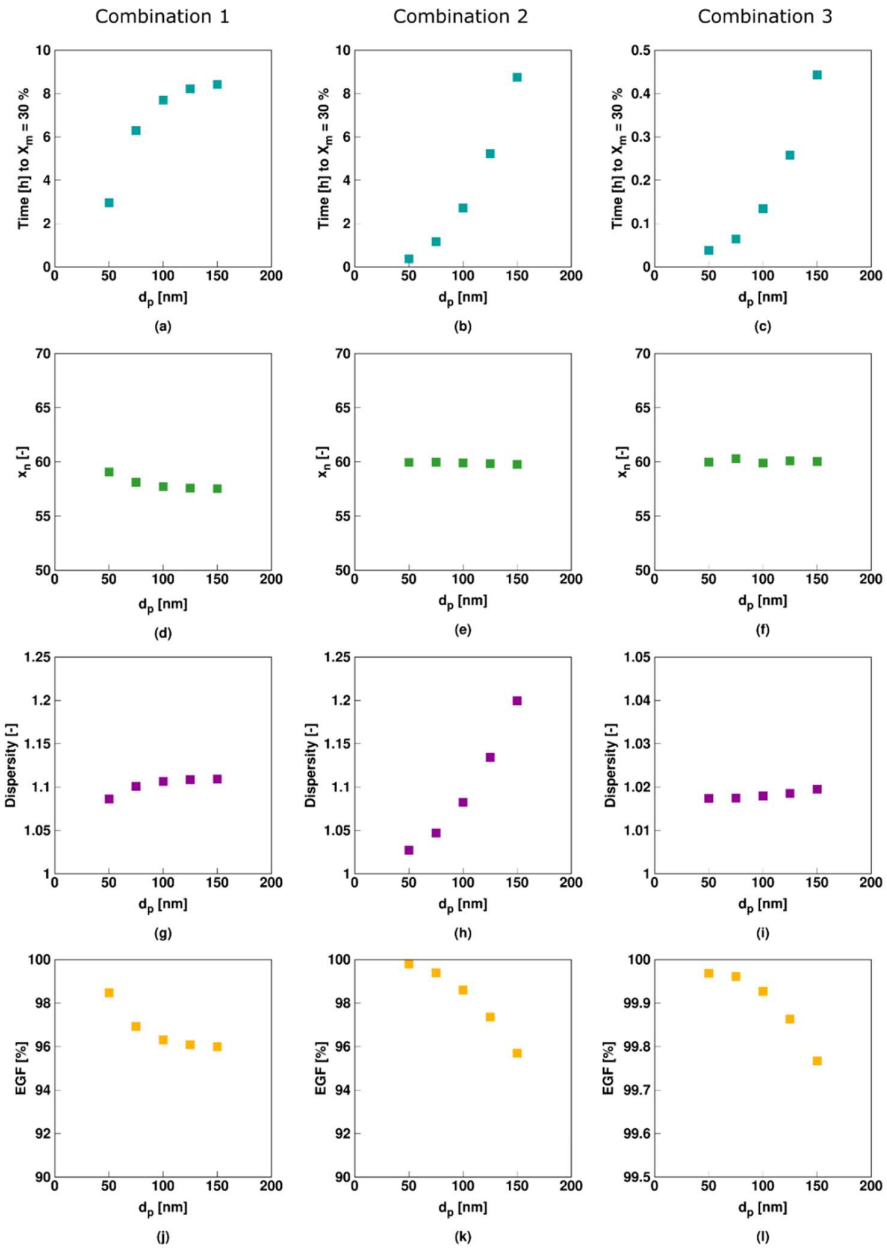

***Figure 5.12**: Influence of the (average) particle size (d_p) on the time to reach 30% monomer conversion X_M ((a)-(c), blue), the number average chain length (x_n, (d)-(f), green), dispersity ((g)-(i), purple) and EGF ((j)-(l), orange) for model parameters Comb1 (first column), Comb2 (second column) and Comb3 (third column) in Table 5.1. $[Sty]_0/[R_0X]_0$=200, $[R_0X]_0/[KPS]_0$= 3, $[KPS]_0 = 4\ 10^{-3}$ mol L^{-1}, $m_{MMA,0}$ = 20 g, and $m_{H2O,0}$ = 80 g. X_M is 30% and X_{R0X} is 100% for all simulation points.*

In contrast, regardless the parameter combination, x_n is practically unaffected by d_p (Figure 5.12 (d)-(f)), which is consistent with the general observation under bulk/solution conditions that

this average polymer response is less sensitive to process variations. The relation between d_p and dispersity (Figure 5.12 (g)-(i)) is strongly varying depending on the parameters combination, highlighting the potential of dispersity measurements besides conventional monomer conversion measurements to study the nature of possible RAFT retardations. For Comb1 a plateau behavior results with increasing d_p with dispersity values around 1.1, whereas for Comb2 an accelerated increase is obtained with increasing d_p with values above 1.2. For Comb3, on the other hand, a plateau behavior with decreasing d_p is observed, with although always very low dispersity values (close to 1).

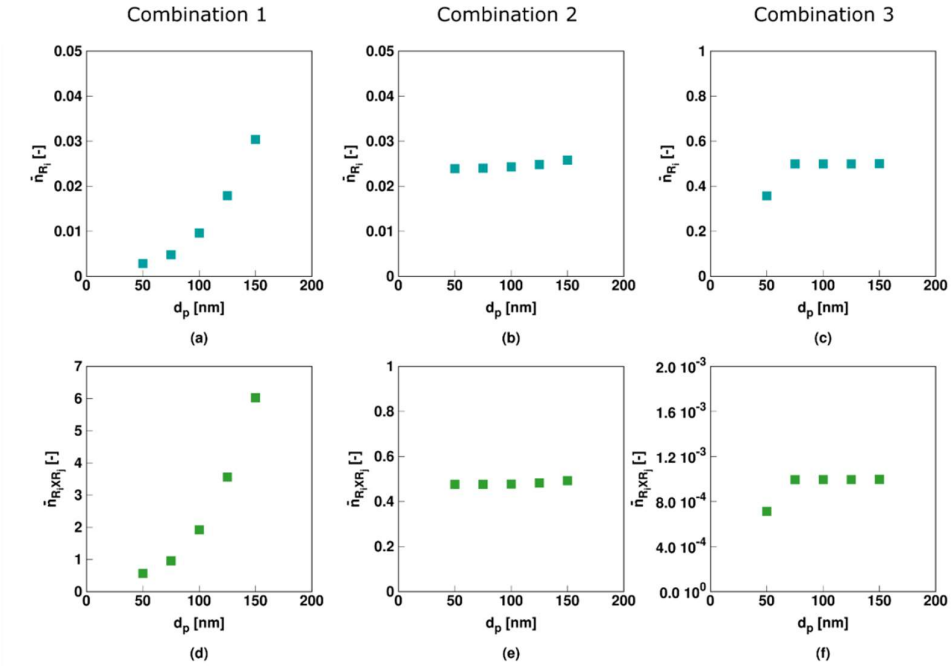

***Figure 5.13**: Corresponding average number of macro- and RAFT intermediate radicals for Figure 5.12 (X_M of 30%); for completeness other average radical numbers in Figure C4 of the Appendix C.*

As shown in Figure 5.13, only for Comb1 (slow RAFT fragmentation) the average number of macroradicals and R_iXR_j radicals per particle is significantly affected by the average particle size. Besides for Comb3 at a small particle size of 50 nm, both Comb2 and Comb3 are rather unaffected, with notably average values around 0.5 for the RAFT intermediate radical in Comb2 and the conventional macroradical in Comb 3. This implies the establishment of a kind of

balancing of exchange reaction rates in Comb 2 and Comb 3 which is not met in Comb 1 where the intermediate RAFT radical cannot easily disappear, as there is slow RAFT fragmentation and no RAFT cross-termination.

This can be further investigated through the radical reaction probabilities shown in Figure 5.14 that are calculated based on all particles jointly. It follows that the probabilities of propagation and addition (first two rows) are unaffected by d_p for all three parameter combinations as these reactions involve, respectively, monomer and dormant species which are present in relatively large concentrations in each particle so that compartmentalization does not matter, at least in a Smith-Ewart based modeling approach. In contrast (RAFT cross-) termination involves radicals only and as a result the related probabilities (last two rows) vary with particle size. Similar to the polymerization rate trends (related to Figure 5.12 (a)-(c)), these termination probabilities (Figure 5.14 (g)-(j)) increase with increasing d_p with the increase slowing down for Comb1 and increasing for Comb2 and Comb3. For Comb3 the termination probability is as such extremely low (e.g. 10^{-7}) and its actual impact is almost negligible, highlighting again the ideal nature of this RAFT agent.

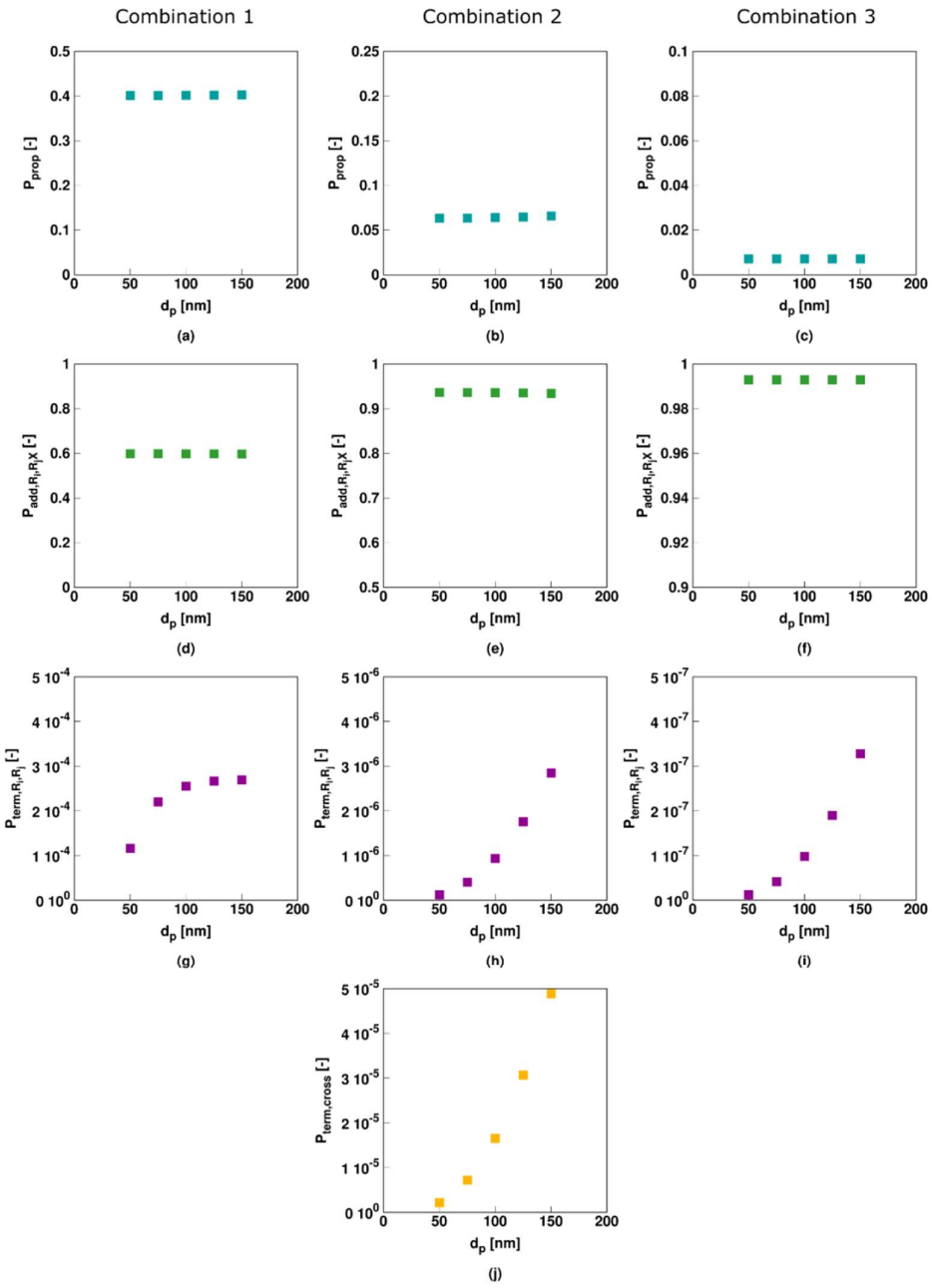

***Figure 5.14**: Corresponding radical reaction probabilities for the macroradicals for Figure 5.12 (X_M of 30%); top to bottom: propagation, RAFT addition, (conventional) termination and RAFT cross-termination; For completeness, RAFT-intermediate radical rates in Figure C5 of Appendix C*

Hence, the relation between the parameter combination for RAFT exchange and the d_p effect in Figure 5.12 needs to be related to the relative importance of termination, in agreement with the suggestions by Tobita et al.[90–92] For Comb 2 the dominant termination rate is the RAFT-

cross termination rate (probabilities of e.g. 10^{-5}), with the conventional radical termination rate matching the d_p dependence of RAFT-cross termination but a negligible effect as such due to too low probabilities (e.g. 10^{-6}). A lower d_p leads in Comb 2 to more segregation, stating that two species can only react when they are present in the same particle, blocking more cross-termination, which results in a stronger polymerization rate acceleration until a d_p is reached at which cross-termination becomes kinetically insignificant. An acceleration is also obtained with Comb 1, as there the segregation effect on the conventional termination is still active with low but still significant probabilities (e.g. 10^{-4}). Here the d_p dependence is although different with at the higher d_p – in the studied d_p range- bulk-like behavior and thus constant reaction probabilities. Such different dependence is also reflected in the evolutions for the average polymer properties, increasing the potential to explain rate retardations in RAFT miniemulsion polymerization. It is clear that the identification of a rate acceleration is insufficient as both a slow RAFT transfer and a polymerization with significant RAFT cross-termination are characterized by such feature. Only upon a close inspection of the d_p dependency and other characteristics a proper distinction is theoretically possible.

5.4 Conclusions

The added value of studying miniemulsion RAFT polymerization in a range of conditions to clarify the nature of a possible RAFT retardation is theoretically highlighted based on multi-dimensional Smith-Ewart equations. Essential is the effect of the average particle size on the relative importance of termination reactions. In practice, focus should be not restricted to examining differences in the monomer conversion profile for slow RAFT fragmentation and significant cross-termination but also the relation between the average particle size and the control over average properties should be investigated. In particular, the dispersity and end-group functionality variation with d_p can be used to differentiate slow RAFT fragmentation

from significant RAFT-cross termination. Moreover, a comparison with the FRP conversion profile is still recommended to confirm whether the RAFT agent can be considered as ideal.

The developed modeling tool can be used to better understand RAFT miniemulsion kinetics. For a slow RAFT fragmentation, zero-one kinetics cannot be assumed, at least if the particle size is sufficiently high. For a fast RAFT cross-termination zero-one kinetics are obtained but multiple radical types need to be considered and the dead polymer product is dominantly star product. Once the degenerative mechanism can be safely assumed a direct switch can be made from a five- to a two-dimensional Smith-Ewart equation based description, strongly simplifying the overall kinetic description.

5.5 References

1. Thickett, S.C.; Gilbert, R.G. Emulsion polymerization: State of the art in kinetics and mechanisms. *Polymer (Guildf).* **2007**, *48*, 6965–6991.

2. Cunningham, M.F. Controlled/living radical polymerization in aqueous dispersed systems. *Prog. Polym. Sci.* **2008**, *33*, 365–398.

3. Destarac, M. Controlled radical polymerization: Industrial stakes, obstacles and achievements. *Macromol. React. Eng.* **2010**, *4*, 165–179.

4. Zetterlund, P.B.; Thickett, S.C.; Perrier, S.; Bourgeat-Lami, E.; Lansalot, M. Controlled/Living Radical Polymerization in Dispersed Systems: An Update. *Chem. Rev.* **2015**, *115*, 9745–9800.

5. Matyjaszewski, K.; Spanswick, J. Controlled / living radical polymerization. *Materialstoday* **2005**, *8*, 26–33.

6. Grishin, D.F.; Grishin, I.D. Controlled radical polymerization: Prospects for application for industrial synthesis of polymers (Review). *Russ. J. Appl. Chem.* **2011**, *84*, 2021–2028.

7. Zetterlund, P.B.; Kagawa, Y.; Okubo, M. Controlled/living radical polymerization in dispersed systems. *Chem. Rev.* **2008**, *108*, 3747–94.

8. Matyjaszewski, K. Controlled radical polymerization: State-of-the-art in 2011. *ACS Symp. Ser.* **2012**, *1100*, 1–13.

9. Save, M.; Guillaneuf, Y.; Gilbert, R.G. Controlled radical polymerization in aqueous dispersed media. *Aust. J. Chem.* **2006**, *59*, 693–711.

10. Asua, J.M. *Polymer Reaction Engineering*; Blackwel Publishing Ltd: Oxford, 2007;

11. Matyjaszewski, K. Controlled Radical Polymerization: Mechanisms. *Curr. Opin. Solid State Mater. Sci.* **1996**, *1*, 769–776.

12. Matyjaszewski, K. *Advances in Controlled / Living Radical Polymerization*; American Chemical Society: Washington, DC, 2003;

13. Barner, L.; Davis, T.P.; Stenzel, M.H.; Barner-Kowollik, C. Complex macromolecular architectures by reversible addition fragmentation chain transfer chemistry: Theory and practice. *Macromol. Rapid Commun.* **2007**, *28*, 539–559.

14. Fierens, S.; D'hooge, D.; Van Steenberge, P.; Reyniers, M.-F.; Marin, G. Exploring the Full Potential of Reversible Deactivation Radical Polymerization Using Pareto-Optimal Fronts. *Polymers (Basel).* **2015**, *7*, 655–679.

15. D'Hooge, D.R.; Van Steenberge, P.H.M.; Reyniers, M.F.; Marin, G.B. Fed-batch control and visualization of monomer sequences of individual ICAR ATRP gradient copolymer chains. *Polymers (Basel).* **2014**, *6*, 1074–1095.

16. Brandl, F.; Drache, M.; Beuermann, S. Kinetic Monte Carlo Simulation Based Detailed Understanding of the Transfer Processes in Semi-Batch Iodine Transfer Emulsion Polymerizations of Vinylidene Fluoride. *Polymers (Basel).* **2018**, *10*, 1008.

17. Barner-Kowollik, C. *Handbook of RAFT Polymerization*; Wiley-VCH: Weinheim, 2008;

18. Moad, G.; Chiefari, J.; Chong, Y.K.; Krstina, J.; Mayadunne, R.T. a; Postma, A.; Rizzardo, E.; Thang, S.H. Living free radical polymerization with reversible addition – fragmentation chain transfer (the life of RAFT). *Polym. Int.* **2000**, *49*, 993–1001.

19. De Rybel, N.; Van Steenberge, P.H.M.; Reyniers, M.-F.; D'hooge, D.R.; Marin, G.B. How chain length dependencies interfere with the bulk RAFT polymerization rate and microstructural control. *Chem. Eng. Sci.* **2018**, *177*, 163–179.

20. Gilbert, R.G. *Emulsion polymerization: a mechanistic approach*; Academic Press Inc.: London, 1995;

21. Charleux, B.; Monteiro, M.J.; Heuts, H. Living Radical Polymerisation in Emulsion and Miniemulsion. In *Chemistry and Technology of Emulsion Polymerisation*; John Wiley & Sons: New York, 2013; pp. 105–143.

22. Rawlston, J. a *Multiscale Modeling of Free-Radical Polymerization Kinetics*; for the Degree Doctor of Philosophy in the School of Chemical and Biomolecular Engineering, Georgia Institute of Technology, May 2010;

23. Prescott, S.W.; Ballard, M.J.; Rizzardo, E.; Gilbert, R.G. Rate optimization in controlled radical emulsion polymerization using RAFT. *Macromol. Theory Simulations* **2006**, *15*, 70–86.

24. Asua, J.M. Challenges for industrialization of miniemulsion polymerization. *Prog. Polym. Sci.* **2014**, *39*, 1797–1826.

25. Matyjaszewski, K.; Davies, T.P. *Handbook of Radical Polymerisation*; John Wiley & Sons: Hoboken, 2002;

26. Mastan, E.; Li, X.; Zhu, S. Modeling and theoretical development in controlled radical polymerization. *Prog. Polym. Sci.* **2015**, *45*, 71–101.

27. D'hooge, D.R.; Van Steenberge, P.H.M.; Reyniers, M.-F.; Marin, G.B. The strength of multi-scale modeling to unveil the complexity of radical polymerization. *Prog. Polym. Sci.* **2016**, *58*, 59–89.

28. Zetterlund, P.B. Controlled/living radical polymerization in nanoreactors: compartmentalization effects. *Polym. Chem.* **2011**, *2*, 534–549.

29. Zetterlund, P.B.; Okubo, M. Compartmentalization in nitroxide-mediated radical polymerization in dispersed systems. *Macromolecules* **2006**, *39*, 8959–8967.

30. Cano-Valdez, A.; Saldívar-Guerra, E.; González-Blanco, R.; Cunningham, M.F.; Herrera-Ordóñez, J. Nitroxide Mediated Radical Emulsion Polymerization: Mathematical Modeling. *Macromol. Symp.* **2017**, *374*, 1–11.

31. Tobita, H. Threshold particle diameters in miniemulsion reversible-deactivation radical polymerization. *Polymers (Basel).* **2011**, *3*, 1944–1971.

32. Prescott, S.W.; Ballard, M.J.; Rizzardo, E.; Gilbert, R.G. Radical Loss in RAFT-mediated emulsion polymerizations. *Macromolecules* **2005**, *38*, 4901–4912.

33. Liu, S.; Hermanson, K.D.; Kaler, E.W. Reversible Addition−Fragmentation Chain Transfer Polymerization in Microemulsion. *Macromolecules* **2006**, *39*, 4345–4350.

34. Qiu, J.; Charleux, B.; Matyjaszewski, K. Controlled/living radical polymerization in aqueous media: homogeneous and heterogeneous systems. *Prog. Polym. Sci.* **2001**, *26*, 2083–2134.

35. Monteiro, M.J.; Cunningham, M.F. Polymer Nanoparticles via Living Radical Polymerization in Aqueous Dispersions: Design and Applications. *Macromolecules* **2012**, *45*, 4939–4957.

36. Monteiro, M.J.; Hodgson, M.; De Brouwer, H. Influence of RAFT on the rates and molecular weight distributions of styrene in seeded emulsion polymerizations. *J. Polym. Sci. Part A Polym. Chem.* **2000**, *38*, 3864–3874.

37. Landfester, K.; Willert, M.; Antonietti, M. Preparation of polymer particles in nonaqueous direct and inverse miniemulsions. *Macromolecules* **2000**, *33*, 2370–2376.

38. Ting, S.R.S.; Min, E.H.; Zetterlund, P.B. Reversible AdditionFragmentation Chain Transfer (RAFT) polymerization in miniemulsion based on in situ surfactant generation. *Aust. J. Chem.* **2011**, *64*, 1033–1040.

39. Jansen, T.G.T.; Meuldijk, J.; Lovell, P. a.; van Herk, A.M. On the Reaction Characteristics of Miniemulsion Polymerization with Aqueous Phase Initiation - Experiments and Modeling. *Macromol. React. Eng.* **2015**, *9*, 19–31.

40. Perrier, S.; Takolpuckdee, P. Macromolecular design via reversible addition-fragmentation chain transfer (RAFT)/xanthates (MADIX) polymerization. *J. Polym. Sci. Part A Polym. Chem.* **2005**, *43*, 5347–5393.

41. Yang, L.; Luo, Y.; Li, B. The Influence of Surfactant Coverage of the Minidroplets on RAFT Miniemulsion Polymerization. *J. Polym. Sci. Part A Polym. Chem.* **2006**, *44*.

42. Derboven, P.; Steenberge, P.H.M. Van; Reyniers, M.; Barner-kowollik, C.; Dagmar, R.D.; Marin, G.B.; D'hooge, D.R.; Marin, G.B.; Dagmar, R.D.; Marin, G.B. Chain transfer in degenerative RAFT polymerization revisited : a comparative study. *Macromol. Theory Simulations* **2016**, *25*, 104–115.

43. Devlaminck, D.J.G.; Van Steenberge, P.H.M.; De Keer, L.; Reyniers, M.-F.; D'hooge, D.R. A detailed mechanistic study of bulk MADIX of styrene and its chain extension. *Polym. Chem.* **2017**, *8*, 6948–6963.

44. Kubo, K.; Goto, A.; Sato, K.; Kwak, Y.; Fukuda, T. Kinetic study on reversible addition-fragmentation chain transfer (RAFT) process for block and random copolymerizations of styrene and methyl methacrylate. *Polymer (Guildf).* **2005**, *46*, 9762–9768.

45. Moad, G.; Flagship, C.M.; Ave, B. *Controlled Radical Polymerization: Mechanisms*; American Chemical Society: Washington, DC, 2015;

46. Derboven, P.; Van Steenberge, P.; Reyniers, M.-F.; Barner-Kowollik, C.; D'hooge, D.R.; Marin, G.B. A novel method for the measurement of degenerative chain transfer coefficients: proof of concept and experimental validation. *Polym. Chem.* **2016**, *7*, 3334–3349.

47. De Rybel, N.; Van Steenberge, P.H.M.; Reyniers, M.-F.; Barner-Kowollik, C.; D'hooge, D.R.; Marin, G.B. An Update on the Pivotal Role of Kinetic Modeling for the Mechanistic Understanding and Design of Bulk and Solution RAFT Polymerization. *Macromol. Theory Simulations* **2017**, *26*, 1600048.

48. Wang, A.R.; Zhu, S. Effects of Diffusion-Controlled Radical Reactions on RAFT Polymerization. *Macromol. Theory Simulations* **2003**, *12*, 196–208.

49. D'hooge, D.R.; Reyniers, M.F.; Marin, G.B. The crucial role of diffusional limitations in controlled radical polymerization. *Macromol. React. Eng.* **2013**, *7*, 362–379.

50. Devlaminck, D.J.G.; Van Steenberge, P.H.M.M.; Reyniers, M.-F.M.-F.; D'hooge, D.R.D.R. Deterministic modeling of RAFT miniemulsion conversion and average chain length characteristics: invalidity of zero-one nature at higher monomer conversions. *Macromolecules* **2018**, 10.1021/acs.macromol.8b02111.

51. Peklak, A.D.; Butté, A. Modeling of diffusion limitations in bulk RAFT polymerization. *Macromol. Theory Simulations* **2006**, *15*, 546–562.

52. Achilias, D.S. A review of modeling of diffusion controlled polymerization reactions. *Macromol. Theory Simulations* **2007**, *16*, 319–347.

53. Barner-Kowollik, C.; Russell, G.T. Chain-length-dependent termination in radical polymerization: Subtle revolution in tackling a long-standing challenge. *Prog. Polym. Sci.* **2009**, *34*, 1211–1259.

54. O'Driscoll, K.F. *Comprehensive Polymer Science*; Pergamon Press London, 1989;

55. Russell, G.T. The kinetics of free-radical polymerization: fundamental aspects. *Aust. J. Chem.* **2002**, *55*, 399–414.

56. McLeary, J.B.; Klumperman, B. RAFT mediated polymerisation in heterogeneous media. *Soft Matter* **2006**, *2*, 45–53.

57. Barner-Kowollik, C.; Quinn, J.F.; Morsley, D.R.; Davis, T.P. Modeling the reversible addition-fragmentation chain transfer process in cumyl dithiobenzoate-mediated styrene homopolymerizations: Assessing rate coefficients for the addition-fragmentation equilibrium. *J. Polym. Sci. Part A Polym. Chem.* **2001**, *39*, 1353–1365.

58. Monteiro, M.J.; De Brouwer, H. Intermediate radical termination as the mechanism for retardation in reversible addition-fragmentation chain transfer polymerization. *Macromolecules* **2001**, *34*, 349–352.

59. Moad, G. Mechanism and Kinetics of Dithiobenzoate-Mediated RAFT Polymerization: status of dilemma. *Macromol. Chem. Phys.* **2014**, *215*, 9–26.

60. Moad, G.; Rizzardo, E.; Thang, S.H. Living Radical Polymerization by the RAFT Process—A Third Update. *Aust. J. Chem.* **2012**, *65*, 985–1076.

61. Moad, G.; Rizzardo, E.; Thang, S.H. Living radical polymerization by the RAFT process A second update. *Aust. J. Chem.* **2009**, *62*, 1402–1472.

62. Barner-Kowollik, C.; Buback, M.; Charleux, B.; Coote, M.L.; Drache, M.; Fukuda, T.; Goto, A.; Klumperman, B.; Lowe, A.B.; Mcleary, J.B.; et al. Mechanism and Kinetics of

Dithiobenzoate-Mediated RAFT Polymerization. I. The Current Situation. *J. Polym. Sci. Part A Polym. Chem.* **2006**, *44*, 5809–5831.

63. Konkolewicz, D.; Hawkett, B.S.; Gray-Weale, A.; Perrier, S. RAFT Polymerization Kinetics : Combination of Apparently Conflicting Models. *Macromolecules* **2008**, *41*, 6400–6412.

64. Kwak, Y.; Goto, A.; Tsujii, Y.; Murata, Y.; Komatsu, K.; Fukuda, T. A Kinetic Study on the Rate Retardation in Radical Polymerization of Styrene with Addition−Fragmentation Chain Transfer. *Macromolecules* **2002**, *35*, 3026–3029.

65. Goto, A.; Sato, K.; Tsujii, Y.; Fukuda, T.; Moad, G.; Rizzardo, E.; Thang, S.H. Mechanism and Kinetics of RAFT-Based Living Radical Polymerizations of Styrene and Methyl Methacrylate. *Macromolecules* **2001**, *34*, 402–408.

66. McLeary, J.B.; Calitz, F.M.; McKenzie, J.M.; Tonge, M.P.; Sanderson, R.D.; Klumperman, B. Beyond Inhibition: A 1H NMR Investigation of the Early Kinetics of RAFT-Mediated Polymerization with the Same Initiating and Leaving Groups. *Macromolecules* **2004**, *37*, 2383–2394.

67. Calitz, F.M.; Tonge, M.P.; Sanderson, R.D.; Step, D. Kinetic and Electron Spin Resonance Analysis of RAFT Polymerization of Styrene. **2006**, 5–8.

68. Geelen, P.; Klumperman, B. Intermediate radical termination in reversible addition-fragmentation chain transfer-mediated polymerization: Identification of termination products. *Macromolecules* **2007**, *40*, 3914–3920.

69. Ranieri, K.; Delaittre, G.; Barner-Kowollik, C.; Junkers, T. Direct access to dithiobenzonate RAFT agent fragmenting rate coefficients by ESR spin-trapping. **2014**, 2023–2028.

70. Kwak, Y.; Goto, A.; Fukuda, T. Rate Retardation in Reversible Addition - Fragmentation Chain Transfer (RAFT) Polymerization: Further Evidence for Cross-Termination Producing 3-Arm Star Chain. *Macromolecules* **2004**, *37*, 1219–1225.

71. Meiser, W.; Buback, M. Assessing the RAFT equilibrium constant via model systems: An EPR study-response to a comment. *Macromol. Rapid Commun.* **2011**, *32*, 1490–1494.

72. Li, C.; He, J.; Liu, Y.; Zhou, Y.; Yang, Y. Probing the RAFT process using a model reaction between alkoxyamine and dithioester. *Aust. J. Chem.* **2012**, *65*, 1077–1089.

73. Konkolewicz, D.; Siauw, M.; Gray-Weale, A.; Hawkett, B.S.; Perrier, S. Obtaining kinetic information from the chain-length distribution of polymers produced by RAFT. *J. Phys. Chem. B* **2009**, *113*, 7086–7094.

74. Ting, S.R.S.; Davis, T.P.; Zetterlund, P.B. Retardation in RAFT polymerization: Does cross-termination occur with short radicals only? *Macromolecules* **2011**, *44*, 4187–4193.

75. Junkers, T.; Delaittre, G.; Chapman, R.; Günzler, F.; Chernikova, E.; Barner-Kowollik, C. Thioketone-mediated polymerization with dithiobenzoates: Proof for the existence of stable radical intermediates in RAFT polymerization. *Macromol. Rapid Commun.* **2012**, *33*, 984–990.

76. Klumperman, B.; Van Den Dungen, E.T. a; Heuts, J.P. a; Monteiro, M.J. RAFT-mediated polymerization- A story of incompatible data? *Macromol. Rapid Commun.* **2010**, *31*, 1846–1862.

77. Barner-Kowollik, C.; Coote, M.L.; Davis, T.P.; Radom, L.; Vana, P. The reversible addition-fragmentation chain transfer process and the strength and limitations of modeling: Comment on “The magnitude of the fragmentation rate coefficient.” *J. Polym. Sci. Part A Polym. Chem.* **2003**, *41*, 2828–2832.

78. Wang, A.R.; Zhu, S.; Kwak, Y.; Goto, A.; Fukuda, T.; Monteiro, M.S. A difference of six orders of magnitude: A reply to “The magnitude of the fragmentation rate coefficient.” *J. Polym. Sci. Part A Polym. Chem.* **2003**, *41*, 2833–2839.

79. Vana, P.; Davis, T.P.; Barner-Kowollik, C. Kinetic analysis of reversible addition fragmentation chain transfer (RAFT) polymerizations: Conditions for inhibition, retardation, and optimum living polymerization. *Macromol. Theory Simulations* **2002**, *11*, 823–835.

80. Zhang, M.; Ray, W.H. Modeling of “living” free-radical polymerization with RAFT chemistry. *Ind. Eng. Chem. Res.* **2001**, *40*, 4336–4352.

81. Monteiro, M.J. Modeling the molecular weight distribution of block copolymer formation in a reversible addition-fragmentation chain transfer mediated living radical polymerization. *J. Polym. Sci. Part A Polym. Chem.* **2005**, *43*, 5643–5651.

82. McLeary, J.B.; Tonge, M.P.; Klumperman, B. A mechanistic interpretation of initialization processes in RAFT-mediated polymerization. *Macromol. Rapid Commun.* **2006**, *27*, 1233–1240.

83. Drache, M.; Schmidt-Naake, G.; Buback, M.; Vana, P. Modeling RAFT polymerization kinetics via Monte Carlo methods: Cumyl dithiobenzoate mediated methyl acrylate polymerization. *Polymer (Guildf).* **2005**, *46*, 8483–8493.

84. Coote, M.L.; Radom, L. Ab initio evidence for slow fragmentation in RAFT polymerization. *J. Am. Chem. Soc.* **2003**, *125*, 1490–1491.

85. Coote, M.L. Ab initio study of the addition-fragmentation equilibrium in RAFT polymerization: When is polymerization retarded? *Macromolecules* **2004**, *37*, 5023–5031.

86. Junkers, T.; Barner-Kowollik, C.; Coote, M.L. Revealing model dependencies in “assessing the RAFT equilibrium constant via model systems: An EPR study.” *Macromol. Rapid Commun.* **2011**, *32*, 1891–1898.

87. Junkers, T. RAFT kinetics revisited: Revival of the RAFT debate. *J. Polym. Sci. Part A Polym. Chem.* **2011**, *49*, 4154–4163.

88. Buback, M.; Meiser, W.; Vana, P. Mechanism of CPDB-mediated RAFT polymerization of methyl methacrylate: Influence of pressure and RAFT agent concentration. *Aust. J. Chem.* **2009**, *62*, 1484–1487.

89. Prescott, S.W. Chain-length dependence in living/controlled free-radical polymerizations: Physical manifestation and Monte Carlo simulation of reversible transfer agents. *Macromolecules* **2003**, *36*, 9608–9621.

90. Tobita, H. On the discrimination of RAFT models using miniemulsion polymerization. *Macromol. Theory Simulations* **2013**, *22*, 399–409.

91. Tobita, H. Effects of retardation and variation of monomer concentration in RAFT miniemulsion polymerization. *Macromol. Theory Simulations* **2011**, *20*, 709–720.

92. Tobita, H.; Yanase, F. Monte Carlo simulation of controlled/living radical polymerization in emulsified systems. *Macromol. Theory Simulations* **2007**, *16*, 476–488.

93. Lansalot, M.; Davis, T.P.; Heuts, J.P.A. RAFT miniemulsion polymerization: Influence of the structure of the RAFT agent. *Macromolecules* **2002**, *35*, 7582–7591.

94. Luo, Y.; Liu, B.; Wang, Z.; Gao, J.; Li, B. Butyl Acrylate RAFT Polymerization in Miniemulsion. *J. Polym. Sci. Part A-Polymer Chem.* **2007**, *45*, 2304–2315.

95. Tsavalas, J.G.; Schork, F.J.; De Brouwer, H.; Monteiro, M.J. Living Radical Polymerization by reversible addition-fragmentation chain transfer in ionically stabilized miniemulsions. *Macromolecules* **2001**, *34*, 3938–3946.

96. Devlaminck, D.J.G.; Van Steenberge, P.H.M.; Reyniers, M.-F.; D'hooge, D.R. Deterministic Modeling of Degenerative RAFT Miniemulsion Polymerization Rate and

Average Polymer Characteristics: Invalidity of Zero–One Nature at Higher Monomer Conversions. *Macromolecules* **2018**, 10.1021/acs.macromol.8b02111.

97. Suzuki, K.; Kanematsu, Y.; Miura, T.; Minami, M.; Satoh, S.; Tobita, H. Experimental method to discriminate RAFT models between intermediate termination and slow fragmentation via comparison of rates of miniemulsion and bulk polymerization. *Macromol. Theory Simulations* **2014**, *23*, 136–146.

98. Tobita, H. Fundamentals of RAFT miniemulsion polymerization kinetics. *Macromol. Symp.* **2010**, *288*, 16–24.

99. Wang, Z.; Zhang, Q.; Zhan, X.; Chen, F.; Rao, G.; Xiong, J. Preparation, kinetics and microstructures of well-defined PS-b-PS/Bd diblock copolymers via RAFT miniemulsion polymerization. *J. Polym. Res.* **2013**, *20*, 288–301.

100. Suzuki, K.; Nishimura, Y.; Kanematsu, Y.; Masuda, Y.; Satoh, S.; Tobita, H. Experimental Validation of Intermediate Termination in RAFT Polymerization with Dithiobenzoate via Comparison of Miniemulsion and Bulk Polymerization Rates. *Macromol. React. Eng.* **2012**, *6*, 17–23.

101. Altarawneh, I.S.; Gomes, V.G.; Srour, M.H. Polymer Chain Extension in Semibatch Emulsion Polymerization with RAFT-Based Transfer Agent: The influence of Reaction Conditions on Polymerization Rate and Product Properties. *J. Appl. Polym. Sci.* **2009**, *114*, 2356–2372.

102. Altarawneh, I.S.; Gomes, V.G.; Srour, M.S. The Influence of Xanthate-Based Transfer Agents on Styrene Emulsion Polymerization: Mathematical Modeling and Model Validation. *Macromol. React. Eng.* **2008**, *2*, 58–79.

103. Luo, Y.; Wang, R.; Yang, L.; Yu, B.; Li, B.; Zhu, S. Effect of Reversible Addition-Fragmentation Transfer (RAFT) reactions on (mini)emulsion polymerization kinetics and estimate of RAFT equilibrium constant. *Macromolecules* **2006**, *39*, 1328–1337.

104. Li, X.; Wang, W.J.; Weng, F.; Li, B.G.; Zhu, S. Targeting copolymer composition distribution via model-based monomer feeding policy in semibatch RAFT mini-emulsion copolymerization of styrene and butyl acrylate. *Ind. Eng. Chem. Res.* **2014**, *53*, 7321–7332.

105. Jung, S.M.; Gomes, V.G. Miniemulsion polymerisation via reversible addition fragmentation chain transfer in pseudo-bulk regime. *Macromol. React. Eng.* **2011**, *5*, 303–315.

106. Peklak, A.D.; Butte, A. Kinetic Model of Reversible Addition Fragmentation Chain Transfer Polymerization of Styrene in Seeded Emulsion. *J. Polym. Sci. Part A Polym. Chem.* **2006**, *44*, 6114–6135.

107. Smulders, W.; Gilbert, R.G.; Monteiro, M.J. A kinetic investigation of seeded emulsion polymerization of styrene using reversible addition-fragmentation chain transfer (RAFT) agents with a low transfer constant. *Macromolecules* **2003**, *36*, 4309–4318.

108. Pepels, M.P.F.; Holdsworth, C.I.; Pascual, S.; Monteiro, M.J. RAFT-Mediated emulsion polymerization of styrene with low reactive xanthate agents: Microemulsion-like behavior. *Macromolecules* **2010**, *43*, 7565–7576.

109. Butté, A.; Peklak, A.D.; Storti, G.; Morbidelli, M. RAFT Polymerization in Bulk and Emulsion. *Radic. Polym. Kinet. Mech.* **2007**, *246*, 168–181.

110. Luo, Y.; Yu, B. Monte Carlo Simulation of Droplet Nucleation in RAFT Free Radical Miniemulsion Polymerization. *Polym. Plast. Technol. Eng.* **2005**, *43*, 1299–1321.

111. Wang, A.R.; Zhu, S. Modeling the Reversible Addition – Fragmentation Transfer Polymerization Process. *J. Polym. Sci. Part A Polym. Chem.* **2003**, *41*, 1553–1566.

112. Houshyar, S.; Keddie, D.J.; Moad, G.; Mulder, R.J.; Saubern, S.; Tsanaktsidis, J. The scope for synthesis of macro-RAFT agents by sequential insertion of single monomer units. *Polym. Chem.* **2012**, *3*, 1879.

113. Dossi, M.; Storti, G.; Moscatelli, D. Initiation Kinetics in Free-Radical Polymerization: Prediction of Thermodynamic and Kinetic Parameters Based on ab initio Calculations. *Macromol. Theory Simulations* **2010**, *19*, 170–178.

114. Buback, M.; Gilbert, R.G.; Hutchinson, R.A.; Klumberman, B.; Kuchta, F.-D.; Manders, B.G.; O'Driscoll, K.F.; Russell, G.T.; Schweer, J. Critically evaluated rate coefficients for free-radical Propagation rate coefficient for styrene. *Macromol. Chem. Phys.* **1995**, *196*, 3267–3280.

115. Johnston-Hall, G.; Monteiro, M.J. Bimolecular Radical Termination: New Perspectives and Insights. *J. Polym. Sci. Part a-Polymer Chem.* **2008**, *46*, 3155–3176.

116. Derboven, P.; D'hooge, D.R.; Reyniers, M.-F.; Marin, G.B.; Barner-Kowollik, C. The Long and the Short of Radical Polymerization. *Macromolecules* **2015**, *48*, 492–501.

117. Moad, G.; Solomon, D.H. *The chemistry of radical polymerization*; Elsevier: Oxford, 2006;

118. Van Steenberge, P.H.M.; D.R., D.; Reyniers, M.F.; Marin, G.B.; Cunningham, M.F. 4-Dimensional modeling strategy for an improved understanding of miniemulsion NMP of acrylates initiated by SG1-macroinitiator. *Macromolecules* **2014**, *47*, 7732–7741.

119. Hui, A.W.; Hamielec, A.E. Thermal Polymerization of Styrene at High Conversion and Temperatures. An Experimental Study. *J. Appl. Polym. Sci.* **1972**, *16*, 749–769.

120. Steenberge, P.H.M. Van; D'hooge, D.R.; Wang, Y.; Zhong, M.; Reyniers, M.-F.; Konkolewicz, D.; Matyjaszewski, K.; Marin, G.B. Linear Gradient Quality of ATRP Copolymers. *Macromolecules* **2012**, *45*, 8519–8531.

121. Bevington, J.C.; Melville, H.W.; Taylor, R.P. The termination reaction in radical polymerizations. II. Polymerizations of styrene at 60° and of methyl methacrylate at 0 and 60°, and the copolymerization of these monomers at 60°. *J. Polym. Sci.* **1954**, *14*, 463–476.

122. Fierens, S.K.; D'hooge, D.R.; Van Steenberge, P.H.M.; Reyniers, M.-F.; Marin, G.B. MAMA-SG1 initiated nitroxide mediated polymerization of styrene: From Arrhenius parameters to model-based design. *Chem. Eng. J.* **2014**, *278*, 407–420.

123. Khuong, K.S.; Jones, W.H.; Pryor, W. a; Houk, K.N. The mechanism of the self-initiated thermal polymerization of styrene. Theoretical solution of a classic problem. *J. Am. Chem. Soc.* **2005**, *127*, 1265–77.

124. Kotoulas, C.; Krallis, A.; Pladis, P.; Kiparissides, C. A comprehensive kinetic model for the combined chemical and thermal polymerization of styrene up to high conversions. *Macromol. Chem. Phys.* **2003**, *204*, 1305–1314.

125. Vivaldo-Lima, E.; Mendoza-Fuentes, A.D.J. Development of a kinetic model for INIFERTER controlled/"living" free-radical polymerization considering diffusion-controlled effects. *Polym. React. Eng.* **2002**, *10*, 193–226.

126. Peklak, A.D.; Butté, A.; Storti, G.; Morbidelli, M. Gel effect in the bulk reversible addition-fragmentation chain transfer polymerization of methyl methacrylate: Modeling and experiments. *J. Polym. Sci. Part A Polym. Chem.* **2006**, *44*, 1071–1085.

127. Garg, D.K.; Serra, C.A.; Hoarau, Y.; Parida, D.; Bouquey, M.; Muller, R. Analytical solution of free radical polymerization: Applications- implementing gel effect using AK model. *Macromolecules* **2014**, *47*, 7370–7377.

128. Tefera, N.; Weickert, G.; Westerterp, K.R. Modeling of Free Radical Polymerization up to High Conversion . I . A Method for the Selection of Models by Simultaneous Parameter Estimation. *J. Appl. Polym. Sci.* **1996**, *63*, 1649–1661.

129. Carswell, T.G.; Hill, D.J.T.; Londero, D.I.; O'Donnell, J.H.; Pomery, P.J.; Winzor, C.L. Kinetic parameters for polymerization of methyl methacrylate at 60??C. *Polymer (Guildf).* **1992**, *33*, 137–140.

130. Mastan, E.; Zhu, S. Method of moments: A versatile tool for deterministic modeling of polymerization kinetics. *Eur. Polym. J.* **2015**, *68*, 139–160.

131. D'hooge, D.R.; Reyniers, M.-F.; Marin, G.B. Methodology for Kinetic Modeling of Atom Transfer Radical Polymerization. *Macromol. React. Eng.* **2009**, *3*, 185–209.

132. Wang, W.; Zhou, Y.; Shi, L.; Luo, Z.-H. Modeling of the Atom Transfer Radical Copolymerization Processes of Methyl Methacrylate and 2-(Trimethylsilyl) Ethyl Methacrylate under Batch, Semibatch, and Continuous Feeding: A Chemical Reactor Engineering Viewpoint. *Ind. Eng. Chem. Res.* **2014**, *53*, 11873–11883.

133. Zhou, Y.-N.; Luo, Z.-H. State-of-the-Art and Progress in Method of Moments for the Model-Based Reversible-Deactivation Radical Polymerization. *Macromol. React. Eng.* **2016**, *10*, 516–534.

134. Smith, W. V.; Ewart, R.H. Kinetics of emulsion polymerization. *J. Chem. Phys.* **1948**, *16*, 592–599.

135. Zetterlund, P.B.; Okubo, M. Compartmentalization in NMP in dispersed systems: Relative contributions of confined space effect and segregation effect depending on nitroxide type. *Macromol. Theory Simulations* **2009**, *18*, 277–286.

136. Prescott, S.W.; Ballard, M.J.; Gilbert, R.G. Average termination rate coefficients in emulsion polymerization: Effect of compartmentalization on free-radical lifetimes. *J. Polym. Sci. Part A Polym. Chem.* **2005**, *43*, 1076–1089.

137. Jia, Z.; Monteiro, M.J. Kinetic simulations of RAFT-mediated microemulsion polymerizations of styrene. *ACS Symp. Ser.* **2012**, *1100*, 293–304.

138. Zetterlund, P.B. Nitroxide-Mediated Radical Polymerization in Dispersed Systems: Compartmentalization and Nitroxide Partitioning. *Macromol. Theory Simulations* **2009**, 11–23.

Chapter 6: Macroemulsion RAFT polymerization: a kinetic study toward the production of core-shell nanoparticles using a xanthate agent

6.1 Introduction

Free radical polymerization (FRP) can be carried out operating several diverse techniques due to its inherent compatibility with a wide range of solvents.[1,2] The most environmentally-friendly are waterborne emulsion polymerization methods where the heat generated by the exothermic FRP process can be readily absorbed and dissipated by the water phase.[3,4]

The most commonly (industrially) applied emulsion polymerization technique is so-called macroemulsion polymerization.[5] A macroemulsion initially consists of water as the continuous phase, a water-soluble initiator, surfactant and a slightly water-soluble monomer which is mainly present in the form of large droplets (1 - 100 μm).[6] If the surfactant concentration exceeds its critical micelle concentration (CMC), the surfactant molecules arrange themselves to form small micelles (5-10 nm). Radicals formed after initiator decomposition in the aqueous phase react with the small amount of monomer available producing oligomeric radicals. If the oligomeric radical reaches a critical chain length (i_{crit} = 2 for styrene), these species become too hydrophobic to remain in the aqueous phase and entry in a micelle can occur, transforming the micelle into a polymer particle.[7] Polymerization continues in the particle until a second radical enters and termination occurs with the first radical. Monomer disappearing in the particles due to polymerization is replenished by monomer diffusing from the droplets, as long as these are not yet completely consumed, through the aqueous phase to the particles.[8] Ideally, no reactions occur inside these monomer droplets and, hence, they only act as reservoirs (up to intermediate monomer conversions).[9] During a macroemulsion polymerization, the reactants are confined within discrete confined spaces, better known as compartmentalization.[10] This results in a segregation effect, with only species located in the same particle able to react, and a confined space effect according to which two species located in the same particle react at a higher rate

in a small particle compared to in a large particle.[11–13] Consequently, high polymerization rates and high molar mass polymer product can be obtained with minimal residual monomer remaining at the end of the polymerization process.[6]

Nevertheless, due to the short time scale of dead polymer formation, the FRP reaction mechanism results in the lack of control over the macromolecular structure, typically leading to broad chain length distributions (CLDs).[14,15] This inherent disadvantage of radical polymerization could be overcome by the introduction of so-called reversible deactivation radical polymerization (RDRP) techniques, also known as controlled radical polymerization (CRP). These techniques rely on the temporary deactivation of the active growing macroradicals into so-called dormant macrospecies via the addition of a controlling/mediating agent.[2,14,16–19] If most of the chains are initiated at the same time and if the activation/deactivation procedure occurs fast enough, the chains which do not terminate will grow concurrently, leading to very narrow CLDs, at least if the fraction of dormant species (also known as the end group functionality (EGF)) is high. Moreover, the reactivation of the dormant species allows the preparation of complex polymer architectures (*e.g.* block, hyperbranched, star) inaccessible via conventional FRP.[20] One of the most industrially promising RDRP techniques is reversible addition-fragmentation chain transfer (RAFT) polymerization as similar rates to FRP can be achieved while being versatile in terms of monomer compatibility.[21,22]

$$R_i + R_0X \underset{k_{\mathrm{frag},a}}{\overset{k_{add,a}}{\rightleftharpoons}} R_0XR_i \underset{k_{add,b}}{\overset{k_{\mathrm{frag},b}}{\rightleftharpoons}} R_0 + R_iX \quad \text{(a)}$$

$$R_0 + M \xrightarrow{k_{pR_0}} R_1 \quad \text{(b)}$$

$$R_i + (R_jX) \underset{k_{\mathrm{frag}}}{\overset{k_{add}}{\rightleftharpoons}} R_iXR_j \underset{k_{add}}{\overset{k_{\mathrm{frag}}}{\rightleftharpoons}} R_\mathrm{j} + R_iX \quad \text{(c)}$$

Figure 6.1*: Key reaction mechanism for the RAFT process showing only the so-called pre-equilibrium (reactions in a), chain initiation by RAFT leaving group (reaction b) and main exchange (reactions c) for simplicity;* $k_{add(,a/b),frag(,a/b)}$ *and* k_{pR_0}*: rate coefficient for addition/fragmentation and chain initiation by the RAFT leaving group;* R_i *,* R_0X *,* R_iX *,* R_0XR_i *,* R_iXR_j *, M,* R_0 *: macroradical, initial RAFT agent, dormant macrospecies, intermediate radical of the pre-equilibrium, intermediate radical of the main exchange, monomer and RAFT leaving group radical; i and j : representations of the chain length.*

In RAFT polymerization, the control over the chain growth is obtained through the reversible transfer mechanism shown in Figure 6.1. Initially, the growing macroradicals cannot only terminate as in conventional FRP but deactivation can also occur via the addition to a chain transfer agent (CTA, R_0X, reaction a in Figure 6.1).[22–24] This intermediate can either fragment back to the original species or it can fragment forming a dormant macrospecies (R_iX) and a new small leaving group radical (R_0) capable of reinitiating the polymerization process (reaction b in Figure 6.1). Moreover, a growing macroradical can also add to a dormant macrospecies which leads to an exchange of the radical function after fragmentation in the proper direction (reaction c in Figure 6.1).[25]

Early attempts to implement RAFT in macroemulsion polymerization resulted in poor colloidal stability, slow polymerization rates or a loss of control over the molar mass and dispersity.[26–32] Moreover, if RAFT agents capable of controlling the chain growth in homogeneous polymerization processes are attempted in emulsion processes, then particles containing large concentrations of oligomeric species during the early stages of macroemulsion polymerization

are formed. Unfortunately, the chemical potential of the monomer inside these particles is lower than in non-nucleated droplets, resulting in a superswelling effect where monomer transfers from the droplets to the particles until an equilibrium is reached.[33] Due to this effect, particles can swell up to 100 times their unswollen volume and thereby inflict particle coagulation or even phase separation.[9,27,31,34–37]

To this day, xanthates are the only class of RAFT agents that can straightforwardly be employed successfully in conventional macroemulsion polymerization.[6,35,38–43] For completeness, it is mentioned that due to historical reasons of its discovery, RAFT polymerization employing xanthates as mediating agents is often referred to as macromolecular design by interchange of xanthates (MADIX).[23,44] These RAFT agents contain an oxygen atom possessing a delocalizable electron pair in the α-position with respect to the thiocarbonlythio functional group, reducing the S=C double-bond character and, consequently, making radical addition to the RAFT moiety less favorable (cf. Chapter 3). As a result, polymeric species (as opposed to oligomeric species) are formed from the onset of the polymerization, which circumvents the superswelling issue although simultaneously resulting in poor molar mass control.[6,38,45] For example, Altarawneh *et al.*[6,45–47] investigated the RAFT macroemulsion polymerization of styrene mediated by (O-ethyl xanthate)-2-ethyl propionate and the influence of process parameters on the polymer and latex characteristics. It was shown that increasing the initial concentration of the "controlling agent" can be used to decrease the polymerization rate, number average molar mass and particle size although broad CLDs were always obtained and no linear growth of the average molar mass was achieved as a function of the monomer conversion. The influence of decreasing the controlling agent concentration on the polymerization rate acceleration was attributed to exit of the RAFT leaving group radicals which increases the probability of termination in the aqueous phase or, after reentry, in another particle already containing a radical. However, the polymerization rate could be increased by

increasing the surfactant or initiator concentration. Moreover, the obtained polystyrene polymer product could be successfully extended with *n*-butyl acrylate resulting in relatively pure polystyrene-block-poly(*n*-butyl acrylate) polymer chains. Optimal results in terms of EGF and dispersity for the chain extension were obtained employing semi-batch operation under starved-feed conditions, where the monomer feed rate is kept low to favor the RAFT transfer process over propagation.[45] The decrease of the S=C double-bond character due to the delocalizable electron pair in xanthates inherently results in high dispersity (≥2) polymer product. However, as shown by Monteiro *et al.*[35,48] for the RAFT macroemulsion polymerization of styrene, introducing an electron withdrawing group such as trifluoroethyl next to the oxygen atom results in an improved conservation of the S=C double-bond character. Ideally this results in a dispersity slightly below 1.5, the theoretical lower limit for free radical polymerization in which recombination is the dominant mode of termination.

Despite the delocalization of the oxygen electron pair generally resulting in poor molar mass control, the resulting charged resonance structure may have advantages, *e.g.* it has been postulated that xanthates are surface active.[27,41] This means that these RAFT controlling agents will always remain in the vicinity of the surface of the particles. Consequently, if a homopolymer latex is chain-extended under semi-batch operation, it becomes possible to produce covalently linked core-shell nanoparticles consisting of block copolymers where the core is comprised of the first polymer and the shell of the second polymer.[20,41,42,49,50] This surface activity is beneficial to facilitate the transport of the RAFT agent from droplet to particle, potentially at the cost of rate retardation due to more pronounced radical exit, as the RAFT leaving group radicals will be formed in the vicinity of the particle/aqueous phase boundary.[32] Smulders *et al.*[20,41] demonstrated the surface activity of (O-ethyl xanthate)-2-ethyl propionate by producing polystyrene-block-poly(*n*-butyl acrylate) core-shell nanoparticles via seeded macroemulsion polymerization for the synthesis of the core and subsequent semi-batch

macroemulsion polymerization for the synthesis of the shell. In seeded macroemulsion polymerization, seed particles (*e.g.* poly(methyl methacrylate) particles) are added to the reaction mixture in order to avoid undesired prolonged nucleation, resulting in better control of the particle size distribution (PSD). It was shown that a low monomer feed rate can reduce the dispersity of the obtained polymer product and that the dispersity of the final block copolymer (≈1.3) is lower than either of the individual blocks (respectively 2 and 1.4). Similarly, Monteiro *et al.*[27,42] prepared polystyrene-block-poly(n-butyl acrylate-co-acetoacetoxyethyl methacrylate) core-shell nanoparticles, without the use of initial seed particles, using (O-ethyl xanthate)-ethylbenzene as RAFT agent. Slow semi-batch feed conditions were again applied to promote the formation of block copolymers over homopolymers during the shell formation step.

In this chapter, the RAFT macroemulsion polymerization of styrene mediated by (O-ethyl xanthate)-2-ethyl propionate (agent from Chapter 3) and the impact of process variables on polymer and latex properties are investigated. Hence, a switch is made from mini (Chapter 4 and 5) to macro-emulsion. Focus on the relevance of partitioning is achieved through dedicated experimental analysis. Furthermore, the expected surface activity of this RAFT agent is verified by the subsequent chain extension of the polystyrene latex with *n*-butyl acrylate under semi-batch conditions.

6.2 Experimental

6.2.1 Materials

Styrene (Sty, ≥99%, Sigma-Aldrich) and *n*-butyl acrylate (*n*BuA, ≥99%, Sigma-Aldrich) were passed through a column filled with basic aluminium oxide (Sigma-Aldrich) to remove the stabilizer (4-tert-butylcatechol for Sty and monomethyl ether hydroquinone for *n*BuA). Potassium persulfate (KPS, ≥99%), sodium dodecyl sulfate (SDS, ≥99%), sodium bicarbonate ($NaHCO_3$, ≥99.7%), sodium chloride (NaCl, ≥99.5)%, ethyl propionate (EP, 99%), hydroquinone (HQ, ≥99%), tetrahydrofuran (THF, ≥99%), acetonitrile (ACN, ≥99.9%) ,and

water with 0.1% (v/v) trifluoroacetic acid were purchased from Sigma-Aldrich and used as received. Distilled water was further purified through a Millipore Milli-Q Plus system. (O-ethyl xanthate)-2-ethyl propionate (OEXEP, RAFT agent) was synthesized according to the literature procedure[51] discussed in Chapter 3.

6.2.2 Ethyl propionate and OEXEP partitioning experiments in the absence of polymerization

Partitioning experiments of ethyl propionate and OEXEP were carried out by adding 35g of H_2O, 15g of styrene (with inhibitor) and a varying amount (1-2.5g) of ethyl propionate or OEXEP in a 100 ml three neck flask. The flask was heated to 70°C in an oil bath and constantly stirred at 350 rpm for three hours. Afterwards, stirring was stopped and the mixture was allowed to stand isothermally for one hour to allow the aqueous and organic phase to separate. Samples were withdrawn from the separated phases and analyzed by means of high performance liquid chromatography (HPLC) in order to determine the analyte concentrations via predetermined calibration curves. The required partitioning coefficients could then be obtained by determining the slope of the $[X]_{org}$ vs $[X]_{aq}$ plots as discussed further (X: component under investigation, see Eq 1). This part was done in collaboration with Kyann De Smit at that time a Master thesis student.

6.2.3 Synthesis of polystyrene latex based on isothermal macroemulsion RAFT polymerization

A typical isothermal RAFT macroemulsion polymerization of styrene was performed as follows (n_0(Sty)/ n_0(OEXEP)/n_0(KPS) = 50/1/0.1; $[SDS]_0$ = 5 x CMC (CMC = 8.18 10^{-3} mol L^{-1} or equivalently, 2.36g L^{-1} at 25°C); 70/30 (w/w) H_2O/Sty). A mixture of styrene (30g), H_2O (65.4g), SDS (0.8g), OEXEP (1.3g), and $NaHCO_3$ (0.2g) was added to a 100 ml Radleys Reactor-Ready™ Duo Lab Reactor as available at the Laboratory for Chemical Technology (LCT). The solution was degassed for 1 hour by bubbling nitrogen gas through the mixture while stirring at 350 rpm (IKA Eurostar 60). Afterwards, the reactor content was heated to 70°C

(Huber Unistat 450). Temperature control was possible through *in situ* measurements via a thermocouple inserted in the reactor. When the desired polymerization temperature was reached, an aqueous KPS solution (4.6g, 35g/L, degassed with nitrogen) was injected, marking the onset of the polymerization process. Samples (1.5mL) were withdrawn from the reactor at predefined reaction times and polymerization in the samples was halted by the addition of a few drops of an aqueous hydroquinone solution (1m%).

6.2.4 Extension toward polystyrene-block-poly(n-butyl acrylate) core-shell nanoparticles

Polystyrene-block-poly(*n*-butyl acrylate) core-shell nanoparticles were prepared via a two-step procedure. In the first step, a polystyrene latex was prepared as follows. A mixture of styrene (12.4g), H_2O (37.1g), SDS (0.2g), OEXEP (0.3g), and $NaHCO_3$ ($6.6\ 10^{-3}$g) was added to a 100 ml 3-neck flask, containing a magnetic stirrer bar and equipped with a Dimroth condenser and thermocouple. The solution was degassed for 1 hour by bubbling argon gas through the mixture while stirring at 350 rpm. Afterwards, the flask was immersed in a preheated oil bath at 70°C and constantly stirred at 350 rpm. When the desired polymerization temperature was reached, an aqueous KPS solution (1.0g, 8g/L, individually degassed with argon) was injected, marking the onset of the polymerization process. Samples (1.5 mL) were withdrawn from the reactor at predefined reaction times and polymerization in the samples was halted by the addition of a few drops of an aqueous hydroquinone solution (1wt%). In the second step, the latex prepared in the first step (22.0g), *n*BuA (3.7g), H_2O (16.7g), SDS ($1.5\ 10^{-1}$g) and $NaHCO_3$ ($1.0\ 10^{-2}$g) were mixed in a 100 ml 3-neck flask and stirred (350 rpm) overnight in an ice bath. Subsequently, a Dimroth condenser and thermocouple were added to the flask which was then heated to 70°C in a preheated oil bath. When the desired polymerization temperature was reached, an aqueous KPS solution (2.0g, 2.5g/L, degassed with argon) was injected, marking the onset of the polymerization process and subsequently fresh *n*BuA (degassed with argon) was added via a

syringe pump (0.04ml/min). Samples (1.5mL) were again withdrawn from the reactor similarly as in the first step of the procedure.

6.2.5 Analytical techniques

Monomer conversion (X_m) was measured via gravimetry. The efficiency of the OEXEP synthesis (molar purity: 97±1%) was determined by means of proton nuclear magnetic resonance (^{1}H NMR) using a Bruker Avance II spectrometer equipped with a Broadband Observe (BBO) probe at 400 MHz and ambient temperature with $CDCl_3$ as solvent. Number/mass average molar mass ($M_{n/m}$) and dispersity ($Đ$) were measured via SEC, injecting dried polymer samples dissolved in THF. A PL-GPC50 plus instrument equipped with a PL-AS RT auto sampler and a refractive index (RI) detector, one Resipore 50 x 7.5 mm guard column and two Resipore 300 X 7.5 mm columns in series were used. The flow rate was 1 mL min^{-1} and the analysis temperature was 30 °C. Calibration for homopolymerization and chain extension was performed with narrow polystyrene standards (Medium EasiVials kit, Agilent Technologies), ranging from 1.62 x 10^2 to 4.83 x 10^5 g mol^{-1}. Data acquisition and processing were performed using the PL Cirrus GPC/SEC software. The size of the latex particles was measured via dynamic light scattering (DLS) using a Zetasizer Nano ZS (Malvern Instruments) after dilution in a 0.9 wt% NaCl solution. HPLC was used to determine the analyte concentrations needed for the determination of the partitioning coefficients using a Zorbax Eclipse XDB-C18 column and a 50/50 (v/v) mixture of acetonitrile and water with an aqueous solution of 0.1% (v/v) trifluoroacetic acid. Detection was achieved using a UV-VIS detector at 280 nm and 30°C.

6.3 Results and Discussion

6.3.1 Relevance of partitioning

The initial conditions of a macroemulsion polymerization are inherently more complex than for their bulk or solution counterpart. The heterogeneous nature results in a distribution of the

reaction species over an organic and aqueous phase and proper knowledge of this distribution is required to fully understand the kinetic events during the polymerization. This knowledge can be achieved by means of the partitioning coefficient (Γ), which is defined as the ratio of the equilibrium concentration of the compound in the organic phase to its equilibrium concentration in the aqueous phase. During a macroemulsion RAFT polymerization, it is important that the controlling agent is mainly present in the organic phase, ultimately the particles. Polymerization occurs almost exclusively in the particles and hence dormant macrospecies can only be formed if the RAFT agent is present there and transported from the droplets to the particles.[22,38]

Figure 6.2a shows the concentration of OEXEP, the RAFT agent considered in this work, in the organic (styrene) phase as a function of the concentration in the aqueous phase (absence of polymerization). Consequently, Γ_{OEXEP} can be obtained by determining the slope of the resulting curve. In this case, Γ is very high ($2\ 10^3$) which implies that indeed the majority of the RAFT agent is initially stored in the organic (styrene) phase as required.[52,53] Hence, even though OEXEP, a xanthate type of RAFT agent, can be considered to be surface active, it will still prefer the styrene phase over the aqueous phase. Nevertheless, it can still be expected that the surface activity will aid the transfer from the droplets to the particles.

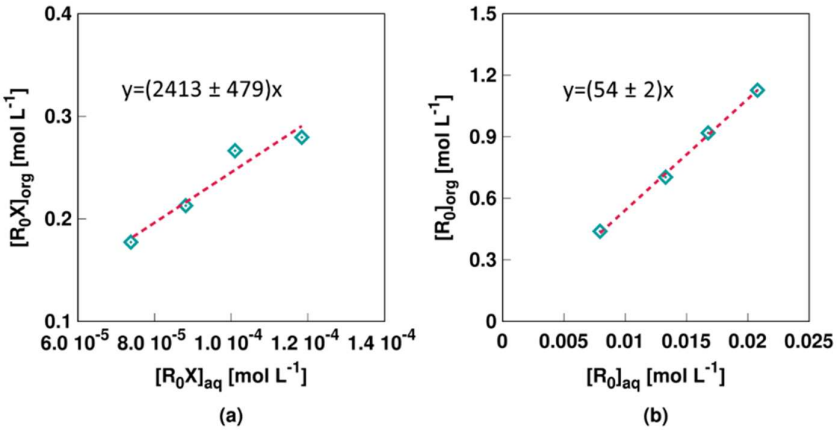

Figure 6.2: *Results of the partitioning experiments showing the equilibrium concentration of the initial RAFT agent OEXEP (R_0X, a) and ethyl propionate mimicking the RAFT leaving group radical (R_0, b) in the organic (styrene) phase as a function of the equilibrium concentration in the aqueous phase. The partitioning coefficients can be determined by the slope of the resulting curves.*

Moreover, the partitioning coefficient is also related to the entry and exit rate coefficients of the concerned species. For example, for the RAFT leaving group radical R_0 which can be mimicked by ethyl propionate, the neutral form of the RAFT leaving group radical, Γ_{R0} can be written as:

$$\Gamma_{R0} = \frac{[R_{0,org}]}{[R_{0,aq}]} = \frac{k_{entry,R_0}}{k_{exit,R_0} v_p N_A} \qquad (1)$$

with $k_{entry,R0}$ the entry rate coefficient (L mol^{-1} s^{-1}) of R_0, $k_{exit,R0}$ the exit rate coefficient (s^{-1}) of R_0, v_p the particle volume and N_A the Avogadro(242 constant.

As shown in Figure 6.2b, Γ_{R0} can be determined as 5 10^1 which means that R_0 still prefers the organic phase over the aqueous phase although to a lesser extent than R_0X. Even though Γ_{R0} by itself is only a thermodynamic quantity pertaining to an equilibrium state, *i.e.* it is related to the ratio of two rate coefficients, the relatively low value (at least compared to R_0X) does indicate a significant amount of exit of R_0 could possibly occur, especially considering that these species are formed close to the particle boundary due to the surface activity of R_0X.

6.3.2 Relevance of reaction conditions for core synthesis

Figure 6.3 shows the influence of the initial amount of KPS, the conventional initiator, on the polymer properties. A first general observation that can be made is that no control over chain growth and a high dispersity product is obtained. As explained in Chapter 3, this is typical for the RAFT polymerization of styrene mediated by a xanthate type of RAFT agent. Nonetheless, increasing the amount of initiator results in an increase of the polymerization rate (Figure 6.3a) as more primary radicals are generated. As explained in Chapter 3, investigating RAFT polymerization in bulk considering the same (OEXEP) RAFT agent, dormant chains are formed after a single RAFT exchange and the formation of these species can be compared to chain transfer with a conventional chain transfer agent, resulting in a constant (average) chain length throughout the polymerization (Figure 6.3b). Nevertheless, increasing the amount of KPS results in a decrease of the number average molar mass (Figure 6.3b). This can be explained by considering the analytical approximation for the instantaneous number average molar mass assuming a zero-one system:[27]

$$M_{n,inst} = \frac{k_p[M_p](MM_{mon})}{k_{tr,0}[R_0X_p] + \rho} \quad (2)$$

with k_p the propagation rate coefficient, $k_{tr,0}$ the (degenerative) rate coefficient for transfer with the initial RAFT agent, $[M_p]$ the monomer concentration in the particles, $[R_0X_p]$ the concentration of the RAFT agent in the particles, MM_{mon} the molar mass of styrene and ρ the (overall) radical entry rate. Note that considering the work of Chapter 4/5 and the relative small particle sizes (Figure 6.3d), the zero-one approximation is reasonable.

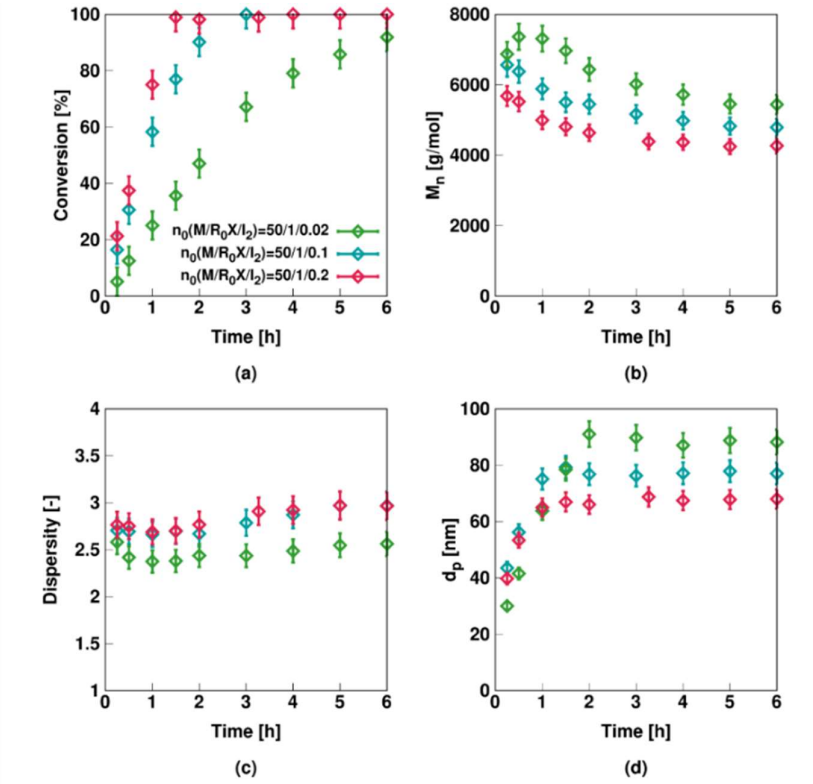

***Figure 6.3**: Influence of the initial amount of KPS (I_2) on the monomer conversion (a), the number average molar mass (b), the dispersity (c) and the average particle size (d_p) as a function of time for the isothermal macroemulsion RAFT polymerization of styrene at 70°C mediated by OEXEP. Green: n_0(Sty)/n_0(OEXEP)/n_0(KPS) = 50/1/0.02, blue: n_0(Sty)/n_0(OEXEP)/n_0(KPS) = 50/1/0.1, red: n_0(Sty)/n_0(OEXEP)/n_0(KPS) = 50/1/0.2. $[SDS]_0$ = 5 x CMC; 70/30 (w/w) H_2O/Sty; CMC=8.18 10^{-3} mol L^{-1}=2.36g L^{-1} at 25°C.*

As a result, increasing the amount of KPS will increase the radical entry rate (and the subsequent (instantaneous) termination rate) which results in a decrease of the number average molar mass. Importantly, the extent of the effect of the amount of KPS on the number average mass is directly correlated with the (initial) RAFT agent concentration in the particles. If this concentration is high, the amount of KPS will have a low influence on the number average molar mass. Moreover, the dispersity of the polymer products in all experiments is high (>2). Theoretically, the dispersity of a polymer mixture where most of the chains are formed by a transfer event is equal to 2. The slightly larger values presented in this work can at least partially

be explained by the changing conditions (concentrations and viscosity) throughout the polymerization process and the difficulties determining the dispersity for broad CLDs obtained via macroemulsion polymerization. Finally, increasing the amount of KPS will slightly decrease the average particle size d_p (Figure 6.3d). In principle, an increase of the initiator concentration will result in more particles being nucleated and hence smaller particles. However, for the experiments in Figure 6.3, the duration of interval 1 (see Chapter 1), where nucleation occurs, is very small leading to a limited effect on d_p.

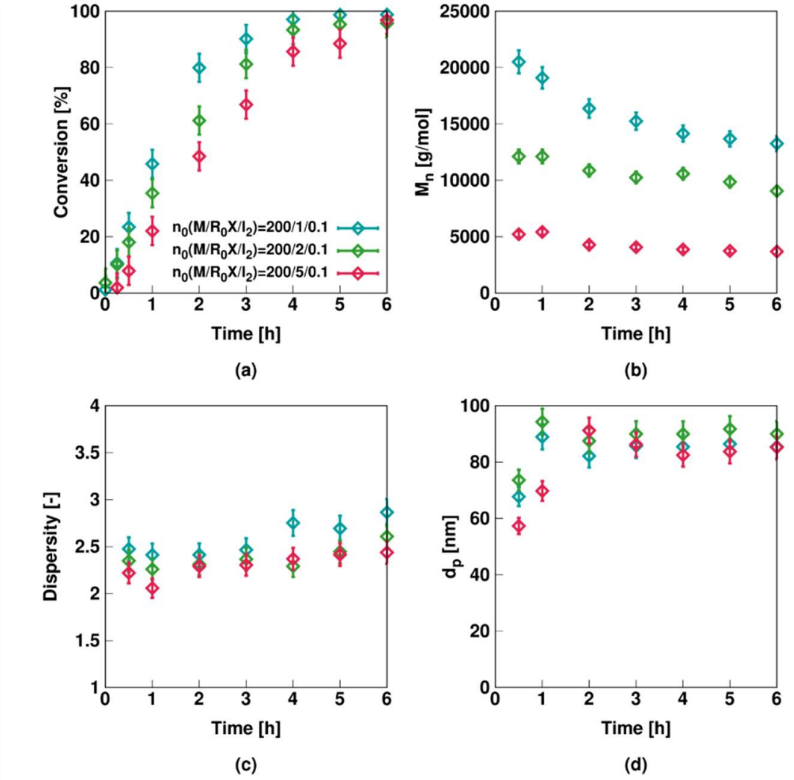

***Figure 6.4**: Influence of the initial amount of OEXEP (R_0X) on the monomer conversion (a), the number average molar mass (b), the dispersity (c) and the average particle size (d_p) as a function of time for the RAFT macroemulsion polymerization of styrene at 70°C initiated by KPS. blue: n_0(Sty)/n_0(OEXEP)/n_0(KPS) = 200/1/0.1, green: n_0(Sty)/n_0(OEXEP)/n_0(KPS) = 200/2/0.1, red: n_0(Sty)/n_0(OEXEP)/n_0(KPS) = 200/5/0.1. $[SDS]_0$ = 5 x CMC; 70/30 (w/w) H_2O/Sty; CMC=8.18 10^{-3} mol L^{-1}=2.36g L^{-1} at 25°C.*

As shown in Figure 6.4a, the polymerization rate can also be increased by decreasing the initial amount of OEXEP. As xanthates are characterized by high fragmentation rate coefficients,[6] the observed influence of the rate by the amount of R_0X cannot be explained by a slow fragmentation or RAFT cross termination effect (see Chapter 5). Considering the partitioning results explained above, a more suitable explanation is the possible exit of R_0 which can, after subsequent re-entry, result in an increase of the termination rate. Furthermore, considering the low transfer rate coefficients of xanthates in combination with styrene (see Chapter 3), this retardation effect will be present throughout the entire polymerization process. However, similar to the results in bulk polymerization (see Chapter 3), even though no control over chain growth is obtained, the initial amount of R_0X can be used to control the number average chain length as shown in Figure 6.4b. Again, high dispersity (>2) product is obtained regardless of the amount of OEXEP. Finally, increasing the amount of OEXEP results in an almost negligible decrease of the average particle size (Figure 6.4d). Similar to the explanation for KPS, the short duration of interval 1 (see Chapter 1) does not allow the exit and subsequent reentry of R_0 radicals to have a very significant effect on the total number of particles.

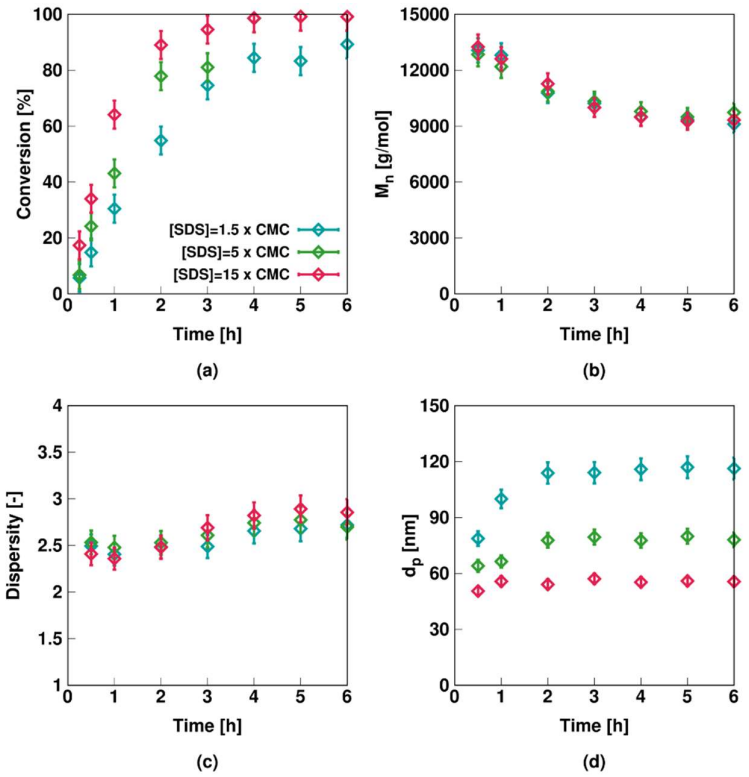

***Figure 6.5**: Influence of the SDS (surfactant) concentration on the monomer conversion (a), the number average molar mass (b), the dispersity (c) and the average particle size (d_p) as a function of time for the RAFT macroemulsion polymerization of styrene at 70°C initiated by KPS and mediated by OEXEP. n_0(Sty)/n_0(OEXEP)/n_0(KPS) = 100/1/0.1, blue: $[SDS]_0$ = 1.5 x CMC, green = 5 x CMC, red = 15 x CMC; 70/30 (w/w) H_2O/Sty; CMC=8.18 10^{-3} mol L^{-1}=2.36g L^{-1} at 25°C).*

Figure 6.5 shows the influence of the amount of surfactant (SDS) on the polymer and process properties. Increasing the surfactant concentration results in an increase of the polymerization rate (Figure 6.5a) and a decrease of the average particle size (Figure 6.5d) as the total number of particles that can be stabilized increases. Consequently, increasing the amount of surfactant can be an easy approach to increase the polymerization rate and decrease the particle size without altering the number average molar mass (Figure 6.5b) and dispersity (Figure 6.5c) t as these are predominantly determined by the amount of monomer and R_0X. However, an

important note is that too high amounts of surfactant can have a detrimental effect on application properties such as for example film formation.[27]

6.3.3 Extension to core-shell synthesis

Although, as expected, "RDRP control" over chain growth could not be achieved, the real strength of the use of xanthates during a RAFT macroemulsion polymerization is the possibility to prepare block copolymers possibly resulting in core shell nanoparticles. In order to investigate this approach, a homopolymerization of styrene (similar to the experiments mentioned in Figure 6.3-5) was performed and a subsequent chain extension with *n*-butyl acrylate employing a semi batch operation was realized of which the results are shown in Figure 6.6. During the polymerization of styrene, ultimately forming the core part of the particles, an approximately constant number average chain length and dispersity was again obtained. However, during the chain extension with *n*-butyl acrylate, ultimately making up the shell part, a linear growth of the chain length and a decrease of the dispersity can be observed. Moreover, as shown in Figure 6.6d, the CLD of the styrene core product is shifted to the right at the end of the shell formation. These results indicate the formation of block copolymers, as the formation of a majority of *n*-butyl acrylate homopolymers would result in a bimodal CLD characterized by a large (>>2) dispersity.

Furthermore, during the second step, the average particle size increases with reaction time indicating that the particles formed during the first stage continue to grow. Taking into account that a semi-batch operation is used and *n*-butyl acrylate is thus not allowed to enter the bulk of the particles, and the RAFT agent is considered to be surface active, it can be expected that indeed covalently linked core-shell nanoparticles consisting of polystyrene-block-poly(n-butyl acrylate) are formed. Unequivocal validation of the core-shell hypothesis can only be obtained by dedicated experimental (*e.g.* TEM) characterization methods which was outside the scope of this chapter. The experimental homopolymerization results discussed in this work can

provide a preliminary idea of the underlying micro- (polymerization kinetics) and mesoscale phenomena (mass transfer; nucleation and growth). However, a complete understanding of the complex heterogeneous RAFT macroemulsion polymerization mechanism can only be achieved by a modelling approach similar to the work discussed in Chapters 4-5, as will be developed in future studies.

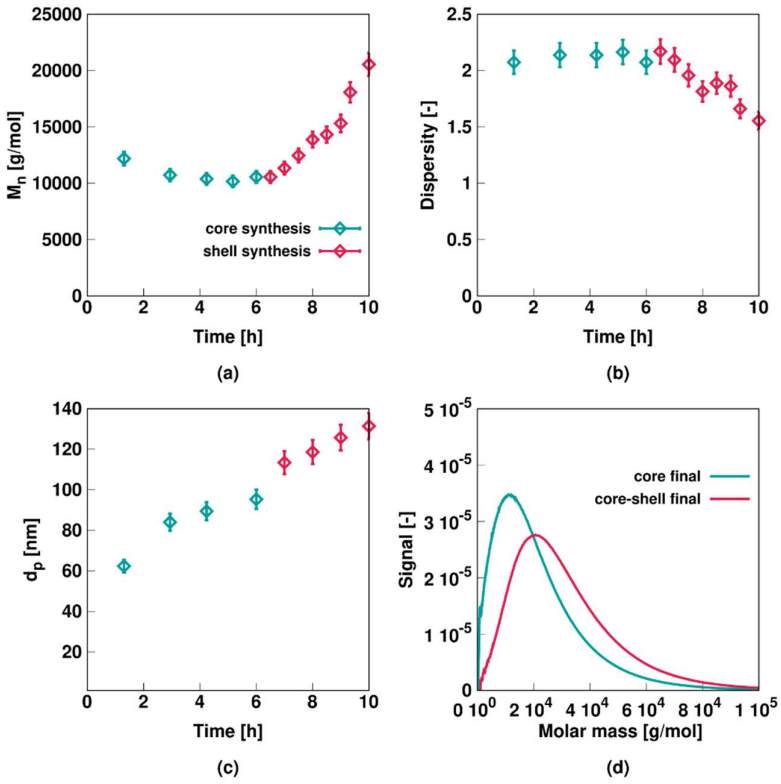

***Figure 6.6**: Number average molar mass (a), dispersity (b) and average particle size (c) as a function of time for the polystyrene core synthesis (blue) and subsequent chain extension (shell formation, red) with n-butyl acrylate. Also shown is the molar mass distribution plot (d) at the end of the core synthesis (6 hours of polymerization time) and shell synthesis (10 hours of total polymerization time).*

6.4 Conclusions

An experimental kinetic study on the macroemulsion RAFT homopolymerization of styrene using xanthates as controlling agents (also known as MADIX) is performed to gain a better understanding of the process-polymer property relationship. Even though no typical RDRP

control over chain growth and high dispersity product is always obtained, the number average molar mass can be decreased by increasing the initial amount of the controlling agent or conventional initiator. Moreover, the polymerization rate can be increased by increasing the amount of initiator or surfactant or by decreasing the amount of controlling agent. Additionally, the average particle size can be increased slightly by decreasing the amount of initiator or controlling agent but can be better controlled by the amount of surfactant. Finally, it could be shown that the obtained polystyrene latex can be extended to create polystyrene-block-poly(*n*-butyl acrylate) polymer particles which will most likely be organized forming a core-shell structure. These results already give a preliminary idea of the underlying of both micro- and mesoscale phenomena. However, a complete understanding can only be achieved by further development of the models discussed in Chapter 4-5, as will be executed in the future at LCT.

6.5 References:

1 S. W. Prescott, M. J. Ballard, E. Rizzardo and R. G. Gilbert, *Aust. J. Chem.*, 2002, **55**, 415.

2 J. M. Asua, *Polymer Reaction Engineering*, Blackwel Publishing Ltd, Oxford, 2007.

3 R. G. Gilbert, *Emulsion polymerization: a mechanistic approach*, Academic Press Inc., London, 1995.

4 N. Yeole, D. Hundiwale and T. Jana, *J. Colloid Interface Sci.*, 2011, **354**, 506–510.

5 F. Joseph Schork and J. Guo, *Macromol. React. Eng.*, 2008, **2**, 287–303.

6 I. S. Altarawneh, V. G. Gomes and M. S. Srour, *Macromol. React. Eng.*, 2008, **2**, 58–79.

7 Y. Dong and D. C. Sundberg, *Macromolecules*, 2002, **35**, 8185–8190.

8 B. C. Chamberlain, D. H. Napper and R. G. Gilbert, *J. Chem. Soc. Faraday Trans. II*, 1982, **78**, 59.

9 F. J. Schork, Y. Luo, W. Smulders, J. P. Russum, A. Butté and K. Fontenot, *Adv. Polym. Sci.*, 2005, **175**, 129–255.

10 P. B. Zetterlund, Y. Kagawa and M. Okubo, *Chem. Rev.*, 2008, **108**, 3747–94.

11 B.-G. Li and W.-J. Wang, *Macromol. React. Eng.*, 2015, **9**, 385–395.

12 H. Tobita, *Macromol. Symp.*, 2008, **261**, 36–45.

13 P. B. Zetterlund, S. C. Thickett, S. Perrier, E. Bourgeat-Lami and M. Lansalot, *Chem. Rev.*, 2015, **115**, 9745–9800.

14 J. Qiu, B. Charleux and K. Matyjaszewski, *Prog. Polym. Sci.*, 2001, **26**, 2083–2134.

15 I. W. Hamley, *Developments in block copolymer science and technology*, John Wiley & Sons, Chichester, 2004.

16 M. Destarac, *Macromol. React. Eng.*, 2010, **4**, 165–179.

17 G. Odian, *Principles of Polymerization*, John Wiley & Sons, New York, 2004.

18 G. Moad and D. H. Solomon, *The chemistry of radical polymerization*, Elsevier, Oxford, 2006.

19 G. T. Russell, *Aust. J. Chem.*, 2002, **55**, 399–414.

20 W. Smulders, R. G. Gilbert and M. J. Monteiro, *Macromolecules*, 2003, **36**, 4309–4318.

21 S. Perrier, *Macromolecules*, 2017, **50**, 7433–7447.

22 C. Barner-Kowollik, *Handbook of RAFT Polymerization*, Wiley-VCH, Weinheim, 2008.

23 S. Perrier and P. Takolpuckdee, *J. Polym. Sci. Part A Polym. Chem.*, 2005, **43**, 5347–5393.

24 M. R. Hill, R. N. Carmean and B. S. Sumerlin, *Macromolecules*, 2015, **48**, 5459–5469.

25 J. Chiefari, Y. K. B. Chong, F. Ercole, J. Krstina, J. Jeffery, T. P. T. Le, R. T. A. Mayadunne, G. F. Meijs, C. L. Moad, G. Moad, E. Rizzardo, S. H. Thang and C. South, 1998, **31**, 5559–5562.

26 G. Moad, J. Chiefari, Y. K. Chong, J. Krstina, R. T. a Mayadunne, A. Postma, E. Rizzardo and S. H. Thang, *Polym. Int.*, 2000, **49**, 993–1001.

27 M. J. Monteiro and J. De Barbeyrac, *Macromolecules*, 2001, **34**, 4416–4423.

28 M. J. Monteiro, M. Sjöberg, J. Van Der Vlist and C. M. Göttgens, *J. Polym. Sci. Part A Polym. Chem.*, 2000, **38**, 4206–4217.

29 I. Uzulina, S. Kanagasabapathy and J. Claverie, *Macromol. Symp.*, 2000, **150**, 33–38.

30 D. Charmot, P. Corpart, H. Adam, S. Z. Zard, T. Biadatti and G. Bouhadir, *Macromol. Symp.*, 2000, **150**, 23–32.

31 M. J. Monteiro, M. Hodgson and H. De Brouwer, *J. Polym. Sci. Part A Polym. Chem.*, 2000, **38**, 3864–3874.

32 S. W. Prescott, University of Sydney, 2003.

33 M. J. Monteiro, *Macromolecules*, 2010, **43**, 1159–1168.

34 C. N. Urbani, H. N. Nguyen and M. J. Monteiro, *Aust. J. Chem.*, 2006, **59**, 728–732.

35 M. J. Monteiro, M. M. Adamy, B. J. Leeuwen, A. M. van Herk and M. Destarac, *Polym. Prepr.*, 2005, **46**, 353–354.

36 J. G. Tsavalas, F. J. Schork, H. De Brouwer and M. J. Monteiro, *Macromolecules*, 2001, **34**, 3938–3946.

37 J. J. Vosloo, M. P. Tonge and R. D. Sanderson, *Macromolecules*, 2002, **35**, 4894–4902.

38 M. P. F. Pepels, C. I. Holdsworth, S. Pascual and M. J. Monteiro, *Macromolecules*, 2010, **43**, 7565–7576.

39 M. M. Adamy, A. M. van Herk, M. Destarac and M. J. Monteiro, *Macromolecules*, 2003, **36**, 2293–2301.

40 S. W. Prescott, M. J. Ballard, E. Rizzardo and R. G. Gilbert, *Macromol. Theory Simulations*, 2006, **15**, 70–86.

41 W. Smulders and M. J. Monteiro, *Macromolecules*, 2004, **37**, 4474–4483.

42 M. J. Monteiro and J. De Barbeyrac, *Macromol. Rapid Commun.*, 2002, **23**, 370–374.

43 S. Pascual, C. N. Urbani and M. J. Monteiro, *Macromol. React. Eng.*, 2010, **4**, 257–263.

44 L. Seiler, J. Loiseau, F. F. Leising, P. Boustingorry, S. Harrisson and M. Destarac, *Polym. Chem.*, 2017, **8**, 3825–3832.

45 I. S. Altarawneh, V. G. Gomes and M. H. Srour, *Macromol. React. Eng.*, 2012, **6**, 8–16.

46 I. S. Altarawneh, V. G. Gomes and M. H. Srour, *J. Appl. Polym. Sci.*, 2009, **114**, 2356–2372.

47 I. S. Altarawneh, V. G. Gomes and M. H. Srour, *Polym. Int.*, 2009, **58**, 1427–1434.

48 M. J. Monteiro, M. M. Adamy, B. J. Leeuwen, A. M. Van Herk and M. Destarac, *Macromolecules*, 2005, **38**, 1538–1541.

49 Y. Zhu, X. Gao and Y. Luo, *J. Appl. Polym. Sci.*, 2016, **133**, 1–11.

50 S. M. Jung and V. G. Gomes, , DOI:10.1080/03602559.2013.763358.

51 WO 1998058974, 1998.

52 L. Bentein, D. R. D'hooge, M.-F. Reyniers and G. B. Marin, *Polymer (Guildf).*, 2012, **53**, 681–693.

53 J. W. Ma, M. F. Cunningham, K. B. McAuley, B. Keoshkerian and M. K. Georges, *J. Polym. Sci. Part A Polym. Chem.*, 2001, **39**, 1081–1089.

Chapter 7: General conclusions and future outlook

7.1 General conclusions

In this PhD thesis, a combination of kinetic modeling and experimental work is applied to gain fundamental understanding of the mechanism of reversible addition-fragmentation chain transfer (RAFT) polymerization applying both bulk and (mini)emulsion techniques. On the one hand, the modeling approach relies on the essential determination of accurate RAFT polymerization specific rate coefficients, including the proper description of diffusional limitations, while taking into account all relevant kinetic events, hence minimizing the integrated approximations. On the other hand, dedicated experimental data is needed to validate the obtained modeling results and relies on the purposeful choice of experimental conditions, which can be tuned by preliminary model screening, and characterization techniques. The work has already resulted - at this stage - in 2 published contributions and 1 submitted contribution in respected journals in the polymer science field. It has also been disseminated at several national and international conferences.

In **Chapter 1**, a brief introduction is given to free radical polymerization (FRP) and reversible deactivation radical polymerization (RDRP) techniques, with focus mainly on RAFT polymerization. The different emulsion polymerization techniques are stated alongside both the advantages and challenges of employing these techniques in combination with RAFT polymerization. This chapter is used to provide a general explanation of the chemical methods on which the other chapters rely on.

Chapter 2 allows to provide an introduction to the modelling of polymerization kinetics using computer simulation methods. Firstly, the two major computational polymerization modeling methods, deterministic and stochastic methods, are discussed. In deterministic modeling, a set of differential equations is integrated which often demands to reduce the number of equations

for computational purposes, for example via the method of moments approach, even though this results in a loss of molecular information about individual chains. Alternatively, stochastic modeling, e.g. kinetic Monte Carlo, considers each reaction as a random event chosen based on its probability and stores the entire reaction event history, making it possible to obtain in detail the polymer structure, e.g. comonomer sequences. For complex reaction schemes, this can require a high computational cost. Secondly, an overview of the state-of-the art of kinetic modeling of RAFT bulk/solution and emulsion polymerization is given. The multi-phase character of RAFT emulsion polymerization requires a more complex mathematical description compared to the bulk countercase. Mostly the deterministic modeling approach using Smith-Ewart differential equations is used to describe the evolution of the particle type distribution. In view of Chapter 4 and 5, these Smith-Ewart equations are elaborated considering a simplified FRP miniemulsion scheme. Established analytical equations for certain limiting cases are used to validate the investigated modeling approach.

In **Chapter 3**, the degenerative transfer coefficients for the RAFT polymerization of styrene commenced with (O-ethyl xanthate)-2-ethyl propionate, a xanthate type of RAFT agent, are determined by applying a multi-responsive regression analysis. The validity of the degenerative mechanism has been confirmed. The coefficients are obtained based on the extended method of moments deterministic modeling technique and experimental data on RAFT agent and styrene conversion, number and mass average molar mass, and end-group functionality (EGF). Notably, this latter property is obtained by a combination of dialysis to remove unreacted RAFT agent and elemental analysis. Furthermore, both the homopolymerization and its chain extension with fresh styrene or *n*-butyl acrylate is visualized *in silico*, applying a kinetic Monte Carlo modeling approach. It is highlighted that the xanthate type of RAFT agent results in a low RAFT reactivity ($C_{tr(,0)} < 1$) due to the presence of a delocalizable oxygen electron pair in α-position to the thiocarbonylthio functional group, decreasing the S=C double bound

character. Consequently, both "blocks" of the chain extension are formed through a unconventional single exchange, which implies a transfer behavior as in conventional FRP. It should be stressed that this insight is only possible by the joint experimental and modeling approach followed in this PhD thesis.

In **Chapter 4**, attention is shifted towards RAFT miniemulsion polymerization. More specifically, the RAFT miniemulsion polymerization of methyl methacrylate with cyanoprop-2-yl dithiobenzoate as initial RAFT agent is studied considering a literature-based degenerative RAFT mechanism and a two-dimensional Smith-Ewart model which accounts for the number of macro- and leaving group radicals per nanoparticle. Firstly however, bulk literature data is used to validate the accuracy of the rate coefficients and the description of the micro-scale diffusional limitations on termination and RAFT transfer. Consequently, miniemulsion literature data have been used to determine the exit and entry rate coefficients concerning the RAFT leaving group radical. These meso-scale consecutive entry/exit events result in a retardation effect as long as RAFT agent is present. Moreover, it is demonstrated that it is not afforded to assume zero-one kinetics, as often done in previous studies, as instantaneous termination cannot be established at high monomer conversion as the reaction mixture becomes to viscous. Additionally, at high average chain length, the diffusional limitations on RAFT transfer become relevant as well which leads to a significant fraction of nanoparticles containing several (macro)radicals. Finally, the developed model is used to identify the optimal average particle size in view of design of the polymerization rate and control over the average polymer properties. Note that again the combination of experimental and modeling work allowed to achieve these new kinetic insights.

In **Chapter 5**, the kinetic model of the previous chapter is extended to a 5-dimensonal Smith-Ewart based model. This allows the comparison of the degenerative and non-degenerative RAFT miniemulsion polymerization reaction scheme as the three possible intermediate radical

species (R_0XR_0, R_iXR_0 and R_iXR_j) are accounted for as well. Styrene was chosen as monomer and the consideration of a macro-RAFT agent allows to avoid the complexities related to exit/entry of the RAFT leaving group radical. It is shown that with a too low RAFT fragmentation rate coefficient it is generally not afforded to consider zero-one kinetics and that with significant RAFT cross-termination the dead polymer product is dominantly originating from the RAFT intermediate radical. Moreover, a degenerative description of the RAFT mechanism is only allowed if slow fragmentation or cross-termination effects are insignificant, hence under the conditions of an ideal RAFT agent. Nonetheless, the possibility to describe the non-degenerative RAFT miniemulsion polymerization scheme allows the identification of the nature of the RAFT retardation as the impact of the average particle size on both the monomer conversion profile, dispersity and EGF is significantly different making it possible to differentiate the slow-fragmentation from the cross-termination hypothesis. Additionally, comparison with the FRP conversion profile is still recommended to highlight whether an ideal RAFT agent can be claimed.

In **Chapter 6**, an experimental study of RAFT macroemulsion polymerization of styrene with (O-ethyl xanthate)-2-ethyl propionate, the same controlling agent as used in Chapter 2, is discussed. Similar as during bulk polymerization, this xanthate type of RAFT agent does not result in control over chain growth, leading to a high dispersity polymer product. Nevertheless, the concentration of the controlling agent can be used to alter the desired number average molar mass whereas the polymerization rate can be increased by increasing the amount of initiator or surfactant or by decreasing the amount of controlling agent. Furthermore, the surfactant concentration can be used to control the average particle size as well. Importantly, the main advantage of the use of a xanthate type of RAFT agent is related to its surface activity. It is shown that the obtained polystyrene latex can be extended via semi-batch operation to create polystyrene-block-poly(n-butyl acrylate) polymer particles which will most likely be organized

forming a core-shell structure. These results can be considered to be a stepping stone for future extension of the model discussed in Chapter 4 and 5 in order to include macroemulsion polymerization, which is more industrially relevant compared to miniemulsion polymerization.

7.2 Future outlook

The work performed in this thesis has the goal to develop computer based models capable of describing and designing sophisticated polymer synthesis procedures through both bulk and emulsion RAFT polymerization. The model is fully developed for bulk processes. At this moment, the model can also be fully used to investigate and optimize RAFT miniemulsion polymerization mechanisms. However, in terms of industrial relevance, (RAFT) macroemulsion polymerization is more interesting as the polymerization procedure is more straightforward, even though the mechanism itself is more complex. Consequently, the model developed in Chapters 4 and 5 need to be extended towards this objective. An essential step would be the incorporation of RAFT seeded macroemulsion polymerization. The seed latex defines the number of particles, making it still unnecessary to account for the micelle-particle transition. Nonetheless, opposite to miniemulsion polymerization where the obtained average particle size is roughly equal to average initial droplet size, modeling of macroemulsion polymerization will demand the need to define the particle growth mechanism.

Importantly, as discussed in this work, xanthates are one of the most interesting classes of RAFT agents to employ in this heterogeneous polymerization technique as it typically results in colloidal stability. However, its surface activity will result in a concentration gradient in the particles as these molecules will prefer the vicinity of the particle-water interface over the bulk of the particle. Consequently, (at least) two individual volumes in the (average) particle will need to be considered, linked via transfer processes between them. Individual balances for the micelles, surfactant molecules and particles should allow the transition towards *ab initio* macro-emulsion polymerization.

Furthermore, if RAFT macroemulsion homopolymerization is completely incorporated, the following update should be the development of a model capable of describing the core-shell copolymer synthesis. At this stage only lab scale modeling has been developed where each phase, *e.g.* the aqueous phase, can be described by a single average concentration for each species. However, on an industrial (or pilot) scale, concentration and temperature gradients will be present. In order to account for these, at least macro-scale reactor segments will be required with again transfer coefficients describing the movement of species from one segment to another. Importantly, the computational effort needed to solve the set of equations will increase with increasing model complexity. Consequently, management of the computational efficiency will be crucial in future model extension.

The work performed in this PhD thesis has been a successful start of a journey towards the development of industrially relevant (RAFT) macroemulsion polymerization modeling but many steps are still needed. Each step will require their own dedicated experiments for model validation and each new development step will increase the knowledge concerning the design of next-generation polymer emulsions.

Appendix A: Supporting information for Chapter 3

A.1 Overview of the experimental conditions: homopolymerization

Table A1*: Overview of the initial conditions used in the experimental study of homopolymerization MADIX of styrene at 70°C, selecting OEXEP as initial RAFT agent and AIBN as conventional initiator; 4 m% n-decane was added as internal standard for GC analysis;* $V_{Sty,0}$*=35 mL.*

Entry	$[Sty]_0$	$[Sty]_0/[OEXEP]_0$	$[OEXEP]_0/[AIBN]_0$	$[Sty]_0/[OEXEP]_0/[AIBN]_0$
1	7.56	50	30	50/1/0.033
2	7.55	50	10	50/1/0.1
3	7.53	50	5	50/1/0.2
4	7.51	40	50	40/1/0.02
5	7.68	100	20	100/1/0.05
6	7.76	200	10	200/1/0.1
7	7.67	100	10	100/1/0.1

A.2 Synthesis procedure of (O-ethyl xanthate)-2-ethyl propionate (OEXEP), the initial RAFT agent (R_0X) used in Chapter 3

OEXEP was synthesized according to the literature procedure.[1] Ethyl 2-bromopropionate (50.3 g, 0.278 mol) was dissolved in 500 mL ethanol and mixed with potassium O-ethyl dithiocarbonate (50.7 g, 0.316 mol) under argon atmosphere. The mixture was stirred for 6 hours in the absence of light at 0°C. Afterwards 500 mL water was added and the obtained OEXEP was extracted by a 1:2 (v:v) mixture of diethyl ether and pentane. The solvent and residual ethyl 2-bromopropionate were removed by evaporation under vacuum. Upon analysis (see Section A3 of Appendix A) a product molar purity of 97±1% was obtained.

A.3 Determination of purity of (O-ethyl xanthate)-2- ethyl propionate (OEXEP)

The purity of OEXEP, synthesized according to the procedure mentioned in the Section A2, has been determined by means of ^{1}H NMR analysis (Figure A1 ,left) of the obtained product and following equation:

$$molar\ purity = \frac{\int D}{\int D + \int H} = \frac{3.00}{3.00 + 0.08} = 0.974 \qquad \text{(A1)}$$

Ethyl 2-bromopropionate can be identified as main impurity and no other significant impurities or side products could be detected, as confirmed by GC analysis (Figure A1 ,right).

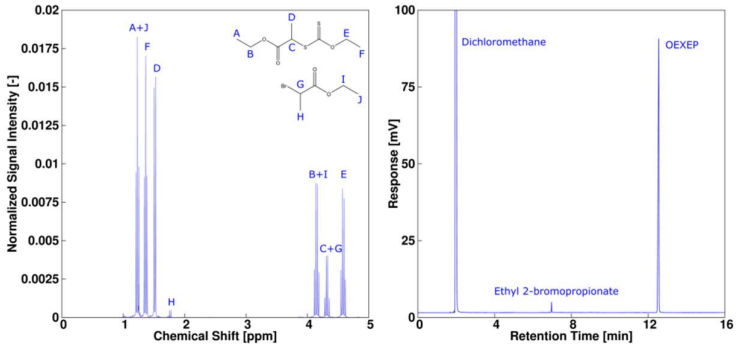

***Figure A1**: ^{1}H NMR (left) and GC (right) analysis of the synthesized OEXEP used as initial RAFT agent in the present work*

A.4 Overview of the experimental conditions: chain extension with styrene

***Table A2**: Overview of the initial conditions used in the experimental study of MADIX chain extension with styrene at 70°C; the initial polystyrene was obtained by purifying the product of Entry 3 in Table A1 after 8h of reaction time; AIBN was used as conventional initiator; 4 mt% n-decane was added as internal standard for GC analysis; with $[RX]_0$ the concentration of dormant polystyrene as determined by Equation 7 of Chapter 3.*

Entry	$[Sty]_0$	$[Sty]_0/[RX]_0$	$[RX]_0/[AIBN]_0$	$[Sty]_0/[RX]_0/[AIBN]_0$
1	6.07	175	20	175/1/0.05
2	4.93	85	25	85/1/0.04
3	5.06	95	100	95/1/0.01

A.5 Justification of the Equation 7 of Chapter 3

The number average chain length x_n can be written as the ratio of the sum of the first moment of the dead, living and dormant species to the zero moment of these species:

$$x_n = \frac{\sum_{i=1}^{\infty} i([P_i] + [R_i] + [R_iX])}{\sum_{i=1}^{\infty}([P_i] + [R_i] + [R_iX])} \tag{A2}$$

As $[\mathrm{A}] = \frac{\mathrm{n_A}}{\mathrm{V}}$ with [A] the concentration of A, $\mathrm{n_A}$ the molar amount of A and V the volume:

$$x_n = \frac{\sum_{i=1}^{\infty} i \frac{1}{V}\left(n_{P_i} + n_{R_iX} + n_{R_i}\right)}{\sum_{i=1}^{\infty} \frac{1}{V}\left(n_{P_i} + n_{R_iX} + n_{R_i}\right)} \tag{A3}$$

Multiplying each side with the molar amount of all RiX species:

$$x_n \sum_{i=1}^{\infty}\left(n_{R_iX}\right) = \frac{\sum_{i=1}^{\infty} i\left(n_{P_i} + n_{R_iX} + n_{R_i}\right)}{\sum_{i=1}^{\infty}\left(n_{P_i} + n_{R_iX} + n_{R_i}\right)} \sum_{i=1}^{\infty}\left(n_{R_iX}\right) \tag{A4}$$

The amount of dormant chains can be related to the end-group functionality (EGF):

$$x_n \sum_{i=1}^{\infty}\left(n_{R_iX}\right) = \sum_{i=1}^{\infty} i\left(n_{P_i} + n_{R_iX} + n_{R_i}\right) EGF \tag{A5}$$

Rearranging and multiplying both the numerator and denominator of the right hand side with the monomer molar mass M_{sty} results in the equation of the molar amount of R_iX as mentioned in Chapter 3 (Equation 7).

$$\sum_{i=1}^{\infty}\left(n_{R_iX}\right) = \frac{M_{Sty} \sum_{i=1}^{\infty} i\left(n_{P_i} + n_{R_iX} + n_{R_i}\right)}{M_{Sty}\, x_n} EGF \tag{A6}$$

$$n_{R_iX} = \frac{m_{PS}}{M_n} EGF \tag{A7}$$

A.6 Confirmation of accuracy of conversion determination by gas chromatography

Monomer and RAFT agent conversion (X_m and X_{R0X}) were determined by means of gas chromatography (GC), as explained in Chapter 3. The accuracy of the technique can be verified by ^{1}H nuclear magnetic resonance (NMR). As shown in Figure A2, the conversion values obtained by both techniques are in excellent agreement (entry 7 in Table A1).

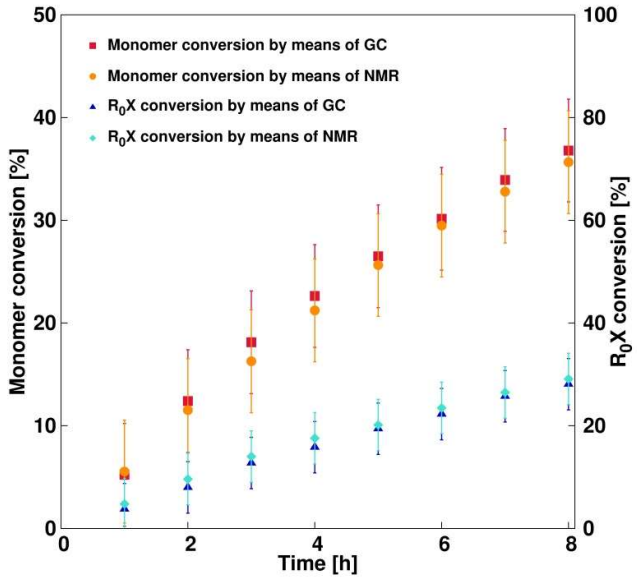

***Figure A2**: Comparison of monomer and R_0X conversion data via GC (■, red = X_m; ▲, dark blue = X_{R0X}) and NMR (●, orange = X_m; ◆, light blue = X_{R0X}) for MADIX of styrene at 70°C, selecting OEXEP as initial RAFT agent and AIBN as conventional initiator: Entry 7 in Table A1.*

A.7 Calculation of the molar amount of end-groups in a polystyrene sample, necessary for the calculation of Equation 8 of Chapter 3.

The three molar amounts in Equation (8) of Chapter 3 can be calculated from the elemental analysis results:

$$n(I) = \frac{w(N)\, m_s}{M(N)} \tag{A7}$$

$$n(X) = \frac{w(S)\, m_s}{2\, M(S)} \tag{A8}$$

$$n(R_0) = n(X) \tag{A9}$$

with $w(A)$ (A=N and S) the mass fraction of nitrogen and sulphur, m_s the mass of the elemental analysis sample, and $M(A)$ (A = N and S) the molar mass of nitrogen and sulphur. Equation (A9) assumes a negligible contribution of termination between individual R_0 species (R_0R_0 formation) and chain transfer of R_0 to monomer, which is valid in the present work as shown in Section A8 of Appendix A

A.8 Verification of the negligible contribution of termination between R_0 species and chain transfer of R_0 to monomer

The EGF values mentioned in Chapter 3 are determined by means of elemental analysis, more precisely by investigating the nitrogen and sulphur peak in the CHNS chromatogram. These two peaks allow to determine the amounts of the I and X end-groups respectively. However, the elemental analysis chromatogram does not allow the direct calculation of the amount of R_0 end-groups. Nonetheless, this can be easily overcome by assuming that the number of R_0 end-groups is equal to the number of X end-groups, as a new X end-group can only be produced by the simultaneous generation of an R_0 which will in turn initiate a new chain. However, this equality only holds up if each R_0 effectively generates a new chain and hence, does not terminate by recombination with another R_0 radical or by chain transfer to monomer.

Figure A3 depicts the rate of termination and chain transfer to monomer of R_0 radicals over the overall consumption rate of R_0 radicals (Entry 3 in Table A1, similar values for other entries of Table A1, simulation achieved by rate coefficients mentioned in Table A3). As clearly visible, the contribution of these reactions are negligible and consequently the number of R_0-end groups can be considered to be equal to the number of *X*-end groups.

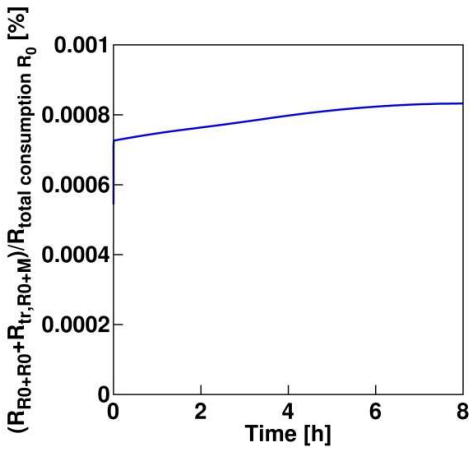

Figure A3*: The rate of termination of R_0 radicals by recombination with another R_0 radical or by chain transfer to monomer over the overall consumption rate of R_0 radicals as a function of time (h); Entry 3 in Table A1.*

A.9 Importance of end-groups obtained by chain transfer to monomer with macroradicals

The EGF values mentioned in Chapter 3 are determined by calculating the number of *X*, R_0 and *I* end groups. However, when chain transfer to monomer by macroradicals is significant, styryl and H end-groups are possible as well, complicating the EGF calculation. Nonetheless, as shown in Figure A4, under the conditions investigated in Chapter 3, these chain transfer reactions do not contribute significantly to the average polymer properties. Consequently, the EGF can be determined by solely investigating the number of *X*, R_0 and *I* end- groups.

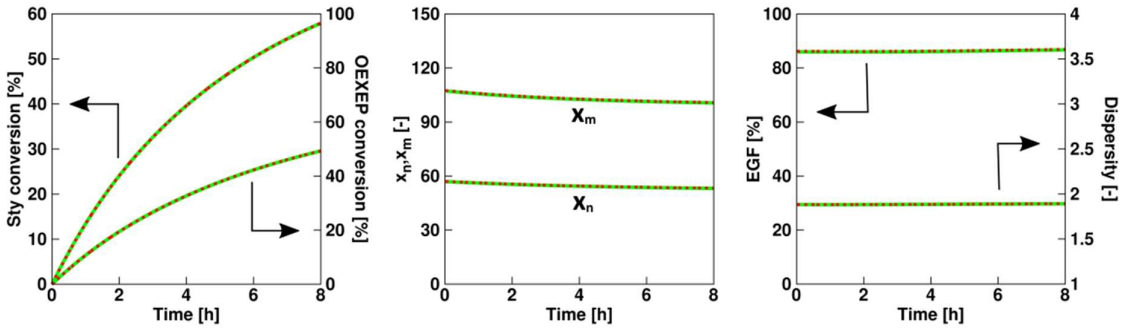

***Figure A4**: Investigation of the influence of chain transfer to monomer reactions on the monomer and R_0X conversion, number/mass average molar mass, EGF and dispersity: chain transfer to monomer taken into account: solid green line; not taken into account: dotted red line; Entry 3 in Table A1; Rate coefficients as mentioned in Table A3*

A.10 Evaluation of the need for the use of the correct reaction volume for the kinetic Monte Carlo simulations

The aforementioned extension of the *k*MC procedure enables tracking of the monomer incorporation and possible short chain branch formation for individual macrospecies of a representative polymer sample (e.g. 10^5 polymer chains). For copolymerization processes this implies knowledge of the exact location of the comonomer units along each of the different polymer chains. Specifically for block copolymer synthesis, the contribution of off-spec (homo)polymer chains can be easily detected and the individual block lengths are readily available, as illustrated previously for RDRP techniques based on the so-called persistent radical effect,[2] i.e. atom transfer radical polymerization (ATRP) and nitroxide mediated polymerization (NMP).[3] In the present work, for the first time, the microstructure of individual polymer chains for degenerative RAFT block copolymerization is visualized based on *k*MC simulations, for styrene and *n*BuA as comonomers, OEXEP as initial RAFT agent, and AIBN as conventional radical initiator. It should be stressed that in contrast to traditional ATRP and NMP processes, new (short) chains are continuously formed by I_2 decomposition and further

chain growth. This requires a very careful evaluation of the *k*MC reaction volume to be used (>> 10^5 chains) to ensure that the polymer microstructure is accurately represented.

Firstly, the volume needs to be large enough to ensure a good representation of all species present. Small volumes will result in a faulty amount of low concentration species, *e.g.* macroradicals, and consequently in an incorrect simulation of the reactions making use of these species. Secondly, although larger volumes can overcome this issue, it comes at a cost of longer simulation times. Hence, accurate and pragmatic simulation results can only be obtained by considering a proper reaction volume. Practically, this can be achieved by investigating a small reaction volume and increasing it until a convergence of the results is obtained. This guarantees appropriate results within a minimum amount of calculation time. Figure A5 shows the outcome of a kinetic Monte Carlo simulation (Entry 3 in Table A1) for three different reaction volumes. As clearly can be observed, a too small volume (~10^{-17}L; red full line) leads to erroneous results as increasing the volume (~10^{-16}L; dashed green line) results in a different outcome. Increasing the volume even more (~10^{-15}L; dashed blue line) does not result in a change of the outcome but only in a significant longer necessary simulation time (X_m=0.58).

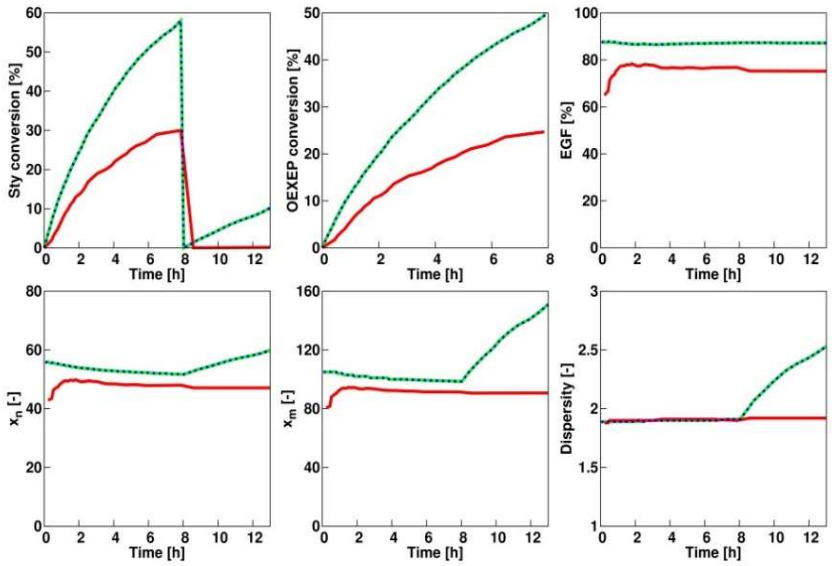

Figure A5: Influence of the reaction volume on the kinetic Monte Carlo simulation; solid red line: V=1.28 x 10-17 L; solid green line: V=1.28 x 10-16 L; dashed blue line: V=1.28 x 10-15 L; 0-8h: entry 3 in Appendix A in Table A1; 8-13h: entry 3 in Appendix A in Table A2; Reaction coefficients as mentioned in Table A3; clearly the red lines are inaccurate.

A.11 Comparison of simulated average characteristics of the extended method of moments and kinetic Monte Carlo (kMC) model

As shown below, the simulated average characteristics of both computational methods converge.

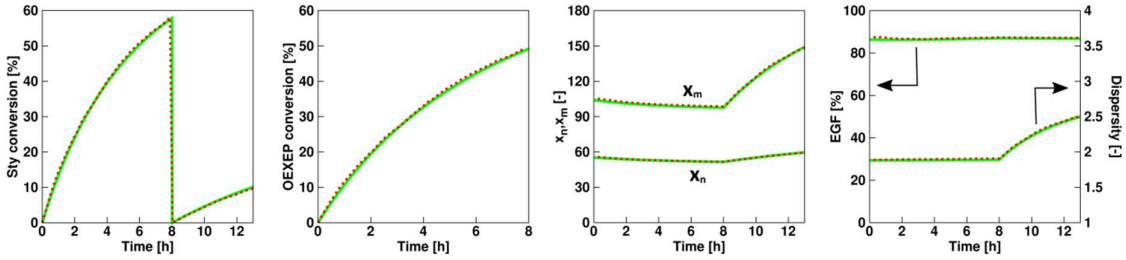

Figure A6: Comparison of monomer and OEXEP (R0X) conversion, number/mass average molar mass (xn/m), EGF and dispersity (Đ) obtained by extended method of moments model (solid green line) and kMC model (dotted red line); 0-8h: entry 3 in Appendix A in Table A1; 8-13h: entry 3 in Appendix A in Table A2.

A.12 Demonstration of kinetic insignificance of transfer coefficient $k_{-tr,0}$

The transfer coefficient $k_{-tr,0}$ is defined as the rate coefficient of the reaction of a RAFT leaving group radical R_0 and a dormant macroradical R_iX, resulting in the initial RAFT agent R_0X and a macroradical R_i:

$$R_0^{\bullet} + R_iX \xrightarrow{k_{-tr,0}} R_0X + R_i^{\bullet}$$

Figure A7 shows the average polymer properties as a function of time, and the fraction of the R_0 radicals consumed by the reaction shown above as a function of monomer conversion obtained by simulations with $k_{-tr,0}$=0 L mol^{-1} s^{-1} (green) and $k_{-tr,0}$=100* $k_{tr,0}$ (red, other parameters as in Table A3, Entry 3 in Table A1). As no difference in the prediction of the average polymer properties can be observed, $k_{-tr,0}$ can be considered to be kinetically insignificant and a value of 0 L mol^{-1}s^{-1} can be used for the simulations, simplifying both the model and the parameter estimation of other transfer coefficients ($k_{tr,0}$ and k_{tr}). R_0 will dominantly react with monomer, initiating new growing macroradicals, or with other (macro)radicals, forming new dead (macro)species.

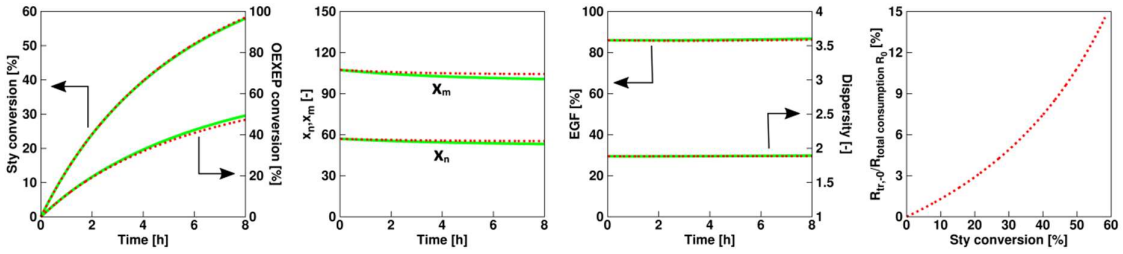

***Figure A7**: The average polymer properties as a function of time and the fraction of the R_0 radicals consumed by the reaction shown above as a function of monomer conversion obtained by simulations with $k_{-tr,0}$=0 L mol^{-1} s^{-1} (green) and $k_{-tr,0}$=100* $k_{tr,0}$ (red, other parameters as in Table A3, Entry 3 in Table A1)*

A.13 Demonstration of kinetic insignificance of transfer between initiator radicals (I) and initial RAFT agent (R_0X)

In addition to the exchange reaction between macroradicals (R_i) and the initial RAFT agent (R_0X), exchange between initiator radicals (I) and R_0X can occur as well. This leads to a new dormant IX species which can in turn react with R_i or R_0:

$$I + R_0X \xrightarrow{k_{tr,IR0X}} IX + R_0$$

$$R_i + IX \xrightarrow{k_{tr,RiIX}} R_iX + I$$

$$R_0 + IX \xrightarrow{k_{tr,R0IX}} R_0X + I$$

Assuming for simplicity $k_{tr,RiIX} = k_{tr,0}$ and $k_{tr,R0IX} = 10k_{tr,0}$ (based on $k_{pR0} = 10k_p$ as shown in Table A3), the average polymer properties as a function of time by simulations with $k_{tr,IR0X} = 0$ L mol^{-1} s^{-1} or $k_{tr,IR0X} = 100k_{tr,0}$ show no significant differences as shown in Figure A8. Consequently, the reaction between I and R_0X can be neglected and I will dominantly initiate new chains by reaction with monomer.

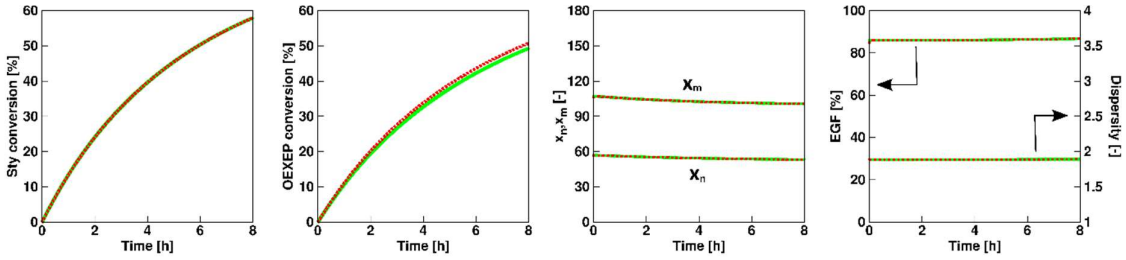

***Figure A8**: The average polymer properties as a function of time obtained by simulations with $k_{tr,IR0X} = 0$ L mol^{-1} s^{-1} (green) and $k_{tr,IR0X} = 100k_{tr,0}$ (red, other parameters as in Table A3, Entry 3 in Table A1)*

A.14 Overview of the reactions and kinetic parameters for the homopolymerization and chain extension with styrene.

An overview of the reactions considered and the corresponding rate coefficients can be found in Table A3.

Table A3*: Overview of the reactions and rate coefficients (monomer: styrene) with* I_2, $I^\bullet$, M, $R_0^\bullet, R_i^\bullet$, P_i, R_0X, R_iX*: conventional radical initiator, initiator fragment, monomer, RAFT leaving group, macroradical (chain length i≥1), dead polymer species, initial RAFT agent, dormant macrospecies; 70°C; for termination apparent rate coefficients with given value the one of* $k_{t,app}^{1,1}$ *(see also further).*

Reaction	Equation	k (L mol^{-1} s^{-1})	ref
Dissociation[a]	$I_2 \xrightarrow{f,k_{dis}} 2I^\bullet$	$4.4\ 10^{-5}$	4
Chain Initiation	$I^\bullet + M \xrightarrow{k_{pI}} R_1^\bullet$	$5.2\ 10^{3}$	5
	$R_0^\bullet + M \xrightarrow{k_{pR_0}} R_1^\bullet$	$5.1\ 10^{3}$	(b)
Propagation	$R_i^\bullet + M \xrightarrow{k_p} R_{i+1}^\bullet$	$4.8\ 10^{2}$	6
Chain transfer to monomer	$R_0^\bullet + M \xrightarrow{k_{trM,0}} R_1^\bullet + P_0$	$2.0\ 10^{-2}$	(c)
	$R_i^\bullet + M \xrightarrow{k_{trM}} R_1^\bullet + P_i$	$2.0\ 10^{-2}$	7
Termination by recombination	$R_0^\bullet + R_0^\bullet \xrightarrow{k_{tc,00}} P_0$	$2\ 10^{8.7}$	8,9
	$R_0^\bullet + R_i^\bullet \xrightarrow{k_{tc,0}} P_i$	$2\ 10^{8.7}$	8,9
	$R_i^\bullet + R_j^\bullet \xrightarrow{k_{tc,app}^{i,j}} P_{i+j}$	$2\ 10^{8.7}$	8,9
RAFT exchange[f]	$R_i^\bullet + R_0X \xrightarrow{k_{tr,0}} R_iX + R_0^\bullet$	$(3.8 \pm 0.1)\ 10^{2}$	(d)
	$R_i^\bullet + R_jX \xrightarrow{k_{tr}} R_iX + R_j^\bullet$	$(2.1 \pm 0.4)\ 10^{2}$	(e)

(a) (apparent) efficiency *f:* see Subsection c; (b) see Subsection b; (c) rate coefficient assumed identical as the rate coefficient for the macroradical; (d) obtained by regression analysis to an extensive set of experimental data (Figure A10, Figure 3.5 and 3.6): *F*-value=1.08 10^4; tabulated *F*-value: 4.84; $k_{tr\text{-}0}$ kinetically insignificant (see Subsection S12); (e) obtained by regression analysis to an extensive set of experimental data (Figure 3.10): *F*-value=1.71 10^3; tabulated *F*-value: 4.84; corresponding $C_{tr,0}$: 0.80±0.02 and C_{tr}: 0.44±0.07; (f) first exchange only important if still R_0X (see Figure A11) present (reverse exchange can be always neglected), second one only relevant upon R_0X removal followed by chain extension (see main text).

The (apparent) termination rate coefficient, the intrinsic rate coefficient concerning chain initiation by the RAFT leaving group R_0, and the (apparent) conventional initiator efficiency are discussed more in depth below.

a. Apparent termination rate coefficient

In order to accurately describe the diffusion-controlled mechanism of bimolecular termination in radical polymerization, the composite k_t model[8] (aka RAFT-CLD-T model) was used. This model allows to calculate an apparent homotermination rate coefficient ($k_{tc,app}^{i,i}$; i=chain length; only considering termination by recombination) dependent on the chain length i and the polymer mass fraction m_p (and thus monomer conversion X_m):

For $i < i_{gel}$

$$k_{tc,app}^{i,i} = k_t^{1,1}\, i^{-\alpha_s} \qquad \text{for } i < i_{SL} \tag{A10}$$

$$k_{tc,app}^{i,i} = k_t^{1,1}\, i_{SL}^{(\alpha_L-\alpha_s)}\, i^{-\alpha_s} \qquad \text{for } i \geq i_{SL} \tag{A11}$$

For $i \geq i_{gel}$

$$k_{tc,app}^{i,i} = k_t^{1,1}\, i_{SL}^{(\alpha_{gel}-\alpha_s)}\, i^{-\alpha_{gel}} \qquad \text{for } i < i_{SL} \tag{A12}$$

$$k_{tc,app}^{i,i} = k_t^{1,1}\, i_{SL}^{(\alpha_L-\alpha_s)}\, i^{(\alpha_{gel}-\alpha_L)}\, i^{-\alpha_{gel}} \qquad \text{for } i \geq i_{SL} \tag{A13}$$

with $k_t^{1,1}$ the (apparent) termination rate coefficient for radicals with chain length 1, α_s the exponent for termination of short chains in dilute solution, α_L the exponent for long chains in dilute solution, α_{gel} the exponent for chains in the gel regime, i_{SL} the crossover chain length

between short- and long-chain behavior, i_{gel} the chain length at the onset of the gel-effect. An overview of these parameters can be found in Table A4.[8–10]

From the apparent homotermination rate coefficients, the apparent cross-termination rate coefficient $k_{tc,app}^{i,j}$ is calculated for simplicity using the geometric mean:

$$k_{tc,app}^{i,j} = \sqrt{k_{tc,app}^{i,i}\, k_{tc,app}^{j,j}} \tag{A14}$$

An averaged (zero order) apparent termination rate coefficient can be calculated at any moment:

$$\langle k_{tc,app} \rangle = \frac{\sum_{i=1}^{\infty}\sum_{j=1}^{\infty}(1+\delta_{ij})k_{tc,app}^{i,j}[R_i][R_j]}{\left(\sum_{i=1}^{\infty}[R_i]\right)^2} \tag{A15}$$

with δ_{ij} the Kronecker Delta Function. When employing the kinetic Monte Carlo technique, each macroradical R_i is tracked individually and Equation (A15) can be calculated exactly. However, when applying the deterministic extended method of moments method this information is not available. Nonetheless, Equation (A15) can still be approximately used by considering the Flory-Schulz distribution to obtain the macroradical chain length distribution:[11]

$$f_n(i) = \frac{1}{x_{n,r}}\, exp\left(-\frac{i}{x_{n,r}}\right) \tag{A16}$$

with $f_n(\mathrm{i})$ the number fraction of macroradicals with chain length i and $x_{n,r}$ the associated number average chain length.

For the validation of the Flory-Schulz distribution for the macroradical CLD in the present work, the reader is referred to Chapter 3.

***Table A4**: Parameters used for the composite k_t model; monomers: styrene (Sty) and methyl acrylate (MA; related to next subsection: these parameters were used for n-butyl acrylate simulations as a first approximation); m_p: polymer mass fraction*

Monomer	T(K)	$\mathbf{k_t^{1,1}}$	$\boldsymbol{\alpha_S}$	$\mathbf{i_{SL}}$	$\boldsymbol{\alpha_L}$	$\boldsymbol{\alpha_{gel}}$	$\mathbf{i_{gel}}$
Sty	363	$2 \times 10^{8.7}$	0.53	30	0.15	$1.22m_p$-0.11	$3.30m_p^{-2.13}$
MA	323	See Table A6	0.78	18	0.15	$0.81m_p$-0.05	$6.9m_p^{-2.2}$

b. Chain initiation by RAFT leaving group (R_0)

The RAFT leaving group R_0 is identical to an ethyl acrylate radical. As a result, the rate coefficient of the reinitiation reaction (k_{pR_0}) can be assessed by considering the propagation rate coefficient of poly(ethyl acrylate) radicals to styrene, ignoring possible chain length dependencies. This rate coefficient can be assessed using the rate coefficient of the homopolymerization of ethyl acrylate and the monomer reactivity ratio r_{EA}:

$$r_{EA} = \frac{k_{p,EAEA}}{k_{p,EASty}} \tag{A17}$$

$$k_{pR_0} \approx k_{p,EASty} = \frac{k_{p,EAEA}}{r_{EA}} \tag{A18}$$

Using a reactivity ratio r_{EA} of 0.22 as determined by Brar et al. [12] and a homopropagation rate coefficient $k_{p,EAEA}$ of 1117 L mol^{-1} s^{-1} at 70°C as mentioned by Gao et al. [13], a k_{pR_0}= 5077 L mol^{-1} s^{-1} results. Note that this value is as good as identical as the one for the other chain initiation.

c. Apparent conventional initiator efficiency

An apparent conventional initiator efficiency f_{app} dependent on monomer conversion X_m can be calculated as described by Buback *et.al.*:[14]

$$f_{app} = \frac{D_I}{D_I + D_{term}} \tag{A19}$$

with D_I the diffusion coefficient of the cyanoisopropyl radical and $D_{term} = 5.3\ 10^{-1}\ m^2 s^{-1}$ a correction factor related to the rate of termination between two cyanoisopropyl radicals.

***Table A5**: Parameters used to calculate the apparent initiator efficiency (Equation (A17) - (A19) as described by Buback et al.[14] for AIBN as conventional radical initiator and styrene as monomer.*

Parameter	Description	Value
$D_{0,I}\ (m^2 s^{-1})$	Pre-exponential factor for diffusion	$1.95\ 10^{-4}$
$E_I\ (kJ\ mol^{-1})$	Activation energy for diffusion	31
$R\ (J\ mol^{-1} K^{-1})$	Universal gas constant	8.314
$T\ (K)$	Temperature	$333 - 363$
$w_1\ (-)$	Mass fraction of monomer	0-1
$w_2\ (-)$	Mass fraction of polymer	0-1
$V_1^*\ (m^3 mol^{-1})$	Specific critical hole free volume of monomer [(a)]	$9.46\ 10^{-7}$
$V_2^*\ (m^3 mol^{-1})$	Specific critical hole free volume of polystyrene	$8{,}50\ 10^{-7}$
$\frac{K_{11}}{\lambda}\ (m^3\ kg^{-1}\ K^{-1})$	Parameter for specific hole free volume monomer [(a)]	$1.49\ 10^{-9}$
$\frac{K_{12}}{\lambda}\ (m^3\ kg^{-1}\ K^{-1})$	Parameter for specific hole free volume polymer	$5.82\ 10^{-10}$
$K_{21} - T_{g1}\ (K)$	Parameter for specific hole free volume monomer [(a)]	-84
$K_{22} - T_{g1}\ (K)$	Parameter for specific hole free volume polymer	-327
$\xi_{i2}\ (-)$	Critical jumping unit volume ratio for cyanoispropyl radical to polymer	0.36
$\xi_{12}\ (-)$	Critical jumping unit volume ratio for monomer to polymer	0.59

(a) Ethylbenzene used as model compound.

According to the free volume theory, D_I can be calculated via:

$$D_I = D_{0,I} \exp\left(-\frac{E_I}{RT}\right) \exp\left(\frac{-w_1 V_1^* \xi_{i2}/\xi_{12} + w_2 V_2^* \xi_{12}}{V_{FH}/\lambda}\right) \quad \text{(A20)}$$

$$\frac{V_{FH}}{\lambda} = \frac{K_{11}}{\lambda} w_1 \left(K_{21} - T - T_{g1}\right) + \frac{k_{12}}{\lambda}\, w_2 (K_{22} + T - T_{g1}) \quad \text{(A21)}$$

Table A5 gives an overview of the description and value of the parameters used in Equation (A18) and (A19).

A.15 Reactions and kinetic parameters for chain extension with n-butyl acrylate

The reactions and rate coefficients to investigate the chain extension of dormant polystyrene with n-butyl acrylate are mentioned in Table A6, neglecting chain transfer to monomer, backbiting and β-scission. The actual apparent termination reactivity is calculated by averaging the RAFT-CLD-T value for pure polystyrene and pure poly(n-butyl acrylate), according to the number of monomer units of each type being incorporated on an overall basis.

***Table A6**: Overview of the reactions and rate coefficients (extension of polystyrene with monomer n-butyl acrylate (nBuA)) with $I^{\bullet}, M, R_i^{\bullet}, P_i, R_iX$: initiator fragment, monomer (nBuA), macroradical (chain length i≥1), dead polymer species, dormant macrospecies; $R_{nB,i}^{\bullet}$ and $R_{S,i}^{\bullet}$: macroradical with chain length i and n-butyl acrylate (nB) and styrene (S) as terminal unit; 60°C; for termination apparent rate coefficients averaging with respect to composition.*

Reaction	Equation	k (L mol^{-1} s^{-1})	Ref
Dissociation	$I_2 \xrightarrow{f,k_{dis}} 2I^{\bullet}$	1.1 10^{-5}	4
Chain Initiation	$I^{\bullet} + M \xrightarrow{k_{pI}} R_{nB,1}^{\bullet}$	4.0 10^{3}	(a)
Propagation	$R_{nB,i}^{\bullet} + M \xrightarrow{k_{pnBnB}} R_{nB,i+1}^{\bullet}$	3.4 10^{4}	15
	$R_{S,i}^{\bullet} + M \xrightarrow{k_{pSnB}} R_{nB,i+1}^{\bullet}$	4.8 10^{2}	(b)
Termination by recombination	$R_{nB,i}^{\bullet} + R_{nB,j}^{\bullet} \xrightarrow{k_{tc,app}^{i,j}} P_{i+j}$	1.3 10^{9}	16,(c)
Termination by disproportionation	$R_{nB,i}^{\bullet} + R_{nB,j}^{\bullet} \xrightarrow{k_{td,app}^{i,j}} P_i + P_j$	1.3 10^{9}	16,(c)
RAFT exchange[(e)]	$R_{nB,i}^{\bullet} + R_{S,j}X \xrightarrow{k_{tr,nBS}} R_{nB,i}X + R_{S,j}^{\bullet}$	4.6 × 10^{4}	(d)

(a) taken identical as reaction with styrene for simplicity; (b) calculated by means of the monomer reactivity ratio[17,18] $r = {k_{p,SS}}/{k_{p,SnBa}} = 0.71$; (c) with ${k_{tc}}/{k_{td}} = 0.9$; (d) obtained by fitting to experimental data (Figure 3.14); corresponding C_{tr}: 1.35; (e) other exchanges can be neglected as kinetically insignificant (see Figure A16). Styrene radicals first add to *n*BuA based on preliminary screening.

A.16 Inefficient removal of unreacted R_0X (OEXEP) via precipitation

In order to determine the end-group functionality (EGF) of the synthesized MADIX polystyrene polymers and to efficiently investigate the chain extension of these polymers, unreacted R_0X (OEXEP) needs to be removed. Due to the high dispersity associated with the bulk polymerization of styrene in the presence of a xanthate-type RAFT agent, conventional methods such as precipitation are not recommended as this would result, next to the removal of R_0X, in the significant loss of the low molar mass polymer chains as shown in Figure A3 (dashed blue

line vs solid red line). Consecutive precipitation was here performed by dissolving the polymer samples in a minimum amount of toluene and slowly adding it to cold methanol. A much more suited experimental procedure is dialysis (coinciding dashed blue and dotted green line in Figure A9) as this does not alter the SEC trace. For more information on the dialysis procedure and the confirmation of the complete removal of non-macromolecules such as styrene and OEXEP, the reader is referred to Chapter 3.

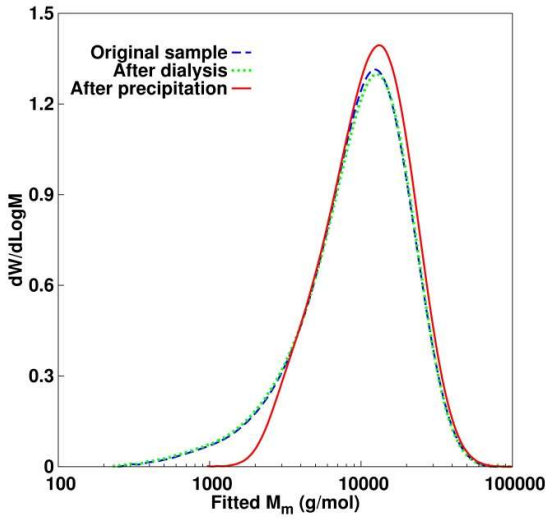

Figure A9*: SEC data illustrating the loss of low-molar mass polymer chains if precipitation is used. Dialysis results in the preservation of all chains; dashed blue line: original polymer sample, dotted green line: polymer sample after dialysis, solid red line: polymer sample after precipitation in cold methanol; Entry 1 in Table A1,* X_m*=0.33*

A.17 The effect of TCL on the homopolymerization of styrene in the presence of (O-ethyl xanthate)-2- ethyl propionate and a fixed $[R_0X]_0/[I_2]_0$

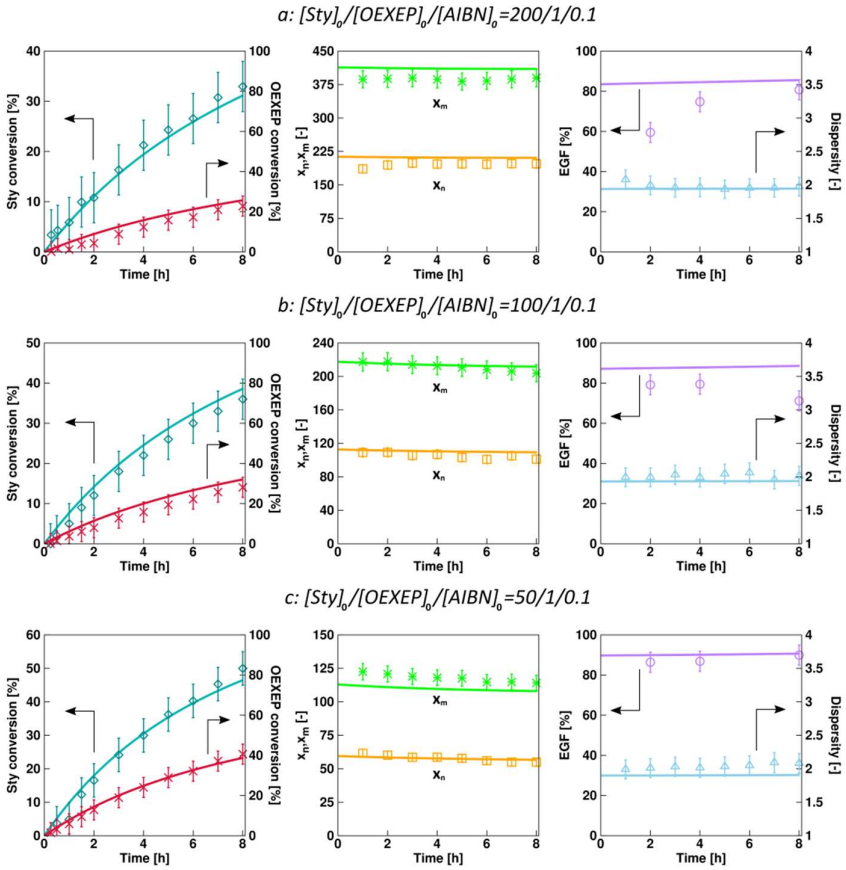

***Figure A10**: Comparison between simulations and experiments (next to Figure 3.5 and 3.6 in Chapter 3; entry 2, 6 and 7 in Table A1).*

A.18 Demonstration of kinetic insignificance of transfer coefficient k_{tr} during homopolymerization experiments

The transfer coefficients $k_{tr,0}$ and k_{tr} are defined as the rate coefficient of the reaction of a macroradical and respectively a RAFT agent R_0X and a dormant macrospecies R_iX. Figure A11 shows the average polymer properties as a function of time obtained by simulations with k_{tr}=0 L mol^{-1} s^{-1} (green) and $k_{tr}=10k_{tr,0}$ (red, other parameters as in Table A3) during a homopolymerization experiment (Entry 3 in Table A1). As no difference in the prediction of

the average polymer properties can be observed, k_{tr} can be considered to be kinetically insignificant and a value of 0 L $mol^{-1}s^{-1}$ can be used for the simulations, simplifying the estimation of $k_{tr,0}$.

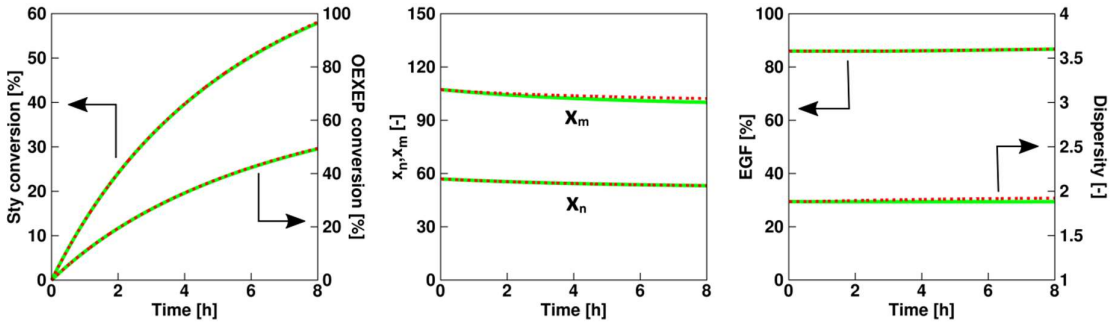

***Figure A11**: The average polymer properties as a function of time obtained by simulations with k_{tr}=0 L mol^{-1} s^{-1} (green) and k_{tr}=10$k_{tr,0}$ (red, other parameters as in Table A3, Entry 3 in Table A1)*

A.19 Determination of $C_{tr,0}$ via the methods of Moad and Mayo

The methods of Moad and Mayo are often applied to determine the $C_{tr,0}$ value in MADIX when low values (<10) are expected by examining the slope of ln([R_0X]) vs ln([M]) (Moad) or $1/x_n$ vs $[R_0X]_0/[M]_0$ (Mayo).[19–24] Figure A12 and Table A7 give an overview of the results after application of both methods on the experimental data discussed in Chapter 3 (Table A1).

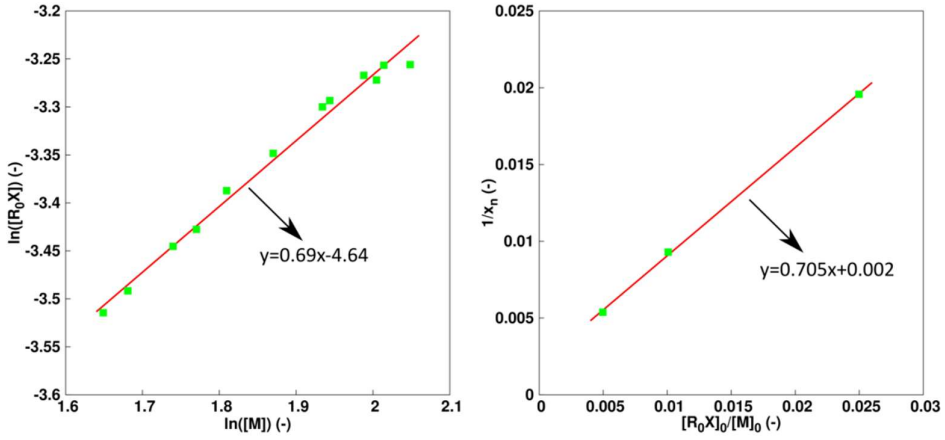

***Figure A12**: Example of the use of the method of Moad (left; Entry 6 in Table A1) and the method of Mayo (right; Entry 4,5 and 6 in Table A1; identical $[I_2]_0$) for the determination of $C_{tr,0}$*

The method of Moad results in a $C_{tr,0}$ of 0.69±0.04 (Table A7; one example in Figure A12: left). The method of Mayo leads to a value of 0.71±0.02 (Figure A12 right).

***Table A7**: Application of the method of Moad on the experiments shown in Table A1 for the determination of $C_{tr,0}$*

Entry in Table A1	$C_{tr,0}$
1	0.66
2	0.75
3	0.73
4	0.63
5	0.68
6	0.69
7	0.73
Average	0.69±0.04

A.20 Limitations of the method of Mayo for determining $C_{tr,0}$

The method of Mayo was originally developed to determine the transfer coefficient (C_{tr}) for chain transfer with solvent in the radical polymerization of styrene.[22] Later, this method has been often used in literature[20,24–26] to determine C_{tr} of other reactants. Strictly the kinetic chain length (ν), which is related to the number average chain length of the actual polymer (no radicals) that is experimentally accessible, is needed. For the RAFT CTA in the present work this ν is given by:

$$\nu = \frac{k_p[M][R_{tot}]}{k_{trM}[M][R_{tot}] + k_{tr,0}[R_0X][R_{tot}] + k_{tc}[R_{tot}][R_{tot}]} \quad \text{(A22)}$$

with $k_{p,/rM/tr0/tc}$ the rate coefficient for propagation, chain transfer to monomer, transfer to R_0X and termination by recombination (no correction factor as strict definition on radical level and total concentration), considering only termination by recombination as termination event and assuming that the obtained polymer has undergone only a single transfer event (k_{tr}=0, as justified by Appendix A Section A18).

Taking the reciprocal and introducing $C_{tr,0} = k_{tr,0}/k_p$ and $C_M = k_{trM}/k_p$, Equation (A22) is transformed in:

$$\frac{1}{\nu} = C_M + \frac{k_{tc}[R_{tot}]}{k_p[M]} + C_{tr,0}\frac{[R_0X]}{[M]} \tag{A23}$$

which is known as the Mayo equation and is often written as:

$$\frac{1}{\nu} = C_M + \frac{1}{\nu_0} + C_{tr,0}\frac{[R_0X]}{[M]} \tag{A24}$$

with ν_0 the kinetic chain length in absence of chain transfer.

At low monomer conversion, $[R_0X]/[M]$ can be considered constant and equal to the initial ratio $[R_0X]_0/[M]_0$. Consequently, by performing several experiments with varying $[R_0X]_0/[M]_0$, $C_{tr,0}$ can be determined by the slope of ν^{-1} vs $[R_0X]_0/[M]_0$ plot if ν_0^{-1} is independent of that ratio. As discussed thoroughly by Smulders[27], this can be expected if the same initiator amount is used for all the experiments, the re-initiation rate of the RAFT leaving group radical (R_0) is high, sufficiently fast fragmentation takes place, and k_{tc} and $[R_i]$ are independent of $[R_0X]_0/[M]_0$.

However, more important and often ignored, *v* represents the average number of monomer units of the macroradicals *before* their termination by recombination or chain transfer, and is not necessarily equal to the related experimentally determinable number average chain length x_n. For example, in absence of chain transfer and with thus only termination by recombination as termination event, x_n is equal to twice the kinetic chain length, not taking into account end-

groups, whereas when chain transfer is the dominant chain stopping event and the EGF approaches 1, x_n will be equal to v.

In order to assess the validity of the Mayo equation in Chapter 3, the approximation of the number average chain length of the radicals by the overall chain length needs to be verified. As shown in Figure A13 (left), for a reference experiment (Entry 5 in Table A1), this is not the case due to the EGF being significantly lower than 1 and consequently shifting the overall x_n to somewhat higher values. Nonetheless, x_n of the dormant chains (R_iX) and the dead chains (P_i) are approximately equal to, respectively, once and twice the x_n of the macroradicals. Importantly, the small difference between the x_n of the macroradicals or dormant species and the overall x_n does result in a lower value of $C_{tr,0}$ (0.75 vs 0.80; with 0.80 also the value with method presented in present work) as shown in Figure A13 (right). This slight mismatch leads to an incorrect simulation of the MADIX average chain length characteristics in an complete kinetic model (see main text). In conclusion, the Mayo method can only be used to obtain an assessment of $C_{tr,0}$ for the conditions investigated in Chapter 3.

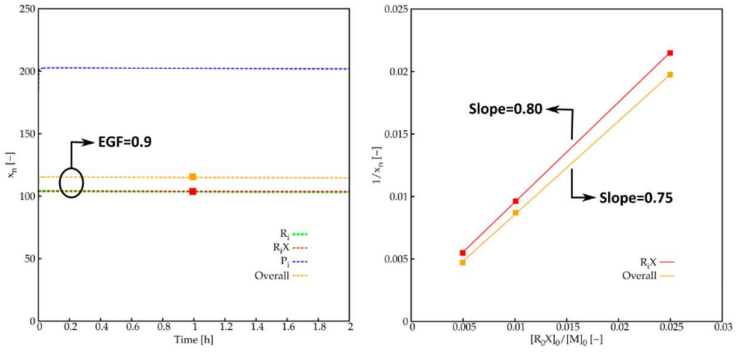

***Figure A13**: left: number average chain length (x_n) of radicals (green), dormant chains (red), dead chains (blue) and overall (orange) as a function of time for Entry 5 in Table A1; right: Application of the method of Mayo on model output of Entry 4, 5 and 6 in Table A1 (identical $[I_2]_0$) by means of $x_n(R_iX)$ (red squares) and x_n(overall) (orange squares, as typically done in practice); lines represent trend lines through the data points; Parameters as mentioned in Table A3; theoretical $C_{tr,0}$ from model=$k_{tr,0}/k_p$=384/479=0.80; $c_{tr,0}$ by means of $x_n(R_iX)$ =0.80 and x_n(overall)=0.75*

A.21 Influence of $[R_0X]_0/[I2]_0$ and $[M]_0/[R0X]_0$ on the R_0X conversion

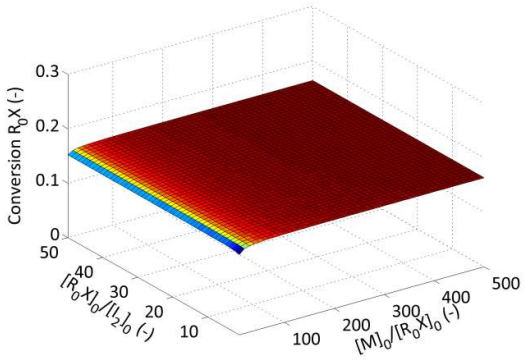

***Figure A14**: R_0X conversion (X_{R_0X}) as a function of $[R_0X]_0/[I_2]_0$ (ranging from 1 to 50) and $[M]_0/[R_0X]_0$ (ranging from 10 to 500); simulated data have been achieved by means of the parameters given in Table A3 with R_0X=(O-ethyl xanthate)-2-ethyl propionate, M=Sty, and I_2=AIBN; 70°C; X_m=20%.*

A.22 Demonstration of the importance of accurate determination of k_{tr} of exchange between polystyrene macroradicals and dormant polystyrene

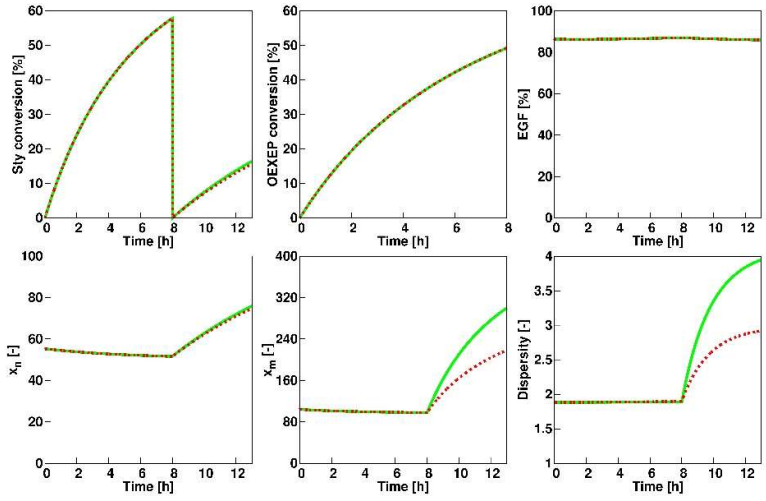

***Figure A15**: The average polymer properties as a function of time for simulations of the chain extension of dormant polystyrene with fresh styrene (entry 1 in Table A2) with k_{tr}= 2.1 x 10² L mol^{-1} s^{-1} (green, see Table A3) as obtained by regression analysis and $k_{tr}=k_{tr,0}$=3.8 x 10² L mol^{-1} s^{-1} (red, see Table A3). Other parameters as in Table A3*

A.23 Determination of the kinetically significant transfer coefficients during chain extension of dormant polystyrene with n-butyl acrylate in solution

When considering the chain extension of dormant polystyrene with n-butyl acrylate, four possible RAFT exchange reactions exist as two macroradical and dormant species types are feasible:

$$R^{\bullet}_{nBuA,i} + R_{Sty,j}X \xrightarrow{k_{tr,nBuASty}} R_{nBuA,i}X + R^{\bullet}_{Sty,j}$$

$$R^{\bullet}_{nBuA,i} + R_{nBuA,j}X \xrightarrow{k_{tr,nBuAnBuA}} R_{nBuA,i}X + R^{\bullet}_{nBuA,j}$$

$$R^{\bullet}_{Sty,i} + R_{Sty,j}X \xrightarrow{k_{tr,StySty}} R_{Sty,i}X + R^{\bullet}_{Sty,j}$$

$$R^{\bullet}_{Sty,i} + R_{nBuA,j}X \xrightarrow{k_{tr,StynBuA}} R_{Sty,i}X + R^{\bullet}_{nBuA,j}$$

with $R^{\bullet}_{nBuA,i}$ and $R^{\bullet}_{Sty,i}$ a macroradical with chain length i and n-butyl acrylate (*n*BuA) and styrene (Sty) as terminal unit, and $R_{nBuA,j}X$ and $R_{Sty,j}X$ a dormant macrospecies with chain length i and n-butyl acrylate (*n*BuA) and styrene (Sty) as terminal unit next to the xanthate functional group *X*.

However, as shown in Figure A16, only $k_{tr,nBuASty}$ will influence the average polymer properties and the other transfer coefficients can be considered kinetically insignificant, reducing the complexity of the model and simplifying the estimation of $k_{tr,nBuASty}$. Styrene macroradicals, generated by the exchange of dormant polystyrene with *n*BuA macroradicals, will swiftly react with *n*BuA monomer forming again macroradicals with an *n*BuA terminal unit, explaining the insignificance of $k_{tr,StySty}$ and $k_{tr,Sty nBuA}$. Futhermore, similarly to the chain extension reaction with fresh styrene (see Figure 3.10), a single activation-growth-deactivation cycle is performed per chain, resulting in the absence of reactivation of dormant poly(styrene-b-*n*BuA) blockcopolymer and hence the insignificance of $k_{tr,nBuAnBuA}$. This can be explained by the low

concentration of dormant poly(styrene-b-*n*BuA) compared to the initial dormant polystyrene at low conversions, as shown in Figure A17.

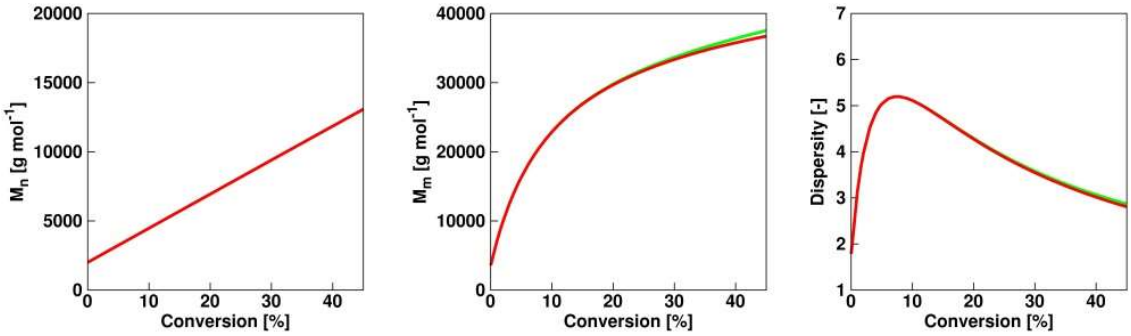

***Figure A16**: The average polymer chain length properties as a function of time obtained by simulations with (i) $k_{tr,nBuAnBuA} = k_{tr,StySty} = k_{tr,StynBuA} = 0$ L mol^{-1} s^{-1} and $k_{tr,nBuASty} = 4.6\ 10^4$ L mol^{-1} s^{-1} (full green line), and (ii) for simplicity: $k_{tr,StySty} = k_{tr,StynBuA} = 2.1\ 10^2$ L mol^{-1} s^{-1} and $k_{tr,nBuASty} = k_{tr,nBuAnBuA} = 4.6\ 10^4$ L mol^{-1} s^{-1} (dotted red line); other parameters as in Table A6; simulated output with stochastic method; Conditions: [Toluene]= 6 mol L^{-1}, [n-BuA]=2.0 mol L^{-1}, [n-BuA]/ [$R_{i,sty}$X]/ [AIBN]=198/1/1; T=60°C; Parameters: Table A6*

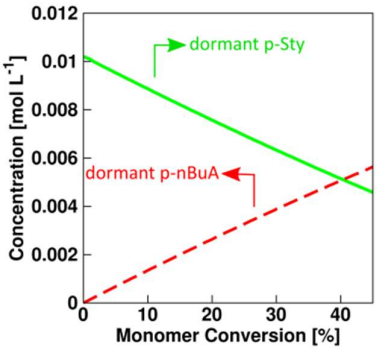

***Figure A17**: The concentration of dormant polystyrene (green) and dormant poly(styrene-b-nBuA) (red) during the extension of dormant polystyrene with nBuA; Conditions: [Toluene]= 6 mol L^{-1}, [n-BuA]=2.0 mol L^{-1}, [n-BuA]/ [$R_{i,sty}$X]/ [AIBN]=198/1/1; T=60°C*

A.24 References

1 WO 1998058974, 1998.

2 H. Fischer and M. Souaille, *Macromol. Symp.*, 2001, **174**, 231–240.

3 C. Toloza Porras, D. R. D'hooge, P. H. M. Van Steenberge, M. F. Reyniers and G. B. Marin, *Macromol. React. Eng.*, 2013, **7**, 311–326.

4 M. T. Erben and S. Bywater, *J. Am. Chem. Soc.*, 1955, **77**, 3712–3714.

5 K. Heberger and H. Fischer, *Int. J. Chem. Kinet.*, 1993, **25**, 249–263.

6 M. Buback, R. G. Gilbert, R. A. Hutchinson, B. Klumberman, F.-D. Kuchta, B. G. Manders, K. F. O'Driscoll, G. T. Russell and J. Schweer, *Macromol. Chem. Phys.*, 1995, **196**, 3267–3280.

7 A. W. Hui and A. E. Hamielec, *J. Appl. Polym. Sci.*, 1972, **16**, 749–769.

8 G. Johnston-Hall and M. J. Monteiro, *J. Polym. Sci. Part a-Polymer Chem.*, 2008, **46**, 3155–3176.

9 P. Derboven, D. R. D'hooge, M.-F. Reyniers, G. B. Marin and C. Barner-Kowollik, *Macromolecules*, 2015, **48**, 492–501.

10 G. Johnston-Hall and M. J. Monteiro, *Macromolecules*, 2008, **41**, 727–736.

11 E. Mastan, D. Zhou and S. Zhu, *J. Polym. Sci. Part A Polym. Chem.*, 2014, **52**, 639–651.

12 A. S. Brar and Sunita, *Makromol. Chemie*, 1993, **194**, 1707–1720.

13 J. Gao, N. McManus and A. Penlidis, *Macromol. Chem. Phys.*, 1997, **198**, 843–859.

14 M. Buback, B. Huckestein, F. Kuchta and G. T. Russell, *Macromol. Chem. Phys.*, 1994, **195**, 2117–2140.

15 J. M. Asua, S. Beuermann, M. Buback, P. Castignolles, B. Charleux, R. G. Gilbert, R. A. Hutchinson, J. R. Leiza, A. N. Nikitin, J. P. Vairon and A. M. Van Herk, *Macromol. Chem. Phys.*, 2004, **205**, 2151–2160.

16 J. Barth, M. Buback, P. Hesse and T. Sergeeva, *Macromolecules*, 2010, **43**, 4023–4031.

17 X. Li, W. J. Wang, F. Weng, B. G. Li and S. Zhu, *Ind. Eng. Chem. Res.*, 2014, **53**, 7321–7332.

18 L. K. Kostanski and A. E. Hamielec, *Polymer (Guildf).*, 1992, **33**, 3703–3710.

19 M. M. Adamy, A. M. van Herk, M. Destarac and M. J. Monteiro, *Macromolecules*, 2003, **36**, 2293–2301.

20 B. Y. K. Chong, J. Krstina, T. P. T. Le, G. Moad, A. Postma, E. Rizzardo and S. H. Thang, *Macromolecules*, 2003, **36**, 2256–2272.

21 G. Moad, J. Chiefari, Y. K. Chong, J. Krstina, R. T. A. Mayadunne, A. Postma, E. Rizzardo and S. H. Thang, *Polym. Int.*, 2000, **49**, 993–1001.

22 F. R. Mayo, *J. Am. Chem. Soc.*, 1943, **65**, 2324–2329.

23 M. Destarac, C. Brochon, J. M. Catala, A. Wilczewska and S. Z. Zard, *Macromol. Chem. Phys.*, 2002, **203**, 2281–2289.

24 P. Derboven, P. H. M. Van Steenberge, M. Reyniers, C. Barner-kowollik, D. R. D'hooge and G. B. Marin, *Macromol. Theory Simulations*, 2016, **25**, 104–115.

25 J. Chiefari, R. T. A. Mayadunne, C. L. Moad, G. Moad, E. Rizzardo, A. Postma, M. A. Skidmore and S. H. Thang, *Macromolecules*, 2003, **36**, 2273–2283.

26 J. Chiefari, Y. K. B. Chong, F. Ercole, J. Krstina, J. Jeffery, T. P. T. Le, R. T. A. Mayadunne, G. F. Meijs, C. L. Moad, G. Moad, E. Rizzardo, S. H. Thang and C. South, 1998, **31**, 5559–5562.

27 W. W. Smulders, Technische Universiteit Eindhoven, 2002.

Appendix B: Supporting info for Chapter 4

B.1 Calculation of the apparent conventional initiator efficiency of AIBN

During a bulk polymerization, the viscosity of the reaction mixtures increases with increasing monomer conversion which results in a decrease of the apparent conventional initiator efficiency fapp. fapp can be calculated as described by Buback et.al.:1

$$f_{app} = \frac{D_I}{D_I + D_{term}} \tag{B1}$$

with D_I the diffusion coefficient of the cyanoisopropyl radical and $\mathrm{D_{term}} = 5.3\ 10^{-10}\mathrm{m^2 s^{-1}}$ a correction factor related to the rate of termination between two cyanoisopropyl radicals. This approach was also used in the bulk study of De Rybel *et al*.[2]

According to the free volume theory, D_I can be calculated via:

$$D_I = D_{0,I} \exp\left(-\frac{E_I}{RT}\right) \exp\left(\frac{-w_1 V_1^* \xi_{i2}/\xi_{12} + w_2 V_2^* \xi_{12}}{V_{FH}/\lambda}\right) \tag{B2}$$

$$\frac{V_{FH}}{\lambda} = \frac{K_{11}}{\lambda} w_1 \left(K_{21} - T - T_{g1}\right) + \frac{k_{12}}{\lambda}\, w_2 (K_{22} + T - T_{g1}) \tag{B3}$$

Table B1 gives an overview of the description and value of the parameters used in Equation (B2) and (B3). These parameters were originally determined for the bulk polymerization of styrene with AIBN as conventional initiator but can be used here as well as a first approximation with some small adjustments based on the experimental monomer conversion data.

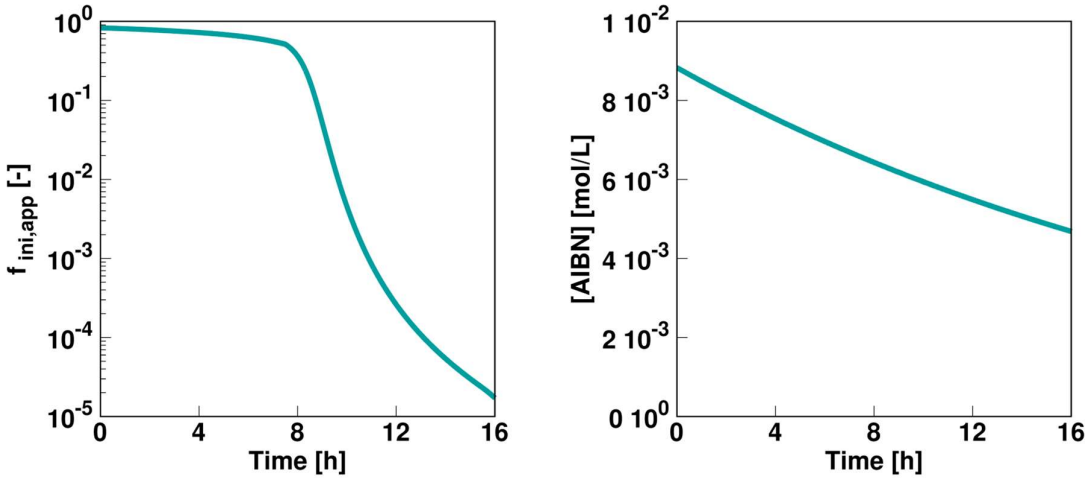

Figure B1*: Apparent initiator efficiency (left) and AIBN concentration (right) as a function of time for the bulk polymerization of MMA mediated by CPDB and initiated with AIBN (Experiment B1 in Table 2 in Chapter 4); initiator efficiency as calculated by the free volume theory (see above).*

***Table B1**: Parameters used to calculate the apparent initiator efficiency (Equation (B1)- (B3) as described by Buback et al.[1] for AIBN as conventional radical initiator and MMA as monomer. Values slightly adjusted from values originally determined for styrene as monomer.*

Parameter	Description	Value
$D_{0,I}\ (m^2 s^{-1})$	Pre-exponential factor for diffusion	$1.95\ 10^{-4}$
$E_I\ (kJ\ mol^{-1})$	Activation energy for diffusion	24
$R\ (J\ mol^{-1} K^{-1})$	Universal gas constant	8.314
$T\ (K)$	Temperature	$333 - 363$
$w_1\ (-)$	Mass fraction of monomer	0-1
$w_2\ (-)$	Mass fraction of polymer	0-1
$V_1^*\ (m^3 mol^{-1})$	Specific critical hole free volume of monomer [(a)]	$9.46\ 10^{-7}$
$V_2^*\ (m^3 mol^{-1})$	Specific critical hole free volume of polymer	$8.50\ 10^{-7}$
$\frac{K_{11}}{\lambda}\ (m^3\ kg^{-1}\ K^{-1})$	Parameter for specific hole free volume monomer [(a)]	$1.49\ 10^{-9}$
$\frac{K_{12}}{\lambda}\ (m^3\ kg^{-1}\ K^{-1})$	Parameter for specific hole free volume polymer	$5.82\ 10^{-10}$
$K_{21} - T_{g1}\ (K)$	Parameter for specific hole free volume monomer [(a)]	-84
$K_{22} - T_{g1}\ (K)$	Parameter for specific hole free volume polymer	-327
$\xi_{i2}\ (-)$	Critical jumping unit volume ratio for cyanoispropyl radical to polymer	0.60
$\xi_{12}\ (-)$	Critical jumping unit volume ratio for monomer to polymer	0.59

(a) Ethylbenzene used as model compound.

B.2 Determination of chain initiation rate coefficient of the AIBN radical fragment and the RAFT leaving group radical (R_0)

The R_0 radical has the same chemical structure as an AINB radical fragment. However, the rate coefficient for the chain initiation reaction between an AIBN radical fragment and MMA is unknown. Consequently, this coefficient was assessed based on the known chain initiation coefficient for styrene[3] and the ratio of the propagation rate coefficients of styrene[4] and MMA[5]:

$$k_{p,R_0}(MMA) = \frac{k_p(MMA)}{k_p(Sty)} k_{p,R_0}(Sty) = \frac{8.2\ 10^2}{3.4\ 10^2} 4.0\ 10^3 = 9.5\ 10^3 \qquad \text{(B4)}$$

B.3 Calculation of the average apparent termination rate coefficient

In order to accurately describe the diffusion-controlled mechanism of bimolecular termination in radical polymerization, the composite k_t model[6] (RAFT-CLD-T model) was used. This model allows to calculate an apparent homotermination rate coefficient ($k_{t,app}^{i,i}$; i=chain length) dependent on the chain length i and the polymer mass fraction m_p (and thus the monomer conversion X_m):

For $i < i_{gel}$

$$k_{t,app}^{i,i} = k_t^{1,1}\ i^{-\alpha_s} \qquad \text{for } i < i_{SL} \qquad \text{(B5)}$$

$$k_{t,app}^{i,i} = k_t^{1,1}\ i_{SL}^{(\alpha_L - \alpha_s)}\ i^{-\alpha_L} \qquad \text{for } i \geq i_{SL} \qquad \text{(B6)}$$

For $i \geq i_{gel}$

$$k_{t,app}^{i,i} = k_t^{1,1}\, i_{gel}^{(\alpha_{gel}-\alpha_s)}\, i^{-\alpha_{gel}} \qquad \text{for } i < i_{SL} \tag{B7}$$

$$k_{t,app}^{i,i} = k_t^{1,1}\, i_{SL}^{(\alpha_L-\alpha_s)}\, i_{gel}^{(\alpha_{gel}-\alpha_L)}\, i^{-\alpha_{gel}} \qquad \text{for } i \geq i_{SL} \tag{B8}$$

with $k_t^{1,1}$ the (apparent) termination rate coefficient for radicals with chain length 1, α_s the exponent for termination for termination of short chains in dilute solution, α_L the exponent for long chains in dilute solution, α_{gel} the exponent for chains in the gel regime, i_{SL} the crossover chain length between short- and long-chain behavior, i_{gel} the chain length at the onset of the gel-effect.

An overview of these parameters can be found in Table B2.

Table B2*: Parameters used for the composite k_t model with MMA as monomer; m_p: polymer mass fraction*

$\mathbf{k_t^{1,1}}$	$\boldsymbol{\alpha_S}$	$\mathbf{i_{SL}}$	$\boldsymbol{\alpha_L}$	$\boldsymbol{\alpha_{gel}}$	$\mathbf{i_{gel}}$
$1.3\ 10^9$	0.65	100	0.15	$1.66m_p$-0.06	$0.53m_p^{-2.5}$

As the complete chain length distribution of the macroradicals is not calculated in the frame of the present work, Equation (B5)-(B8) are calculated using the number average chain length of the macroradical species.

The (apparent) rate coefficients for the termination by recombination and disproportionation can then be calculated by means of f_{tc} = 0.32, [7–9] the fraction of termination occurring by recombination:

$$k_{tc,app} = f_{tc} k_{t,app} \tag{B9}$$

$$k_{td,app} = (1 - f_{tc}) k_{t,app} \tag{B10}$$

B.4 Calculation of the apparent degenerative RAFT transfer rate coefficient

The apparent degenerative RAFT transfer rate coefficient can be calculated using the encounter pair model as described by D'hooge *et al.*[10]:

$$k_{tr,app} = \left(\frac{1}{k_{tr,chem}} + \frac{2}{k_{tr,diff}}\right)^{-1} \quad \text{(B11)}$$

with $k_{tr,app}$ the apparent RAFT transfer rate coefficient, $k_{tr,che}$ the intrinsic RAFT transfer rate coefficient (see Table 1 in Chapter 4) and $k_{tr,diff}$ the diffusional contribution for RAFT transfer.

The diffusional term was calculated using the equations of the composite k_t model[6] as explained in Section B3 with the adjustment of $k_t^{1,1}$, i_{SL} and α_s as tuned by comparison with the available experimental data of the bulk polymerization of MMA mediated by CPDB and initiated by 2,2-azobis(2-methyl-propionitrile) (AIBN) at 333K. A similar approach was considered by De Rybel *et al.* in their bulk study.[2]

An overview of the parameters used for the diffusional contribution for RAFT transfer in the encounter pair model as calculated using the composite k_t model can be found in Table B3.

Table B3*: Parameters used for the calculation of the diffusional contribution for RAFT transfer using the composite k_t model with MMA as monomer; m_p: polymer mass fraction*

$k_t^{1,1}$	α_S	i_{SL}	α_L	α_{gel}	i_{gel}
$6.3\ 10^8$	2.1	40	0.15	$1.66m_p$-0.06	$0.53m_p^{-2.5}$

B.5 Demonstration of kinetic insignificance of chain transfer to monomer in the miniemulsion RAFT polymerization experiments and of transfer coefficient $k_{-tr,0}$ in the bulk RAFT polymerization experiment

Chain transfer of a growing macroradical with a monomer molecule makes the total reaction mechanism of RAFT miniemulsion polymerization much more complex as not only a new compartmentalized species, namely the monomer radical, needs to be considered but exit of this monomeric radical extends the aqueous reaction scheme as well. In order to investigate the impact of chain transfer to monomer and subsequent exit of the formed monomeric radical on the polymer properties, these reactions were added to the developed kinetic model and the model parameters are shown in Table B4.

Table B4: Overview of reactions and rate coefficients related to chain transfer of macroradicals ($R_{i,p}^{\bullet}$) to monomer (M_p) inside the polymer particles. Exit of the formed monomeric radical ($M_p^{\bullet}$) is either taken into account ($k_{exitM} = 10^8 L\, mol^{-1} s^{-1}$) or neglected ($k_{exitM} = 0\, L\, mol^{-1} s^{-1}$) as shown in Figure B2.

Reaction	Equation	k ((L mol^{-1}) s^{-1})	ref
Chain transfer to monomer	$R_{i,p}^{\bullet} + M_p \xrightarrow{k_{trM}} M_p^{\bullet} + P_{i,p}$	$1.0\ 10^{-2}$	11
Exit[(a)] of $\boldsymbol{M_p^{\bullet}}$	$M_p^{\bullet} \xrightarrow{k_{exitM}} M_{aq}^{\bullet}$	$0\ or\ 10^8$	Chapter 4
Chain initiation	$M_p^{\bullet} + M_p \xrightarrow{k_{pM_p}} R_{2,p}^{\bullet}$	$8.2\ 10^2$	(b)
	$M_{aq}^{\bullet} + M_{aq} \xrightarrow{k_{pM_{aq}}} R_{2,aq}^{\bullet}$	$8.2\ 10^2$	(b)

(a) Rate coefficient expressed in units s^{-1}; (b) considered to be equal to k_p as a first approximation

As shown in Figure B2, under the conditions investigated in Chapter 4, chain transfer to monomer and monomeric radical exit do not significantly contribute to the average polymer properties. Consequently, these reactions were neglected in the kinetic model discussed in Chapter 4.

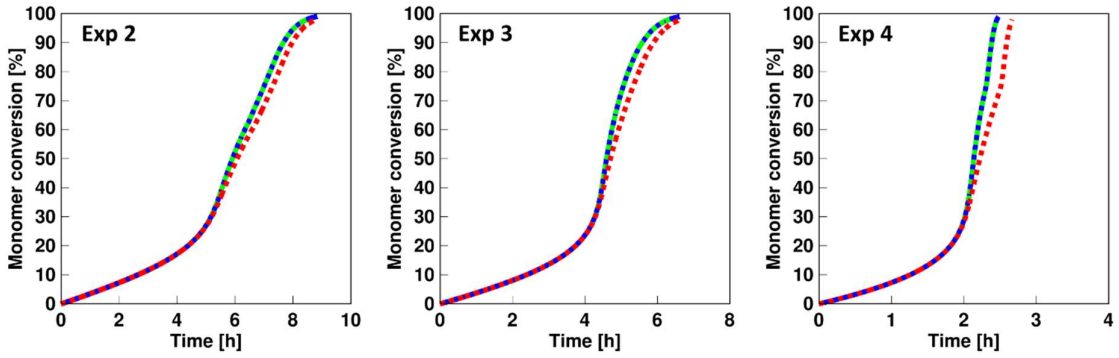

***Figure B2**: Influence of chain transfer to monomer and monomeric radical exit on the conversion plots of Experiment ME1 (left), ME2 (middle) and ME3 (right), experimental conditions as mentioned in Table 2 (Chapter 4). Influence on number average molar mass and dispersity as a function of conversion are similar and not shown for simplicity. Green:* $k_{trM} = 0\ L\ mol^{-1}s^{-1}$ *and* $k_{ExitM} = 0\ s^{-1}$*, blue:* $k_{trM} = 1.0\ 10^{-2}\ L\ mol^{-1}s^{-1}$ *and* $k_{ExitM} = 0\ s^{-1}$*, red: :* $k_{trM} = 1.0\ 10^{-2}\ L\ mol^{-1}s^{-1}$ *and* $k_{ExitM} = 10^{8}\ s^{-1}$*, other rate coefficients as mentioned in Table 1 (Chapter 4).*

The transfer coefficient $k_{-tr,0}$ is defined as the rate coefficient of the reaction of a RAFT leaving group radical R_0 and a dormant macrospecies R_iX (i≥1), resulting in the initial RAFT agent R0X and a macroradical R_i:

$$R_0^{\bullet} + R_iX \xrightarrow{k_{-tr,0}} R_0X + R_i^{\bullet}$$

Figure B3 shows the average polymer properties as a function of time or monomer conversion obtained by simulations with $k_{-tr,0}$=0 L mol^{-1} s^{-1} (green) and $k_{-tr,0}$=100* $k_{tr,0}$ (red, other parameters as in Table 1 in Chapter 4, Exp B1 in Table 2 in Chapter 4). As no difference in the prediction of the average polymer properties can be observed, $k_{-tr,0}$ can be considered to be kinetically insignificant and a value of 0 L mol^{-1}s^{-1} can be used for the simulations. R_0 radicals

will dominantly react with monomer, initiating new growing macroradicals, or with other (macro)radicals, forming new dead (macro)species.

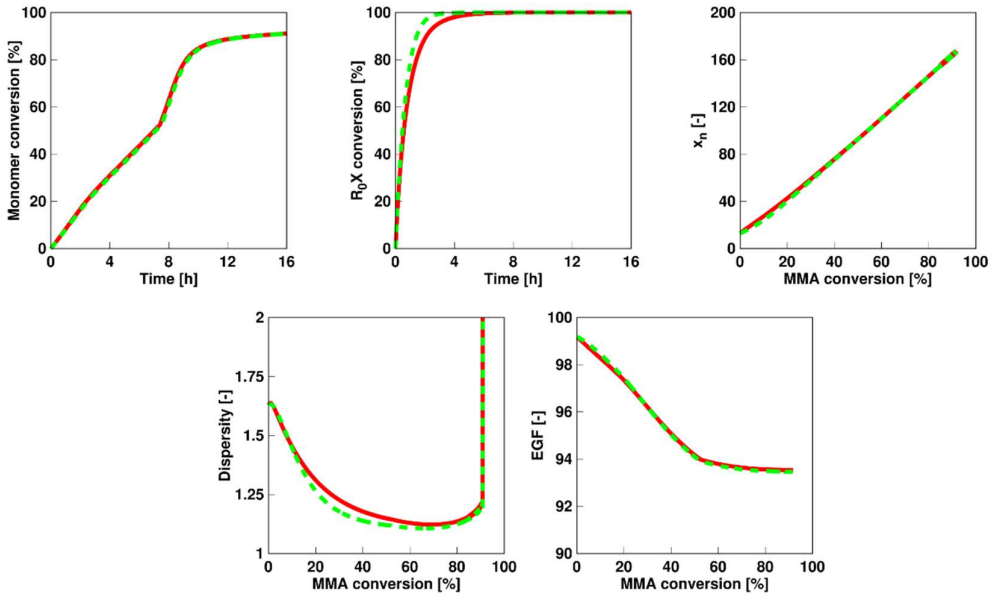

Figure B3*: The average polymer properties as a function of time obtained by simulations with* $k_{-tr,0}$*=0 L mol*$^{-1}$ *s*$^{-1}$ *(green) and* $k_{-tr,0}$*=100* *$k_{tr,0}$ *(red); other parameters as in Table 1 in Chapter 4, Exp B1 in Chapter 4).*

B.6 Overview of the continuity equations for the integration of the higher order moments equations

The number average chain length and the dispersity can be modeled as a function of polymerization time if the higher order moments equations are solved (similar approach as covered in Bentein *et al.*[12] and Van Steenberge *et al.*[13]) . Below, an overview of all relevant equations is given with $[R_iX_p], [R_0X_p], [P_{i,p}], [R_{i,p}]$ the concentration in the particles of the dormant macrospecies (with chain length *i*), initial RAFT agent, dead species and macroradicals; $[R'_{2,aq}]$ and $[R_{4,aq}]$ concentration in the aqueous phase of radicals with chain length 2 initiated by an R_0 group and radicals with chain length 4 initiated by an initiator fragment; $\bar{n}(R_i)$ and $\bar{n}(R_0)$ the average number of macroradicals and RAFT leaving group

radicals per particle; $\tau_{0/1/2}, \mu_{0/1/2}, \lambda_{1/2}$ the zeroth, first and second moment of the dormant species, the zeroth, first and second moment of the dead species and the first and second moment of the macroradicals; $k_p, k_{pR_0}, k_{tr0}, k_{tr}, k_{tc,app}, k_{td,app}, k_{tc,0}, k_{entr\ \ _2'}, k_{entry\ _4}$,the rate coefficients for propagation, chain initiation by R_0, the RAFT transfer with the initial RAFT agent, the RAFT transfer with dormant macrospecies, the apparent termination by recombination, the apparent termination by disproportionation, the termination between macroradicals and R_0 , the entry of an oligomer with chain length 2 initiated by R_0, the entry of an oligomer with chain length 4 initiated by R_0; N_a, v_p, V_{aq} Avogadro's constant, the volume of a particle, the volume of the aqueous phase. The extra moment equations with compartmentalization effects accounted via the direct link with $\bar{n}(R_i)$ and $\bar{n}(R_0)$:

$$\begin{aligned}\frac{d\lambda_1}{dt} &= \frac{d\sum_i i[R_i]}{dt} \\ &= [M_p]\left(k_p\frac{\bar{n}(R_i)}{N_a v_p} + k_{pR_0}\frac{\bar{n}(R_0)}{N_a v_p}\right) + 2k_{entryR_2'}N_p\frac{[R'_{2,aq}]}{N_A V_{aq}} \\ &+ 4k_{entryR_4}N_p\frac{[R_{4,aq}]}{N_A V_{aq}} + k_{tr}\left(\frac{\bar{n}(R_i)}{N_a v_p}\tau_1 - \lambda_1\tau_0\right) \\ &- \left(k_{tc,app,c} + 2k_{td,app,c}\right)\frac{\bar{n}(R_i)}{N_a v_p}\lambda_1 - k_{tc,0,c}\lambda_1\frac{\bar{n}(R_0)}{N_a v_p} \\ &- k_{tr,0}\lambda_1[R_0X_p]\end{aligned} \tag{B12}$$

$$\frac{d\lambda_2}{dt} = \frac{d\sum_i i^2[R_i]}{dt}$$

$$= [M_p]\left(k_p \frac{\bar{n}(R_i)}{N_a v_p} + 2k_p\lambda_1 + k_{pR_0}\frac{\bar{n}(R_0)}{N_a v_p}\right) + 4k_{entryR_2'}N_p\frac{[R'_{2,aq}]}{N_A V_{aq}}$$

$$+ 16k_{entryR_4}N_p\frac{[R_{4,aq}]}{N_A V_{aq}} + k_{tr}\left(\frac{\bar{n}(R_i)}{N_a v_p}\tau_2 - \lambda_2\tau_0\right) \quad \text{(B13)}$$

$$- \left(k_{tc,app,c} + 2k_{td,app,c}\right)\frac{\bar{n}(R_i)}{N_a v_p}\lambda_2 - k_{tc,0,c}\lambda_2\frac{\bar{n}(R_0)}{N_a v_p}$$

$$- k_{tr,0}\lambda_2[R_0X_p]$$

$$\frac{d\tau_1}{dt} = \frac{d\sum_i i[R_iX_p]}{dt} = k_{tr,0}\lambda_1[R_0X_p] + k_{tr}\left(\lambda_1\tau_0 - \frac{\bar{n}(R_i)}{N_a v_p}\tau_1\right) \quad \text{(B14)}$$

$$\frac{d\tau_2}{dt} = \frac{d\sum_i i^2[R_iX_p]}{dt} = k_{tr,0}\lambda_2[R_0X_p] + k_{tr}\left(\lambda_2\tau_0 - \frac{\bar{n}(R_i)}{N_a v_p}\tau_2\right) \quad \text{(B15)}$$

$$\frac{d\mu_1}{dt} = \frac{d\sum_{i\geq 1} i[P_{i,p}]}{dt} = \left(k_{tc,app,c} + 2k_{td,app,c}\right)\frac{\bar{n}(R_i)}{N_a v_p}\lambda_1 + k_{tc,0,c}\lambda_1\frac{\bar{n}(R_0)}{N_a v_p} \quad \text{(B16)}$$

$$\frac{d\mu_2}{dt} = \frac{d\sum_{i\geq 1} i^2[P_{i,p}]}{dt} = \left(k_{tc,app,c} + 2k_{td,app,c}\right)\frac{\bar{n}(R_i)}{N_a v_p}\lambda_2 + k_{tc,0,c}\lambda_2\frac{\bar{n}(R_0)}{N_a v_p} \quad \text{(B17)}$$

B.7 Comments related to the entry/exit rate coefficients for the RAFT miniemulsion polymerization of MMA

The kinetic description of RAFT miniemulsion is complicated by the possible partitioning of small molecules resulting in the necessity of the consideration of exit and entry events. To a first approximation, only R_0 exit and entry rate coefficients are considered. Both the entry and exit rate coefficient are dependent on the average polymer particle diameter (d_p) and interrelated by the partitioning coefficient Γ:[12,13]

$$k_{entry R_0} = C_{entry} N_A D_{R_0,aq} d_p \quad \text{(B18)}$$

$$k_{exit,R_0} = C_{exit} D_{R_0,or} d_p^{-2} \quad \text{(B19)}$$

$$\Gamma = \frac{[R_{0,org}]}{[R_{0,aq}]} = \frac{6 C_{entry} D_{R_0,aq}}{\pi C_{exit} D_{R_0,or}} \quad \text{(B20)}$$

with N_A the Avogadro constant (mol^{-1}), $D_{R_0,aq/or}$ the diffusion coefficient of R_0 in the organic/aqueous phase (dm^2 s^{-1}) and $C_{entry/exit}$ the proportionality constants for R_0 exit/entry from/into a polymer particle (-)

The particle dependency of the entry and exit rate coefficient is visualized in Figure B4.

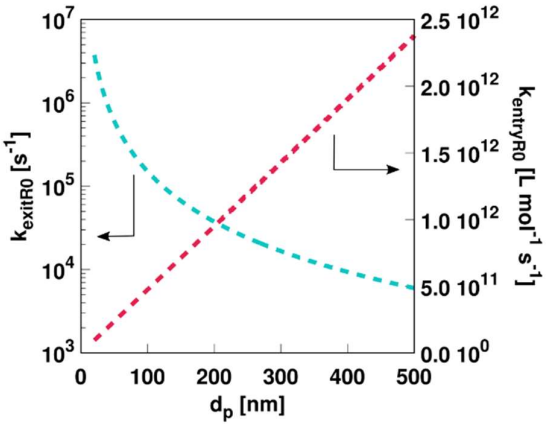

Figure B4*: The rate coefficient of entry and exit of R0 as a function of particle size, as calculated by means of Equation B19 and B20.*

In Chapter 4, a typical value of 10 was used for the partitioning coefficient (Γ).[14,15] The tuning of $C_{exit} D_{R_0,or} = 1.5\ 10^{-7}$dm-2 s-1 allowed the calculation of $C_{entry} D_{R_0,aq} = 7.9\ 10^{-7}$ dm-2 s-1 (cf. Figure 4 in Chapter 4)

***Table B5**: Entry and exit rate coefficient for R_0 from/into a polymer particle with diameter d_p in the miniemulsion of MMA at 333K.*

Exp	$d_p\ (nm)$	$k_{exitR_0}(s^{-1})$	$k_{entryR_0}(L\ mol^{-1}s^{-1})$
ME1	$2.0\ 10^2$	$3.8\ 10^4$	$9.5\ 10^{11}$
ME2	$1.4\ 10^2$	$7.7\ 10^4$	$6.6\ 10^{11}$
ME3	$1.0\ 10^2$	$1.5\ 10^5$	$4.7\ 10^{11}$

A sensitivity analysis of the exit and entry rate coefficients was performed and can be found below. This shows that the simulated output mainly depends on k_{exit,R_0} and not k_{entryR_0}, justifying the fitting of the former and calculation of the latter.

a. Sensitivity analysis of $C_{exit}D_{R_0,or}$ with $C_{entry}D_{R_0,aq} = 7.9\ 10^{-7}\ dm^2s^{-1}$

***Table B6**: Overview of the influence of $\boldsymbol{C_{exit}D_{R_0,or}}$ on the exit rate coefficient of $\boldsymbol{R_0}$ ($\boldsymbol{k_{exitR_0}}$) and the partitioning coefficient (Γ) with $\boldsymbol{C_{entry}D_{R_0,aq} = 7.9\ 10^{-7}\ dm^2s^{-1}}$ for the miniemulsion experiments mentioned in Table 2 (Chapter 4).*

Exp	$d_p\ (nm)$	$C_{exit}D_{R_0,or}(dm^2s^{-1})$	$k_{exitR_0}(s^{-1})$	$k_{entryR_0}(L\ mol^{-1}s^{-1})$	Γ
ME1	$2.0\ 10^2$	$1.5\ 10^{-6}$	$3.8\ 10^5$	$9.5\ 10^{11}$	1.0
ME1	$2.0\ 10^2$	$1.5\ 10^{-7}$	$3.8\ 10^4$	$9.5\ 10^{11}$	10.0
ME1	$2.0\ 10^2$	$1.5\ 10^{-8}$	$3.8\ 10^3$	$9.5\ 10^{11}$	100.0
ME2	$1.4\ 10^2$	$1.5\ 10^{-6}$	$7.7\ 10^5$	$6.6\ 10^{11}$	1.0
ME2	$1.4\ 10^2$	$1.5\ 10^{-7}$	$7.7\ 10^4$	$6.6\ 10^{11}$	10.0
ME2	$1.4\ 10^2$	$1.5\ 10^{-8}$	$7.7\ 10^3$	$6.6\ 10^{11}$	100.0
ME3	$1.0\ 10^2$	$1.5\ 10^{-6}$	$1.5\ 10^6$	$4.7\ 10^{11}$	1.0
ME3	$1.0\ 10^2$	$1.5\ 10^{-7}$	$1.5\ 10^5$	$4.7\ 10^{11}$	10.0
ME3	$1.0\ 10^2$	$1.5\ 10^{-8}$	$1.5\ 10^4$	$4.7\ 10^{11}$	100.0

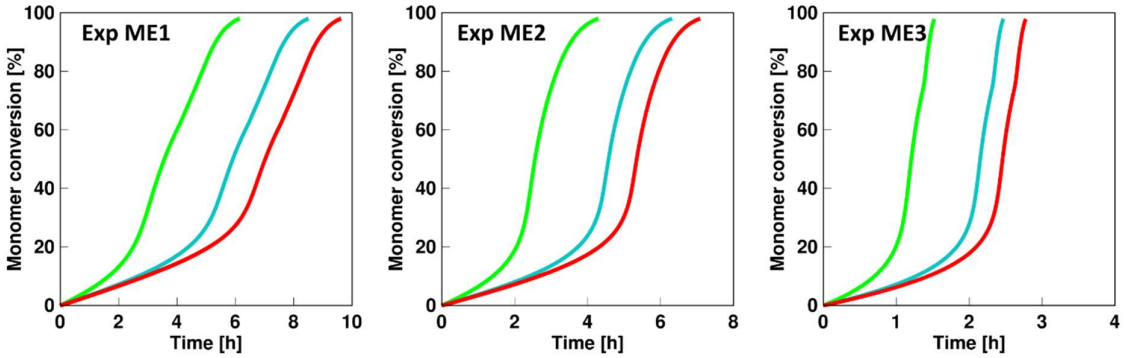

***Figure B5**: Influence of $C_{exit}D_{R_0,or}$ with $C_{entry}D_{R_0,aq} = 7.9\ 10^{-7}\ dm^2s^{-1}$ on the conversion plots of Experiment ME1 (left), ME2 (middle) and ME3 (right), experimental conditions as mentioned in Table 2 (Chapter 4). Green: $C_{exit}D_{R_0,or} = 1.5\ 10^{-8}dm^2s^{-1}$, Red: $C_{exit}D_{R_0,or} = 1{,}5\ 10^{-6}dm^2s^{-1}$, Blue: $C_{exit}D_{R_0,or} = 1{,}5\ 10^{-7}dm^2s^{-1}$. Exit and entry rate coefficients as mentioned in Table B6, other rate coefficients as mentioned in Table 1 (Chapter 4).*

b. Sensitivity analysis of $C_{entry}D_{R_0,aq}$ with $C_{exit}D_{R_0,or} = 1.5\ 10^{-7} dm^2\ s^{-1}$

***Table B7**: Overview of the influence of $\boldsymbol{C_{entry}D_{R_0,aq}}$ on the entry rate coefficient of $\boldsymbol{R_0}$ ($\boldsymbol{k_{entry,R_0}}$) and the partitioning coefficient (Γ) with $\boldsymbol{C_{exit}D_{R_0,or} = 1.5\ 10^{-7}\ dm^2 s^{-1}}$ for the miniemulsion experiments mentioned in Table 2 (Chapter 4).*

Exp	$d_p\ (nm)$	$C_{entry}D_{R_0,aq}(\ dm^2 s^{-1})$	$k_{exitR_0}(s^{-1})$	$k_{entryR_0}(L\ mol^{-1}s^{-1})$	Γ
ME1	$2.0\ 10^2$	$7.9\ 10^{-9}$	$3.8\ 10^4$	$9.5\ 10^9$	0.1
ME1	$2.0\ 10^2$	$7.9\ 10^{-7}$	$3.8\ 10^4$	$9.5\ 10^{11}$	10.0
ME1	$2.0\ 10^2$	$7.9\ 10^{-5}$	$3.8\ 10^4$	$9.5\ 10^{13}$	1000.0
ME2	$1.4\ 10^2$	$7.9\ 10^{-9}$	$7.7\ 10^4$	$6.6\ 10^9$	0.1
ME2	$1.4\ 10^2$	$7.9\ 10^{-7}$	$7.7\ 10^4$	$6.6\ 10^{11}$	10.0
ME2	$1.4\ 10^2$	$7.9\ 10^{-5}$	$7.7\ 10^4$	$6.6\ 10^{13}$	1000.0
ME3	$1.0\ 10^2$	$7.9\ 10^{-9}$	$1.5\ 10^5$	$4.7\ 10^9$	0.1
ME3	$1.0\ 10^2$	$7.9\ 10^{-7}$	$1.5\ 10^5$	$4.7\ 10^{11}$	10.0
ME3	$1.0\ 10^2$	$7.9\ 10^{-5}$	$1.5\ 10^5$	$4.7\ 10^{13}$	1000.0

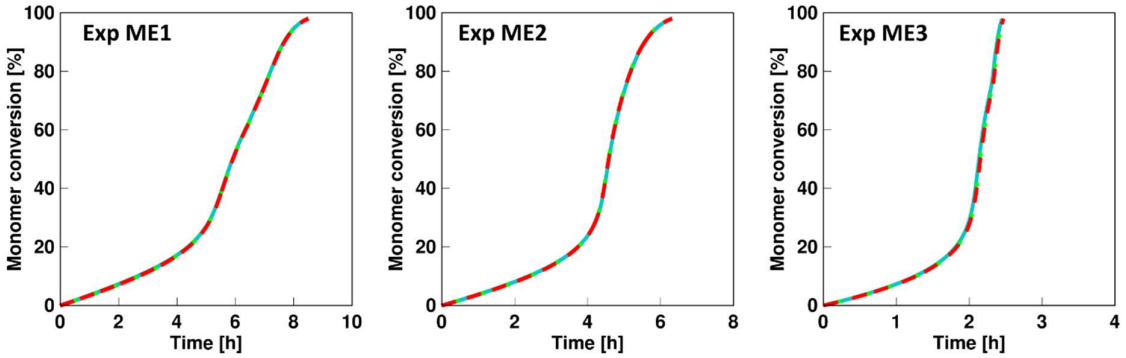

***Figure B6**: Influence of $C_{entry}D_{R_0,aq}$ with $C_{exit}D_{R_0,or} = 1.5\ 10^{-7}\ dm^2s^{-1}$ on the conversion plots of Experiment ME1 (left), ME2 (middle) and ME3 (right), experimental conditions as mentioned in Table 2 (Chapter 4). Green: $C_{entry}D_{R_0,aq} = 7.9\ 10^{-9}\ dm^2s^{-1}$, Red: $C_{entry}D_{R_0,aq} = 7.9\ 10^{-7} dm^2s^{-1}$, Blue: $C_{entry}D_{R_0,aq} = 7.9\ 10^{-5dm^2s^{-1}}$. Exit and entry rate coefficients as mentioned in Table B6, other rate coefficients as mentioned in Table 1 (Chapter 4). All lines are coinciding.*

B.8 Investigation of invalidity of zero-one kinetics for experiment ME1

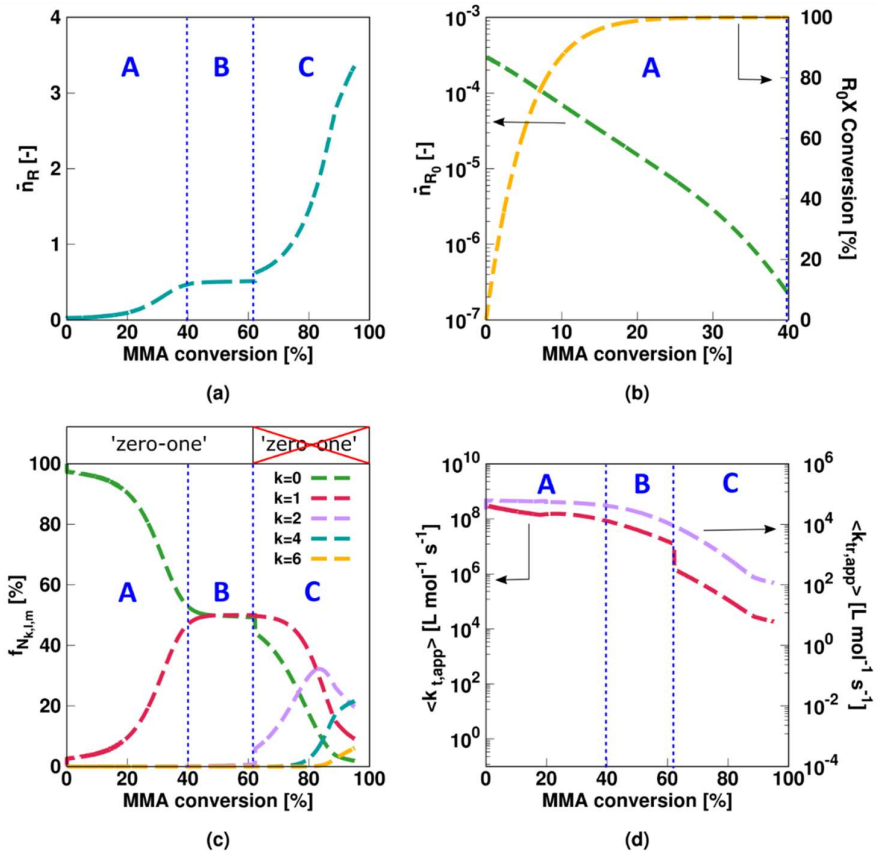

***Figure B7**: Results with complete model (diffusional limitations on termination and RAFT transfer) for the average number of macroradicals per particle ($\bar{n}_R$, (a), blue), average number of leaving group radicals per particle ($\bar{n}_{R_0}$, (b), green), R_0X conversion ((b), orange), fraction of particles with 0 up to 6 macroradicals present (c), average apparent overall termination rate coefficient ($\langle k_{t,app} \rangle = \langle k_{tc,app} \rangle + \langle k_{td,app} \rangle$, (d), red, for calculation see Section B3 in Appendix B) and the average apparent transfer rate coefficient ($\langle k_{tr,app} \rangle$, (d), purple, for calculation see Section B4 in Appendix B) as a function of MMA conversion for Experiment ME1 (conditions as mentioned in Table 2 of Chapter 4 and calculated with model parameters given in Table 1 of Chapter 4.)*

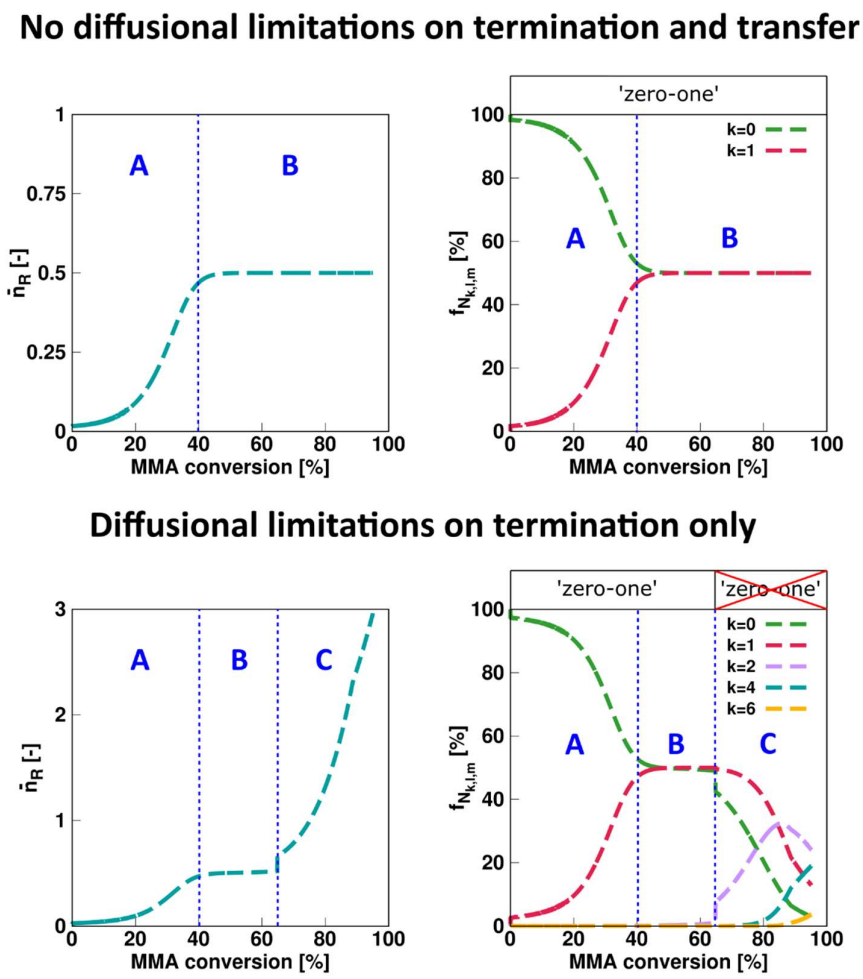

***Figure B8**: Top row: the average number of macroradicals per particle ($\bar{n}_{R_i}$blue) and the average number of leaving group radicals per particle ($\bar{n}_{R_0}$) in case intrinsic kinetics are assumed for ME1 in Table 2 in Chapter 4 (no diffusional limitations on termination and RAFT transfer); bottom row: updates in case diffusional limitations on termination are accounted for. Results imply that the invalidity of zero-one kinetics is due to diffusional limitation on termination only for this condition, similar to results of ME2 in Table 1 (see Figure 10 in Chapter 4).*

B.9 Influence of TCL ([MMA]$_0$/[CPDB]$_0$) on the RAFT agent conversion and probability of exit of R_0

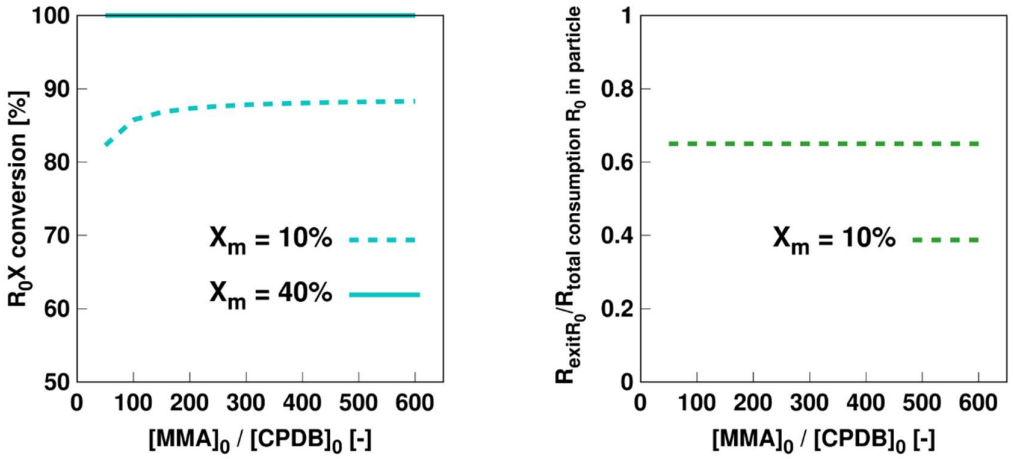

Figure B9: *Influence of TCL ([MMA]$_0$/[CPDB]$_0$) on the RAFT agent conversion and the ratio of the rate of the exit of the leaving group radicals to the overall consumption (or disappearance) rate in all particles; d_p = 100 nm, all other experimental conditions as in experiment ME1 in Table 2 of Chapter 4 except for $m_0(R_0X)$; X_m=10% (dashed lines) and X_m=40% (full lines, only shown for left Figure as R_0X conversion is 100%); model parameters as given in Table 1 of Chapter 4.*

B.10 Reaction probability of macroradicals in particles containing two macroradicals or one macroradical and one leaving group radical

The reaction probabilities involving a macroradical in a particle containing one macroradical and one leaving group radical and a particle containing two macroradicals are shown in Figure B10. Although propagation has the highest probability of occurring, after a short interval, the macroradical will terminate with either a leaving group radical (left) or another macroradical (right). With the former having a higher reaction probability compared to the latter due to the chain length dependent apparent termination rate coefficient.

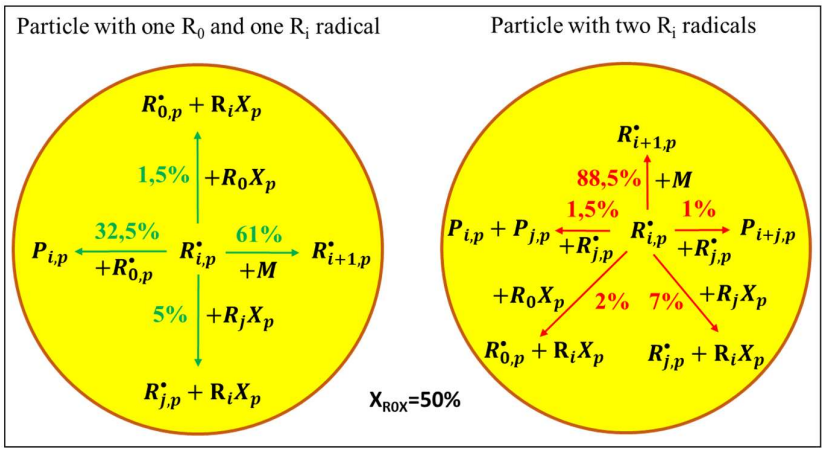

***Figure B10**: Reaction probabilities involving the macroradical in particles with one macroradical and a leaving group radical (left) and two macroradicals (right); situation at 50% conversion of initial RAFT agent (X_m = 3.5); ME3 in Table 2 of Chapter 4; parameters Table 1 of Chapter 4.*

Although the termination probabilities may seem to be quite high in these particles, it is important to realize that the overall termination probability during a RAFT miniemulsion polymerization are much lower due to the segregation effect as shown in Figure B11 (left). The termination probabilities in a particle containing two macroradicals (purple) and in a particle containing a macroradical and a leaving group radical (orange) are higher than the termination probability in a comparable bulk experiment (red), but the overall termination probability (blue) is much lower as most of the particles will contain no (black) or only one macroradical (grey) and particles in which termination can occur are in a great minority as shown in Figure B11 (right).

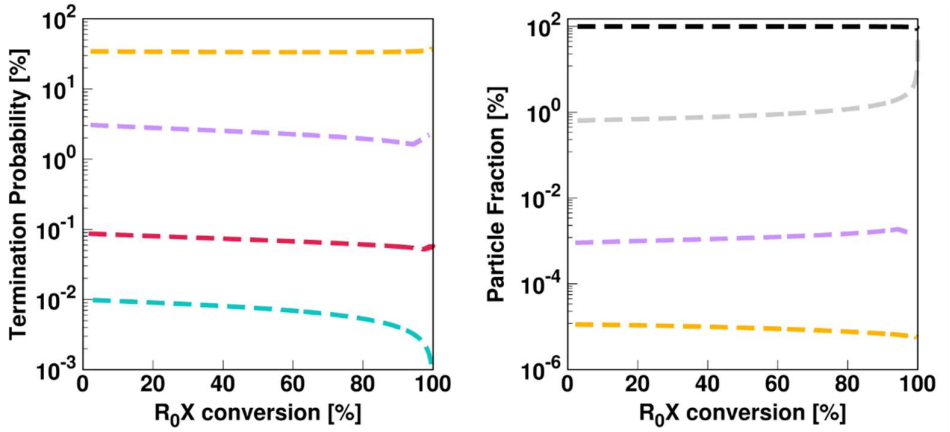

***Figure B11**: Left: Termination probabilities in bulk RAFT polymerization (red) and in RAFT miniemulsion overall (blue), in particles containing two macroradicals (purple) and in particles containing a macroradical and a leaving group radical (orange); Right: Fraction of particles containing no radicals (black), one macroradical (grey), two macroradicals (purple) and one macroradical and one leaving group radical (orange); B1 and ME3 in Table 2 of Chapter 4; parameters Table 1 of Chapter 4.*

B.11 Extra information regarding lower EGF with increasing TCL (Figure 13c in Chapter 4)

Increasing the TCL implies a lower amount of initial R0X used in the RAFT miniemulsion. As a result, as shown in Figure B12 left, a lower amount of dormant macrospecies are formed. Increasing the TCL also results in a reduction of the dead macrospecies as well (Figure B12 right). Nevertheless, as clearly visible in Figure B12, the decrease of the concentration of the dormant macrospecies with increasing TCL outweighs the decrease of the concentration of the dead species resulting in a decrease of the EGF as shown in Figure 13c in Chapter 4.

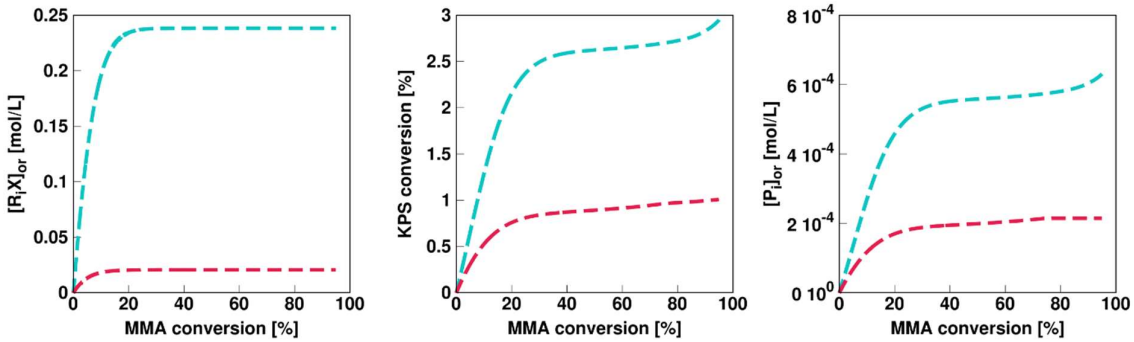

***Figure B12**: The total concentration of dormant macrospecies in all particles (left), the KPS (conventional initiator) conversion and the concentration of all dead macrospecies (right) as a function of MMA conversion for a TCL of 50 (blue) and 600 (red))); d_p = 100 nm, all other experimental conditions as in experiment ME1 in Table 2 of Chapter 4 except for $\boldsymbol{m_0(R_0X)}$; model parameters as given in Table 1 of Chapter 4.*

B.12 Influence of targeted chain length (TCL) on the monomer conversion

As shown in Figure B13, a lower TCL leads to longer polymerization times as the retardation effect at low monomer conversion due to R_0 exit is prolonged as more initial R_0X present results in more R_0 being generated in general.

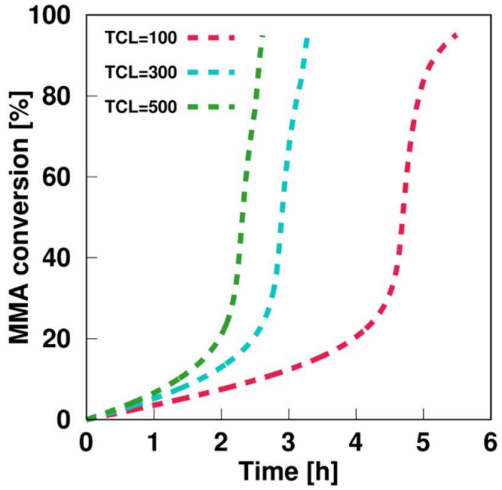

***Figure B13**: Influence of TCL on the monomer conversion; TCL = 100 (red), 300 (blue) and 500 (green); d_p = 100 nm, all other experimental conditions as in experiment ME1 in Table 2 of Chapter 4 except for $m_0(R_0X)$; model parameters as given in Table 1 of Chapter 4.*

B.13 Influence of the (average) particle size (d_p) on the total number of particles

As shown in Figure B14, if only the (average) particle size (d_p) is varied and the total volume of the organic phase is constant, the total number of particles decreases with increasing particle size.

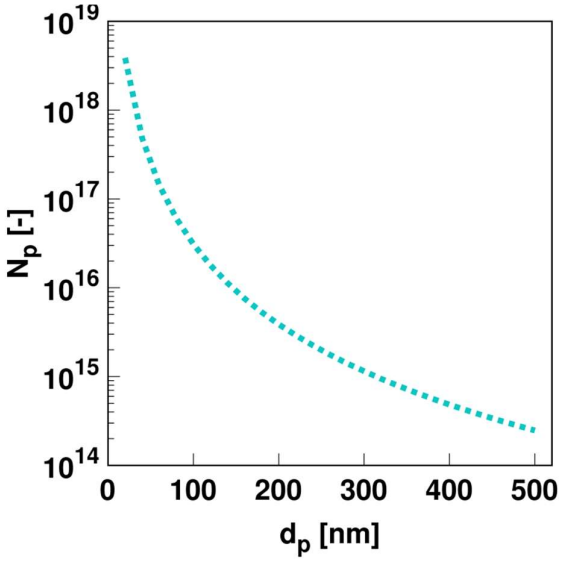

***Figure B14**: Influence of (average) particle size (d_p) on the total number of particles present; Experimental conditions as in experiment ME1 in Table 2 of Chapter 4 (targeted chain length of 192)*

B.14 References:

1 Buback, M.; Huckestein, B.; Kuchta, F.; Russell, G. T. Initiator Efficiencies in 2,2'-Azoisobutyronitrile-Initiated Freeradical Polymerizations of Styrene. *Macromol. Chem. Phys.* **1994**, *195*, 2117–2140.

2 De Rybel, N.; Van Steenberge, P. H. M.; Reyniers, M.-F.; Barner-Kowollik, C.; D'hooge, D. R.; Marin, G. B. An Update on the Pivotal Role of Kinetic Modeling for the Mechanistic Understanding and Design of Bulk and Solution RAFT Polymerization. *Macromol. Theory Simulations* **2017**, *26*, 1600048.

3 Heberger, K.; Fischer, H. Rate Constants for the Addition of the 2-Cyano-2-Propyl Radical Alkenes in Solution. *Int. J. Chem. Kinet.* **1993**, *25* (4), 249–263.

4 Buback, M.; Gilbert, R. G.; Hutchinson, R. A.; Klumberman, B.; Kuchta, F.-D.; Manders, B. G.; O'Driscoll, K. F.; Russell, G. T.; Schweer, J. Critically Evaluated Rate Coefficients for Free-Radical Propagation Rate Coefficient for Styrene. *Macromol. Chem. Phys.* **1995**, *196*, 3267–3280.

5 Beuermann, S.; Buback, M. Rate Coefficients of Free-Radical Polymerization Deduced from Pulsed Laser Experiments. *Prog. Polym. Sci.* **2002**, *27* (2), 191–254.

6 Johnston-Hall, G.; Monteiro, M. J. Bimolecular Radical Termination: New Perspectives and Insights. *J. Polym. Sci. Part a-Polymer Chem.* **2008**, *46* (10), 3155–3176.

7 Fierens, S. K.; Van Steenberge, P. H. M.; Reyniers, M. F.; Marin, G. B.; D'hooge, D. R. How Penultimate Monomer Unit Effects and Initiator Influence ICAR ATRP of N-Butyl Acrylate and Methyl Methacrylate. *AIChE J.* **2017**, *63* (11), 4971–4986.

8 Nakamura, Y.; Yamago, S. Termination Mechanism in the Radical Polymerization of Methyl Methacrylate and Styrene Determined by the Reaction of Structurally Well-Defined Polymer End Radicals. *Macromolecules* **2015**, *48* (18), 6450–6456.

9 Buback, M.; Günzler, F.; Russell, G. T.; Vana, P. Determination of the Mode of Termination in Radical Polymerization via Mass Spectrometry. *Macromolecules* **2009**, *42* (3), 652–662.

10 D'hooge, D. R.; Reyniers, M. F.; Marin, G. B. The Crucial Role of Diffusional Limitations in Controlled Radical Polymerization. *Macromol. React. Eng.* **2013**, *7*, 362–379.

11 Moad, G.; Solomon, D. H. *The Chemistry of Radical Polymerization*; Elsevier, 2006.

12 Bentein, L.; D'hooge, D. R.; Reyniers, M.-F.; Marin, G. B. Kinetic Modeling of Miniemulsion Nitroxide Mediated Polymerization of Styrene: Effect of Particle Diameter and Nitroxide Partitioning up to High Conversion. *Polymer (Guildf).* **2012**, *53* (3), 681–693.

13 Van Steenberge, P. H. M.; D.R., D.; Reyniers, M. F.; Marin, G. B.; Cunningham, M. F. 4-Dimensional Modeling Strategy for an Improved Understanding of Miniemulsion NMP of Acrylates Initiated by SG1-Macroinitiator. *Macromolecules* **2014**, *47*, 7732–7741.

14 Shang, Y.; Shan, G.-R. IBN Partition between St Monomer/Polymer and Water and Its Application in Miniemulsion Polymerization Initiated by AIBN. *AIChE J.* **2012**, *58* (10), 3135–3143.

15 Shang, Y.; Shan, G.; Pan, P. Kinetic and Molecular Weight Modeling of Miniemulsion Polymerization Initiated by Oil-Soluble Initiators. *Macromol. Chem. Phys.* **2015**, *216*, 884–893.

Appendix C: Supporting info for Chapter 5

C.1 Calculation of the average apparent termination rate coefficient

The diffusion-controlled mechanism of bimolecular termination in radical polymerization can be accurately described using the composite k_t model (RAFT-CLD-T model).[1] This model allows to calculate an apparent homotermination rate coefficient ($k_{t,app}^{i,i}$; i=chain length) dependent on the chain length i and the polymer mass fraction m_p (and thus the monomer conversion X_m):

For $i < i_{gel}$

$$k_{t,app}^{i,i} = k_t^{1,1}\, i^{-\alpha_s} \qquad \text{for } i < i_{SL} \tag{C1}$$

$$k_{t,app}^{i,i} = k_t^{1,1}\, i_{SL}^{(\alpha_L-\alpha_s)}\, i^{-\alpha_L} \qquad \text{for } i \geq i_{SL} \tag{C2}$$

For $i \geq i_{gel}$

$$k_{t,app}^{i,i} = k_t^{1,1}\, i_{gel}^{(\alpha_{gel}-\alpha_s)}\, i^{-\alpha_{gel}} \qquad \text{for } i < i_{SL} \tag{C3}$$

$$k_{t,app}^{i,i} = k_t^{1,1}\, i_{SL}^{(\alpha_L-\alpha_s)}\, i_{gel}^{(\alpha_{gel}-\alpha_L)}\, i^{-\alpha_{gel}} \qquad \text{for } i \geq i_{SL} \tag{C4}$$

in which $k_t^{1,1}$ is the (apparent) termination rate coefficient for radicals with chain length 1, α_s the exponent for termination for termination of short chains in dilute solution, α_L the exponent for long chains in dilute solution, α_{gel} the exponent for chains in the gel regime, i_{SL} the

crossover chain length between short- and long-chain behavior, i_{gel} the chain length at the onset of the gel-effect.

An overview of these parameters can be found in Table C1.

***Table C1**: Parameters[1,2] used for the composite k_t model with MMA as monomer; m_p: polymer mass fraction*

$\mathbf{k_t^{1,1}}$	$\boldsymbol{\alpha_S}$	$\mathbf{i_{SL}}$	$\boldsymbol{\alpha_L}$	$\boldsymbol{\alpha_{gel}}$	$\mathbf{i_{gel}}$
10^9	0.53	30	0.15	$1.22m_p$-0.11	$3.30m_p^{-2.13}$

For simplicity, Equation (C1)-(C4) are calculated using the number average chain length of the macroradical species as the complete chain length distribution of the macroradicals is not calculated in the frame of the present work.

C.2 Calculation of the apparent RAFT exchange related rate coefficients

The coupled parallel encounter pair model as described by D'hooge *et al.*[3] can be used to calculated the apparent rate coefficients for the RAFT addition, fragmentation, cross termination and transfer reactions involving only chain length *i* via:

$$k_{add,app}^{i,i} = \left(\frac{1}{k_{add,chem}} + \frac{1}{k_{add,diff}^{i,i}}\right)^{-1} \quad \text{(C5)}$$

$$k_{frag,app}^{i,i} = \left(\frac{1}{k_{frag,chem}} + \frac{K_{eq,1}}{k_{frag,diff}^{i,i}}\right)^{-1} \quad \text{(C6)}$$

$$k_{tcross,app}^{i,i,i} = \left(\frac{1}{k_{tcross,chem}} + \frac{1}{k_{tcross,diff}^{i,i,i}}\right)^{-1} \quad \text{(C7)}$$

$$k_{tr,0,app} = \left(\frac{1}{k_{tr,0,chem}} + \frac{1}{k_{tr,0,diff}} + \frac{1}{K_{eq,2}k_{-tr,0,diff}}\right)^{-1} \quad \text{(C8)}$$

$$k_{-tr,0,app} = \left(\frac{1}{k_{-tr,0,chem}} + \frac{1}{k_{-tr,0,diff}} + \frac{K_{eq,2}}{k_{tr,0,diff}}\right)^{-1} \quad \text{(C9)}$$

$$k_{tr,app} = \left(\frac{1}{k_{tr,chem}} + \frac{2}{k_{tr,diff}}\right)^{-1} \quad \text{(C10)}$$

with $k_{add,app}^{i,i}$, $k_{frag,app}^{i,i}$, $k_{tcross,app}^{i,i,i}$ and $k_{(-)tr(,0),app}^{i,i}$ the apparent RAFT addition, fragmentation, cross termination and transfer rate coefficient; $k_{add,chem}$, $k_{frag,chem}$, $k_{tcross,chem}$ and $k_{(-)tr(,0),chem}$ the intrinsic RAFT addition, fragmentation, cross termination and transfer rate coefficient (see Table 1 in Chapter 5); $k_{add,diff}^{i,i}$, $k_{frag,diff}^{i,i}$, $k_{tcross,diff}^{i,i,i}$ and $k_{(-)tr(,0),diff}^{i,i}$ the diffusional contribution for RAFT addition, fragmentation, cross termination and transfer.

with:

$$K_{eq,1} = \frac{k_{add,chem}}{k_{frag,chem}} \quad \text{(C11)}$$

$$K_{eq,2} = \frac{k_{tr,0,chem}}{k_{-tr,0,chem}} \quad \text{(C12)}$$

In the present work, the diffusional contributions are approximated by the corresponding one when considering the composite k_t model[1] (see Section C1) for the apparent termination rate coefficient as this can also be described by the classical encounter pair theory:

$$k_{t,diff}^{i,i} \approx k_{add,diff}^{i,i} \approx k_{frag,diff}^{i,i} \approx k_{tcross,diff}^{i,i,i} \approx k_{(-)tr(,0),diff}^{i,i} \quad \text{(C13)}$$

in which the intrinsic termination rate coefficient ($k_{t,chem}$) is approximated by $k_t^{1,1}$ (see Section C1). This approach is justified to a first approximation considering that the diffusion behavior

of the species involved in the RAFT reactions mentioned above is similar to the diffusion behavior of the corresponding terminating radicals.

Similar as for termination (Section C1), the number average chain length of the radicals are used to calculate the actual apparent rate coefficients.

C.3 Prove of the insignificance of the RAFT cross termination rate coefficient for Comb3 (ideal RAFT agent)

As shown in Figure 1 in Chapter 5, the RAFT cross termination rate coefficient is kinetically insignificant for Comb3 as the same results are obtained when a value of 0 L mol^{-1} s^{-1} is used compared to a value of 10^8 L mol^{-1} s^{-1}.

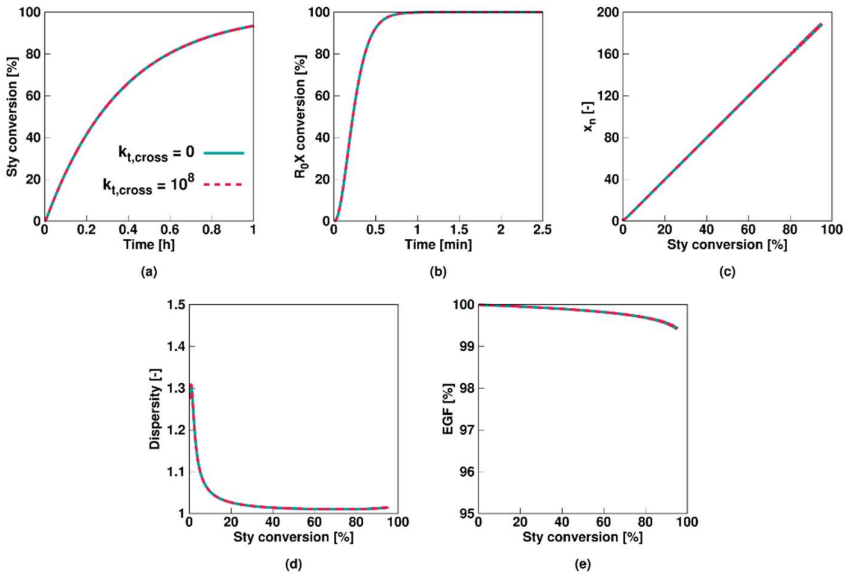

***Figure C1**: Overview of average characteristics for non-degenerative miniemulsion RAFT polymerization of styrene at 343 K with KPS and an oligomeric RAFT agent. Monomer conversion (a) and initial RAFT agent (R_0X) conversion (b) as a function of time and number average chain length x_n (c), dispersity (d) and end-group functionality (EGF) (e) as a function of styrene conversion. Model parameters for Comb3 in Table 1 in Chapter 5 without cross termination (blue) and with cross termination ($k_{t,cross}$ = 10^8 L mol^{-1} s^{-1}) taken into account. $[Sty]_0/[R_0X]_0 = 200$, $[R_0X]_0/[KPS]_0 = 3$, $[KPS]_0 = 4\ 10^{-3}$ mol L^{-1}, and d_p = 100 nm, $m_{MMA,0}$ = 20 g, $m_{H2O,0}$ = 80 g*

C.4 Comparison between results of non-degenerative and degenerative model for Comb3

As shown in Figure 2 in Chapter 5, identical results are obtained when a non-degenerative or a degenerative model is used for Comb3. This implies that all intermediate species are very short-lived, as also can be seen in Figure 11 in Chapter 5, and no side reactions involving these species are kinetically relevant (see also Section C3).

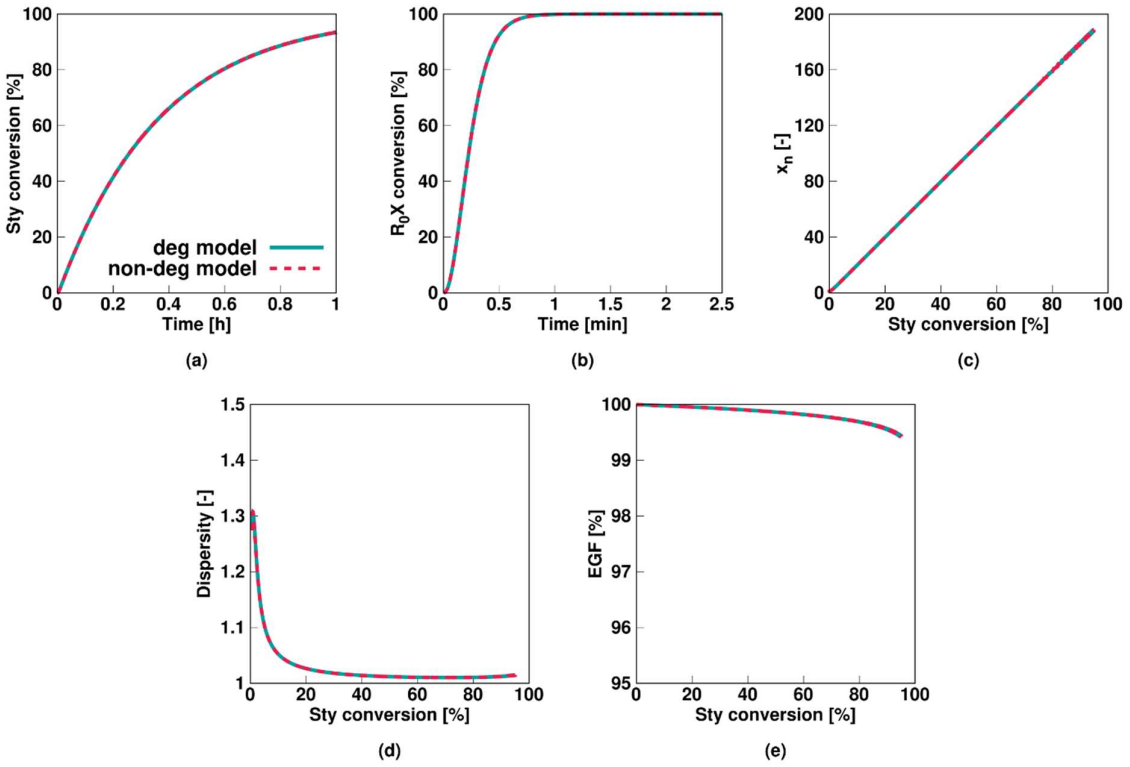

***Figure C2**: Overview of the degenerative (blue full line) and non-degenerative (dashed red line) simulation data for miniemulsion RAFT polymerization of styrene at 343 K with KPS and an oligomeric RAFT agent. Monomer conversion (a) and initial RAFT agent (R0X) conversion (b) as a function of time and number average chain length xn (c), dispersity (d) and EGF (d) as a function of styrene conversion. Model parameters for Comb3 in Table 1 of Chapter 5. $[Sty]_0/[R_0X]_0$=200 , $[R_0X]_0/[KPS]_0$= 3 , $[KPS]_0$ = 4 10^{-3} mol L^{-1} , d_p = 100 nm, $m_{MMA,0}$ = 20 g, $m_{H2O,0}$ = 80 g*

C.5 Influence of diffusional limitations on the apparent rate coefficients for Comb1

Figure C3 shows the influence of the diffusional limitations as taken into account via the formulas mentioned in Section C1 and C2 on the apparent rate coefficient for termination via recombination (a), addition of R_i to R_jX (b) and fragmentation of the intermediate radical to R_i and R_jX (c) for Comb1 (Table 1 of Chapter 5).

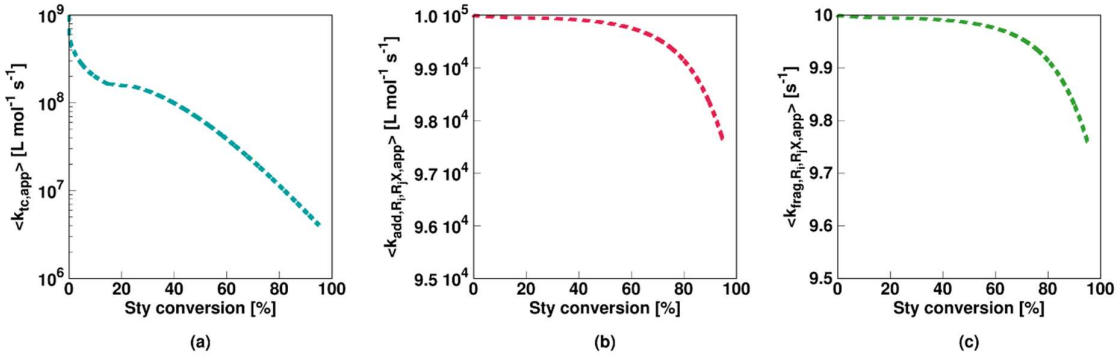

Figure C3: *Overview of the apparent termination by recombination (a), addition of R_i to R_jX (b) and fragmentation to R_i to R_jX (c) rate coefficients as calculated by the formulas mentioned in Section C1 and C2 for miniemulsion RAFT polymerization of styrene at 343 K with KPS and an oligomeric RAFT agent. Model parameters for Comb1 in Table 1 of Chapter 5. $[Sty]_0/[R_0X]_0$=200 , $[R_0X]_0/[KPS]_0$= 3 , $[KPS]_0 = 4\ 10^{-3}$ mol L^{-1} , d_p = 100 nm , $m_{MMA,0}$ = 20 g, $m_{H2O,0}$ = 80 g; note no RAFT cross-termination.*

C.6 Influence of the (average) particle size on the average number of leaving group related radicals per particle

Figure C4 shows the influence of the (average) particle size on average number of leaving group (blue), R_0XR_i (green) and R_0XR_0 (purple) radicals per particle for model parameters Comb1 (first column), Comb2 (second column) and Comb3 (third column) at 30% monomer conversion. At this monomer conversion, the conversion of initial RAFT agent (R_0X) is 100% resulting in a negligible amount of these leaving group related radicals. For a more in depth investigation of the influence of the (average) particle size on the three investigated model parameter sets, the reader is referred to Chapter 5.

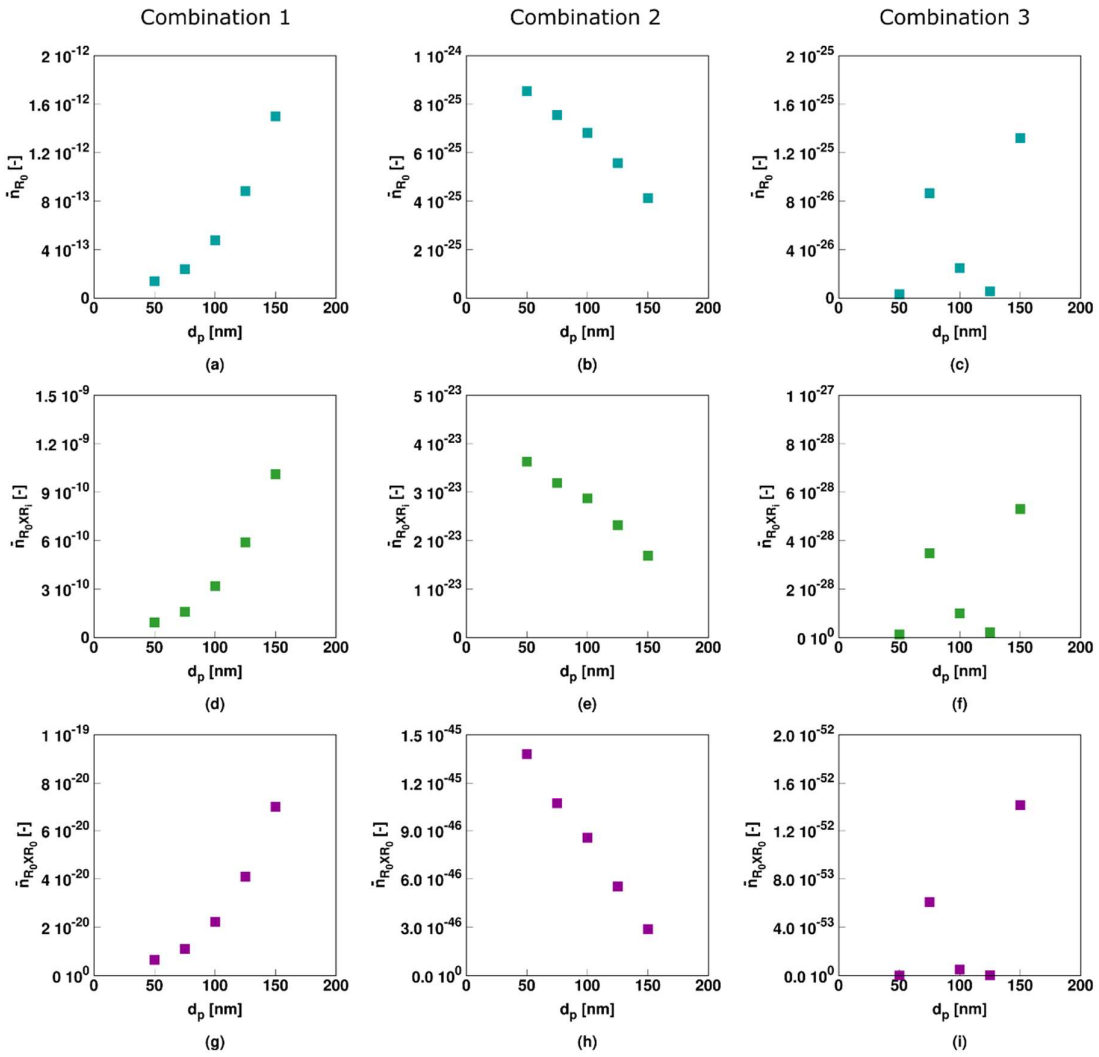

Figure C4*: Influence of the (average) particle size (dp) on the average number of leaving group ((a)-(c), blue), R_0XR_i ((d)-(f), green) and R_0XR_0 ((g)-(i), purple) radicals per particle for model parameters Comb1 (first column), Comb2 (second column) and Comb3 (third column) in Table 1 of Chapter 5. [Sty]0/[R0X]0=200 , [R0X]0/[KPS]0= 3 , [KPS]0 = 4 10-3 mol L-1 , mMMA,0 = 20 g, mH2O,0 = 80 g. XM is 30% and XR0X is 100% for all simulation points.*

C.7 Influence of the (average) particle size on rates involving the macro-RAFT intermediate radical.

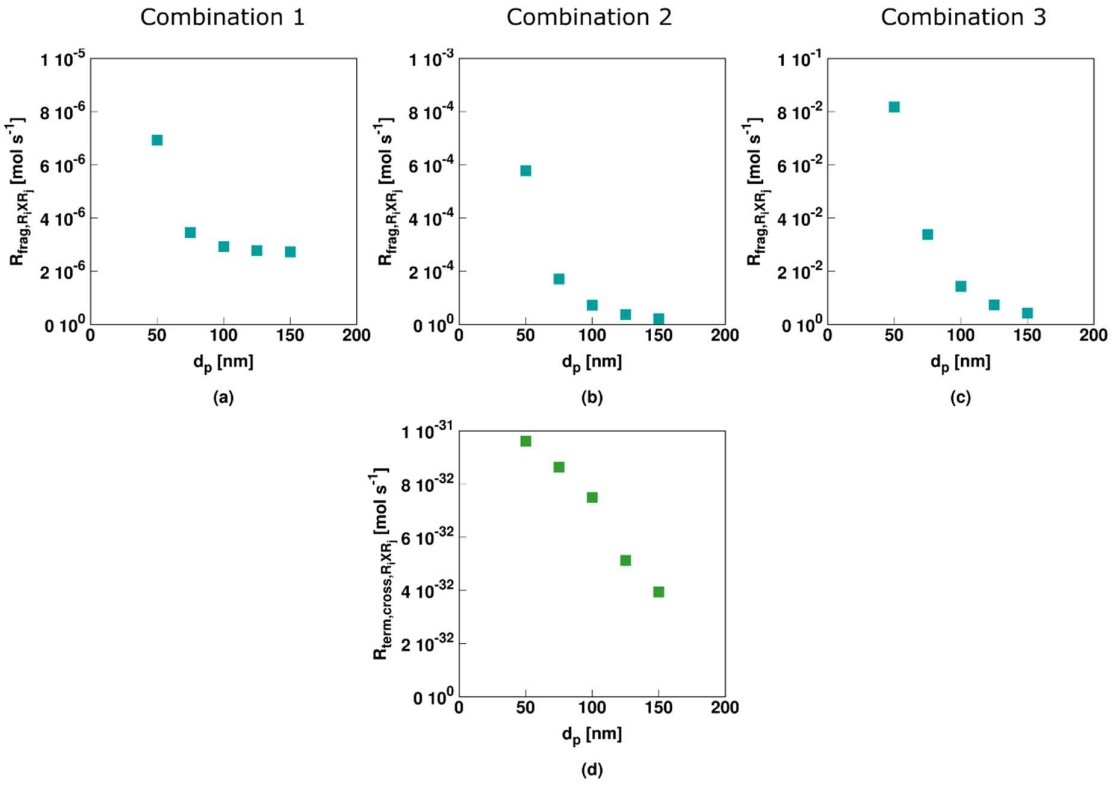

Figure C5: *Fragmentation and RAFT cross-termination rates for R_iXR_j radicals related to Figure 14 in Chapter 5.*

Figure C5 shows the corresponding rates for Figure 14 in Chapter 5, taking the macro-RAFT intermediate radical as reference. It specifically follows that for Comb1 at the higher d_p a bulk-like character is is obtained. Notably for Comb 3 the RAFT fragmentation rates are the highest. Furthermore, in Comb2, the RAFT cross-termination rate is the lowest at the highest d_p but relatively the importance of RAFT-cross termination is higher (less segregation).

C.8 Population balances necessary to describe the temporal evolution of the polymer particles

The population balances of the five-dimensional Smith-Ewart model as necessary for the non-degenerative model (Table 1 of Chapter 5), describing the temporal evolution of polymer particles having k macroradicals, l R_0 radicals, m R_iXR_0 radicals, n R_iXR_j radicals and o R_0XR_0 radicals ($N_{k,l,m,n,o}$; $k,l,m,n,o \geq 0$) are given by:

$$
\begin{aligned}
\frac{dN_{k,l,m,n,o}}{dt} = {} & \frac{k_{tc,app}}{2v_pN_A}\Big((k+2)(k+1)N_{k+2,l,m,n,o} - k(k-1)N_{k,l,m,n,o}\Big) \\
& + k_{ent\quad_2}\big[R_{2,aq}\big](N_{k-1,l,m,n,o} - N_{k,l,m,n,o}) \\
& + k_{pR_0}\big[M_p\big]\Big((l+1)N_{k-1,l+1,m,n,o} - lN_{k,l,m,n,o}\Big) \\
& + \frac{k_{tc,00}}{2v_pN_A}\Big((l+2)(l+1)N_{k,l+2,m,n,o} - l(l-1)N_{k,l,m,n,o}\Big) \\
& + \frac{k_{tc,0}}{v_pN_A}\Big((k+1)(l+1)N_{k+1,l+1,m,n,o} - klN_{k,l,m,n,o}\Big) \\
& + k_{add,R_0,R_iX}\big[R_iX_p\big]\Big((l+1)N_{k,l+1,m-1,n,o} - lN_{k,l,m,n,o}\Big) \\
& + k_{add,R_i,R_jX}\big[R_jX_p\big]\Big((k+1)N_{k+1,l,m,n-1,o} - kN_{k,l,m,n,o}\Big) \\
& + k_{add,R_0,R_0X}\big[R_0X_p\big]\Big((l+1)N_{k,l+1,m,n,o-1} - lN_{k,l,m,n,o}\Big) \\
& + k_{add,R_i,R_0X}\big[R_0X_p\big]\Big((k+1)N_{k+1,l,m-1,n,o} - kN_{k,l,m,n,o}\Big) \\
& + k_{frag,R_0,R_iX}\Big((m+1)N_{k,l-1,m+1,n,o} - mN_{k,l,m,n,o}\Big) \\
& + k_{frag,R_i,R_0X}\Big((m+1)N_{k-1,l,m+1,n,o} - mN_{k,l,m,n,o}\Big) \\
& + k_{frag,R_i,R_jX}\Big((n+1)N_{k-1,l,m,n+1,o} - nN_{k,l,m,n,o}\Big) \\
& + k_{frag,R_0,R_0X}\Big((o+1)N_{k,l-1,m,n,o+1} - oN_{k,l,m,n,o}\Big) \\
& + \frac{k_{tcross}}{v_pN_A}\Big((k+1)(m+1)N_{k+1,l,m+1,n,o} - kmN_{k,l,m,n,o}\Big) \\
& + \frac{k_{tcross}}{v_pN_A}\Big((l+1)(m+1)N_{k,l+1,m+1,n,o} - lmN_{k,l,m,n,o}\Big) \\
& + \frac{k_{tcross}}{v_pN_A}\Big((k+1)(n+1)N_{k+1,l,m,n+1,o} - knN_{k,l,m,n,o}\Big) \\
& + \frac{k_{tcross}}{v_pN_A}\Big((l+1)(n+1)N_{k,l+1,m,n+1,o} - lnN_{k,l,m,n,o}\Big) \\
& + \frac{k_{tcross}}{v_pN_A}\Big((k+1)(o+1)N_{k+1,l,m,n,o+1} - koN_{k,l,m,n,o}\Big) \\
& + \frac{k_{tcross}}{v_pN_A}\Big((l+1)(o+1)N_{k,l+1,m,n,o+1} - loN_{k,l,m,n,o}\Big)
\end{aligned}
\tag{C14}
$$

C.9 The continuity equations of the species in the aqueous phase, the abundant species in the particles and the associated equations for the average chain length characteristics

The continuity equations of the species in the aqueous phase, the abundant species in the particles and the pseudo-bulk approximation of the higher order moment equations of the macrospecies are given by:

$$\frac{d[I_{2,aq}]}{dt} = -fk_{dis}[I_{2,aq}] \tag{C15}$$

$$\frac{d[I_{aq}]}{dt} = 2fk_{dis}[I_{2,aq}] - k_{pI}[I_{aq}][M_{aq}] \tag{C16}$$

$$\frac{d[R_{1,aq}]}{dt} = k_{pI}[I_{aq}][M_{aq}] - k_p[R_{1,aq}][M_{aq}] \tag{C17}$$

$$\frac{d[R_{2,aq}]}{dt} = k_p[R_{1,aq}][M_{aq}] - k_{EntryR2}N_p\frac{[R_{2,aq}]}{N_A V_{aq}} \tag{C18}$$

$$\frac{d[M_{aq}]}{dt} = -k_{pI}[I_{aq}][M_{aq}] - k_p[R_{1,aq}][M_{aq}] \tag{C19}$$

$$\frac{d[M_p]}{dt} = -k_p\frac{\bar{n}(R_i)}{N_a v_p}[M_p] - k_{pR_0}\frac{\bar{n}(R_0)}{N_a v_p}[M_p] \tag{C20}$$

$$\begin{aligned}\frac{d\tau_0}{dt} &= \frac{d\sum_{i>0}[R_i X_p]}{dt} \\ &= k_{frag,R_0,R_iX}\frac{\bar{n}(R_0XR_i)}{N_a v_p} + k_{frag,R_i,R_jX}\frac{\bar{n}(R_iXR_j)}{N_a v_p} \\ &\quad - k_{add,R_0,R_iX}\frac{\bar{n}(R_0)}{N_a v_p}\tau_0 - k_{add,R_i,R_jX}\frac{\bar{n}(R_i)}{N_a v_p}\tau_0\end{aligned} \tag{C21}$$

$$\frac{d\mu_0}{dt} = \frac{d\sum_{i\geq 1}[P_{i,p}]}{dt}$$

$$= \frac{k_{tc,app}}{2}\frac{\bar{n}(R_i)}{N_a v_p}\frac{\bar{n}(R_i)}{N_a v_p} + k_{tc,0}\frac{\bar{n}(R_i)}{N_a v_p}\frac{\bar{n}(R_0)}{N_a v_p}$$

$$+ k_{tcross}\frac{\bar{n}(R_i)}{N_a v_p}\frac{\bar{n}(R_0 X R_i)}{N_a v_p} + k_{tcross}\frac{\bar{n}(R_0)}{N_a v_p}\frac{\bar{n}(R_0 X R_i)}{N_a v_p} \quad \text{(C22)}$$

$$+ k_{tcross}\frac{\bar{n}(R_i)}{N_a v_p}\frac{\bar{n}(R_i X R_j)}{N_a v_p} + k_{tcross}\frac{\bar{n}(R_0)}{N_a v_p}\frac{\bar{n}(R_i X R_j)}{N_a v_p}$$

$$+ k_{tcross}\frac{\bar{n}(R_i)}{N_a v_p}\frac{\bar{n}(R_0 X R_0)}{N_a v_p}$$

$$\frac{d[P_{0,p}]}{dt} = \frac{k_{tc,00}}{2}\frac{\bar{n}(R_0)}{N_a v_p}\frac{\bar{n}(R_0)}{N_a v_p} + k_{tcross}\frac{\bar{n}(R_0)}{N_a v_p}\frac{\bar{n}(R_0 X R_0)}{N_a v_p} \quad \text{(C23)}$$

$$\frac{d[R_0 X_p]}{dt} = k_{frag,R_i,R_0 X}\frac{\bar{n}(R_0 X R_i)}{N_a v_p} + k_{frag,R_0,R_0 X}\frac{\bar{n}(R_0 X R_0)}{N_a v_p}$$

$$- k_{add,R_0,R_0 X}\frac{\bar{n}(R_0)}{N_a v_p}[R_0 X_p] - k_{add,R_i,R_0 X}\frac{\bar{n}(R_i)}{N_a v_p}[R_0 X_p] \quad \text{(C24)}$$

$$\frac{d\lambda_1}{dt} = \frac{d\sum_i i[R_i]}{dt}$$

$$= [M_p]\left(k_p\frac{\bar{n}(R_i)}{N_a v_p} + k_{pR_0}\frac{\bar{n}(R_0)}{N_a v_p}\right) + 2k_{entryR_2}N_p\frac{[R_{2,aq}]}{N_A V_{aq}}$$

$$- k_{tc,app,c}\frac{\bar{n}(R_i)}{N_a v_p}\lambda_1 - k_{tc,0,c}\lambda_1\frac{\bar{n}(R_0)}{N_a v_p} - k_{add,R_i,R_0 X}\lambda_1[R_0 X_p]$$

$$- k_{add,R_i,R_j X,c}\lambda_1\tau_0 + k_{frag,R_i,R_0 X}\Omega_1^0 + k_{frag,R_i,R_j X}\Omega_{1,0} \quad \text{(C25)}$$

$$- k_{tcross,c}\lambda_1\frac{\bar{n}(R_0 X R_0)}{N_a v_p} - k_{tcross,c}\lambda_1\frac{\bar{n}(R_0 X R_i)}{N_a v_p}$$

$$- k_{tcross,c}\lambda_1\frac{\bar{n}(R_i X R_j)}{N_a v_p}$$

$$\frac{d\lambda_2}{dt} = \frac{d\sum_i i^2[R_i]}{dt}$$

$$= [M_p]\left(k_p \frac{\bar{n}(R_i)}{N_a v_p} + 2k_p\lambda_1 + k_{pR_0}\frac{\bar{n}(R_0)}{N_a v_p}\right) + 4k_{entryR_4}N_p\frac{[R_{2,aq}]}{N_A V_{aq}}$$

$$- k_{tc,app,c}\frac{\bar{n}(R_i)}{N_a v_p}\lambda_2 - k_{tc,0,c}\lambda_2\frac{\bar{n}(R_0)}{N_a v_p} - k_{add,R_i,R_0X}\lambda_2[R_0X_p]$$

$$- k_{add,R_i,R_jX,c}\lambda_2\tau_0 + k_{frag,R_i,R_0X}\Omega_2^0 + k_{frag,R_i,R_jX}\Omega_{2,0} \quad \text{(C26)}$$

$$- k_{tcross,c}\lambda_2\frac{\bar{n}(R_0XR_0)}{N_a v_p} - k_{tcross,c}\lambda_2\frac{\bar{n}(R_0XR_i)}{N_a v_p}$$

$$- k_{tcross,c}\lambda_2\frac{\bar{n}(R_iXR_j)}{N_a v_p}$$

$$\frac{d\tau_1}{dt} = \frac{d\sum_i i[R_iX_p]}{dt}$$

$$= k_{frag,R_0,R_iX}\Omega_1^0 + k_{frag,R_i,R_jX}\Omega_{1,0} - k_{add,R_0,R_iX}\frac{\bar{n}(R_0)}{N_a v_p}\tau_1 \quad \text{(C27)}$$

$$- k_{add,R_i,R_jX,c}\frac{\bar{n}(R_i)}{N_a v_p}\tau_1$$

$$\frac{d\tau_2}{dt} = \frac{d\sum_i i^2[R_iX_p]}{dt}$$

$$= k_{frag,R_0,R_iX}\Omega_2^0 + k_{frag,R_i,R_jX}\Omega_{2,0} - k_{add,R_0,R_iX}\frac{\bar{n}(R_0)}{N_a v_p}\tau_2 \quad \text{(C28)}$$

$$- k_{add,R_i,R_jX,c}\frac{\bar{n}(R_i)}{N_a v_p}\tau_2$$

$$\frac{d\mu_1}{dt} = \frac{d\sum_{i\geq 1} i[P_{i,p}]}{dt}$$

$$= k_{tc,app,c}\frac{\bar{n}(R_i)}{N_a v_p}\lambda_1 + k_{tc,0,c}\lambda_1\frac{\bar{n}(R_0)}{N_a v_p} + k_{tcross,c}\Omega_1^0\frac{\bar{n}(R_i)}{N_a v_p}$$

$$+ k_{tcross,c}\Omega_{1,0}\frac{\bar{n}(R_i)}{N_a v_p} + k_{tcross,c}\lambda_1\frac{\bar{n}(R_0XR_0)}{N_a v_p} + k_{tcross,c}\Omega_1^0\frac{\bar{n}(R_0)}{N_a v_p} \quad \text{(C29)}$$

$$+ k_{tcross,c}\Omega_{1,0}\frac{\bar{n}(R_0)}{N_a v_p}$$

$$\frac{d\mu_2}{dt} = \frac{d\sum_{i\geq 1} i^2[P_{i,p}]}{dt}$$

$$= k_{tc,app,c}\frac{\bar{n}(R_i)}{N_a v_p}\lambda_2 + k_{tc,0,c}\lambda_2\frac{\bar{n}(R_0)}{N_a v_p} + k_{tcross,c}\Omega_2^0\frac{\bar{n}(R_i)}{N_a v_p}$$

$$+ k_{tcross,c}\Omega_{2,0}\frac{\bar{n}(R_i)}{N_a v_p} + k_{tcross,c}\lambda_2\frac{\bar{n}(R_0XR_0)}{N_a v_p} + k_{tcross,c}\Omega_2^0\frac{\bar{n}(R_0)}{N_a v_p} \quad \text{(C30)}$$

$$+ k_{tcross,c}\Omega_{2,0}\frac{\bar{n}(R_0)}{N_a v_p}$$

$$\frac{d\Omega_1^0}{dt} = \frac{d\sum_{i\geq 1} i[R_0XR_{i,p}]}{dt}$$

$$= k_{add,R_0,R_iX}\frac{\bar{n}(R_0)}{N_a v_p}\tau_1 + k_{add,R_i,R_0X}\lambda_1[R_0X_p] - k_{frag,R_i,R_0X}\Omega_1^0 \quad \text{(C31)}$$

$$- k_{frag,R_0,R_iX}\Omega_1^0 - k_{tcross,c}\Omega_1^0\frac{\bar{n}(R_i)}{N_a v_p} - k_{tcross,c}\Omega_1^0\frac{\bar{n}(R_0)}{N_a v_p}$$

$$\frac{d\Omega_2^0}{dt} = \frac{d\sum_{i\geq 1} i^2[R_0XR_{i,p}]}{dt}$$

$$= k_{add,R_0,R_iX}\frac{\bar{n}(R_0)}{N_a v_p}\tau_2 + k_{add,R_i,R_0X}\lambda_2[R_0X_p] - k_{frag,R_i,R_0X}\Omega_2^0 \quad \text{(C32)}$$

$$- k_{frag,R_0,R_iX}\Omega_2^0 - k_{tcross,c}\Omega_2^0\frac{\bar{n}(R_i)}{N_a v_p} - k_{tcross,c}\Omega_2^0\frac{\bar{n}(R_0)}{N_a v_p}$$

$$\frac{d\Omega_{1,0}}{dt} = \frac{d\sum_{i\geq 1}\sum_{j\geq 1} i[R_iXR_j]}{dt}$$

$$= k_{add,R_i,R_jX,c}\left(\lambda_1\tau_0 + \frac{\bar{n}(R_i)}{N_a v_p}\tau_1\right) - 2k_{frag,R_i,R_jX}\Omega_{1,0} \quad \text{(C33)}$$

$$- k_{tcross,c}\Omega_{1,0}\frac{\bar{n}(R_i)}{N_a v_p} - k_{tcross,c}\Omega_{1,0}\frac{\bar{n}(R_0)}{N_a v_p}$$

$$\frac{d\Omega_{2,0}}{dt} = \frac{d\sum_{i\geq 1}\sum_{j\geq 1} i^2[R_iXR_j]}{dt}$$

$$= k_{add,R_i,R_jX,c}\left(\lambda_2\tau_0 + \frac{\bar{n}(R_i)}{N_a v_p}\tau_2\right) - 2k_{frag,R_i,R_jX}\Omega_{2,0} \quad \text{(C34)}$$

$$- k_{tcross,c}\Omega_{2,0}\frac{\bar{n}(R_i)}{N_a v_p} - k_{tcross,c}\Omega_{2,0}\frac{\bar{n}(R_0)}{N_a v_p}$$

$$\frac{d\Omega_{1,1}}{dt} = \frac{d\sum_{i\geq 1}\sum_{j\geq 1} ij[R_iXR_j]}{dt}$$

$$= 2k_{add,R_i,R_jX,c}\lambda_1\tau_1 - 2k_{frag,R_i,R_jX}\Omega_{1,1} - k_{tcross,c}\Omega_{1,1}\frac{\bar{n}(R_i)}{N_a v_p} \quad \text{(C35)}$$

$$- k_{tcross,c}\Omega_{1,1}\frac{\bar{n}(R_0)}{N_a v_p}$$

with the number and mass average chain length of the R_iXR_j radicals defined as

$$x_{n,R_iXR_j} = \frac{\Omega_{1,0}}{\frac{\bar{n}(R_iXR_j)}{N_a v_p}} \quad \text{(C36)}$$

$$x_{m,RiXR_j} = \frac{\Omega_{2,0} + \Omega_{1,1}}{\Omega_{1,0}} \quad \text{(C37)}$$

C.10 References:

1. Johnston-Hall, G.; Monteiro, M.J. Bimolecular Radical Termination: New Perspectives and Insights. *J. Polym. Sci. Part a-Polymer Chem.* **2008**, *46*, 3155–3176.

2. Derboven, P.; D'hooge, D.R.; Reyniers, M.-F.; Marin, G.B.; Barner-Kowollik, C. The Long and the Short of Radical Polymerization. *Macromolecules* **2015**, *48*, 492–501.

3. D'hooge, D.R.; Reyniers, M.F.; Marin, G.B. The crucial role of diffusional limitations in controlled radical polymerization. *Macromol. React. Eng.* **2013**, *7*, 362–379.